The background is a stylized, low-poly illustration of a soil profile. The top portion shows green grass blades against a light blue sky. Below the surface, the soil is depicted in various shades of brown and tan, with a jagged, faceted texture that suggests organic matter and soil structure. The overall style is modern and graphic.

***Mechanistic modelling
of the vertical
soil organic matter
profile***

Maarten C. Braakhekke

Mechanistic modelling of the vertical soil organic matter profile

Maarten C. Braakhekke

Thesis committee

Promotor

Prof. Dr P. Kabat
Professor of Earth System Science
Wageningen University
Director General
International Institute for Applied Systems Analysis, Laxenburg, Austria

Co-promotors

Dr C. Beer
Associate professor, Department of Applied Environmental Science and Bolin Centre
for Climate Research
Stockholm University, Stockholm, Sweden

Dr M. Reichstein
Director, Department Biogeochemical Integration
Max-Planck Institute for Biogeochemistry, Jena, Germany

Dr M.R. Hoosbeek
Associate professor, Earth System Science Group
Wageningen University

Other members

Dr M. van Oijen, Centre for Ecology & Hydrology, Edinburgh, Scotland
Prof. Dr L. Brussaard, Wageningen University
Prof. Dr W. de Vries, Wageningen University
Dr V. Brovkin, Max Planck Institute for Meteorology, Hamburg, Germany

This research was conducted under the auspices of the Graduate School for Socio-Economic and Natural Sciences of the Environment (SENSE).

Mechanistic modelling of the vertical soil organic matter profile

Maarten C. Braakhekke

Thesis

submitted in fulfilment of the requirements for the degree of doctor
at Wageningen University

by the authority of the Rector Magnificus

Prof. Dr M.J. Kropff,

in the presence of the

Thesis Committee appointed by the Academic Board

to be defended in public

on Friday 24 January 2014

at 11 a.m. in the Aula.

Maarten C. Braakhekke
Mechanistic modelling of the vertical soil organic matter profile,
192 pages.

PhD thesis, Wageningen University, Wageningen, NL (2014)
With references, with summaries in Dutch and English

ISBN 978-94-6173-828-8

Table of Contents

1	Introduction	9
2	SOMPROF: a vertically explicit soil organic matter model	25
3	Modelling the vertical soil organic matter profile using Bayesian parameter estimation	67
4	The use of radiocarbon to constrain current and future soil organic matter turnover and transport in a temperate forest	107
5	General discussion and conclusions	143
	References	161
	Summary	179
	Samenvatting	182
	About the author	187

Preface

This thesis is the result of work carried out largely in Jena, Germany, at the Biogeochemical Model-Data Integration Group, in the Max-Planck Institute for Biogeochemistry. When I started there in 2006 there were only three people, including myself. Over the course of six years it has grown into a successful group with over thirty researchers, and has now become the Department of Biogeochemical Integration. I am grateful to have been part of this process. My time in this young, dynamic research group has shaped me in many ways as a scientist. Most importantly it has convinced me of the importance of observations and involving them in a formal way in the development of process-oriented models. A smaller, yet not unimportant part of my time was spent at the Earth System Science Group of Wageningen University. Similar to the MDI group in Jena, the ESS group was young when I joined but has grown to be large, successful, and very diverse.

It has been a long ride. Fortunately I had some good people around me that supported me along the way. I will mention the most important of these here.

First, my supervisors: Christian Beer and Markus Reichstein in Jena, and Marcel Hoosbeek, Bart Kruijt, and Pavel Kabat in Wageningen. Thank you for your advice during our many meetings, for allowing me the freedom to carry out my research as I thought best, and for keeping faith in that I would bring it to completion.

In Jena, Thomas Wutzler, Bernhard Ahrens, Jens Kattge, and Nuno Carvalhais: our many discussions about modelling and model-data integration have been an inspiration. Many thanks also to Marion Schrumppf for selflessly providing your great data, even if it hadn't yet been published, and for your ever thorough manuscript reviews.

To those at the Earth System Science Group in Wageningen: although I spent relatively little time with you during my PhD work, you always made me feel at home when I was there. Thank you for your pleasant company.

Hans Vloemans and Bas Kempen, my paranymphs and dear friends since the early days of our soil science study in Wageningen: thank you for supporting me, particularly in the last hour of my PhD work. To my other friends in the Netherlands: despite my extended absence it never felt as if I had left the group, for which I am very grateful. My friends in Jena, some of whom have moved on to other places: thank you for your great friendship. I'd like to think that spending time with people of more than ten different nationalities has made me a more open-minded person.

My final “thank yous” are reserved for my family: my brother Coen Braakhekke and his wife Esther, and children Fenne, Robbe, and Suze; and most importantly my parents, Wim and Ellen Braakhekke. Thank you for your encouragement, unconditional faith, and great hospitality during the times when I was working in Wageningen. Ellen, our many phone calls have been a constant source of moral support. Wim, you have been my main inspiration for choosing science as a profession. It is no coincidence that I ended up in nearly the same field as you.

Maarten Braakhekke
Heelsum, December 2013

Chapter 1

Introduction

1.1 Motivation

On May 9, 2013 the daily mean atmospheric CO₂ concentration at the Mauna Loa observatory in Hawaii reached 400 ppm for the first time since the start of recordings (National Oceanic and Atmospheric Administration, 2013). This event marked a symbolic milestone in the increasing perturbation of the global carbon cycle, caused mainly by emissions from fossil fuel combustion and land-use change. That the rising levels of CO₂ and other greenhouse gases have potentially major effects on the global climate is now virtually undisputed in the scientific community (Arblaster et al., 2013). However, the precise impacts remain highly uncertain, due to limited understanding of the earth as a system. An important source of this uncertainty are potential feedbacks between the climate system and the global carbon cycle (Jones et al., 2006).

Carbon is a key element in the earth system, being a constituent of the two most important greenhouse gases, CO₂ and CH₄, and a fundamental building block of organisms. It is continually exchanged between the atmosphere and other compartments of the earth system: the hydrosphere, the geosphere, and the biosphere (Schlesinger, 1997). The latter three spheres each store much larger amounts of carbon than what is currently present in the atmosphere. Since the dynamics of these carbon pools are determined by very small differences between large losses and gains, small relative changes in these fluxes have the potential to mitigate or enhance climate change. Hence, large efforts are made to improve understanding of carbon fluxes in each of these spheres and transfer this knowledge to numerical models. This study deals with a large and potentially vulnerable pool of carbon in the terrestrial biosphere: soil organic matter.

Soils are estimated to store between 1220 and 1576 petagram (Pg, 1×10^{15} g) of carbon as organic matter globally in the top meter (Eswaran et al., 1993; Sombroek et al., 1993; Batjes, 1996; Jobbagy and Jackson, 2000), roughly twice the amount currently present in the atmosphere. The flow of carbon from soils to the atmosphere through heterotrophic respiration is estimated at around 55 Pg per year, an order of magnitude higher than the current fossil fuel emissions (Prentice et al., 2001). Rising atmospheric CO₂ concentrations are expected to lead to increased soil carbon input due to increased vegetation productivity and litter fluxes (Schimel, 1995; Norby et al., 2005). Conversely, rising global temperature will accelerate carbon loss by heterotrophic respiration (Davidson and Janssens, 2006). Global simulations suggest that the net effect on the soil carbon balance will initially be positive, but will decrease and possibly become negative during the next 50–100 yr (Sitch et al., 2008).

Traditionally, research into soil carbon dynamics has focused mainly on the surface organic layer and the topsoil (0–30 cm), where organic carbon occurs in highest concentrations, is most directly influenced by climate and vegetation, and has highest turnover rates (Trumbore, 2009). Lately, attention is starting to extend to greater soil depths, partially due to accumulating evidence that “deep” organic matter may not be as stable as previously believed (Baisden and Parfitt, 2007; Koarashi et al., 2012). The mechanisms that protect organic matter from decomposition may vary over the profile due to the strong vertical gradients of physical, chemical, and bio-

logical properties that typically occur in soils (Rumpel et al., 2012). Several of these mechanisms are sensitive to changes in environmental conditions. Furthermore, several studies have shown that significant amounts of organic carbon are stored below 1 m depth (Jobbagy and Jackson, 2000; Tarnocai et al., 2009). Finally, the vertical distribution and form of organic matter influences soil physical properties, such as bulk density, and soil moisture and heat transport parameters (Rawls, 1983; Rawls et al., 2003; Koven et al., 2009).

Thus, ecosystem models will benefit from vertically a explicit representation of soil carbon, both to facilitate future extension with new process descriptions, as well as to improve existing parameterizations. Growing awareness of this need is demonstrated by recent efforts to add the vertical dimension to existing soil carbon models (Jenkinson and Coleman, 2008; Koven et al., 2013). However, the mechanisms controlling the vertical soil organic matter distribution have been little investigated. This hinders the determination of the rates and proper mathematical formulations of processes, particularly for models intended for large spatial scales.

1.2 Background

1.2.1 Soil organic matter

Soil organic matter (SOM) is defined as all dead organic compounds in soil, in all forms and states of decay, derived from plant, animal, and microbial biomass¹ (Trumbore and Torn, 2005). Most SOM is ultimately derived from plants, which produce organic products from carbon dioxide and water through the process of photosynthesis. The majority of the net production of photosynthates eventually enters the litter layer and soil through senescence, plant death, and excretion of exudates by roots. Once present in the soil, SOM is processed by the soil foodweb, during which a part is incorporated into decomposer biomass and another part is lost as CO₂ due to respiration. Finally, a small fraction is transformed into recalcitrant organic compounds, collectively called “humus”, which comprises approximately 90% of all SOM (van Breemen and Buurman, 1997). Overall, SOM is an extremely heterogeneous mixture of organic compounds of all decomposition stages, with different chemical structures, turning over at different rates ranging from days to millennia.

The decomposition process is essential for the stabilization of organic carbon. On the other hand, through heterotrophic respiration, decomposition is the main mechanism for carbon loss from soils. Hence, decomposers are key agents in the terrestrial carbon cycle, despite the fact that their biomass constitutes only a small fraction of all organic matter in soils (1–2%; Xu et al. (2013)). The main organisms involved in decomposition are fungi, bacteria, and soil fauna. Mineralization of organic matter is mainly carried out by bacteria and fungi who release exoenzymes that break down and mobilize organic molecules. The resulting substrates diffuse to the microbes and are absorbed and incorporated into biomass (Chapin et al., 2002). Soil

¹In this discussion, “soil organic matter” also refers to material in organic layers on top of the mineral soil, although this not considered SOM in the strict sense.

fauna includes microfauna (nematodes, protozoans), mesofauna (mites, springtails), and macrofauna (earthworms, arthropods) (Brussaard et al., 1997). They play an important role by fragmenting, transforming, and mixing organic matter, as well as by grazing on bacteria and fungi (Chapin et al., 2002; van Delft et al., 2006).

Organic matter decomposition rates are influenced by a range of factors. In the early stages, decomposition is determined mainly by substrate quality, temperature, and moisture. Substrate quality is a general term that refers to the susceptibility of organic matter to decomposition under standard conditions. It is determined by chemical properties (molecular structure, nutrient concentration) and generally negatively correlated to litter C:N or lignin:N ratio (Chapin et al., 2002). Decomposition is positively correlated to temperature due to stimulation of microbial activity and substrate diffusion. Moisture availability promotes decomposer activity, as long as conditions remain aerobic. Very high moisture contents limit oxygen diffusion which slows decomposition, and may ultimately lead to anaerobic respiration and methane (CH₄) production.

As organic matter becomes more decomposed and mixed with minerals, several mechanisms may lead to protection from further breakdown (van Breemen and Burman, 1997; von Lützow et al., 2006; Schmidt et al., 2011). For well drained soils these include: (i) adsorption of organic matter onto mineral surfaces; (ii) formation of water repellent organic structures; (iii) high levels of aluminium and/or iron which are toxic to microbes; (iv) physical disconnection from decomposers due to low concentrations or occlusion in aggregates; (v) energy or nutrient limitation of microbes. These mechanisms all contribute to long term SOM stabilization, but their relative importance is poorly known and varies strongly between soils (von Lützow et al., 2006). Organic matter may become destabilized when environmental and biological factors that control these mechanisms are altered due to changes in land use or vegetation structure.

1.2.2 The vertical soil organic matter profile

Since the biological activity required for organic matter production occurs at or near the soil surface, SOM concentrations in the mineral soil are generally highest in the topsoil and decrease with depth (Jenny, 1980). Exceptions are peat soils (histosols) which have very high organic matter concentrations, potentially up to great depths (Driessen and Dudal, 1991), and podzols (spodosols), which can have locally increasing SOM concentrations due to eluviation and illuviation of mobile SOM fractions (van Breemen and Burman, 1997). Additionally, natural formation of the SOM profile may be disturbed due to erosion and deposition, or anthropogenic influences, such as ploughing and plaggen cultivation (Blume and Leinweber, 2004). However, in most natural and undisturbed soils SOM concentrations monotonically decrease with depth. Generally, the profile is concave—i.e. the gradient decreases with depth—and, if bedrock is sufficiently deep, asymptotically approaches zero. A range of depth functions has been proposed to model the SOM profile, including exponential (Minasny et al., 2006), power (Jobbagy and Jackson, 2000), polynomial (Arrouays and Pelissier, 1994) and Langmuir-derived (Johnson et al., 2011). Addi-

tionally, soil-type specific, piecewise functions have been used to model disturbed and human-influenced soils (Kempen et al., 2011).

The vertical SOM profile differs markedly between soils, ecosystems, and climate regions (Batjes, 1996; Jobbagy and Jackson, 2000, Figure 1.1). Jobbagy and Jackson (2000) analysed a global database of soil organic carbon profiles, and the relationship of the soil carbon distribution with environmental factors. They concluded that the vertical distribution of SOM differs significantly between vegetation types, with the proportion of organic carbon in the top 20 cm relative to the total in the first meter ranging between 29 % for cold arid shrublands to 57 % in cold humid forests. These differences are mainly related to the varying root distributions and root/shoot ratios of these vegetation types. The amount of organic carbon in the top 20 cm was found to be most strongly correlated with climate, whereas the clay fraction is more important in deeper layers. Globally, it is estimated that approximately 36 % of organic matter occurs below 1 m depth (Jobbagy and Jackson, 2000). However, due to the small number of published deep SOM stocks this figure is presumably quite uncertain. Very deep SOM profiles, with significant stocks below 5 m depth, have been observed in tropical forests (Trumbore et al., 1995; Telles et al., 2003) and permafrost regions (Zimov et al., 2006; Tarnocai et al., 2009).

1.2.3 The surface organic layer

In ecosystems with significant aboveground litter production and little biological mixing organic matter tends to accumulate at the surface in the form of a organic layer, also termed “ectorganic horizon²”. In dryland soils such layers are mainly found in forests, where a large part of the litter input occurs aboveground. They may also occur in shrublands. In grasslands a layer with high organic matter concentration may form due to accumulation of root litter (“endorganic horizon”) but such layers are usually considered part of the mineral soil (van Delft et al., 2006). The humus in surface organic layers is generally classified as mor or moder. Mor humus occurs when conditions are most unfavourable and decomposition occurs largely by fungi. Under somewhat more favorable conditions the humus may be partially processed by mesofauna and consist of moder: fecal pellets, mainly from arthropoda (van Breemen and Buurman, 1997; van Delft et al., 2006).

The thickness of the organic layer varies greatly between ecosystems and is determined by the balance between litter deposition versus decomposition and biological mixing (Olson, 1963). In ecosystems with active soil fauna and fast decomposition the organic layer may be (almost) absent, whereas under unfavorable conditions the organic layer can accumulate to great thickness (van Delft et al., 2006). A typical example are peat soils, where decomposition is slowed by anaerobic conditions due to a high water table. But also in well drained soils very thick (> 1m) organic layers have been reported (Berg and McLaugherty, 2008). Roots often grow preferentially in the organic layer because of the higher nutrient and moisture availability (Schenk and Jackson, 2002a). This in turn accelerates organic layer buildup by additional input due to root turnover (Vogt et al., 1983, 1986).

²In the literature the surface organic layer is also referred to as “litter layer” or “forest floor”

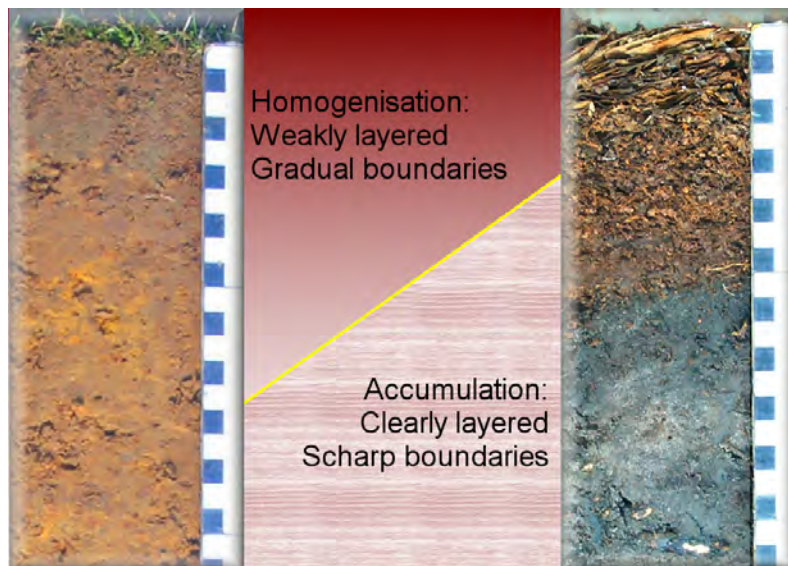


Figure 1.1: Two examples of the organic matter profile, characterized by strong mixing and decomposition (left), and accumulation at the surface (right). From van Delft et al. (2006), reprinted with kind permission of Bas van Delft.

Due to constant deposition of litter at the surface the organic layer is often sharply delineated from the mineral soil, particularly when biological mixing is low (Jenny, 1980). Consequently, the organic layer is typically not considered part of the SOM profile and is often excluded from carbon stock estimates (Batjes, 1996).

Horizon classification systems generally distinguish three major horizons in the surface organic layer of forest soils: (i) The L-horizon: fresh, undecomposed litter, with discernable plant structures; (ii) The F-horizon: partially decomposed (fragmented/fermented) litter; (iii) The H-horizon: strongly decomposed humus without recognizable plant residues³. In soils with fast decomposition and biological mixing the F and H horizon may be thin or absent.

Organic matter dynamics in the organic layer differ significantly from the mineral soil, due to the absence of minerals. Whereas in the mineral soil organic matter decomposition is governed by stabilization processes (see section 1.2.1), in the organic layer decay is mainly determined by litter chemistry, nutrient status, moisture, and temperature (van Breemen and Buurman, 1997). Furthermore, organic layers have markedly different physical properties compared to the mineral soil, including porosity, bulk density, heat conductivity, and hydraulic conductivity (Schaap and Bouten, 1997; Schaap et al., 1997; Lawrence and Slater, 2008; Rinke et al., 2008).

³The L, F, and H horizon codes are used in the Canadian horizon classification system (Soil Classification Working Group, 1998) as well as a recently developed Dutch system for humus form description (van Delft et al., 2006). They correspond to the Oi, Oe, and Oa horizons, respectively, in the U.S.A. and FAO classification systems (Soil Survey Division Staff, 1993; IUSS Working Group WRB, 2007)

1.2.4 Processes related to soil organic matter profile formation

The accumulation of SOM in the vertical profile is an important part of soil formation (Jenny, 1980; van Breemen and Buurman, 1997), taking place on time scales of decades to millennia. Overall, SOM dynamics are determined by the gain and loss due to (above and belowground) litter input and decomposition. When studying the vertical distribution of SOM, the depth dependence of these processes is relevant, as well as vertical transport and erosion and deposition.

Vertical SOM transport can have a major effect on the SOM profile and is generally caused by mixing processes and transport of mobile fractions with the liquid phase (van Breemen and Buurman, 1997; Rumpel and Kögel-Knabner, 2011). In terrestrial soils, mixing of the soil—referred to as “pedoturbation” (Hole, 1961)—can occur by several processes, including the reworking activity of soil fauna (bioturbation) and freezing and thawing (cryoturbation) (Johnson et al., 1987). Cryoturbation occurs mainly in permafrost affected soils, which cover large regions at high latitudes. Since these ecosystems are unfavorable to soil fauna, this process forms a relatively large contribution to organic matter redistribution (Bockheim, 2007). In the global context however, bioturbation and liquid phase transport are presumably the most important transport processes. They are discussed in detail below.

In layers with high organic matter concentrations an important additional transport flux occurs that is generally ignored in SOM profile models. Loss of mass due to decomposition leads to downward shift of material above, while surface litter deposition continually buries older material. This causes advective downward flow of material unrelated to mixing or water movement. Kaste et al. (2007) found this process to be relevant for the vertical distribution of $^{210}\text{Pb}_{\text{ex}}$ in the organic surface horizon of a podzol. This may be simulated by tracking “cohorts”: layers of litter that are deposited within specific time intervals, and thus have similar age. Such models have been applied to simulate peat accumulation (Heinemeyer et al., 2010).

Bioturbation

Bioturbation is defined as the biological reworking of soils and sediments by different kinds of organisms, including rooting plants, and most importantly, burrowing animals (Meysman et al., 2006). Chapin et al. (2002) noted that in temperate regions the mixing activity of earthworms represents a force orders of magnitude larger than other geomorphic processes such as erosion. The potential effects of bioturbators on their habitat are so severe that they have been called “ecosystem engineers” (Meysman et al., 2006).

The rate of soil displacement by bioturbating organisms is usually estimated by measuring deposition of mounds at the soil surface. Paton et al. (1995) reviewed a range of quantitative estimates for different organisms. They concluded that the most important animal groups are earthworms, ants, mammals, and termites. Rates of mounding ranged from 0.0063 to 27 kg m⁻² yr⁻¹. These estimates may not be completely reliable for assessment of rates at regional to global scales since studies tend to focus on sites with high bioturbation rates, and because not all mixing activity is

expressed as mounding at the surface.

In the ideal case, mixing has a homogenizing effect on soil properties: it increases dispersal of particles, reduces concentration gradients, and destroys layering (Johnson et al., 1987). Hence, bioturbation leads to organic matter diffusion and deepening of the SOM profile. However, at small spatial scales the effects of bioturbation are more complex, for several reasons: (i) Certain fractions may be transported preferentially. For example, since mixing by earthworms is mostly related to feeding, it is more likely to affect (fresh) litter than mineral fractions (Johnson et al., 2005). The coarsest fractions, including stones, may be completely unaffected by bioturbation. (ii) Mixing may occur more strongly in one direction than in others (anisotropic mixing). For example termites bring clay particles from considerable depths to the soil surface to for incorporation into their surface mounds (Paton et al., 1995). (iii) The distance of particle translocation may be quite large compared to the scale of the SOM profile (Boudreau, 1986b).

Although the relevance of bioturbation for organic matter redistribution is well recognized (van Breemen and Buurman, 1997; Chapin et al., 2002; Hoosbeek and Scarascia-Mugnozza, 2009), very few studies have been performed on its effects on the SOM profile (Tonnejck and Jongmans, 2008; Yoo et al., 2011), particularly on long time scales. Based on micromorphological analysis and radiocarbon dating, Tonnejck and Jongmans (2008) showed that bioturbation is the main mechanism for SOM input at depth in a volcanic ash soil, more important than liquid phase transport and root input. On shorter time scales, studies of earthworm invasions in forests have demonstrated dramatic effects on organic surface layers (Alban and Berry, 1994; Bohlen et al., 2004). For example, Alban and Berry (1994) found that increasing earthworm populations in a temperate podzol led to a reduction of forest floor mass by 85 % and disappearance of the eluviation (E) horizon in 14 years.

Liquid phase transport

A small part of organic matter in soils is dissolved in the liquid phase. Concentrations of dissolved organic matter (DOM) are typically so low that total organic carbon in solution is negligible compared to the immobile fraction (Michalzik et al., 2001). However, leaching and decomposition fluxes of dissolved organic matter may be important terms in the soil carbon budget (Kalbitz and Kaiser, 2008; Kindler et al., 2011). DOM is also highly relevant to the formation of the SOM profile since it is subject to potentially very fast transport with downward water fluxes and represents a mechanism of organic matter input at depths well below the zone where bioturbation and root input are relevant (Rumpel et al., 2012). Furthermore, adsorption of DOM to the mineral phase is one of the main mechanisms for organic carbon stabilization (Kalbitz and Kaiser, 2008).

Similar to SOM, DOM is not chemically defined but consists of a broad spectrum of organic substances ranging from small molecules to complex humic acids (Kalbitz et al., 2000; Michalzik et al., 2001). The biodegradability of these substances ranges over several orders of magnitude (Kalbitz et al., 2000), with more resistant compounds generally increasing with depth (Kalbitz et al., 2000; Sanderman et al.,

2008).

DOM may originate from several sources, of which the relative contribution are not fully clear (Kalbitz et al., 2000). Leaching of fresh litter contributes strongly to DOM production in the surface organic layer (L horizon). However, for most plant species litter leachate is relatively labile, and thus may not contribute strongly to DOM in the mineral soil (Neff and Asner, 2001). More complex and recalcitrant dissolved organic substances are formed as a byproduct of decomposition. These presumably contribute more to DOM in the mineral soil. DOM is also input by throughfall (Michalzik et al., 2001), and root exudation (Neff and Asner, 2001)

DOM is removed from the soil solution by uptake and decomposition by microbes. A considerable part of DOM is easily degradable, but this fraction decreases with depth (Kalbitz et al., 2000). Another important mechanism for DOM removal is immobilization due to interactions with the solid phase and (co-)precipitation. Through a range of chemical mechanisms DOM is adsorbed to surfaces of minerals (particularly Al and Fe hydroxides and clay) and to lesser extent solid organic matter (Neff and Asner, 2001). These interactions are highly variable and depend on the chemical properties of DOM, the sorbent, and the soil solution. Furthermore, in acid soils DOM may (co-)precipitate with Al and Fe ions, which is an important process for the formation of the illuviation horizon in podzols (van Breemen and Buurman, 1997). As a result of these interactions, vertical transport of DOM is significantly lower than that of water, and DOM concentrations are often much lower in the deep soil than near the surface. Furthermore, the fact that certain compounds are more susceptible to adsorption than others leads to changes of DOM chemistry along the profile (“chromatographic effect”). Since immobilization of DOM dramatically reduces its susceptibility to decomposition, it is considered to be a highly relevant mechanism of soil carbon stabilization (Kaiser and Guggenberger, 2000), particularly in the deep soil (Rumpel et al., 2012). However, the adsorption capacity of minerals is not unlimited, which restricts the capacity for soil layers to store carbon by this mechanism (Hassink, 1997).

The relevance of DOM transport for the SOM profile is often discussed in the context of podzolization (van Breemen and Buurman, 1997). However, it is presumably an important mechanism for SOM transport in all soils where significant downward water fluxes occur (Rumpel and Kögel-Knabner, 2011). DOM movement has been found to be more important in forest soils, particular those with acidic conditions. Nevertheless, very little research has been performed on the effects of liquid phase transport on SOM profile formation on long time scales. DOM dynamics are a very poorly understood part of SOM cycling, as shown by several review studies (Kalbitz et al., 2000; Michalzik et al., 2001; Neff and Asner, 2001). Production, ad- and desorption, and mineralization of DOM all occur by a range of mechanisms that are sensitive to physical, chemical, and biological factors. As a result, laboratory experiments are usually not representative for field conditions, while in field studies effects on various mechanisms are highly confounded, often resulting in conflicting findings. Furthermore, DOM transport occurs for a large part during short storm events and with macropore flow (Kalbitz et al., 2000).

Depth dependence of organic matter input

Only in growing ecosystems does a small fraction of the net primary production (NPP) of vegetation lead to long term biomass increase. In the absence of grazing, most fixed carbon is ultimately delivered to the soil (Schlesinger, 1997). Litter input can be divided into an aboveground fraction: leaves/needles, stems, branches, and fruits; and a belowground fraction, also referred to as rhizodeposition⁴: root turnover, sloughing off of root tissue, and secretion of mucilage and root exudates (Nguyen, 2003). The relative distribution of the litter input over these two fractions, as well as the vertical distribution of the belowground input is highly relevant for the SOM profile. Jobbagy and Jackson (2000) found a significant relationship between vertical SOM distribution and plant functional type, which is partially explained by root/shoot ratio and root biomass distribution.

Since NPP is the source of litter input, its distribution over above- and belowground biomass is a good predictor of the relative proportions of aboveground litter fall and rhizodeposition (Raich and Nadelhoffer, 1989). Herbaceous vegetation types and shrubs allocate the highest fraction of NPP belowground, and forests the lowest fraction (Chapin et al., 2002). Saugier et al. (2001) compiled NPP estimates and concluded that on average 67% and 57% of NPP is allocated belowground for grasslands and arctic tundra, respectively, whereas for temperate and boreal forests this fraction is 39% and 44%. Root to shoot biomass ratios follow a similar pattern (Jackson et al., 1996). Due to the difficulty of measuring NPP, particularly belowground, these figures should be considered indications only (Clark et al., 2001). Furthermore, plants may change their allocation pattern and rooting profile when changes in nutrient and water availability and other environmental factors occur (Jackson et al., 2000).

Decomposition dynamics of above and belowground litter differ substantially due to differences in chemical composition and environmental factors at the deposition site—at the surface or directly within the profile. Root litter has repeatedly been found to be more chemically recalcitrant than aboveground litter due to the presence of substances such as lignin, cutin, and suberin (Rasse et al., 2005). Furthermore, since root input occurs predominantly in the mineral soil it is subject to stabilization mechanisms related to the mineral phase, such as adsorption and occlusion in aggregates (Rasse et al., 2005). Most of the aboveground litter fall is foliar (leaves) which is generally more degradable. Woody litter (stems, branches) is much more resistant, being mainly degraded by certain fungi (Berg and McClaugherty, 2008). However, although woody debris may contribute considerably to the soil carbon stock, woody litter fall constitutes generally only a small fraction of the aboveground litter flux, since wood tissue is not subject to senescence (Berg and McClaugherty, 2008).

Rhizodeposition is vertically distributed over the mineral soil profile and organic surface layers. Jackson et al. (2000) analysed a global data set of root distribution measurements and found that tundra, boreal forests and temperate grasslands generally have the shallowest profiles with 80–90% of the roots occurring in the top 30 cm

⁴There is some debate about the precise definition of “rhizodeposition” (Rasmussen, 2011). Here it is used to refer to all organic matter input from roots.

of the soil. Deserts and temperate coniferous forests were found to have the deepest rooting profiles with only 50 % of the roots in the top 30 cm. Independent of vegetation type, root distribution seems to be mostly determined by soil hydrology, as demonstrated by significant relationships between annual potential evapotranspiration, precipitation, and soil texture (Schenk and Jackson, 2002a). In more water limited ecosystems plants tend to have deeper root profiles to maximize water uptake (Schenk and Jackson, 2002b). Roots may also preferentially grow in the organic surface layer, if present, due to the high nutrient and moisture availability there (Schenk and Jackson, 2002a).

Although rhizodeposition and root biomass are strongly related, they may not have exactly the same profile, since not all roots contribute equally to organic matter input. Fine roots have higher mortality rates and excrete more exudates since they play a greater role in water and nutrient uptake (Anderson et al., 2003). Hence, it is likely that organic matter input by roots is more closely related to the fine root profile, which is more shallow than the overall distribution of roots. Furthermore, radiocarbon analysis shows that also within the fine root fraction turnover rates decrease with depth (Gaudinski et al., 2010).

Depth dependence of soil organic matter properties and dynamics

The chemical properties of SOM change along the vertical profile (Rumpel and Kögel-Knabner, 2011; Vancampenhout et al., 2012). Most well-known are the decrease of C/N ratio, and the enrichment of ^{13}C and ^{15}N (Ehleringer et al., 2000; Nadelhoffer and Fry, 1988; Högberg, 1997). These gradients indicate a change from plant derived to more decomposed and microbial derived organic matter with depth (Rumpel et al., 2002; Rumpel and Kögel-Knabner, 2011; Baisden et al., 2002). It has been suggested that microbial residues are more effectively stabilized by organo-mineral interactions, which have been found to be an important mechanism in the deep soil (Rumpel et al., 2012).

A distinct property of most soils is the decrease of radiocarbon (^{14}C) activity with depth, indicating a higher average age of carbon since uptake from the atmosphere. Near the surface average radiocarbon age is typically in the range of 1 to 100 yr, whereas in the deep soil ages of 10 000 yr or more are no exception (Rumpel and Kögel-Knabner, 2011). Presumably, this age gradient is partially explained by slow downward transport of carbon fractions that are either very recalcitrant, or continually recycled by microbes (Elzein and Balesdent, 1995; Kaiser and Kalbitz, 2012). However, a more important cause may be decreasing average turnover rates along the profile (Persson et al., 2000). The reason for this gradient is not fully understood yet. It may be caused by the selective preservation of recalcitrant compounds combined with downward transport (Elzein and Balesdent, 1995). Also, the dominant source of organic matter in deep soils is root input, which is chemically more recalcitrant than aboveground litter (Rasse et al., 2005).

Another cause of the decreasing turnover rates with depth is the increased occurrence of certain stabilization mechanisms. Several studies have found that organic matter in subsoils is predominantly associated with minerals (Rumpel and Kögel-

Knabner, 2011; Eusterhues et al., 2003) or occluded within aggregates (Moni et al., 2010). A further cause of stabilization in deep soil is physical disconnection between microbes and substrates. Most microbial activity in deep soils is located in so-called hot spots: root and earthworm channels and preferential water flow paths (e.g. cracks). Organic matter outside of these zones may be stabilized due spatial separation from decomposers (Chabbi et al., 2009). Finally, (Fontaine et al., 2007) found that energy limitation of microbes caused by lack of fresh organic matter input may be an important mechanism in subsoils.

1.2.5 Models of soil organic matter decomposition

Numerical modelling is an important part of soil carbon research. In a comprehensive review Manzoni and Porporato (2009) recently listed some 250 models that were developed in the last 80 years. They showed that the number of models is growing exponentially. These models are applied at a variety of spatial and temporal scales, ranging from centimeters to the globe, and hours to hundreds of years, respectively. The mathematical structure of models also varies widely, but Manzoni and Porporato (2009) found that most models are based on similar kinetic laws.

A critical part of a soil carbon model is the formulation of breakdown of organic matter by decomposers. The most widely used and possibly simplest formulation is first order kinetics. This approach does not explicitly account for microbial biomass and activity, but assumes that decomposer community is in equilibrium with the substrate, resulting in a simple linear differential equation (Wutzler and Reichstein, 2008). Since decomposition is mainly a catalytic process, it may be represented more realistically by the Michaelis-Menten formulation, which accounts for the limitation of decomposition by enzyme availability (Blagodatsky and Richter, 1998). Models in which decomposition is linked to an explicitly simulated microbial pool have also been proposed (Fontaine and Barot, 2005; Wutzler and Reichstein, 2008).

Studies using radiocarbon analysis have shown that the heterogeneous nature of SOM in terms of turnover rate needs to be considered in order to correctly reproduce dynamics at different time scales (Trumbore and Torn, 2005). Models have been proposed that describe SOM as a continuous distribution along a quality axis that relates to decomposability (e.g. Bosatta and Ågren, 1985). However, the majority of models describe SOM as several discrete pools or compartments with different kinetic parameters (Manzoni and Porporato, 2009; Schimel et al., 1994; Jenkinson, 1990). Effective turnover rates of these pools range from days, for the most labile substrates, to millennia, for stabilized SOM. Whether SOM pools in models correspond to actual existing fractions or should be seen as artificial constructs is a subject of debate (Christensen, 1996; Smith et al., 2002). In recent publications it has been suggested that chemical recalcitrance of organic matter molecules is of minor importance for SOM decomposition (Kleber, 2010; Schmidt et al., 2011). These authors have called for explicit representation of SOM stabilization mechanisms in soil carbon models.

1.2.6 Soil organic matter profile models

While the overwhelming majority of soil carbon models represent SOM zero-dimensionally, a number of schemes have been published that in some way account for the vertical SOM profile. For example, some models vertically distribute simulated total soil organic carbon or extrapolate topsoil carbon downwards using a predefined depth-function, in order to determine lateral soil carbon transport due to erosion (Rosenbloom et al., 2001; Hilinski, 2001). Several models represent carbon pools in predefined soil layers that differ with respect to physical and chemical parameters, as well as temperature, moisture, and root input. (van Veen and Paul, 1981; Grant et al., 1993). In some cases heat or water transport between layers is included to account for the effects of temperature and moisture on decomposition, or to simulate leaching of mineral nitrogen (Hansen et al., 1991; Li et al., 1992). However, these models do not consider vertical transfer of organic matter between layers.

A number of models of dissolved organic matter (DOM) dynamics have been proposed (Michalzik et al., 2003; Neff and Asner, 2001; Gjettermann et al., 2008; Brovelli et al., 2012). These models account explicitly for production and mineralization of DOM, as well as vertical transport with water flow and ad- and desorption. Transport is usually represented as advection, based on measured or simulated water fluxes. These schemes are mainly developed to reproduce DOM fluxes and concentrations at small scales, and usually require site level calibration or detailed information on soil texture.

The effects of bioturbation in terrestrial soils have been modeled in relation to transport of radionuclides (e.g. Müller-Lemans and van Dorp, 1996; Kaste et al., 2007; Bunzl, 2002) and soil formation (Kirkby, 1977; Salvador-Blanes et al., 2007). More literature exists on modelling of benthic bioturbation and its effects on chemical species in sediments at the bottom of oceans and lakes (e.g. Boudreau, 1986b; Meysman et al., 2005, 2010). Bioturbation is usually modeled as a diffusive process, although it has been shown that this approach is not generally valid (Meysman et al., 2003, 2010). Several alternative schemes have been proposed, both deterministic (Boudreau, 1986a, 1989) and stochastic (Bunzl, 2002; Choi et al., 2002; Meysman et al., 2008).

Perhaps the first model truly aimed at dynamically simulating the SOM profile was developed by Kirkby (1977), as part of a soil formation model. Since then, a number of models have been developed that combine decomposition with vertical transport, represented either as diffusion (O'Brien and Stout, 1978; van Dam et al., 1997; Koven et al., 2009), advection (Nakane and Shinozaki, 1978; Dörr and Münnich, 1989; Bosatta and Ågren, 1996; Feng et al., 1999; Baisden et al., 2002; Jenkinson and Coleman, 2008), or both (Elzein and Balesdent, 1995; Bruun et al., 2007; Freier et al., 2010; Guenet et al., 2013; Koven et al., 2013). Most of these models were developed to explain measurements of SOM and tracer profiles. Fewer were intended for (predictive) simulation of soil carbon cycling (Jenkinson and Coleman, 2008; Koven et al., 2013). Furthermore, little attempt has been made to relate transport mechanisms to bioturbation and liquid phase transport. With some exceptions (Chertov and Ko-

marov, 1997; Chertov et al., 2001; Bottcher and Springob, 2001) most models do not explicitly simulate organic matter in the surface organic layer.

1.2.7 Calibration of soil organic matter models

In mathematical modelling, model parameters may be defined as quantities that specify constant, inherent properties of the system (Bard, 1974). Typical examples of parameters in soil organic matter models include decomposition rate constants, flux partitioning coefficients, and parameters that define responses to environmental factors. A SOM profile model also includes organic matter transport coefficients and shape parameters to define the vertical distribution of root input. Calibration involves the adjustment of parameters intended to improve model predictions compared to observations. For dynamical models also forcing data and initial conditions of the model state variables may be included in calibration (Raupach et al., 2005). In addition to parameter estimates, calibration procedures usually provide estimates of errors on the parameters which can be used to quantify uncertainty of model predictions.

Parameter estimation requires specification of a cost function $J(\theta)$ (also known as “misfit” or “objective” function) which quantifies the mismatch between model predictions $M(\theta)$, based on parameters θ , and observations O in a single number (Raupach et al., 2005). The most common choice is the sum of squared deviations between model predictions and observations (Omlin and Reichert, 1999):

$$J(\theta) = \sum_{n=1}^N \frac{(O_n - M_n(\theta))^2}{\sigma_n^2} \quad (1.1)$$

for N uncorrelated observations with known variances σ_n^2 . When residuals are normally distributed, this formulation is related to the likelihood function $L(\theta)$ of the parameters, according to:

$$L(\theta) = \exp\left(-\frac{1}{2}J(\theta)\right) \quad (1.2)$$

The likelihood is equal to the probability of the observed values given the parameters ($P(O|\theta)$). Thus, for Gaussian residuals the parameter set for which $J(\theta)$ is minimal (also known as the least-squares estimate) is equal to the maximum-likelihood estimate. Various alternative cost functions exist for when model-data residuals are not normally distributed (see e.g. Tarantola, 2005). However, when the distribution does not deviate too much from normal, the least-squares estimate is often a good approximation (Press et al., 1996, ch. 15).

An increasingly used method for parameter estimation for ecological models is Bayesian calibration (van Oijen et al., 2005). This approach is grounded in a wholly different view of model parameters: While the classical (frequentist) approach defines parameters as fixed quantities which are to be estimated, in the Bayesian view parameters are seen as random variables whose probability distributions reflect “degrees of belief” based on the current state of knowledge. The process of updating the state of knowledge based on new information is achieved by conditioning the prior

distribution $P(\theta)$ —representing the knowledge prior to the calibration—on observations in order to obtain the posterior distribution $P(\theta|\mathbf{O})$. This is done according to Bayes' rule:

$$p(\theta|\mathbf{O}) = c p(\theta) p(\mathbf{O}|\theta), \quad (1.3)$$

where $p(\mathbf{O}|\theta)$ is the likelihood function, as used in classical inference, and c is a constant. The incorporation of prior knowledge in the calibration can be highly beneficial for ecological models, where the parameters are often poorly constrained by the observations alone (Omlin and Reichert, 1999). Bayesian calibration is also increasingly applied for SOM models (Yeluripati et al., 2009; Scharnagl et al., 2010; Guenet et al., 2013).

For non-linear models the parameter estimates and their uncertainty must usually be derived using an iterative method. Many of such algorithms exist (Press et al., 1996, ch. 9). Gradient search approaches such as Levenberg-Marquardt or quasi-Newton are aimed at finding the minimum of the cost function and its local gradient. The latter can be used to estimate the uncertainty of the parameters (Omlin and Reichert, 1999). In Bayesian calibration often an approximation of the full posterior distribution is desired. This can be obtained by random sampling using Monte Carlo approaches, such as the Metropolis algorithm (Mosegaard and Sambridge, 2002).

1.3 This study

1.3.1 Research gaps

Despite the existence previous models discussed in section 1.2.6, there are several distinct gaps in research related to SOM profile modelling:

- Most SOM profile models were intended to complement measurements in order to explain observed concentration profiles of soil organic carbon, radiocarbon, or other constituents. As such they typically do not account for effects of soil temperature and moisture.
- None of the SOM profile models represents both the organic layer and the mineral soil profile.
- Typically all vertical SOM transport is lumped into one transport term, diffusion or advection. Several models do include both formulations but generally no effort is made to relate them to specific processes in the field such as bioturbation and liquid phase transport.
- Very few of the published studies present thorough assessment of parameter uncertainty and its effect on the reliability of model predictions. Furthermore, the value of different observations to estimate parameters is not discussed.

1.3.2 Aims & methodology

This study aims to address the above-mentioned research gaps by development of a dynamic and process-oriented description of the vertical soil organic matter profile. Specific attention is given to vertical organic matter transport processes and representation of the surface organic layer, since these represent the most important innovations compared to existing soil carbon models.

While no global simulations studies are presented here, the main intended application of this work is prognostic simulation at large spatial scales, such as in dynamic global vegetation models or earth system models. This poses a number of constraints on the model formulation and implementation. Most importantly, it means the model will be run for unvisited locations, hence its input must be derived from information in gridded data sets of soil properties, or supplied by other models. An additional consideration is the potential combination of the SOM profile model with other process descriptions, such as moisture and heat transport and new formulations of SOM decomposition.

Since few quantitative estimates of the relevant processes are available, a large part of this study focuses on parameter estimation. A Bayesian calibration system is presented which allows incorporation of prior knowledge and quantification of parameter uncertainty arising from measurement errors and the convolution of processes that cannot be observed directly.

1.3.3 Outline

Including the introduction, this thesis comprises five chapters. The model structure and the underlying rationale, as well as analysis of sensitivity to the transport parameters are presented in chapter 2.

In chapter 3 a Bayesian calibration framework is developed, and used to estimate the model parameters for two temperate forests with contrasting conditions and SOM profiles: a coniferous forest in the Netherlands (Loobos) and a deciduous forest in Germany (Hainich). Furthermore, the value of the isotope lead-210 as a tracer for SOM transport is investigated. The parameter distributions are used to gain insight into the relevance of the different processes.

Chapter 4 presents further study on the Hainich site. Specifically, the value of observed radiocarbon activity of both SOM and heterotrophic respiration for constraining the parameters is investigated. Additionally, the potential behavior of the SOM profile under conditions of increasing global CO₂ and temperatures is studied. A prognostic simulation for the Hainich site is performed, based on litter fluxes and soil temperatures predicted by an ecosystem model under the assumption of moderate to strong greenhouse gas emissions.

Finally, chapter 5 summarizes the main findings of this study and presents a reflection of the model structure and the calibration approach. Furthermore, several recommendations for potential improvements to the model structure and calibration approach, as well as for future large scale applications, are made.

Chapter 2

SOMPROF: a vertically explicit soil organic matter model

Most current soil organic matter (SOM) models represent the soil as a bulk without specification of the vertical distribution of SOM in the soil profile. However, the vertical SOM profile may be of great importance for soil carbon cycling, both on short (hours to years) time scale, due to interactions with the soil temperature and moisture profile, as well as on long (years to centuries) time scale because of depth-specific stabilization mechanisms of organic matter. It is likely that a representation of the SOM profile and surface organic layers in SOM models can improve predictions of the response of land surface fluxes to climate and environmental variability. Although models capable of simulating the vertical SOM profile exist, these were generally not developed for large scale predictive simulations and do not adequately represent surface organic horizons. We present SOMPROF, a vertically explicit SOM model, designed for implementation into large scale ecosystem and land surface models. The model dynamically simulates the vertical SOM profile and organic layer stocks based on mechanistic representations of bioturbation, liquid phase transport of organic matter, and vertical distribution of root litter input. We tested the model based on data from an old growth deciduous forest (Hainich) in Germany, and performed a sensitivity analysis of the transport parameters, and the effects of the vertical SOM distribution on temporal variation of heterotrophic respiration. Model results compare well with measured organic carbon profiles and stocks. SOMPROF is able to simulate a wide range of SOM profiles, using parameter values that are realistic compared to those found in previous studies. Results of the sensitivity analysis show that the vertical SOM distribution strongly affects temporal variation of heterotrophic respiration due to interactions with the soil temperature and moisture profile.

Based on: M. C. Braakhekke, C. Beer, M. R. Hoosbeek, M. Reichstein, B. Kruijt, M. Schrumpf, and P. Kabat
Ecological Modelling 222 (2011): 1712–1730

2.1 Introduction

Because soils globally store a huge amount of carbon, the response of soil carbon cycling to future climate change is currently subject to great attention (Trumbore and Czimczik, 2008; Heimann and Reichstein, 2008). Increasing temperatures will lead to accelerated heterotrophic respiration (Davidson and Janssens, 2006), while concurrently the increasing atmospheric CO₂ concentration is expected to cause higher vegetation productivity (Norby et al., 2005), resulting in greater soil carbon input. The present uncertainty with respect to the magnitude of these two mechanisms is demonstrated by the large disagreement of ecosystem models on future land surface CO₂ fluxes (Jones et al., 2003, 2005; Friedlingstein et al., 2006).

The focus of studies of soil carbon dynamics has classically been on the upper 20 to 50 cm of the soil (e.g., Jenkinson and Rayner, 1977; Gregorich et al., 1996). This layer (from hereon referred to as the “topsoil”) is most directly influenced by climate, vegetation and land use, and generally contains much higher organic matter concentrations than the subsoil. Furthermore, the subsoil is below the rooting zone of most crops, while its organic matter appears to be stable on the time scale of anthropogenic climate change (Scharpenseel et al., 1989; Trumbore, 2000). Therefore, application of soil organic matter (SOM) models has focused on a bulk description of the organic matter in the topsoil, without specification of the vertical distribution. (Parton et al., 1987; Schimel et al., 1994).

Recently, interest in organic matter at greater soil depths has grown, mainly for two reasons. First, several recent studies have shown that the deep soil stores a considerable amount of carbon, which had previously not been included into estimates of global stocks (Batjes, 1996; Jobbagy and Jackson, 2000; Tarnocai et al., 2009).

Second, accumulating evidence contests the assumption that deep soil carbon is intrinsically stable. SOM can be stabilized by a myriad of mechanisms, many of which are reversible (von Lützow et al., 2006). Usually, different stabilization mechanisms are operating at different depths within a single soil profile. For example, Fontaine et al. (2007) found that energy limitation of microbes is more important as a stabilization mechanism in the subsoil than in topsoil, although these results were contradicted by Salomé et al. (2010) who found the reverse. Conversely, stabilization due to organo-mineral interactions is occurring in most of the soil profile, but increases in relative importance with depth (Rumpel et al., 2002).

Recent studies suggest that deep soil carbon may become destabilized under changing conditions, depending on the specific stabilization mechanism. For example, increased root exudation and root litter production, occurring under elevated CO₂ levels (Philips et al., 2006; Iversen, 2010) can lead to decomposition of old SOM due to priming of microbial activity (Drigo et al., 2008; Fontaine et al., 2007). Furthermore, it has been suggested that chemically recalcitrant SOM fractions are more sensitive to temperature increase (Conant et al., 2008; Davidson et al., 2006; Knorr et al., 2005), although this is under dispute (Fang et al., 2005; Reichstein et al., 2005). At the same time, physically protected SOM is likely less sensitive to warming, but more vulnerable to physical disturbance (Diochon and Kellman, 2009). Efforts are being made to include different stabilization mechanisms explicitly in SOM models

in order to improve predictions of soil carbon cycling at decadal to centennial time scales (Wutzler and Reichstein, 2008; von Lützow et al., 2008; Manzoni and Porporato, 2009).

But also on short (hourly to annually) time scales the vertical distribution of organic matter plays an important role for soil carbon cycling. Soil properties usually show a strong depth gradient, with strongest temporal variations occurring near the surface. Respiration in surface layers usually responds more strongly to weather fluctuations, whereas subsoil respiration shows less temporal variation (Fierer et al., 2005; Hashimoto et al., 2007; Davidson et al., 2006). Hence, a soil with a deep organic matter distribution is likely to respond differently to short term weather fluctuations than a soil where most organic matter is stored near the surface. Because many factors are simultaneously, and often non-linearly, influencing decomposition rates, aggregating respiration over the profile in models may lead to incorrect results (Subke and Bahn, 2010).

Thus, an explicit representation of the vertical SOM distribution in biogeochemical models could significantly improve predictions of carbon cycling, as well as facilitate addition of new process descriptions. Such a model should include explicit representation of the processes leading to organic matter input at depth: root litter production and downward transport of organic matter. These models (referred to as "SOM profile models" from hereon) have already been proposed more than three decades ago (O'Brien and Stout, 1978; Nakane and Shinozaki, 1978). O'Brien and Stout (1978) applied a diffusion model of downward organic matter transport to explain carbon isotope profiles. Since then, various researchers have applied similar models, including diffusion or advection or both (Dörr and Münnich, 1989; Elzein and Balesdent, 1995; Baisden et al., 2002; Bosatta and Ågren, 1996; Bruun et al., 2007; Jenkinson and Coleman, 2008; Freier et al., 2010).

Most of these models, however, were developed to explain organic carbon and tracer profiles, not for predictive simulations of soil carbon cycling, and as such do not account for the influence of soil temperature and moisture on decomposition. A notable exception is the work of Jenkinson and Coleman (2008) who developed a vertically explicit version of the well-known SOM model RothC (Jenkinson, 1990), by adding two parameters: one that moves SOM down the profile in an advection-like manner, and another that slows decomposition with depth. Though innovative, their scheme was in fact a downward extrapolation of the original model, and is difficult to transfer to a different SOM model.

Furthermore, none of the published models include a representation of the surface organic layer. Consisting mostly of organic material, the organic layer has markedly different properties than the mineral soil, and behaves differently in terms of soil hydrology and heat transport. An explicit representation of this layer in the model would therefore be particularly valuable in the land surface scheme of a global climate model.

Despite past efforts to develop SOM profile models, the development of a general understanding of SOM profile formation has been slow, in part caused by the high complexity and the extremely slow rates of the relevant processes. An additional problem is posed by the lack of a standardized approach to determine transport rates

with inverse modelling. The assumptions inherent to the model structure used in parameter estimation strongly influence the final parameter estimates (Bruun et al., 2007). For example, failure to include a relevant mechanism for subsoil organic matter input will inevitably lead to under- or overestimation of the importance of other processes. The diversity of the models in the published studies is such that the usefulness of direct comparison of transport rates is questionable.

Taken that the ultimate aim is to develop a SOM profile model that can be applied for global simulations, there is a need for a standardized and mechanistic scheme for modelling SOM transport to allow transfer of parameters between models. On the other hand, such a scheme should be parsimonious enough to allow development of a large scale parameter set. The model presented here, SOMPROF, has been developed with these considerations in mind. SOMPROF is based on earlier SOM profile models, with several important additions, including explicit representation of surface organic horizons and the effects of soil temperature and moisture on decomposition. Rather than lumping all SOM transport processes into either a diffusion or an advection term, explicit distinction is made between bioturbation and liquid phase transport. In this paper we present the model and its underlying rationale. Furthermore, we test the sensitivity to the input parameters, and study the effects of the vertical SOM distribution on predicted heterotrophic respiration.

2.2 Theory and model description

We will not give an exhaustive description of SOMPROF here, but instead focus on the parts that are innovative compared to existing SOM models and discuss the rationale behind the model structure. Particular attention is given to the reasoning behind the implementation of the transport processes. A full description, including all model equations, can be found in Appendix 2.A.

In the following description, depth is denoted with z (m) and time with t (yr). Depth is assumed positive downwards and $z = 0$ is set at the top of the mineral soil. Organic matter (OM) quantity C is simulated in the mineral soil as concentrations (kg m^{-3}), and in the organic horizons (L, F and H) as stocks (kg m^{-2}).

2.2.1 General structure

A mechanistic model of the vertical soil organic matter profile must consider the vertical distribution of root litter input and downward organic matter transport processes (Lorenz and Lal, 2005). The mathematical description of vertical transport processes usually comprises terms for diffusion, advection, or both. However, such a scheme is unsuitable for the organic layer. Transport models typically simulate concentrations as unit mass per unit volume. This concentration is only a valid quantity in the context of a mixture consisting of several materials. In the mineral soil, where organic matter is mixed with minerals material, this approach is justified, but in the organic layer, where the organic matter concentration far exceeds the mineral concentration, the organic matter itself forms the bulk and the organic matter concentra-

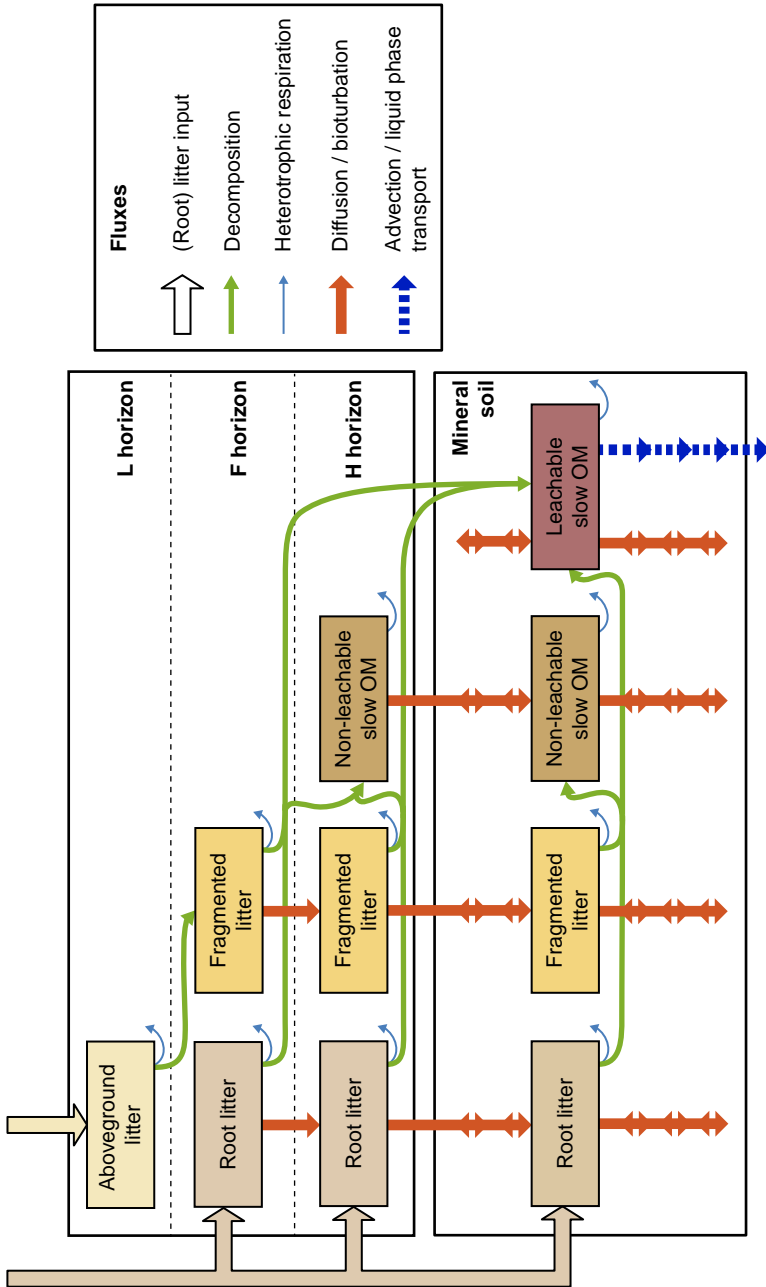


Figure 2.1: Overview of the SOMPROF model.

tion becomes an undefined quantity. The vertical distribution of properties such as organic matter quality and element concentrations is therefore dominated by organic matter input and loss due to litter deposition and decomposition, and cannot be explained by vertical mixing alone. This problem was demonstrated by Kaste et al. (2007) who found that a transport model could well explain the vertical profile of the radioactive lead isotope ^{210}Pb in the mineral soil but not in a thick organic layer. Instead, a model that ignored vertical transport due to mixing and accounted for the effects of litter accumulation and decomposition proved more able to reproduce the observed ^{210}Pb profile.

Hence, in SOMPROF the diffusion-advection model is not applied to the organic layer. The organic layer is explicitly split into three layers: the L, F and H horizon¹ (Figure 2.1). The organic horizons are simulated as separate, homogenous reservoirs of organic matter. When organic matter in one layer is transformed to more decomposed material, it flows to the underlying layer. This represents the process of continuous burial and decomposition that occurs in the organic layer and leads to the formation of a vertical gradient of decomposition stage that is typically observed in the field (van Delft et al., 2006). Bioturbation reduces this gradient by causing downward flow from the F to the H horizon and from the H horizon to the mineral soil. Because we assume that the material in the L horizon is not transported, this horizon is always present if above ground litter input occurs. On the other hand, the F and H horizon may be absent if the bioturbation rate exceeds the input of material. Liquid phase transport (advection) within the organic layer is not explicitly considered; we assume that all material that can be transported with the liquid phase immediately flows to the mineral soil.

In the mineral soil, the organic carbon concentration as a function of depth is simulated using a transport model including diffusion, representing bioturbation, and advection, representing liquid phase transport. Currently, the model does not account for the presence of stones in the mineral soil matrix.

2.2.2 Organic matter pools

SOMPROF follows the classical organic matter pool approach with five types of organic matter (Table 2.1). The organic matter pools are chosen to represent functionally different types of organic matter that differ with respect to decomposition rate and transport behavior. The pools have a serial arrangement: upon decomposition material flows from less to more decomposed pools. This setup was chosen rather than parallel pool arrangement to be able to represent the change of transport behavior when organic matter is transformed.

Above ground litter Above ground litter (AGL) is material accumulating at the surface and is easily decomposable. Since this is typically coarse material, we assume that it is not transported and is therefore only present in the L horizon. No distinction

¹These horizon codes are used to designate organic horizons in several soil classification systems (Soil Classification Working Group, 1998; van Delft et al., 2006) and approximately correspond the Oi, Oe and Oa horizons in the U.S. (Soil Survey Division Staff, 1993) and FAO (IUSS Working Group WRB, 2007) systems.

Table 2.1: The organic matter pools in SOMPROF

Pool	Decomposition rate	Source	Diffusion	Advection
Above ground litter (AGL)	High	External input into L horizon	No	No
Fragmented litter (FL)	Intermediate	Formed from Above ground litter	Yes	No
Root litter (RL)	High	External input into F, H and mineral soil	Yes	No
Non-leachable slow OM (NLS)	Low	Formed from fragmented and root litter	Yes	No
Leachable slow OM (LS)	Low	Formed from fragmented and root litter	Yes	Yes

is made between different types of litter (e.g. leaves, woody debris).

Fragmented litter In the first decomposition step, above ground litter is transformed to fragmented litter (FL) which flows immediately to the F horizon, thus forming the most important organic matter fraction of this layer. This transformation represents early litter decomposition during which material is fragmented. Fragmented litter is assumed to be chemically similar to above ground litter and has a relatively high decomposition rate. However, contrary to above ground litter, fragmented litter can be transported by bioturbation, which thus acts as a mechanism for the introduction of easily degradable material in the H horizon and mineral soil.

Root litter Root turnover provides input for the root litter (RL) pool in the mineral soil and the F and H horizon. We assume root growth, and thus root turnover, to be negligible in the L horizon. Since root litter is largely produced by the turnover of fine roots, we assume that it is chemically similar to above ground litter. But, contrary to above ground litter, it can be transported by bioturbation. The total root litter production rate is specified as model input and vertically distributed according to an exponentially decreasing function of depth, which starts at the top of the F horizon. The root litter input into a given layer is obtained by integrating the distribution function over the layer thickness.

Non-leachable slow organic matter Part of the decomposition products of the fragmented litter and root litter pools flow into the non-leachable slow (NLS) organic matter pool. Non-leachable slow OM comprises chemically stabilized particulate organic matter and forms the basis of the H horizon. It is formed in the organic layer and in the mineral soil and can be transported by bioturbation. Non-leachable slow OM formed from litter in the in the F horizon flows immediately into the H horizon, while NLS-OM formed in the H horizon stays there, although it may subsequently be transported into the mineral soil by bioturbation.

Leachable slow organic matter The leachable slow (LS) organic matter pool represents organic matter adsorbed to the mineral phase. Since this material can enter the liquid phase through desorption, it is transported by advection as well as bioturba-

tion. Hence, liquid phase transport is included in SOMPROF, even though dissolved organic matter is not explicitly represented. The rationale behind this approach is discussed in section 2.2.4. Organic matter adsorption onto the mineral phase is typically very strong and protects organic matter against decomposition, hence the LS organic matter pool is presumably the most stabilized type of organic matter in the model.

2.2.3 Organic matter decomposition

Decomposition of organic matter is simulated according to first order kinetics using a base decomposition rate which is corrected for soil temperature and moisture using response factors (Appendix 2.A.1). A first order decomposition rate k at reference temperature (10 °C) and optimal soil moisture is specified for each organic matter pool as part of the model input. For the response of decomposition to soil temperature we use the modified Arrhenius function from Lloyd and Taylor (1994), in which the temperature sensitivity decreases with increasing temperature. Response to soil moisture is defined according to a sigmoid function from Subke et al. (2003). Measured or modelled depth profiles of temperature and moisture are input, hence the decomposition response factors are depth dependent. If necessary, the profiles are interpolated to the midpoint depths of the organic horizons and the soil layers used for numerical solution (section 2.2.6).

As discussed in section 2.2.2, several pools are transformed to other pools during decomposition. The transformation fluxes are determined by a transformation factor α (-) that specifies how much of the decomposition flux of donor pool flows to the receiving pool. The material that does not flow to another pool ($1 - \sum_j \alpha_{i \rightarrow j}$) is assumed to be lost as CO₂, representing heterotrophic respiration. Note that all transformation factors other than those for the decomposition of the above ground litter, root litter and fragmented litter are zero.

Contrary to some other models, the decomposition rates are not explicitly reduced with depth in SOMPROF. Elzein and Balesdent (1995) showed that with a multi-pool organic matter model, the assumption of explicitly decreasing turnover rates with depth is not required to reproduce ¹⁴C profiles because the change of apparent turnover time with depth emerges from the change of relative distribution of the organic matter pools. Depth specific stabilization mechanisms are currently not yet fully understood, hence, in view of parsimony we do not include these processes at this stage of model development.

2.2.4 Organic matter transport

SOMPROF includes two organic matter transport processes: bioturbation and liquid phase transport. Other transport processes are known to occur in certain soils, such as mixing due to freezing and thawing (cryoturbation) and mixing due to shrinking and swelling. Although locally these processes may be very important, they occur only under specific conditions. In general bioturbation and liquid phase transport can be assumed to be the dominant transport mechanisms in most soils, hence other

transport processes are not explicitly considered (although they may be implicitly included, depending on how the transport parameters are estimated).

Except for the influence of bulk density on the diffusivity (see below), the transport rates are kept constant with depth. In reality this is probably not the case since the soil fauna biomass decreases with depth, and water fluxes and adsorption of dissolved organic matter are likely depth dependent as well. However, past studies have shown that SOM and tracer profiles can be well reproduced using constant transport rates (Dörr and Münnich, 1989; Elzein and Balesdent, 1995; Bruun et al., 2007; Jenkinson and Coleman, 2008). On the other hand, making the transport parameters depth dependent introduces additional degrees of freedom which complicates parameter estimation based on measurements.

Bioturbation

Bioturbation refers to the reworking of soil by soil animals and to a lesser degree by plants (Meysman et al., 2006). The activities of these organisms mix the soil matrix, representing an important mechanism for organic matter flow within the organic layer and mineral soil (Hoosbeek and Scarascia-Mugnozza, 2009; Tonneijck and Jongmans, 2008). Estimates of soil fauna mixing activity are typically expressed as reworking rates, the amount of material moved per unit surface area (Wilkinson et al., 2009). For example, earthworm activity at the population level is often estimated by measuring rates of surface cast deposition. (See Paton et al., 1995, for a comprehensive overview of many bioturbation rate estimates for different animal species and plants.)

In general, bioturbation causes homogenization of soil properties, i.e. net transport of soil constituents inversely proportional to the concentration gradient. Therefore, the effects of bioturbation on the distribution of soil properties has often been modelled using Ficks diffusion equation (Elzein and Balesdent, 1995; van Dam et al., 1997; Kaste et al., 2007). Using mixing length theory developed for turbulent mixing in gasses and fluids, it can be shown that bioturbation can indeed lead to diffusive behavior of soil constituents (Boudreau, 1986b, Appendix 2.B). However, the validity of the diffusion model for stochastic mixing processes such as bioturbation is not self-evident but depends on several criteria. (These have been thoroughly discussed in the context of benthic bioturbation: Boudreau, 1986b; Meysman et al., 2003). Most important, (i) the time between mixing events must be short compared to other processes that influence the concentration profile; (ii) the length scale of the mixing (the distance over which soil particles are moved) must be small compared the scale of the concentration profile and; (iii) the mixing should be isotropic, i.e. equal in both up and down direction.

At small spatial scales ($\sim 1 \text{ m}^{-2}$) bioturbation cannot be expected to meet these criteria. Mixing of soil particles occurs as sudden jumps followed by long periods of rest, hence the local instantaneous concentration of any soil constituent depends strongly on whether or not a mixing event has recently occurred, particularly if mixing is done by larger organisms (e.g. burrowing mammals, uprooted trees).

However, for describing the average transport of many mixing events the diffu-

sion model can be assumed to be valid. Such averaging may be over time, if the mixing is stationary, or over space if the mixing is homogenous (Hinze, 1975, p.5). The latter suggests that at sufficiently large spatial scales within a single ecosystem, the assumption of diffusive behavior is reasonable. Hence, we assume that the diffusion approach is valid at ecosystem scale, for which SOMPROF is designed. Vertical transport due to bioturbation in the mineral soil is defined as:

$$\left. \frac{\partial C_i}{\partial t} \right|_{\text{BT}} = D_{\text{BT}} \frac{\partial^2 C_i}{\partial z^2}, \quad (2.1)$$

where C_i is the organic matter concentration of pool i (kg m^{-3}) and D_{BT} is the diffusivity due to bioturbation ($\text{m}^2 \text{yr}^{-1}$). All organic matter pools are assumed to be transported equally according to (2.1), except for the above ground litter pool, which is not transported (section 2.2.2). At the top of the mineral soil, a flux prescribed boundary condition is used, which is determined by the bioturbation rate (see below). At the bottom of the soil profile, a zero-gradient boundary condition is used, which means that no material is transported by bioturbation over the lower boundary.

Since the diffusive behavior of organic matter is the direct result of the mixing activity of the soil fauna, there must be a unique relationship between the diffusivity D_{BT} and the bioturbation rate B ($\text{kg m}^{-2} \text{yr}^{-1}$). Continuing the mixing length analogy, it can be shown that the diffusivity is composed of the time-averaged correlation between the fluctuation of the vertical advection rate of transported material and the distance over which the material is moved (Boudreau, 1986b, Appendix 2.B). The fluctuation of the vertical advection rate is directly related to the bioturbation rate via the bulk density ρ^{MS} (kg m^{-3}). Furthermore, we assume that there exists a typical distance over which material is moved by the soil fauna, the mixing length l_m (m) which must be determined later. The diffusion can then be estimated from the bioturbation rate as follows:

$$D_{\text{BT}} = \frac{1}{2} \frac{B}{\rho^{\text{MS}}} l_m. \quad (2.2)$$

Note that B refers only the *vertical* component of the mixing. If the bioturbation rate is estimated from ingestion rates of earthworms, it must be multiplied by an additional factor of 0.5 to obtain the mixing rate in the vertical direction (Wheatcroft et al., 1990). Measurements of earthworm cast formation can be assumed to represent vertical mixing only. As said, the diffusion model represents the effective transport behavior of SOM averaged over long time scales and large areas. As such, equations (2.1) and (2.2) should not be viewed as a mechanistic description of the mixing activity of the soil fauna, nor is the mixing length parameter a physical quantity that can be measured. Rather, mixing length theory provides justification for a simple linear empirical relationship between the diffusivity and the soil fauna activity. More specifically, in SOMPROF l_m is used as a tuning parameter that links the bioturbation fluxes within the organic layer (see below) to the transport within the mineral soil.

The bulk density ρ^{MS} can either be specified or estimated (section 2.2.5). From (2.2) it follows that the diffusivity due to bioturbation is inversely proportional to

bulk density. This is consistent with our rationale: the diffusivity is limited only by the capacity of the soil fauna to displace a certain amount of mass per unit time, not by the volume over which this mass is distributed. Hence, the diffusion coefficient must increase with decreasing bulk density to maintain the same rate of mass transport.

For reasons discussed in section 2.2.1, the diffusion model is not applied to the organic surface horizons. Instead, we assume that the total net flux of organic matter from F to H and from H to the mineral soil is equal to the bioturbation rate B (Appendix 2.A.4). We do not consider upward transport of mineral material from the mineral soil to the organic layer. If the mass of a layer is zero, the flux is set to the total input minus the loss from decomposition in this layer, to avoid that the mass becomes negative. The flux from H to mineral soil serves as the upper boundary flux for the transport scheme of the mineral soil.

Liquid phase transport

Liquid phase transport refers to the combined effects of formation, transport, and adsorption and desorption of dissolved organic matter (DOM). Although DOM concentrations are usually very small compared to immobile organic matter, transport in the liquid phase represents a major contribution to downward organic matter movement, particularly in soils with little biological activity (Kalbitz and Kaiser, 2008). DOM, once formed, flows down with infiltrating water and may be reversibly adsorbed to mineral particles upon which it becomes immobile (Kalbitz et al., 2000).

Models of short time scale DOM dynamics have been applied with some success at site scale (e.g. Neff and Asner, 2001; Michalzik et al., 2003). However, DOM fluxes in the field are notoriously difficult to predict due to spatial heterogeneity of mineral composition and DOM chemistry—which determine DOM adsorption behavior—and water infiltration, which is often dominated by macropore flow and storm events (Kalbitz et al., 2000). Consequently, simulation of long time scale SOM profile evolution based on a mechanistic description of DOM transport and adsorption is not feasible. Furthermore, simulation of DOM transport requires accurate simulation of water fluxes at short (sub-daily) time scales, while SOMPROF is designed to be run with daily or longer time steps.

Therefore, downward movement of organic matter as DOM is not modelled explicitly. We define a pool that can potentially enter the liquid phase and be transported downward advectively: leachable slow (LS) organic matter, which is equivalent to the reactive soil pool, introduced by Nodvin et al. (1986). Downward movement with the liquid phase is simulated by defining an effective advection rate v (m yr^{-1}):

$$\left. \frac{\partial C_{\text{LS}}}{\partial t} \right|_{\text{adv}} = -v \frac{\partial C_{\text{LS}}}{\partial z}. \quad (2.3)$$

This scheme is similar to the retardation factor approach, which has been successfully applied in studies of transport of tracers and pollutants in soils (e.g. Huang et al., 1995). This method simulates both the adsorbed and dissolved fraction as one pool by correcting the transport rate of the dissolved fraction with the retardation

factor, which accounts for interactions with the solid phase. The underlying assumptions of the retardation factor approach are that the adsorption isotherm is linear, and that the dissolved and adsorbed fraction are locally in equilibrium with each other. When these conditions hold, the relative distribution of the studied compound over the dissolved and adsorbed fraction is fixed and independent of the concentration in the liquid phase.

In SOMPROF, the retardation factor concept is expanded to organic matter decomposition: the breakdown of organic matter is retarded by adsorption to the mineral phase. Hence, the decomposition rate of LS organic matter is also an effective parameter for both fractions. However, in practice the influence of the dissolved fraction on the effective decomposition rate and total carbon concentration will be negligible since adsorbed organic matter is present in much higher quantities than DOM. Hence, we do not consider the dissolved fraction when comparing with measurements. Note that the LS-OM pool is also transported by bioturbation. The upper boundary condition of (2.3) is comprised of the combined production of LS-OM in the organic layer.

SOMPROF differs from other SOM profile models (e.g. Elzein and Balesdent, 1995) in that only a specific pool is moved advectively, rather than all organic matter. Although this introduces additional model parameters, it is clearly closer to reality since not all organic matter can be transported with the liquid phase. Furthermore, the fraction of organic matter that is potentially mobile presumably increases with depth, since liquid phase transport reaches greater depths than bioturbation and root litter input.

Contrary to bioturbation, liquid phase transport may lead to a loss of organic matter from the system. For a given soil, this depends on the depth at which the lower boundary is set. If it is set shallow enough that the bottom LS-OM concentration is significantly higher than zero, organic matter is lost and is not included in the calculation of organic matter stocks and heterotrophic respiration.

In the organic layer the adsorptive capacity of the solid phase is negligible compared to that in the mineral soil, due to the absence of the mineral material. Therefore, we assume that all LS-OM produced in the organic layer immediately flows into the mineral soil and that the concentration of LS-OM in the organic layer is zero.

2.2.5 Bulk density

The thickness of the organic horizons is estimated from their mass using the bulk density, which is specified as model input separately for the L, F and H horizons (ρ^L , ρ^F , ρ^H). The bulk density in the mineral soil ρ^{MS} is required to convert the mass-based bioturbation rate to the volume-based diffusivity (section 2.2.4). Furthermore, the bulk density profile affects the shape of the organic matter profile. Bulk density is usually strongly correlated with soil organic matter content. If measurements are not available, SOMPROF estimates bulk density from the soil organic matter fraction using an equation proposed by Federer et al. (1993). These authors proposed that the soil is a hypothetical mixture of pure mineral material and pure organic material, that both have a bulk density. Assuming that their bulk densities mix linearly, the bulk

density of the mixture is estimated as:

$$\rho^{\text{MS}} = \frac{\rho_{\text{M}}\rho_{\text{O}}}{f_{\text{O}}^{\text{MS}}\rho_{\text{M}} + (1 - f_{\text{O}}^{\text{MS}})\rho_{\text{O}}}, \quad (2.4)$$

where ρ_{M} and ρ_{O} are the bulk densities of the mineral and organic fractions, respectively (kg m^{-3}), and f_{O} is the organic matter fraction (-). ρ_{O} is set equal to the bulk density of the H horizon.

2.2.6 Model solution and simulation setup

SOMPROM is solved for discrete time steps using standard finite differencing techniques. The model compartments are solved in order from top to bottom: L, F, H, mineral soil. For the organic horizons, first the pools are updated for input and decomposition, using an explicit scheme. Next it is determined whether the maximum bioturbation flux can be met, and if necessary it is adjusted downward. Then the mineral soil is updated using a fully implicit scheme with upwind differencing for advection. To this end, the soil is split into compartments of variable thickness. The compartment thicknesses as well as the depth of the lower boundary can be chosen freely, depending on the available computational resources and the desired resolution of the model output. For the simulations discussed in section 2.3, we used 11 compartments, with thicknesses increasing from 0.5 cm at the surface to 50 cm at the bottom of the profile.

Near the soil surface, the concentration of organic matter may be high enough that its mass is no longer negligible compared to that of the matrix. Therefore, the compartment thicknesses are corrected for change of mass at every time step, once the new concentrations of organic matter are known (Appendix 2.A.4).

To avoid aggregation errors due to the non-linearity of the soil temperature and moisture response function (Appendix 2.A.1), the response factors are calculated before the model run, at the temporal resolution at which they are available (typically at half hourly intervals). These response factors are then averaged to the time step length of the model and used as input. Since the compartments thicknesses change during the simulation, the response factors as well as measured bulk densities (if available) are interpolated at every time step using piecewise cubic Hermite interpolation to obtain values at the midpoint depths of the compartments and organic horizons.

A typical model run consists of two stages: (i) a spin-up stage, starting from bare ground, i.e. without organic matter, during which the model is run with an average annual cycle of soil moisture, soil temperature and litter fall; and (ii) the actual simulation for which measurements of soil temperature, moisture and litter fall are available. The purpose of the spin-up stage is to obtain the initial conditions used for the second stage. The length of the spin-up period can be chosen freely and, in principle, should be the time since the start of the development of the organic matter profile. For many soils it may be acceptable to run the model in spin-up until the slowest carbon pools and the vertical distribution are in equilibrium (~ 1000 years).

Table 2.2: List of model input required to run SOMPROF and values used for the reference simulation.

Parameter	Symbol	Units and value in reference simulation
<i>Litter input</i>		
Aboveground litter input ^a	I_{AGL}^L	0.314 kgC m ⁻² yr ⁻¹ ^b
Total annual root litter input ^a	I_{RL}^{tot}	0.178 kgC m ⁻² yr ⁻¹ ^b
Root litter distribution parameter	β	0.07 m ⁻¹
<i>Decomposition</i>		
Aboveground litter decomposition rate	k_{AGL}	0.5 yr ⁻¹
Root litter decomposition rate	k_{RL}	0.5 yr ⁻¹
Fragmented litter decomposition rate	k_{FL}	0.2 yr ⁻¹
Non-leachable slow OM decomposition rate	k_{NLS}	0.05 yr ⁻¹
Leachable slow OM decomposition rate	k_{LS}	0.005 yr ⁻¹
Aboveground litter - fragmented litter transformation factor	$\alpha_{AGL \rightarrow FL}$	0.8
Fragmented litter - NLS transformation factor	$\alpha_{FL \rightarrow NLS}$	0.15
Fragmented litter - LS transformation factor	$\alpha_{FL \rightarrow LS}$	0.15
Root litter - NLS transformation factor	$\alpha_{RL \rightarrow NLS}$	0.15
Root litter - LS transformation factor	$\alpha_{RL \rightarrow LS}$	0.15
Soil temperature response parameter	E_a	308.56 K
Soil moisture response parameter	a	1
Soil moisture response parameter	b	20
Soil temperature ^a	T	K
Relative soil moisture content ^a	M	-
<i>Organic matter transport</i>		
Bioturbation rate	B	0.4 kg m ⁻² yr ⁻¹
Mixing length	l_m	0.3 m
Advection rate	v	0.002 m yr ⁻¹
<i>Bulk density</i>		
Bulk density L layer	ρ^L	50 kg m ⁻³
Bulk density F layer	ρ^F	100 kg m ⁻³
Bulk density H layer ^c	ρ^H	150 kg m ⁻³
Bulk density mineral soil ^a	ρ^{MS}	kg m ⁻³
Mineral bulk density [§]	ρ_M	kg m ⁻³
<i>Other input</i>		
Spin-up length	-	1000 yr
Depth of bottom boundary	L	0.7 m

^a Time and/or depth dependent

^b Average annual value for the spin-up

^c ρ^H is also used as the organic bulk density ρ_O for determining ρ^{MS} (section 2.2.5).

[§] Not required if ρ^{MS} is specified

2.2.7 Model input

Almost all input data required to run SOMPROF (Table 2.2) depends strongly on soil and ecosystem type. Several of these quantities can be measured directly in the field, including the aboveground and belowground litter production, the soil temperature and moisture and the root (litter input) distribution profile. In a biogeochemical model, these parameters can be supplied by other submodels (e.g. vegetation or land surface models), or derived from the vegetation and soil type.

Decomposition parameters

The parameters of the decomposition submodel include the decomposition rates k at reference temperature (10 °C) and the transformation factors α . The three litter pools (aboveground litter, fragmented litter and root litter) are chemically similar in the sense that they have a relatively high decomposition rate. Typical values range from 0.1 to 1 yr⁻¹ (Paustian et al., 1997; Berg and McLaugherty, 2008). The non-leachable and leachable slow organic matter pools represent stabilized fractions. It is likely that the LS-OM pool is the more recalcitrant of the two, since this pool consists largely of organic matter adsorbed to the mineral phase, which is thought to be very stable (von Lützow et al., 2006; Kaiser and Guggenberger, 2000). Since the LS-OM pool reaches deeper layers than the other pools, the decomposition rate of this fraction should correspond to organic carbon ages and turnover times found in the deep soil, i.e. 10⁻³ to 10⁻² yr⁻¹. The non-leachable slow pool represents organic matter stabilized by other mechanisms (e.g. chemical recalcitrance or spatial inaccessibility), and is assumed to have a decomposition rate between 10⁻¹ and 10⁻² yr⁻¹.

The transformation factors determine the flow between the organic matter pools and lie between 0 and 1. Since these parameters are rather abstract, they are more difficult to predict a priori, but we can gain some insight from parameterizations of other decomposition models with a similar structure (e.g. van Dam et al., 1997; Elzein and Balesdent, 1995). In these models, the efficiency of the decomposition usually increases with successive decomposition steps, meaning that a greater fraction of the organic matter is metabolized. It is likely that little material is lost during the transformation of aboveground litter to fragmented litter, hence we expect $\alpha_{\text{AGL} \rightarrow \text{FL}}$ to be in the higher end of the range, 0.6 to 0.9. The transformation factors for production of leachable and non-leachable slow OM ($\alpha_{\text{FL} \rightarrow \text{NLS}}$, $\alpha_{\text{FL} \rightarrow \text{LS}}$, $\alpha_{\text{RL} \rightarrow \text{NLS}}$, $\alpha_{\text{RL} \rightarrow \text{LS}}$) are presumably closer to zero: 0.05 to 0.4.

The parameters of the temperature and moisture response factors can be found in literature if local measurements are not available (e.g. Lloyd and Taylor, 1994; Subke et al., 2003).

Transport parameters

Compared to decomposition, relatively little research has been done with respect to organic matter transport. The bioturbation rate B is determined by the soil fauna biomass and activity, which in turn strongly depends on soil and vegetation type and climate. Under inhospitable conditions for soil animals the mixing rate may be

virtually zero, whereas very high mixing rates can be found for e.g. tropical soils. Paton et al. (1995) compiled an extensive list of estimates of reworking rates for different types of organisms and climates and found that earthworms are generally the most important organisms for bioturbation. Reported reworking rates ranged from 0.0063 to 27 kg m⁻² yr⁻¹, with two thirds of the rates between 0 and 5 kg m⁻² yr⁻¹. Since most of these estimates were rates of surface cast formation, they noted that these numbers are probably underestimations, since not all species deposit casts at the surface.

The mixing length l_m should ideally represent the typical distance over which soil particles are displaced. However, as discussed in section 2.2.4, in SOMPROF this parameter is of a more empirical nature. Nevertheless, we can expect the mixing length to be roughly in the order of magnitude of the body size of the soil fauna, i.e. 0.01 to 0.5 m. Ideally, this parameter should be relatively constant over different ecosystems.

The advection rate v is determined both by downward water fluxes and adsorption of DOM to mineral surfaces. Since SOMPROF differs from most other models in the sense that only part of the organic matter is transported advectively, little a priori information on this parameter is available. Sanderman et al. (2008) estimated effective DOM advection rates for the total organic matter fraction as a function of depth, based on field concentration measurements and modelled water fluxes. Assuming that in the deep soil most organic material is potentially mobile, their estimate of the effective advection rate for this fraction is approximately 0.2 mm yr⁻¹. Bruun et al. (2007) estimated transport rates from ¹⁴C profile, and found an advection rate of 2.3 mm yr⁻¹ for a fraction of 24% of the total organic matter. Based on profiles of short-lived isotopes (¹³⁷Ce and ²⁴¹Am) produced by nuclear weapon testing, Kaste et al. (2007) reported advection rates ranging from 0.7 to 2 mm yr⁻¹, for different soils.

Bulk density

The bulk densities of the organic layers (ρ^L , ρ^F and ρ^H) are not usually measured in field studies. Since they are needed only to calculate the thickness of the organic layers in order to distribute the root litter input and soil temperature and moisture profiles, their influence on the carbon stocks and distribution is relatively small. For soil carbon cycling simulations they may be set to fixed but reasonable values (Table 2.2). However, for energy and water exchange the bulk density of the organic horizons is more important, due to the effects of the organic layer on soil heat and moisture transport.

If the bulk density of the mineral soil (ρ^{MS}) is not available, it is estimated according to equation (2.4). In this equation, the organic bulk density ρ_o is set equal to the H horizon bulk density. The mineral bulk density depends on the mineral composition, and should be approximately equal to the bulk density at the deep soil, where the organic matter fraction approaches zero.

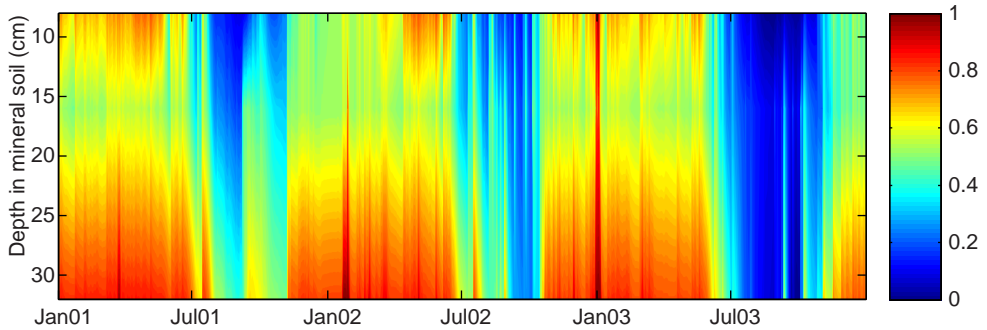


Figure 2.2: Measured relative soil moisture content at Hainich for the period 2001–2003. Measurement depths were 8, 16, 32 cm.

2.3 Simulation preparation

To test the model, a simulation was made using data from Hainich, a deciduous forest in Germany. Predicted soil carbon fractions and stocks are compared to measurements made at the site. However, we did not perform calibration the model parameters to these measurements, which, due to the complexity of the model, is outside of the scope of this paper. The organic carbon measurements are presented for reference, but we do not present any statistics on model performance.

To study the model behavior we prepared several additional simulations for which one or more parameters were changed. This section describes the preparation of the reference simulation. For each additional simulation, the changes with respect to the reference simulation are described in section 2.4.

2.3.1 Site description

Hainich (51°4'45.36"N; 10°27'7.20"E) is an old growth deciduous forest in Central Germany which has been unmanaged for several decades. The climate is temperate suboceanic/subcontinental with an average annual precipitation of 800 mm and an average temperature of 7 to 8 °C. The forest is dominated by beech (*Fagus Sylvatica*, 65%) and ash (*Fraxinus excelsior*, 25%), with a wide range of age classes, up to 250 years. The understorey consists of herbaceous vegetation (*Allium ursinum*, *Mercurialis perennis*, *Anemone nemorosa*) which seasonally completely covers the forest floor (Kutsch et al., 2010).

The soil is classified as Luvisol or Cambisol (IUSS Working Group WRB, 2007; Kutsch et al., 2010) and consists of weathered limestone overlain by a Pleistocene loess layer of varying thickness (10–50 cm). The mineral soil is characterized by a high clay content (60%) and a pH-H₂O of 6.0 to 7.8 (Søe and Buchmann, 2005). About 90% of the root biomass occurs above 40 cm depth. The pH and litter quality of deciduous trees in Hainich support a high soil biological activity, demonstrated

by a thin organic layer and a well developed A horizon of 10 to 15 cm (Søe and Buchmann, 2005). Cesarz et al. (2007) reported earthworm populations of up to 500 individuals per m² for the Hainich forest.

The high clay content and shallow bedrock at Hainich obstruct drainage, which causes the deep soil to be relatively moist throughout the year (Figure 2.2).

2.3.2 Measurements and data processing

10 soil cores to a maximum depth of 70 cm were extracted in March 2004. Organic carbon fraction, root biomass and bulk density of the fine soil fraction were determined for 7 depth increments (0–5 cm; 5–10 cm; 10–20 cm; 20–30 cm; 30–40 cm; 50–60 cm; 60–70 cm). Organic carbon stocks were measured for L and F/H horizons (the individual F and H horizons could not be identified). The mineral soil organic carbon stocks were derived from the organic carbon fraction using the fine soil bulk density. The sampling and measurement procedures are described in Schrumpf et al. (2011).

Soil temperature and moisture were continuously measured at half-hourly intervals for the period 2001 to 2008. Gaps were filled with piecewise Hermite interpolation. Soil temperature was measured for two profiles at 5 depths (2, 5, 15, 30, 50 cm). The average of the two soil temperature profiles was used for model input. Soil moisture was measured for one profile (8, 16, 32 cm; Figure 2.2). The soil moisture volume fraction was converted to relative content by calculating the relative value between the minimum value and the maximum value of the time series for each depth. Next, the half-hourly temperature and relative soil moisture content values were converted to response factors based on the response equations (Appendix 2.A.1), and were subsequently averaged to daily values for the second stage of the simulation. Also, an average annual cycle of monthly values was derived for the spin-up.

Total annual litter fall and root litter production rate was measured for the period 2000 to 2007 (Kutsch et al., 2010). Average values for this period were used for the spin-up.

2.3.3 Simulation setup

For the reference simulation, the decomposition and transport parameters (Table 2.2) were manually tuned based on a priori knowledge of the parameters (section 2.2.7) and model behavior.

During the spin-up phase, the model was run for a period of time to achieve the initial conditions for the second stage of the simulation. Although the oldest trees at Hainich are about 250 years old, development of the soil organic matter profile presumably started much earlier. Therefore, we used a spin-up length of 1000 years, during which the soil effectively reached an equilibrium. During the spin-up, the model was run at a monthly time step, and driven by an average annual cycle of soil temperature and moisture response factors, derived from the available measurements. Also, average annual values for aboveground litter fall and root litter pro-

duction were used during the spin-up (but the aboveground litter fall is distributed over the year, see below).

During the second stage of the simulation, SOMPROF was run at a daily time step for the period 2001 to 2007, and driven by local measurements of soil temperature, moisture and above and belowground litter production. Since no local estimates of the soil moisture and temperature sensitivity are available, the parameter values from Lloyd and Taylor (1994) were used for the temperature response function. The parameters of the soil moisture response were chosen such that respiration starts to decrease sharply when relative soil moisture drops below 20%. To account for seasonal variations, the annual total aboveground litter fall was distributed over the year (for the spin-up as well as the second phase of the simulation) according to a distribution function based on data for a similar forest, taken from Lebrecht et al. (2001). Since no information about the seasonal cycle of root litter production was available, it was kept at a constant rate throughout the year. An exponential function was fitted to the vertical root biomass profile to determine the vertical distribution of root litter input.

The subsoil at Hainich has a high stone content which increases towards the bedrock. Since SOMPROF does not account for stones, the fine soil density (mass of grains smaller than 2 mm per unit total volume) was used as bulk density for the simulations, up to a depth of 40 cm. Since the stoniness increases with depth below this level, the bulk density was kept at the 30–40 cm level below 40 cm. The bulk density for the L, F and H horizons were set to typical values observed in the field. The bottom depth of the soil profile was set at 70 cm.

2.4 Results

2.4.1 Organic carbon stocks and mass fraction profile

Modelled organic carbon stocks and concentration profile for the reference simulation are shown together with measured values in figures 2.3 and 2.4 (center graphs). The modelled results are values from the last year of the spin-up, from a month near the sampling date, to reduce differences with measurements due to seasonal fluctuations.

The predicted stocks and concentrations generally compare well with measurements. However, the organic carbon stock in the F+H horizon is strongly overestimated with respect to the measurements. This may be caused by a too low bioturbation rate or too low decomposition rates of the organic carbon pools. The carbon stocks in the topsoil are underestimated while the subsoil stocks are overestimated. Presumably, a higher bioturbation rate and a lower advection rate would lead to a better fit to the measurements, but without additional data and more thorough calibration the precise reason cannot be determined. Furthermore, the possibility of a bias in the model results is higher for the deep soil, due to the presence of stones, which are not accounted for in SOMPROF.

Although leachable slow (LS) organic matter is absent in the organic layer, it is the

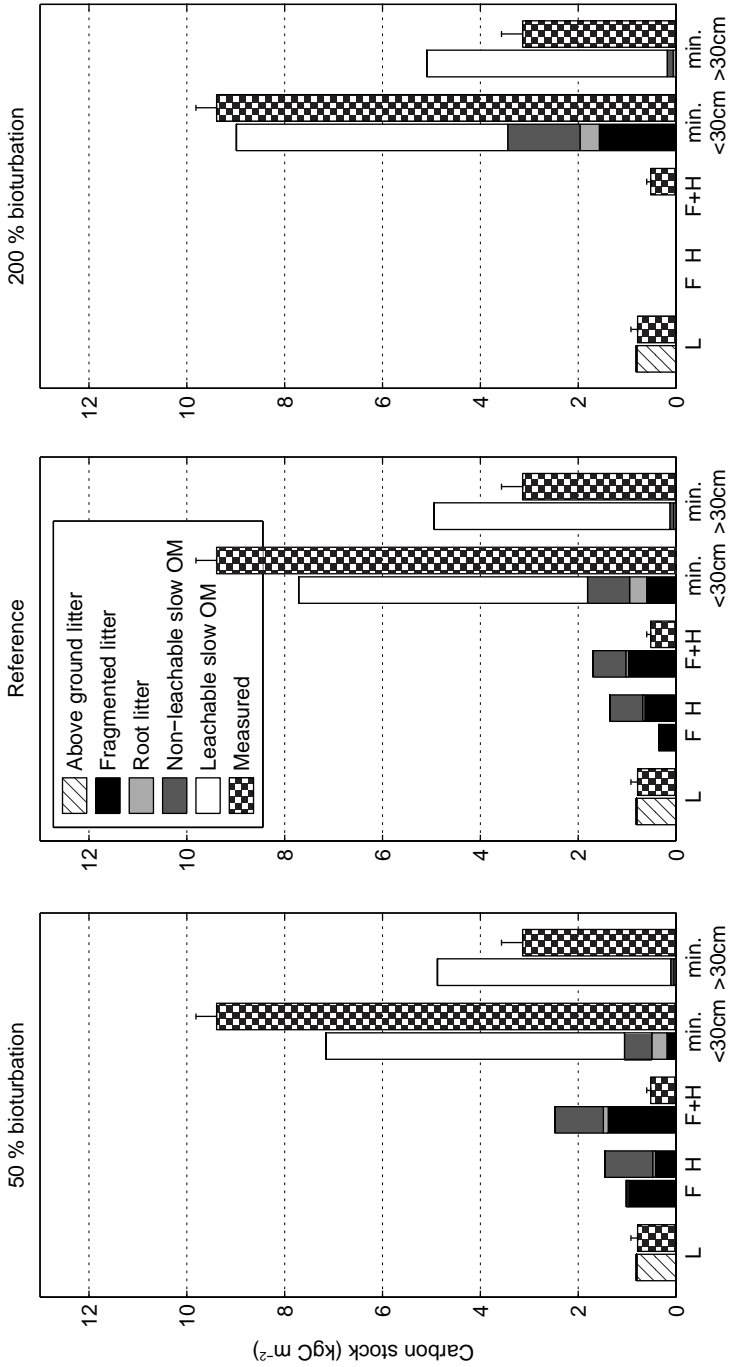


Figure 2.3: Measured organic carbon stocks and modelled stocks for three bioturbation scenarios: $B = 0.2, 0.4, 0.8 \text{ kg m}^{-2} \text{ yr}^{-1}$. All other parameters are as listed in Table 2.2. Measured stocks are mean values; errorbars denote 1 standard error of the mean.

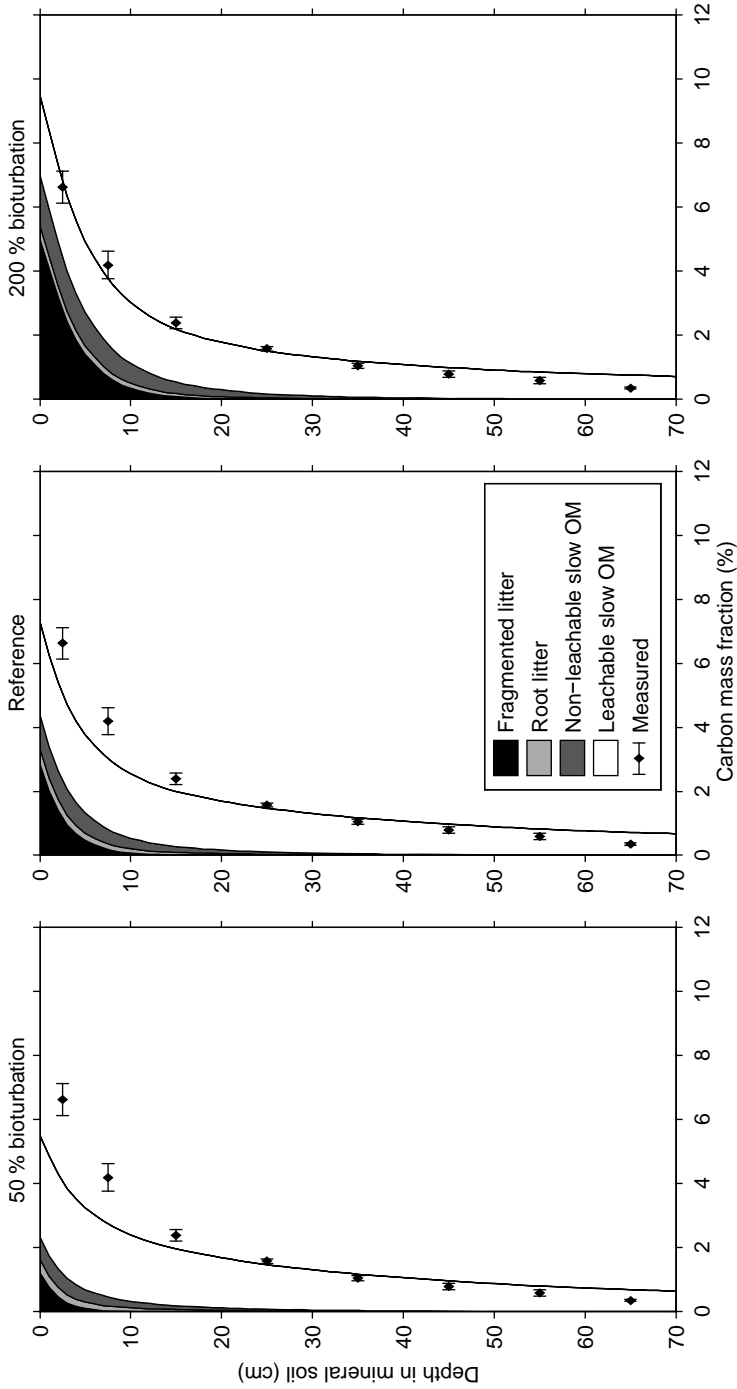


Figure 2.4: Measured organic carbon mass fraction profile in the mineral soil and modelled fraction profiles for three bioturbation scenarios: $B = 0.2, 0.4, 0.8 \text{ kg m}^{-2} \text{ yr}^{-1}$. All other parameters are as listed in Table 2.2. Measured concentrations are mean values; errorbars denote 1 standard error of the mean.

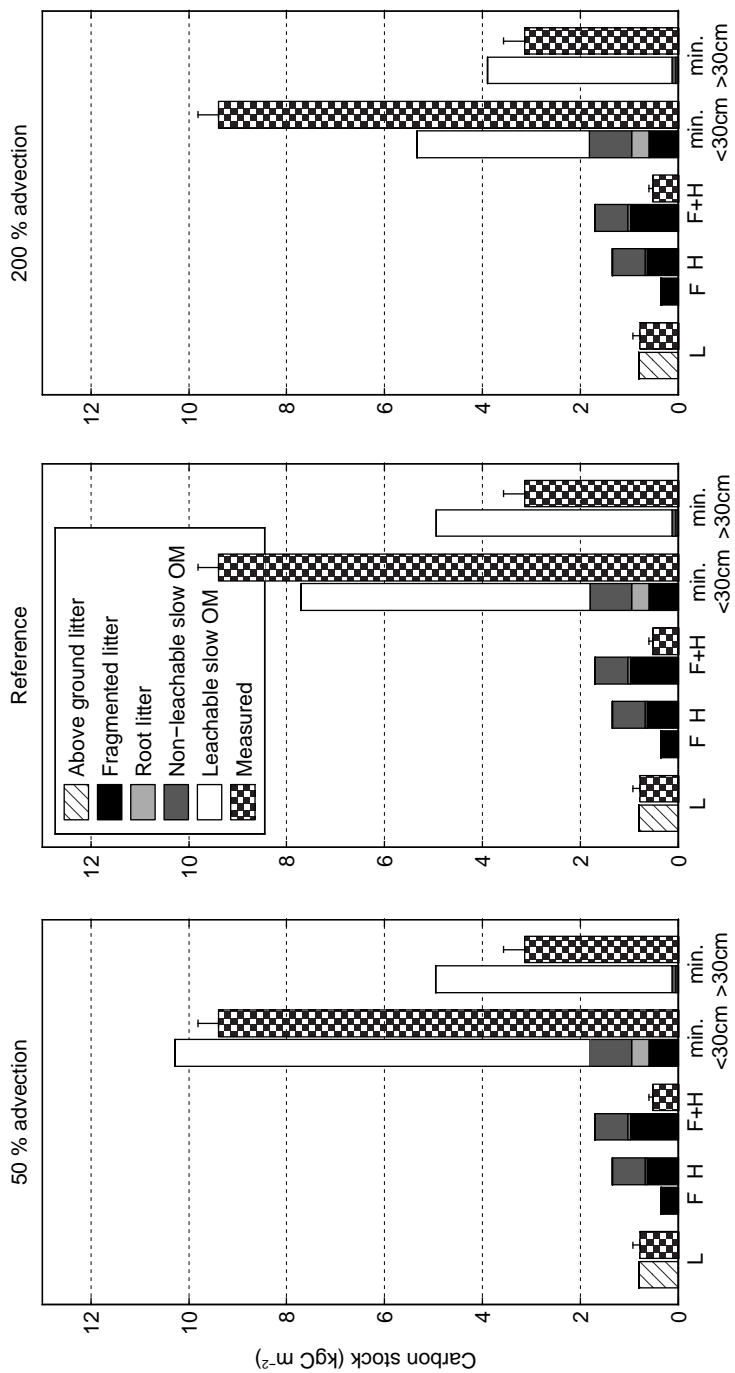


Figure 2.5: Measured organic carbon stocks and modelled stocks for three advection scenarios: $v = 0.001, 0.002, 0.004 \text{ m yr}^{-1}$. All other parameters are as listed in Table 2.2. Measured stocks are mean values; errorbars denote 1 standard error of the mean.

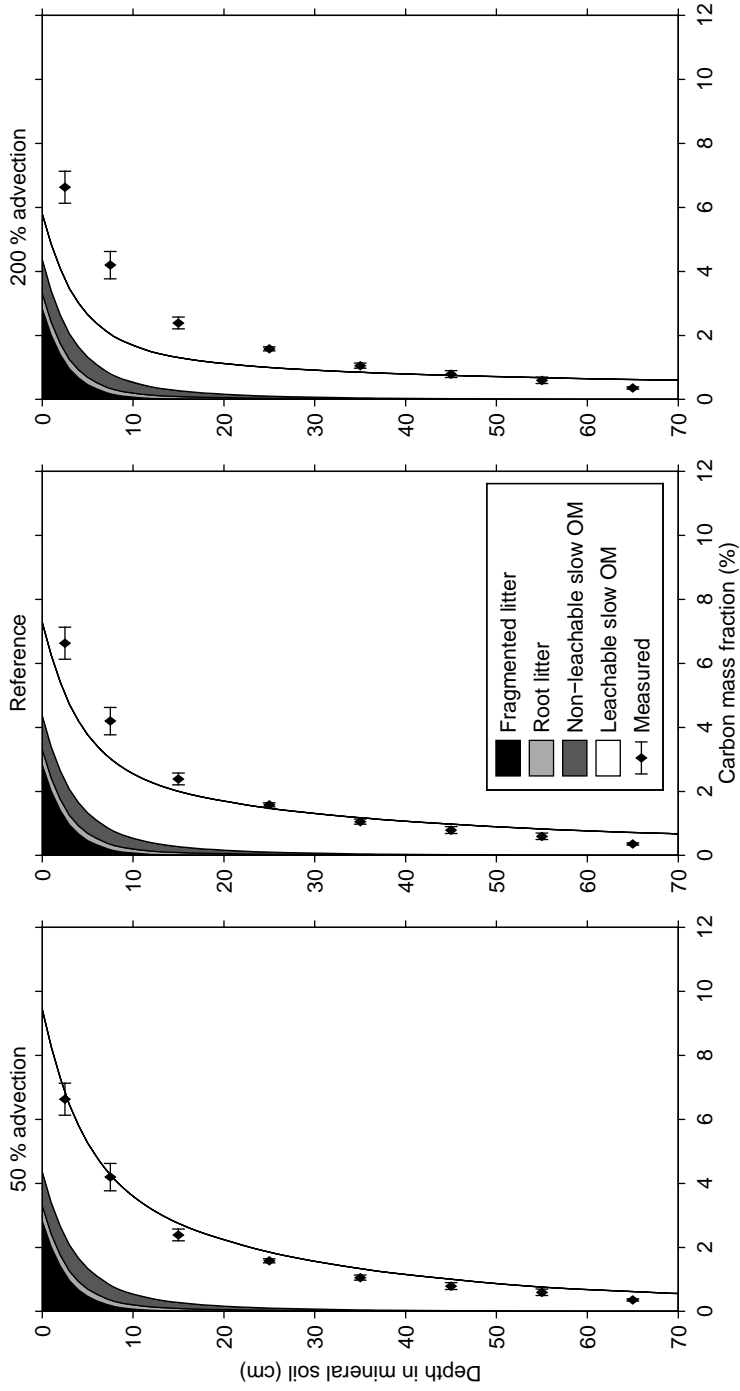


Figure 2.6: Measured organic carbon mass fraction profile in the mineral soil and modelled fraction profiles for three advection scenarios: $v = 0.001, 0.002, 0.004 \text{ m yr}^{-1}$. All other parameters are as listed in Table 2.2. Measured concentrations are mean values; errorbars denote 1 standard error of the mean.

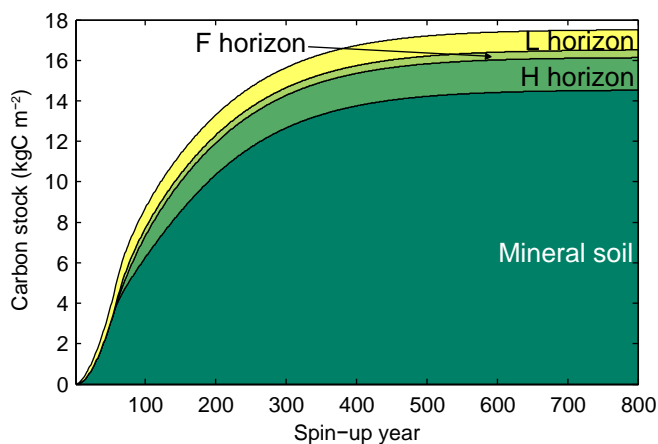


Figure 2.7: Development of the organic carbon stocks for the reference simulation.

largest organic matter pool (11.0 kgC m^{-2} of 15.4 kgC m^{-2} in total) due to its predicted abundance in the complete mineral soil profile. The importance of the LS pool is not surprising, given that it has the lowest decomposition rate of all pools. Fragmented litter dominates the upper 5 cm of the mineral soil, but decreases rapidly with depth, becoming negligible below 10 cm. The root litter and non-leachable slow (NLS) pool reach deeper levels because of direct local input and, in the case of NLS-OM, the relatively low decomposition rate.

2.4.2 Development of the organic carbon stocks

Figure 2.7 shows the development of the carbon pools for the reference simulation. Initially all material produced in the L horizon flows immediately into the mineral soil, preventing buildup of an F or H horizon. When the flux from the L layer exceeds the bioturbation rate, the F and H horizon start to form. In this case this occurs after approximately 50 years.

Under certain conditions, the organic carbon stock of the mineral soil initially increases, peaks, and then decreases again (Figure 2.8). This is caused by a positive feedback in the formation of the F and H horizon due to the fact that root litter input of a layer is indirectly proportional to its mass (via its thickness, section 2.2.2). Initially, in absence of an F or H horizon, all root litter (and its decomposition products) flows into the mineral soil. As the organic layer develops, root litter input gradually shifts to the F and H horizon, leading to reduced organic matter input into the mineral soil.

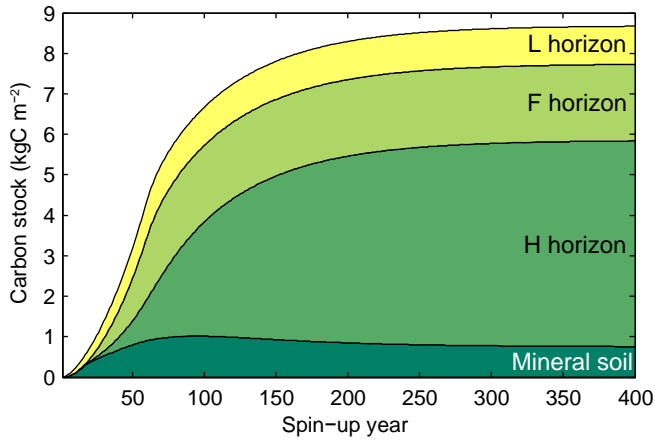


Figure 2.8: Development of the organic carbon stocks for a scenario with high and shallow root litter input and low bioturbation. Input parameters are as follows: $k_{\text{NLS}} = 0.02 \text{ yr}^{-1}$; $k_{\text{LS}} = 0.02 \text{ yr}^{-1}$; $\alpha_{\text{AGL} \rightarrow \text{FL}} = 0.7$; $\alpha_{\text{FL} \rightarrow \text{NLS}} = 0.1$; $\alpha_{\text{FL} \rightarrow \text{LS}} = 0.05$; $\alpha_{\text{RL} \rightarrow \text{NLS}} = 0.2$; $\alpha_{\text{RL} \rightarrow \text{LS}} = 0.05$; $B = 0.1 \text{ kgC m}^{-2} \text{ yr}^{-1}$; $\beta = 0.4 \text{ m}^{-1}$; $I_{\text{RL}} = 0.8 \text{ kgC m}^{-2} \text{ yr}^{-1}$; all other parameters as listed in Table 2.2.

2.4.3 Organic matter transport fluxes

Figure 2.9 depicts the different transport fluxes in the mineral soil. The advective flux is clearly the main transport mechanism in virtually all of the soil profile. Only in the top 2 to 3 cm, is diffusion more important due to the high concentration gradient of fragmented litter there. The relative importance of advection for organic matter transport is caused mainly by the fact that leachable slow organic matter is the largest organic matter pool, due to its low decomposition rate. Interestingly, the diffusive transport rate of LS-OM near the surface is negative, indicating upward transport. This is because the LS-OM concentration peaks at around 5 cm depth, which indicates that the largest input of LS-OM due to root litter and fragmented litter decomposition is around this depth. Presumably, this is a modelling artifact and does not occur in reality.

2.4.4 Sensitivity to transport parameters

Bioturbation rate

The bioturbation rate B controls both the flow of organic matter from the organic horizons, as well as the diffusivity determining the transport within the mineral soil. The effects of a 50% reduction and a 100% increase of the bioturbation rate on the organic carbon stocks and organic carbon profile in the mineral soil are shown in figures 2.3 and 2.4, respectively. Increasing the bioturbation rate causes a shift of material from the organic layer to the mineral soil, leading to complete disappearance

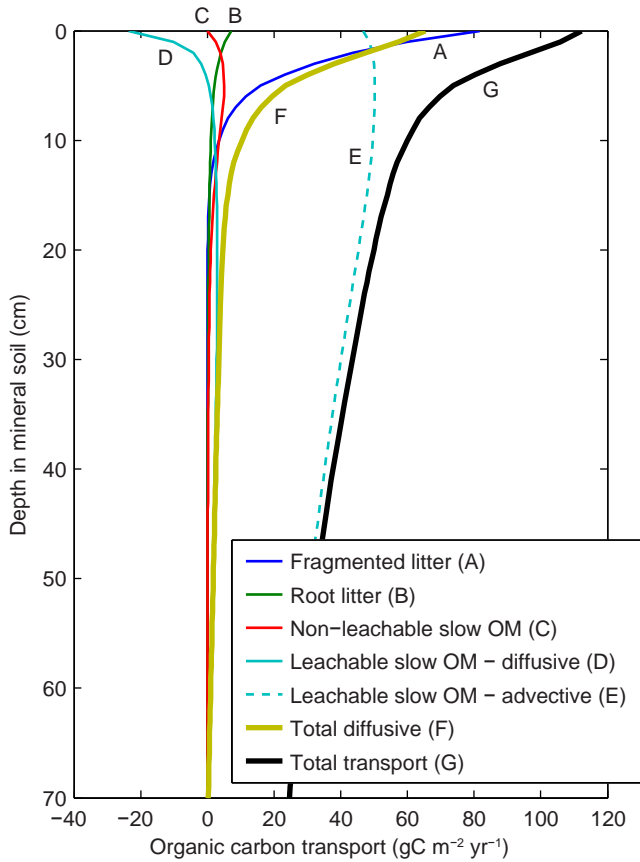


Figure 2.9: Organic carbon transport fluxes in the mineral soil for the reference simulation. Downward fluxes are positive.

of the F and H horizon in the high bioturbation scenario.

The effects of bioturbation are mostly limited to the fragmented litter and non-leachable slow pools. These pools are dependent on bioturbation for downward flow, whereas root litter and leachable slow organic matter are also influenced by direct input and advection, respectively. The change of bioturbation rate has virtually no influence on the carbon stocks below 50 cm.

Advection rate

Figures 2.5 and 2.6 show the organic carbon stocks for the control, a 50 % decrease and a 100 % increase of the advection rate. As would be expected, the advection rate has no influence on the stocks in the organic layers since it does not affect the flow into the mineral soil. The mineral soil stock of leachable slow organic matter

strongly decreases with increasing advection rate, particularly in the topsoil. This is explained by the increased loss of organic carbon over the lower boundary. Interestingly, the organic matter concentration below 50 cm is slightly lower both for the scenario with increased advection and with decreased advection, with respect to the reference simulation. The reason for this is that for the low advection scenario less LS-OM reaches the subsoil, while for the high advection scenario more LS-OM flows out of the system over the lower boundary, both cases leading to lower organic matter concentrations.

The amount of carbon lost at the lower boundary is also strongly dependent on the advection rate: $9.36 \text{ gC m}^{-2} \text{ yr}^{-1}$ for the low advection scenario, $22.6 \text{ gC m}^{-2} \text{ yr}^{-1}$ for the reference and $34.7 \text{ gC m}^{-2} \text{ yr}^{-1}$ for the high advection scenario.

2.4.5 Influence of the SOM profile on heterotrophic respiration

To study the effects of the vertical SOM distribution on heterotrophic respiration, we set up three SOMPROF simulations with different vertical organic matter distributions, by varying the transport rates and the vertical distribution of root litter input (Figure 2.10). The lower boundary of the mineral soil was set to 3 m to assure that virtually all SOM is accounted for in the simulations, and differences in predicted respiration are not due to differences in total carbon stock. Since soil moisture measurements were available only up to a depth of 32 cm, the soil moisture is estimated by non-linear extrapolation up to a depth of 70 cm. Below 70 cm, the soil moisture was held at a constant value.

Figure 2.11 shows the relative contribution of the three organic horizons and the mineral soil to the total heterotrophic respiration, for the three scenarios. The vertical organic matter distribution strongly influences the location of the CO_2 production within the profile. Aside from short time scale fluctuations, this vertical partitioning is quite constant, showing little seasonal variability. A notable exception is the summer of 2003, which was an exceptionally dry and hot period in Europe. During this time, soil moisture decreased severely at Hainich, with lowest values in the organic layer and in the topsoil (Figure 2.2). The vertical partitioning of the heterotrophic respiration changes dramatically during the drought: the mineral soil becomes the dominating source of CO_2 in all three scenarios. These marked differences demonstrate the severity of the drought.

The vertical organic matter distribution also has a significant effect on the temporal variation of total heterotrophic respiration, as shown in Figure 2.12. The amplitude of the fluctuations decreases with deeper organic matter distribution: the deep organic matter scenario has lower respiration rates in summer and higher rates in winter, compared to the other scenarios. Also the response to the 2003 drought (Figure 2.12, inset) is less pronounced for the deep organic matter scenario, although the differences are relatively small because ultimately the whole profile was affected by the drought.

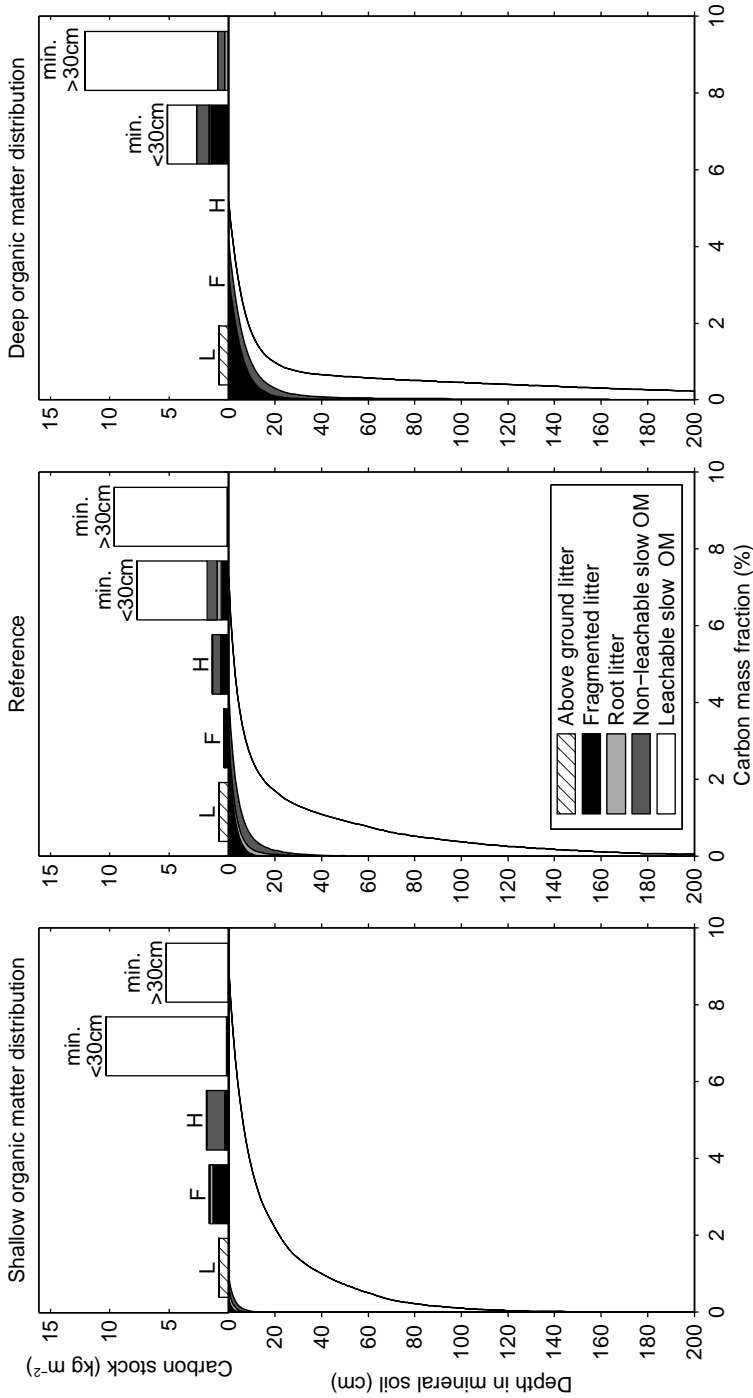


Figure 2.10: Carbon stocks and profile of the organic matter distribution on heterotrophic respiration. Parameters are as follows: Shallow organic matter distribution: $\beta = 0.4 \text{ m}^{-1}$; $B = 0.25 \text{ kg m}^{-2} \text{ yr}^{-1}$ $v = 0.001 \text{ m yr}^{-1}$. Deep organic matter distribution: $\beta = 0.01 \text{ m}^{-1}$; $B = 2 \text{ kg m}^{-2} \text{ yr}^{-1}$ $v = 0.002 \text{ m yr}^{-1}$. For all three scenarios the depth of the lower boundary has been set to 3 m. All other parameters, as well as all parameters for the reference scenario are as listed in Table 2.2.

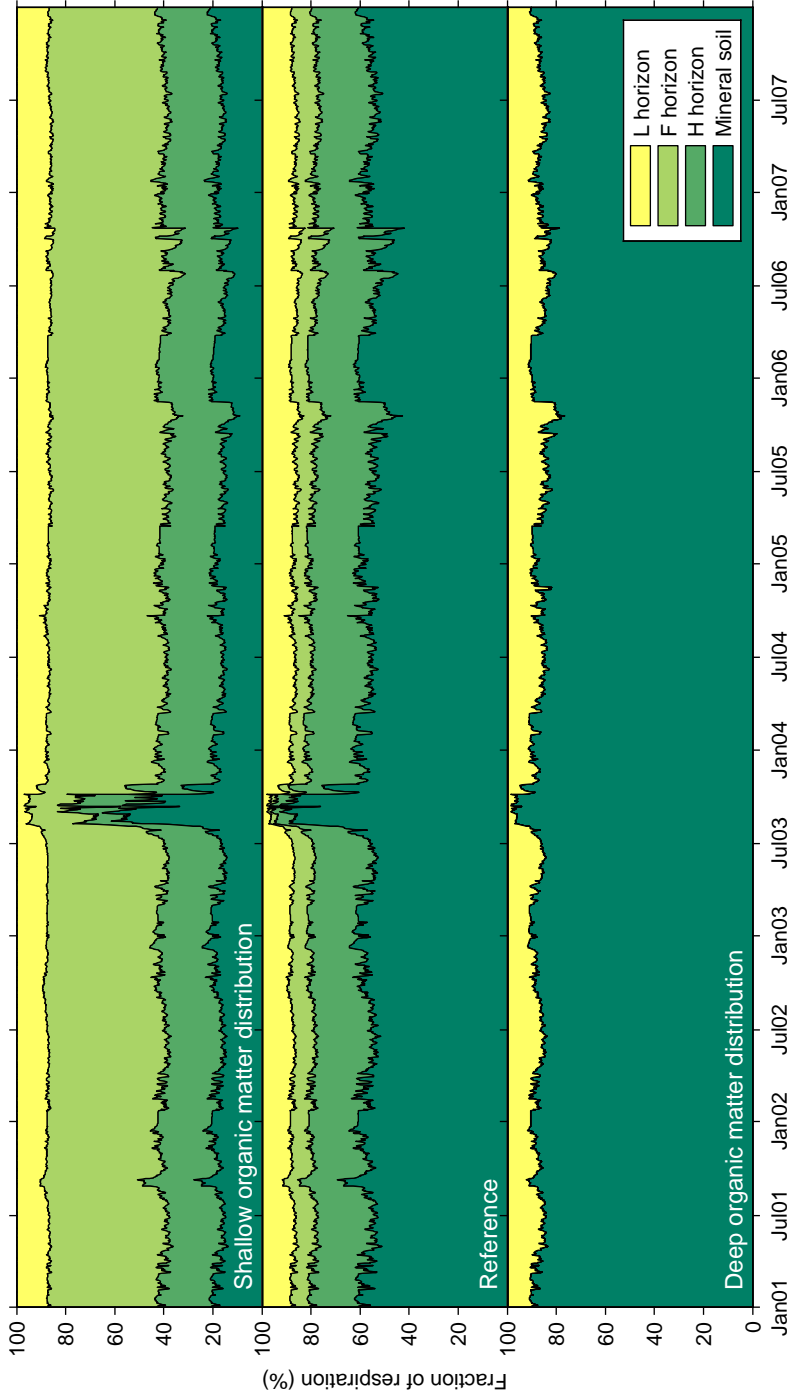


Figure 2.11: Relative contribution of the three organic horizons and the mineral soil of the three organic matter distribution scenarios for the simulation period.

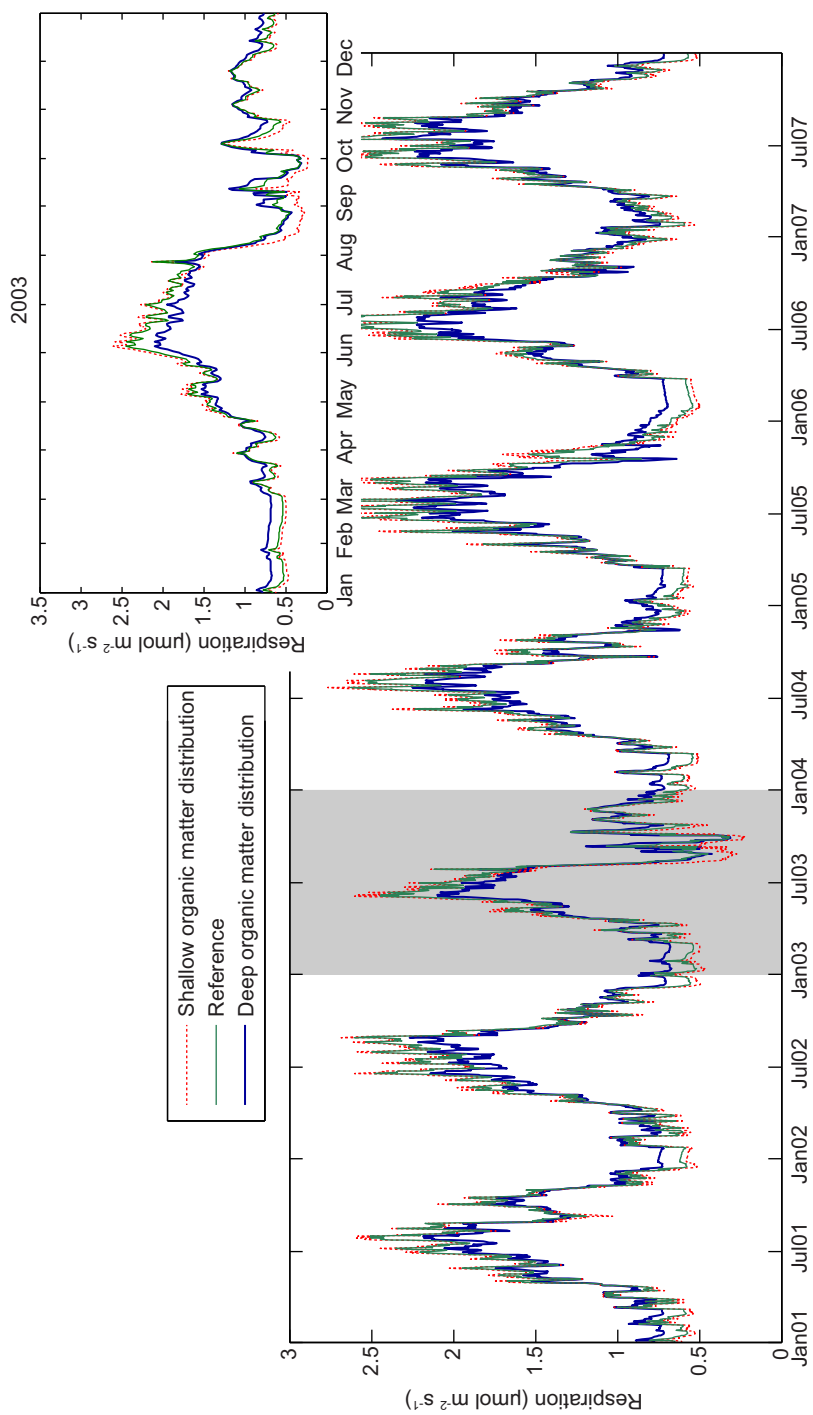


Figure 2.12: Total heterotrophic respiration of the three organic matter distribution scenarios for the simulation period.

2.5 Discussion

2.5.1 Organic carbon stocks and profile

The results depicted in figures 2.3-2.6 show that SOMPROF is able to produce organic carbon stocks and profiles that are realistic compared to measurements. Furthermore, it does so based on input parameter values that lie within ranges suggested by *a priori* knowledge (section 2.2.7), which is encouraging. It must be noted, however, that the model is over-parameterized with respect to the available measurements. This is clear, for example, from the fact that the profile and stocks are roughly equally well reproduced in the high bioturbation scenario (figures 2.3 and 2.4, right graphs) and the low advection scenario (figures 2.5 and 2.6 left graphs), which have distinctly different parameter sets.

In spite of this problem, the results offer some insight into the structure of the mineral SOM profile (figures 2.4 and 2.6). The profile can be divided into a zone near the surface with relatively fast decay of organic matter content with depth, and a zone with a smaller depth gradient in the subsoil. The model results suggest that the two zones are characterized by different organic matter deposition mechanisms: bioturbation in the topsoil and liquid phase transport in the subsoil. The low depth gradient in the subsoil causes a long, downward “tail” of organic matter, which is also often observed in the field. Because of this tail, a power function of depth often yields a better fit to the vertical SOM profile than a one-term exponential decay function (Jobbagy and Jackson, 2000).

In the model results, the leachable slow organic matter pool is dominant throughout most of the profile. This can fully be ascribed to our choice for model parameters: its decomposition rate is lowest of all pools, while it is formed at the same rate as non-leachable slow OM. Nevertheless, measurements at Hainich (Schrumpf, unpublished) show that most organic matter is located in the heavy fraction. Since the heavy fraction can be assumed to be mineral associated organic matter, this corroborates our results.

The positive feedback in the development of the F and H horizon (section 2.4.2) leads, under certain conditions, to interesting behavior in which the mineral soil carbon stock initially increases and later decreases again (Figure 2.8). Although the F/H horizon feedback always occurs if these layers are present, the peaking behavior of the mineral soil stock is observed only in situations where root litter input is the dominant source of organic matter, while being shallowly distributed in the profile. Furthermore, vertical transport of organic matter should play a small role, which means that the mineral soil is mostly dependent on root litter for its soil carbon input. Such conditions may occur, for example, in a forest on a poor soil (i.e. with little soil biological activity) with a productive herbaceous understorey. Although it does not seem unlikely that the predicted behavior could occur for such a site, we did not find chronosequence studies that confirm this, since soil carbon buildup usually involves a succession of vegetation types, accompanied by changes in (root) litter production.

2.5.2 Soil organic matter transport

In our simulations, liquid phase transport of organic matter is the dominant mechanism for SOM movement in most of the profile, due to the abundance of LS-OM (Figure 2.9). Thorough parameter estimation should reveal if this is truly the case for Hainich. However, even if advection dominates, bioturbation should not be ignored as a mechanism for organic matter transport. The bioturbation rate strongly controls the organic carbon stocks in the F and H horizons and determines the amount of easily decomposable material in the topsoil.

SOMPROF behaves differently with respect to bioturbation than existing models that include this process: for a small increase of bioturbation, the increased input of organic matter into the mineral soil is not fully compensated by the increased diffusion rate, leading to *higher* concentrations in the topsoil. Only in absence of an F and H horizon, will an increase of bioturbation rate lead to reduced organic matter concentrations due to faster diffusion. In this respect SOMPROF is more realistic than SOM profile models that ignore the organic layer. This is corroborated by results of Alban and Berry (1994) who found a significant increase of topsoil organic carbon content together with a decrease of organic layer mass for a forest soil which was invaded by earthworms.

Predicted organic carbon loss over the lower boundary due to advection (section 2.4.4) is strongly overestimated compared to *in situ* measurements at Hainich by Kindler et al. (2011), who found fluxes of $1.9\text{--}2.6\text{ gC m}^{-2}\text{ yr}^{-1}$ from the subsoil. The advective loss rates are also relatively high compared to typically observed estimates at other sites (Michalzik et al., 2001). This points to a too high advection rate in the deep soil, which may also partly explain the overestimation of the deep soil organic matter concentration. It is likely that the advection rate of the deep soil is in reality lower than that of the topsoil, since average water infiltration rates decrease with depth (Sanderman et al., 2008). At Hainich this is particularly likely due to the high clay content which obstructs water drainage and adsorbs organic matter. The predicted advective loss of organic matter also depends on the depth at which the lower boundary is set in the model. Leached organic matter can be accounted for simply by lowering the soil depth (compare figures 2.3 and 2.4 with figure 2.10, middle graphs). This raises the question whether leached organic carbon in the field can really be considered lost or if it is retained by adsorption at depths below the lowest measurement depth, in which case it may still contribute to respiration.

2.5.3 Significance of the SOM profile for carbon cycling

The results in section 2.4.5 demonstrate that the vertical SOM distribution can significantly affect soil carbon cycling at short time scales. Since temporal fluctuations of soil moisture and temperature decrease with depth in soil, a deeper distribution of organic matter causes reduced variability of heterotrophic respiration. This suggests that a soil with a deep SOM distribution is less sensitive to short time scale climatic fluctuations than a soil with a shallow distribution. However, since no measurements of soil moisture and temperature were available below 32 and 50 cm respec-

tively, we needed to make assumptions regarding these quantities in the deep soil. A more thorough modelling study is needed to evaluate these effects.

Whether these interactions affect the average long term soil carbon balance is unsure, since, in this case, the vertical SOM distribution affects mostly the amplitude and less the average of the variations. In general, the long term effects depend on the non-linearity of the response functions and the average vertical gradients of the temperature moisture profiles. This suggests that the variability of soil moisture would play a greater role on the long time scale, since its response function is less linear and it generally displays stronger depth gradients than soil temperature. More simulation studies, for different conditions and at larger spatial scales (possibly as part of a dynamic global vegetation model) should reveal if these effects truly play a significant role for soil carbon cycling.

A large part of the merit of a vertically explicit SOM model lies in synergies with other processes that are not yet implemented in SOMPROF. For example, the vertical SOM profile (particularly the presence of an organic surface layer) strongly influences soil heat and moisture transport (Koven et al., 2009; Lawrence and Slater, 2008), which ultimately feed back to soil carbon cycling. Also microbial dynamics may be of importance on long time scales (Fontaine et al., 2007; Allison et al., 2010). Fontaine et al. (2007) showed that deep soil organic carbon can be stabilized due to the absence of fresh organic matter for microbial decomposers. A decomposition model that includes such effects, as part of a vertically explicit scheme, is likely to find markedly different results for deep soil carbon storage.

2.5.4 Model limitations

SOMPROF cannot be applied under all conditions. The organic layer structure corresponds to the humus profile observed in forests. For grassland soils it may not be possible to make the distinction between an organic layer and the mineral soil, since organic matter accumulation occurs mostly in the topsoil due to root turnover. Furthermore, SOMPROF is not suitable for soils where the vertical SOM profile is significantly influenced by processes that are not represented, including ploughing, cryoturbation, erosion and podzolization.

Currently, SOMPROF does not account for stones in the mineral soil matrix. To include these effects the mass balance equations would need to be corrected for the amount of fine soil that is involved with carbon storage and bioturbation. Since the high stone content at Hainich is limited to the deep soil where organic carbon fractions are low, presumably the error in the predicted carbon stocks are small. However, many soils have a high stoniness throughout the profile, which significantly affects the vertical SOM distribution.

Future model development will address several of the issues discussed above to improve the large scale applicability of the model.

2.5.5 Outlook

For further application of SOMPROF, parameter estimation is required to obtain insight into the model parameters, particularly those related to SOM transport, since they are relatively unknown. A problem is posed by equifinality: the ability of the model to produce similar results using significantly different parameter sets. The fact that the different mathematical terms in SOMPROF relate to specific processes somewhat alleviates this problem because it allows *a priori* rough estimates of parameter values to be obtained. Nevertheless, future model testing should investigate whether the model may be simplified in order to facilitate parameter estimation. Furthermore, observational data used for optimization should include additional high-resolution profile data, such as ^{14}C and ^{13}C measurements and respiration rates. Also, since small scale spatial heterogeneity can significantly affect local stocks and profiles, multiple replicate samplings at different locations within one ecosystem or soil type are required.

Application of the model at large spatial scales requires sets of parameters for different ecosystems and soils, or empirical functions relating the parameters to information in available data sets. Bioturbation is strongly linked to climate, litter quality and soil properties such as pH and base saturation. Since conditions that support a high vegetation productivity and litter quality tend to have a large and active soil fauna community as well, vegetation type and productivity may be a good proxy for the bioturbation rate. The advection rate is related to physical and chemical factors, such as water infiltration rates, soil texture, and pH.

It is likely that the spatial variability of the transport parameters is comparable to that of the decomposition parameters since both groups are influenced by the same environmental factors. Therefore, we do not expect that the introduction of a vertical scheme in SOM models as such calls for better representation of spatial heterogeneity compared to current models.

Many existing SOM models can be made vertically explicit by adopting the scheme of SOMPROF. This modification would mainly involve separation of the soil into the mineral soil with a concentration profile, and the organic layer, possibly further subdivided into different horizons. The pool structure of the model to be adjusted must support the change of transport behavior during the decomposition process. Hence, a serial arrangement of pools (with one type of material being transformed to another) is preferable. Furthermore, a specific pool must be defined that is transported advectively, to represent liquid phase mediated transport. Finally, there must be an explicit distinction between aboveground litter and root litter, since these two types represent different input mechanisms.

2.6 Conclusions

SOMPROF is able to reproduce organic carbon stocks and concentration profiles that compare well to measurements, using input parameters that are reasonable compared to prior knowledge. Furthermore, the model is able to produce widely different organic matter profiles, making it applicable to a range of soil types, provided

that the natural process of soil formation has not been disturbed. The model can provide insight into several processes that cannot be addressed with bulk models, such as soil formation, organic matter origin, loss of organic carbon through leaching, and interactions between the SOM profile, heterotrophic respiration and soil temperature and moisture.

Appendix 2.A Full description of SOMPROF

Here a complete description of SOMPROF is given, including all equations. Additional explanation is given in the main text of this paper. Table 2.3 gives complete overview of all symbols used in the equations. Depth (z) is assumed positive downwards and $z = 0$ is set at the top of the mineral soil. In general, subscripts suffixed to model variables denote an organic matter pool, while superscripts denote a location in the vertical profile.

2.A.1 Decomposition

Organic matter decomposition is modelled according to first order kinetics corrected for local soil temperature and moisture. For any organic matter pool i in model compartment p , decomposition is defined as:

$$L_i^p = f(T) g(W) k_i C_i^p, \quad (2.5)$$

where $f(T)$ and $g(W)$ are response functions for soil temperature and moisture. $f(T)$ is defined according to Lloyd and Taylor (1994):

$$f(T) = \exp\left(E_a \left(\frac{1}{T_0 - T_{ref}} - \frac{1}{T - T_{ref}}\right)\right), \quad (2.6)$$

where T is the soil temperature (K), T_{ref} (283.15 K) and T_0 (227.13 K) are reference temperatures, and E_a (K) determines the temperature sensitivity. $g(W)$ is defined according to a modified sigmoid model (Subke et al., 2003):

$$g(W) = \exp(-\exp(a - bW)), \quad (2.7)$$

where W is the fraction of the porosity filled with water (-) and a and b (-) are parameters determining the shape of the soil moisture response.

For several pools, part of the decomposition flux flows into to secondary pools. This is determined by the transformation factor α . The flux from pool i to pool j in model compartment p is defined as:

$$F_{i \rightarrow j}^p = \alpha_{i \rightarrow j} L_i^p. \quad (2.8)$$

Thus, the total formation of the secondary pools in any compartment p , is defined as follows:

$$F_{FL}^p = \alpha_{AGL \rightarrow FL} L_{AGL}^p, \quad (2.9)$$

$$F_{NLS}^p = \alpha_{FL \rightarrow NLS} L_{FL}^p + \alpha_{RL \rightarrow NLS} L_{RL}^p, \quad (2.10)$$

$$F_{LS}^p = \alpha_{FL \rightarrow LS} L_{FL}^p + \alpha_{RL \rightarrow LS} L_{RL}^p. \quad (2.11)$$

Table 2.3: List of symbols and abbreviations.

Symbol	Description	Units
<i>State variables and fluxes</i>		(Organic layer / Mineral soil)
C_i^p	Content of pool i in model compartment $p^{a,b}$	kg m^{-2} / kg m^{-3}
I_i^p	Input of pool i in model compartment $p^{a,b,c}$	$\text{kg m}^{-2} \text{yr}^{-1}$ / $\text{kg m}^{-3} \text{yr}^{-1}$
$F_{i \rightarrow j}^p$	Transformation of pool i to pool j in model compartment $p^{a,b}$	$\text{kg m}^{-2} \text{yr}^{-1}$ / $\text{kg m}^{-3} \text{yr}^{-1}$
F_i^p	Total formation of pool i in model compartment $p^{a,b}$	$\text{kg m}^{-2} \text{yr}^{-1}$ / $\text{kg m}^{-3} \text{yr}^{-1}$
L_i^p	Loss of pool i by decomposition in model compartment $p^{a,b}$	$\text{kg m}^{-2} \text{yr}^{-1}$ / $\text{kg m}^{-3} \text{yr}^{-1}$
$J_i^{p \rightarrow q}$	Bioturbation flux of pool i from model compartment p to $q^{a,b,d}$	$\text{kg m}^{-2} \text{yr}^{-1}$
<i>Model input</i>		
k_i	Decomposition rate of pool i^c	yr^{-1}
T	Soil temperature ^{a,b,c}	K
E_a	Soil temperature response parameter ^c	K
W	Relative soil moisture content ^{a,b,c}	–
a	Soil moisture response parameter ^c	–
b	Soil moisture response parameter ^c	–
$\alpha_{i \rightarrow j}$	Factor for transformation of pool i to pool j^c	–
I_{RL}^{tot}	Total root litter input in the soil profile ^{b,c}	$\text{kg m}^{-2} \text{yr}^{-1}$
β	Root litter distribution parameter ^c	m^{-1}
B	Bioturbation rate ^c	$\text{kg m}^{-2} \text{yr}^{-1}$
l_m	Mixing length ^c	m
D_{BT}	Diffusion coefficient due to bioturbation ^{a,b}	$\text{m}^2 \text{yr}^{-1}$
v	Advection rate ^{c,d}	m yr^{-1}
ρ^p	Bulk density in model compartment $p^{a,b,c}$	kg m^{-3}
ρ_M, ρ_O	Pure mineral and pure organic bulk density ^c	kg m^{-3}
<i>Other variables</i>		
z	Depth ^{a,d}	m
t	Time ^b	yr
f_i^p	Mass fraction of organic matter pool i in model compartment $p^{a,b}$	–
L	Depth of the lower boundary ^c	m
<i>Model compartments (superscripts)</i>		
L	L horizon	N/A
F	F horizon	N/A
H	H horizon	N/A
MS	Mineral soil	N/A
<i>Organic matter pools (subscripts)</i>		
AGL	Aboveground litter	N/A
FL	Fragmented litter	N/A
RL	Root litter	N/A
NLS	Non-leachable slow OM	N/A
LS	Leachable slow OM	N/A
O	Organic matter, sum of all pools	N/A

^a Depth and/or model compartment dependent

^b Time dependent

^c Input parameter

^d Positive downward

2.A.2 Litter input

External input of organic matter occurs for the aboveground litter pool I_{AGL}^L and for the root litter pool $I_{\text{RL}}^{\text{tot}}$. The total root litter input is distributed over the soil profile according to an exponential function of depth which starts at the top of the F horizon:

$$I_{\text{RL}}(z) = I_{\text{RL}}^{\text{tot}} \beta \exp(-\beta(z + \Delta z^F + \Delta z^H)), \quad (2.12)$$

where $I_{\text{RL}}^{\text{tot}}$ is the total root litter production ($\text{kg m}^{-2} \text{yr}^{-1}$), β (m^{-1}) is a shape parameter, and Δz^F and Δz^H are the thickness (m) of the F and H horizon, respectively, and are determined from the total mass of each layer and its bulk density:

$$\Delta z^F = \frac{C_{\text{O}}^F}{\rho^F} = \frac{C_{\text{FL}}^F + C_{\text{RL}}^F}{\rho^F}, \quad (2.13)$$

$$\Delta z^H = \frac{C_{\text{O}}^H}{\rho^H} = \frac{C_{\text{FL}}^H + C_{\text{RL}}^H + C_{\text{NLS}}^H}{\rho^H}. \quad (2.14)$$

The root litter input into the F and H horizon is obtained by integrating (2.12) over the horizon thickness:

$$I_{\text{RL}}^F = \int_{-\Delta z^H - \Delta z^F}^{-\Delta z^H} I_{\text{RL}}(z) dz, \quad (2.15)$$

$$I_{\text{RL}}^H = \int_{-\Delta z^H}^0 I_{\text{RL}}(z) dz. \quad (2.16)$$

2.A.3 Bulk density

If mineral soil bulk density is unknown it is estimated according to a function from Federer et al. (1993):

$$\rho^{\text{MS}} = \frac{\rho_{\text{M}} \rho_{\text{O}}}{f_{\text{O}}^{\text{MS}} \rho_{\text{M}} + (1 - f_{\text{O}}^{\text{MS}}) \rho_{\text{O}}}, \quad (2.17)$$

where ρ_{M} and ρ_{O} are bulk densities for hypothetical pure mineral and pure organic soil and f_{O} is the mass fraction organic matter:

$$f_{\text{O}} = \frac{C_{\text{O}}^{\text{MS}}}{\rho^{\text{MS}}} = \frac{C_{\text{FL}}^{\text{MS}} + C_{\text{RL}}^{\text{MS}} + C_{\text{NLS}}^{\text{MS}} + C_{\text{LS}}^{\text{MS}}}{\rho^{\text{MS}}}. \quad (2.18)$$

Substituting (2.18) into (2.17) and rearranging yields:

$$f_{\text{O}}^{\text{MS}} = \frac{C_{\text{O}}^{\text{MS}} \rho_{\text{O}}}{\rho_{\text{O}}^{\text{MS}} (C_{\text{O}}^{\text{MS}} + \rho_{\text{M}}^{\text{MS}}) - \rho_{\text{M}}^{\text{MS}} C_{\text{O}}^{\text{MS}}}, \quad (2.19)$$

and:

$$\rho^{\text{MS}} = \frac{\rho_{\text{O}}^{\text{MS}} (C_{\text{O}}^{\text{MS}} + \rho_{\text{M}}^{\text{MS}}) - \rho_{\text{M}}^{\text{MS}} C_{\text{O}}^{\text{MS}}}{\rho_{\text{O}}^{\text{MS}}}. \quad (2.20)$$

2.A.4 Organic matter transport

Fluxes between the organic horizons are determined by the bioturbation rate B . In case the stock in an organic horizon is zero, the bioturbation fluxes from that organic horizon are adjusted downward to the total input, if necessary, to avoid negative stocks. Thus, the bioturbation fluxes in the organic layer are defined as follows:

$$J_{\text{FL}}^{\text{F} \rightarrow \text{H}} = \begin{cases} f_{\text{FL}}^{\text{F}} B & \text{if } C_{\text{FL}}^{\text{F}} > 0 \\ \min [(I_{\text{AGL} \rightarrow \text{FL}}^{\text{L}} - L_{\text{FL}}^{\text{F}}), f_{\text{FL}}^{\text{F}} B] & \text{if } C_{\text{FL}}^{\text{F}} = 0 \end{cases}, \quad (2.21)$$

$$J_{\text{RL}}^{\text{F} \rightarrow \text{H}} = \begin{cases} f_{\text{RL}}^{\text{F}} B & \text{if } C_{\text{RL}}^{\text{F}} > 0 \\ \min [(I_{\text{RL}}^{\text{F}} - L_{\text{RL}}^{\text{F}}), f_{\text{RL}}^{\text{F}} B] & \text{if } C_{\text{RL}}^{\text{F}} = 0 \end{cases}, \quad (2.22)$$

$$J_{\text{FL}}^{\text{H} \rightarrow \text{MS}} = \begin{cases} f_{\text{FL}}^{\text{H}} B & \text{if } C_{\text{FL}}^{\text{H}} > 0 \\ \min [(J_{\text{FL}}^{\text{F} \rightarrow \text{H}} - L_{\text{FL}}^{\text{H}}), f_{\text{FL}}^{\text{H}} B] & \text{if } C_{\text{FL}}^{\text{H}} = 0 \end{cases}, \quad (2.23)$$

$$J_{\text{RL}}^{\text{H} \rightarrow \text{MS}} = \begin{cases} f_{\text{RL}}^{\text{H}} B & \text{if } C_{\text{RL}}^{\text{H}} > 0 \\ \min [(I_{\text{RL}}^{\text{H}} + J_{\text{RL}}^{\text{F} \rightarrow \text{H}} - L_{\text{RL}}^{\text{H}}), f_{\text{RL}}^{\text{H}} B] & \text{if } C_{\text{RL}}^{\text{H}} = 0 \end{cases}, \quad (2.24)$$

$$J_{\text{NLS}}^{\text{H} \rightarrow \text{MS}} = \begin{cases} f_{\text{NLS}}^{\text{H}} B & \text{if } C_{\text{NLS}}^{\text{H}} > 0 \\ \min [(F_{\text{NLS}}^{\text{F}} + F_{\text{NLS}}^{\text{H}} - L_{\text{NLS}}^{\text{H}}), f_{\text{NLS}}^{\text{H}} B] & \text{if } C_{\text{NLS}}^{\text{H}} = 0 \end{cases}, \quad (2.25)$$

where f_i^p is the mass fraction of pool i in compartment p :

$$f_i^p = \frac{C_i^p}{C_{\text{O}}^p} = \frac{C_i^p}{C_{\text{FL}}^p + C_{\text{RL}}^p + C_{\text{NLS}}^p + C_{\text{LS}}^p}. \quad (2.26)$$

Note that C_{LS}^p is zero for the organic horizons. In the mineral soil, transport by bioturbation is modelled according to the diffusion equation. The transport due to bioturbation for any pool i (except aboveground litter) is defined as:

$$\left. \frac{\partial C_i}{\partial t} \right|_{\text{BT}} = D_{\text{BT}} \frac{\partial^2 C_i}{\partial z^2}, \quad (2.27)$$

where the diffusion coefficient D_{BT} is defined according to:

$$D_{\text{BT}} = \frac{1}{2} \frac{B}{\rho_{\text{MS}}} l_m. \quad (2.28)$$

Advective transport of the LS pool in the mineral is modelled according to:

$$\left. \frac{\partial C_{\text{LS}}}{\partial t} \right|_{\text{adv}} = -v \frac{\partial C_{\text{LS}}}{\partial z}. \quad (2.29)$$

2.A.5 Governing equations

Organic layer

The complete mass balance equations for the organic matter pools in the organic layer are as follows:

$$\frac{\partial C_{AGL}^L}{\partial t} = I_{AGL}^L - L_{AGL}^L, \quad (2.30)$$

$$\frac{\partial C_{FL}^F}{\partial t} = F_{FL}^L - L_{FL}^F - J_{FL}^{F \rightarrow H}, \quad (2.31)$$

$$\frac{\partial C_{RL}^F}{\partial t} = I_{RL}^F - L_{RL}^F - J_{RL}^{F \rightarrow H}, \quad (2.32)$$

$$\frac{\partial C_{FL}^H}{\partial t} = J_{FL}^{F \rightarrow H} - L_{FL}^H - J_{FL}^{H \rightarrow MS}, \quad (2.33)$$

$$\frac{\partial C_{RL}^H}{\partial t} = I_{RL}^H + J_{RL}^{F \rightarrow H} - L_{RL}^H - J_{RL}^{H \rightarrow MS}, \quad (2.34)$$

$$\frac{\partial C_{NLS}^H}{\partial t} = F_{NLS}^F + F_{NLS}^H - L_{NLS}^H - J_{NLS}^{H \rightarrow MS}. \quad (2.35)$$

Mineral soil

The complete mass balance equations for the organic matter pools in the mineral soil are as follows:

$$\frac{\partial C_{FL}^{MS}}{\partial t} = D_{BT} \frac{\partial^2 C_{FL}^{MS}}{\partial z^2} - L_{FL}^{MS}, \quad (2.36)$$

$$\frac{\partial C_{RL}^{MS}}{\partial t} = D_{BT} \frac{\partial^2 C_{RL}^{MS}}{\partial z^2} + I_{RL}^{MS} - L_{RL}^{MS}, \quad (2.37)$$

$$\frac{\partial C_{NLS}^{MS}}{\partial t} = D_{BT} \frac{\partial^2 C_{NLS}^{MS}}{\partial z^2} + F_{NLS}^{MS} - L_{NLS}^{MS}, \quad (2.38)$$

$$\frac{\partial C_{LS}^{MS}}{\partial t} = D_{BT} \frac{\partial^2 C_{LS}^{MS}}{\partial z^2} - v \frac{\partial C_{LS}^{MS}}{\partial z} + F_{LS}^{MS} - L_{LS}^{MS}. \quad (2.39)$$

2.A.6 Boundary conditions

Upper boundary

The upper boundary conditions for the organic matter pools in the mineral soil are determined by the flux from the organic layer:

$$\left[-D_{BT} \frac{\partial C_{FL}^{MS}}{\partial z} \right]_{z=0} = J_{FL}^{H \rightarrow MS}, \quad (2.40)$$

$$\left[-D_{\text{BT}} \frac{\partial C_{\text{RL}}^{\text{MS}}}{\partial z} \right]_{z=0} = J_{\text{RL}}^{\text{H} \rightarrow \text{MS}}, \quad (2.41)$$

$$\left[-D_{\text{BT}} \frac{\partial C_{\text{NLS}}^{\text{MS}}}{\partial z} \right]_{z=0} = J_{\text{NLS}}^{\text{H} \rightarrow \text{MS}}. \quad (2.42)$$

Since LS-OM formed in the organic layer is assumed to flow immediately into the mineral soil, the upper boundary condition for this pool is defined as the total production in the organic layer:

$$\left[-D_{\text{BT}} \frac{\partial C_{\text{LS}}^{\text{MS}}}{\partial z} + v C_{\text{LS}}^{\text{MS}} \right]_{z=0} = F_{\text{LS}}^{\text{F}} + F_{\text{LS}}^{\text{H}}. \quad (2.43)$$

Lower boundary

For all organic matter pools a zero flux boundary condition is used at depth L :

$$\left[\frac{\partial C_{\text{FL}}^{\text{MS}}}{\partial z} \right]_{z=L} = 0, \quad (2.44)$$

$$\left[\frac{\partial C_{\text{RL}}^{\text{MS}}}{\partial z} \right]_{z=L} = 0, \quad (2.45)$$

$$\left[\frac{\partial C_{\text{NLS}}^{\text{MS}}}{\partial z} \right]_{z=L} = 0, \quad (2.46)$$

$$\left[\frac{\partial C_{\text{LS}}^{\text{MS}}}{\partial z} \right]_{z=L} = 0. \quad (2.47)$$

2.A.7 Numerical solution

Equations (2.30–2.39) with boundary conditions (2.40–2.47) are solved numerically using finite differencing, in the order as they are listed above. The organic matter pools in the organic layer are updated using an explicit scheme, while for the mineral soil an implicit scheme, with upwind differencing for the advection term, is used.

At the end of each time step, the thickness of the mineral soil layers are updated for change of mass. For any compartment n the layer thickness updated according to:

$$\Delta z^{n,\text{new}} = \Delta z^{n,\text{old}} \frac{M_{\text{tot}}^{n,\text{new}}}{M_{\text{tot}}^{n,\text{old}}}, \quad (2.48)$$

where $M_{\text{tot}}^{n,\text{new}}$ and $M_{\text{tot}}^{n,\text{old}}$ are the total compartment mass (kg m^{-2} ; mineral plus organic) for the previous and current time step, respectively. Next, the concentrations of the fractions are recalculated to assure conservation of mass:

$$C_i^{n,\text{new}} = \frac{M_i^{n,\text{new}}}{\Delta z^{n,\text{new}}}. \quad (2.49)$$

Appendix 2.B Derivation of the diffusion equation for bioturbation

Here we derive Fick's diffusion equation from the underlying principles mixing in soils, following mixing length theory. Our derivation is based on Boudreau (1986b) and Hinze (1975, ch. 1 and 5). It must be noted that the derivation is only valid under certain conditions, which are discussed in the main text of this paper, and more extensively in Boudreau (1986b) and Meysman et al. (2003). Alternatively, bioturbation may be pictured as a random walk process (Meysman et al., 2003). This representation is analogous to the turbulent mixing picture presented here and also leads to the diffusion equation in the limiting case.

Bioturbation is the average effect of many short term mixing events—displacements of mass elements of the soil matrix. These mixing events are stochastic in the sense that they occur at random times and depths in the profile. Ignoring bulk density changes, we assume that the average mass displacement is isotropic, i.e. equal in all directions. Here we focus only on the vertical component of the mixing. Since a soil constituent is moved together with the soil matrix, its concentration is a stochastic variable as well. For a single mixing event, the transport of a soil constituent will be of an advective nature (not to be confused the advection caused by liquid phase transport). Material is moved at a certain rate w over a certain distance l . Hence a constituent with local concentration c is will be transported according to:

$$J = wc . \quad (2.50)$$

Since w and c are stochastic variables, we can apply Reynolds decomposition to split them into smooth, time-averaged components, \bar{w} and \bar{c} , and random fluctuating components, w' and c' .

$$\begin{aligned} w &= \bar{w} + w' \\ c &= \bar{c} + c' . \end{aligned} \quad (2.51)$$

Substituting equation (2.51) into (2.50) yields:

$$J = (\bar{w}\bar{c} + w'\bar{c} + \bar{w}c' + w'c') . \quad (2.52)$$

To obtain the average flux as a result of many stochastic mixing events we use time-averaging, to which applies: $\overline{pq'} = 0$, for any two stochastic variables p and q . Furthermore, since the bioturbation process is isotropic, there is on average no net transport in any direction, i.e. $\bar{w} = 0$. Hence, the time-averaged flux is:

$$\bar{J} = \overline{w'c'} . \quad (2.53)$$

If the mixing distance l (which is also a stochastic quantity) is small with respect to the concentration gradient, we can approximate the fluctuation of the concentration with the first order depth derivative of \bar{c} :

$$c' \approx -\frac{1}{2}l' \frac{\partial \bar{c}}{\partial z} . \quad (2.54)$$

Substituting (2.54) into (2.53) yields:

$$\bar{J} \approx \frac{1}{2} \overline{w'l'} \frac{\partial \bar{c}}{\partial z}. \quad (2.55)$$

Thus, the average transport of a soil constituent is controlled by its concentration gradient and the relationship between w' and l' . In turbulent flow, $\overline{w'l'}$ specifies the combined transport by eddies of all length scales. In bioturbation, this term specifies the combined effect of mixing events over all distances. The critical assumption in mixing length theory is that most of the mixing occurs over a typical distance, the mixing length l_m , and that mixing over other distances is negligible. In that case, $\overline{w'l'}$ can be rewritten as:

$$\overline{w'l'} \approx \overline{|w'|} l_m, \quad (2.56)$$

where $\overline{|w'|}$ represents the average transport rate, independent of direction. $\overline{|w'|}$ is presumably directly related to the soil fauna activity. If we convert the soil reworking activity B (mass area⁻¹ time⁻¹) to units of volume (volume area⁻¹ time⁻¹), we obtain a units of speed (length time⁻¹). Hence we propose that $\overline{|w'|}$ can be approximated by:

$$\overline{|w'|} \approx \frac{B}{\rho}, \quad (2.57)$$

where ρ is the bulk density of the soil matrix. Taking the divergence of (2.55) and defining a diffusion coefficient as:

$$D \equiv \frac{1}{2} \frac{B}{\rho} l_m, \quad (2.58)$$

we obtain the diffusion equation:

$$\frac{\partial \bar{c}}{\partial t} \approx \frac{\partial}{\partial z} \left[D \frac{\partial \bar{c}}{\partial z} \right]. \quad (2.59)$$

Chapter 3

Modelling the vertical soil organic matter profile using Bayesian parameter estimation

The vertical distribution of soil organic matter (SOM) in the profile may constitute an important factor for soil carbon cycling. However, the formation of the SOM profile is currently poorly understood due to equifinality, caused by the entanglement of several processes: input from roots, mixing due to bioturbation, and organic matter leaching. In this study we quantified the contribution of these three processes using Bayesian parameter estimation for the mechanistic SOM profile model SOMPROF. Based on organic carbon measurements, 13 parameters related to decomposition and transport of organic matter were estimated for two temperate forest soils: an Arenosol with a mor humus form (Loobos, The Netherlands), and a Cambisol with mull type humus (Hainich, Germany). Furthermore, the use of the radioisotope $^{210}\text{Pb}_{\text{ex}}$ as tracer for vertical SOM transport was studied. For Loobos the calibration results demonstrate the importance of organic matter transport with the liquid phase for shaping the vertical SOM profile, while the effects of bioturbation are generally negligible. These results are in good agreement with expectations given in situ conditions. For Hainich the calibration offered three distinct explanations for the observations (three modes in the posterior distribution). With the addition of $^{210}\text{Pb}_{\text{ex}}$ data and prior knowledge, as well as additional information about in situ conditions, we were able to identify the most likely explanation, which indicated that root litter input is a dominant process for the SOM profile. For both sites the organic matter appears to comprise mainly adsorbed but potentially leachable material, pointing to the importance of organo-mineral interactions. Furthermore, organic matter in the mineral soil appears to be mainly derived from root litter, supporting previous studies that highlighted the importance of root input for soil carbon sequestration. The $^{210}\text{Pb}_{\text{ex}}$ measurements added only slight additional constraint on the estimated parameters. However, with sufficient replicate measurements and possibly in combination with other tracers, this isotope may still hold value as tracer for SOM transport.

Based on: M. C. Braakhekke, T. Wutzler, C. Beer, J. Kattge, M. Schrumpf, B. Ahrens, I. Schöning, M. R. Hoosbeek, B. Kruijt, P. Kabat, and M. Reichstein
Biogeosciences 10 (2013): 399–420

3.1 Introduction

The current lack of understanding of the soil system forms an important contribution to the uncertainty of terrestrial carbon cycle predictions (Heimann and Reichstein, 2008; Trumbore, 2009). To improve simulation of soil carbon cycling, it is necessary to move beyond the simple description of organic matter decomposition that is currently being applied in most large scale models (Reichstein and Beer, 2008). Increasing evidence indicates that decomposition and stabilization are controlled by a range of mechanisms that depend on physical, chemical, and biological factors (von Lützow et al., 2006). These factors vary laterally at landscape scale in relation to climate, vegetation, and soil type. In the vertical dimension, however, they change on a scale of centimeters to meters, since most drivers (e.g. wetting, heating, organic matter input) are exerted on the soil at or near the surface, propagating downwards. Consequently, the conditions that determine soil carbon cycling are highly depth-dependent and different mechanisms may be operating in different layers within one profile (Rumpel et al., 2002; Salomé et al., 2010; Rumpel and Kögel-Knabner, 2011). Therefore, aggregation of processes and soil properties over the profile, or downward extrapolation of topsoil organic carbon, as used in many SOM models (e.g. Parton et al., 1987; Tuomi et al., 2009), is likely an oversimplification, inadequate to support new parameterizations of relevant processes.

Awareness of this problem has spurred recent efforts to develop models that predict the vertical distribution of SOM, based on explicit descriptions of carbon deposition processes in the profile (Jenkinson and Coleman, 2008; Koven et al., 2009, chapter 2). In most soils there are three mechanisms by which organic carbon can be input at any given depth: (i) Organic matter may be deposited in situ by root exudation, sloughing off of root tissue, and root turnover. (ii) Organic matter is transferred within the profile due to movement with the liquid phase. This type of transport is of an advective nature and affects only fractions that are potentially mobile: mainly dissolved and to a lesser degree colloidal organic matter. (iii) Downward dispersal of organic matter occurs due to mixing of the soil matrix. Soil mixing is mostly caused by bioturbation – the reworking activity of soil animals and plant roots – and its effects on organic matter may be simulated mathematically as diffusion, provided the time and space scale of the model are sufficiently large (Boudreau, 1986b, section 2.2.4).

The processes involved in SOM deposition in the profile – root input, liquid phase transport, and bioturbation – are fundamentally different, not only in a physical and mathematical sense, but also in terms of their relationship with environmental factors. Therefore, in order for a SOM profile model to be robust over different ecosystems and soil types, and over changing environmental conditions, the relevant processes should be explicitly represented. Furthermore, the distribution of organic matter over particulate and potentially mobile fractions needs to be accounted for.

Unfortunately, the different processes have been poorly quantified to this date. Published results are inconsistent and past studies have generally focused on a single mechanism, rather than comparing all three (Rasse et al., 2005; Kaiser and Guggenberger, 2000; Tonneijck and Jongmans, 2008). Their extremely low rates, as well

as practical problems impede direct measurements of these processes in the field. Furthermore, the fact that the mechanisms are acting simultaneously complicates inference from SOM profile measurements. Diffusion and advection of decaying compounds such as organic matter, can produce very similar concentration profiles, despite the different natures of these processes. Moreover, root input closely follows the root biomass distribution, which often strongly resembles the SOM profile. Hence, it is generally not possible to derive the rate of each process from the organic carbon profile alone, unless strong assumptions are made. A model that includes all relevant processes may be able to explain an observed soil carbon profile by several different mechanisms – a problem referred to as equifinality (Beven and Freer, 2001).

Thus, additional information is required in order to parameterize dynamic SOM profile models. In past studies, ^{13}C and ^{14}C have been used as tracers to this purpose (Elzein and Balesdent, 1995; Freier et al., 2010; Baisden et al., 2002). Although these isotopes are particularly useful for constraining organic matter turnover times and carbon pathways, their precise information content with respect to the processes involved in SOM profile formation is less clear, since root input leads to direct input of ^{13}C and ^{14}C at depth. In this context, fallout radio-isotopes (e.g. ^{137}Cs , ^{134}Cs , $^{210}\text{Pb}_{\text{ex}}$, ^7Be) may be more effective. Such tracers have two major advantages over carbon isotopes: (i) loss occurs only due to radioactive decay, which is constant and exactly known; and (ii) input occurs only at the soil surface – direct input at depth is negligible. These points imply that the vertical transport rate of such isotopes can be directly inferred from their concentration profiles (Kaste et al., 2007; He and Walling, 1997). Since many radio-isotopes sorb strongly to organic matter molecules, they offer an effective alternative or complement to carbon isotopes for inferring organic matter transport rates in soils (Dörr and Münnich, 1989, 1991). Particularly $^{210}\text{Pb}_{\text{ex}}$ (^{210}Pb in excess of the in situ produced fraction) is a valuable tracer due to its strong adsorption to soil particles, and relatively constant fallout rate (Walling and He, 1999). Past studies have mostly used radio-isotopes for determining erosion and deposition rates (Mabit et al., 2009; Wakiyama et al., 2010), while their use for inferring vertical transport at stable sites has received little attention (Dörr and Münnich, 1989; Kaste et al., 2007; Arai and Tokuchi, 2010; Yoo et al., 2011).

The aim of this study is to examine SOM profile formation with model inversion. We used $^{210}\text{Pb}_{\text{ex}}$ concentration profiles, in addition to soil carbon measurements, to calibrate the model SOMPROF (chapter 2) for two forest sites with contrasting SOM profiles. SOMPROF is a vertically explicit SOM model that simulates the distribution of organic matter over the mineral soil profile and surface organic layers. The aim of the model is to represent SOM profile formation over time scales of years to centuries. It includes simple but explicit representations of the relevant processes: bioturbation, liquid phase transport, root litter input, and decomposition. SOMPROF was developed with large scale application in an earth system model in mind. It was shown to be able to produce SOM profiles that compare well to observations (chapter 2), but parameter sets for different soils and ecosystems have hitherto not been derived.

For both sites, 13 SOMPROF parameters were estimated. We focussed on un-

measurable parameters such as decomposition rate coefficients and organic matter transport rates. The model inversion was performed in a Bayesian framework, allowing prior knowledge of the model parameters to be included and to estimate their posterior uncertainty. In view of the limited understanding of the SOM profile, the aim of this study went beyond simply reducing the uncertainty ranges of the parameters. We also sought to gain qualitative understanding of the model's behavior, specifically its potential ability to explain observations by different mechanisms, and the value of $^{210}\text{Pb}_{\text{ex}}$ data and prior knowledge to improve parameter identification. This work also represents a first step towards testing the validity of SOMPROF for different soils and ecosystems.

We aim to answer the following questions: (i) What is the relative importance of the different processes involved in SOM profile formation? (ii) How much organic matter is present as material potentially transportable with the liquid phase, as compared to immobile particulate material? And, (iii) Are $^{210}\text{Pb}_{\text{ex}}$ profile measurements useful for constraining the model parameters?

3.2 Methods

3.2.1 The SOMPROF model

Here a brief overview of the SOMPROF model is presented. We focus specifically on the model equations in which the estimated parameters are applied, and the $^{210}\text{Pb}_{\text{ex}}$ module. A more exhaustive description and the rationale behind the model structure is presented in chapter 2.

In SOMPROF the soil profile is divided into the mineral soil and the surface organic layer, which is assumed to contain no mineral material and is further subdivided into three horizons: L, F and H (Figure 3.1). These organic horizons are simulated as homogeneous connected reservoirs of organic matter (OM). Decomposition products of litter generally flow from the L to the F horizon and from the F to the H horizon. Additionally, material may be transported downward between the organic horizons and into the mineral soil by bioturbation. For the mineral soil, which comprises both organic matter and mineral material, the model simulates the vertical distribution of the organic matter pools with a diffusion-advection model.

In view of the low rates of the relevant processes and lack of knowledge of initial conditions at the sites, the SOMPROF simulations in this study covered the complete period of SOM profile formation, starting without any organic carbon in the profile. The model was run with a time step length of one month (1/12 yr), for a specified maximum number of years, depending on the age and history of the site, and was driven by repeated annual cycles of measured or estimated soil temperature, moisture and (root) litter production. The main reason for considering temperature and moisture was to remove effects of local climate from the estimated decomposition rate coefficients, which thus are more intrinsic quantities, influenced mostly by local soil and vegetation properties. Furthermore, seasonal fluctuations of the forcing variables were accounted for since the timing of oscillations may have effects on long

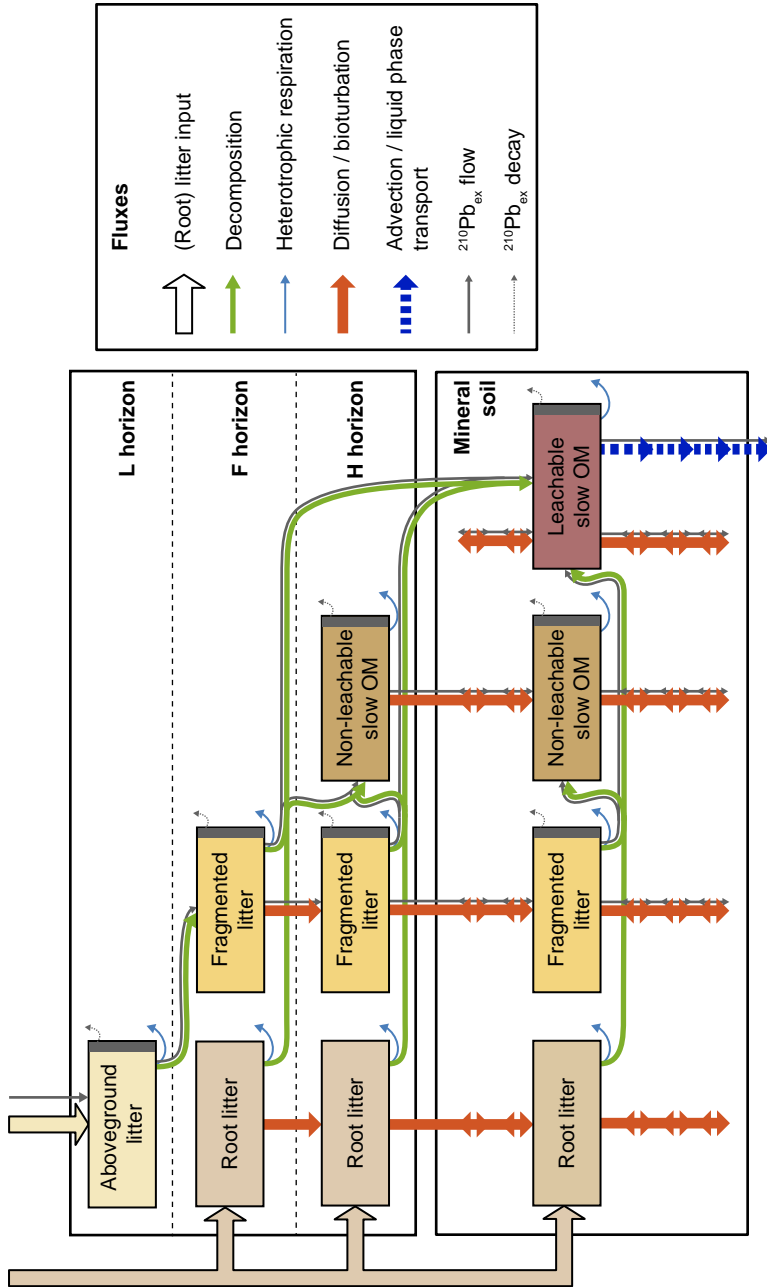


Figure 3.1: Overview of the SOMPROF model and the $^{210}\text{Pb}_{\text{ex}}$ module. The dark gray rectangles indicate $^{210}\text{Pb}_{\text{ex}}$ associated with the organic matter pools.

time scales due to non-linear interactions in the model. We limited the forcing cycle to one year because inter-annual variability is expected to be small compared to seasonal fluctuations and the available measurements were not sufficient to derive longer cycles.

Organic matter pools and decomposition

Organic matter simulated in SOMPROF comprises five pools (Figure 3.1), representing fractions that differ with respect to decomposability, transport behavior, and mechanism of input: aboveground litter (AGL), fragmented litter (FL), root litter (RL), non-leachable slow organic matter (NLS), and leachable slow organic matter (LS). Aboveground and root litter receive external input; fragmented litter and leachable and non-leachable slow OM are formed by decomposition. LS is absent in the organic horizons since the adsorptive capacity there is assumed to be negligible compared to that of the mineral soil.

Organic matter decomposition is simulated as a first-order decay flux, corrected for soil temperature and moisture. For any organic matter pool i the decomposition flux L_i is defined as:

$$L_i = f(T) g(W) k_i C_i, \quad (3.1)$$

where C_i is the concentration (kg m^{-3} , for the mineral soil) or the stock (kg m^{-2} , for the organic horizons), k_i is the decomposition rate coefficient (yr^{-1}) at 10°C and optimal soil moisture, and $f(T)$ and $g(W)$ are response functions for soil temperature and moisture (see section 2.2.3). To avoid errors due to smoothing of the temperature and moisture data to monthly values, the response factors were calculated for the unsmoothed, daily measurements. These response factors were subsequently averaged to monthly values and several years of data were averaged to an average annual cycle, which was used to calculate the decomposition fluxes.

The formation of fragmented litter, non-leachable, and leachable slow OM is defined according to a transformation fraction ($\alpha_{i \rightarrow j}$) which determines the decomposition flux $F_{i \rightarrow j}$ from donor pool i to the receiving pool j :

$$F_{i \rightarrow j} = \alpha_{i \rightarrow j} L_i. \quad (3.2)$$

The organic matter that does not flow to other pools is assumed to be lost as CO_2 .

For the calibration measured organic carbon amounts were always compared to total simulated organic carbon, summed over all pools. Mass fraction in the mineral soil layers was calculated as the organic carbon mass divided by the total mass (mineral plus organic) in each layer. Effective decomposition rate coefficients were determined by dividing the total simulated heterotrophic respiration by the total organic matter stock of the respective layers.

Organic matter transport

All organic matter pools except aboveground litter are transported by bioturbation at equal rate. Conversely, only the leachable slow organic matter pool is transported

by liquid phase transport. All transport parameters are assumed constant and independent of depth, although the diffusivity of organic matter may vary with depth due to bulk density variations (see Equation 3.4).

For the organic layer, organic matter transport due to bioturbation is determined by the bioturbation rate B ($\text{kg m}^{-2} \text{yr}^{-1}$), which represents the mixing activity of the soil fauna, i.e. the amount of material being displaced per unit area and unit time. B is the maximum flux of organic matter that can be moved to the next horizon. In case the potential bioturbation flux for one time step exceeds the amount of organic matter in a horizon, it is adjusted downward. For the mineral soil, a diffusion model is applied to simulate transport due to bioturbation:

$$\left. \frac{\partial C_i}{\partial t} \right|_{\text{BT}} = D_{\text{BT}} \frac{\partial^2 C_i}{\partial z^2}, \quad (3.3)$$

where C_i is the local concentration of organic matter pool i (kg m^{-3}), z is depth in the mineral soil (m, positive downward; $z = 0$ at the top of the mineral soil), and t is time (yr). D_{BT} is the diffusivity ($\text{m}^2 \text{yr}^{-1}$) which is derived from the bioturbation rate according to mixing length theory, as follows (section 2.2.4):

$$D_{\text{BT}} = \frac{1}{2} \frac{B}{\rho^{\text{MS}}} l_{\text{m}}, \quad (3.4)$$

where ρ^{MS} is the local bulk density (kg m^{-3}), which is depth dependent and can either be set to measured values or calculated by the model. l_{m} is the mixing length (m) which links the bioturbation rate to the diffusivity. The upper boundary condition, at the top of the mineral soil, is determined by the flux of material coming from the H horizon.

Dissolved organic matter is not explicitly represented in SOMPROF. Instead, the combined effects of ad- and desorption and water flow on the concentration profile of the leachable slow organic matter pool are simulated as an effective advection process:

$$\left. \frac{\partial C_{\text{LS}}}{\partial t} \right|_{\text{LPT}} = -v \frac{\partial C_{\text{LS}}}{\partial z}, \quad (3.5)$$

where v is the effective organic matter advection rate (m yr^{-1}). Note that the LS pool represents *potentially* leachable material; the bulk of this organic matter is in fact immobile due to adsorption to the mineral phase. Hence, the LS pool is also transportable by bioturbation. The upper boundary condition for LS is determined by the total production in the organic layer.

For all pools a zero-gradient condition is used for the lower boundary. Hence only advection of LS can lead to a loss of organic matter by transport.

$^{210}\text{Pb}_{\text{ex}}$ simulation

^{210}Pb is a radiogenic isotope that is input into the soil due to both atmospheric deposition and in situ formation within the profile. The fallout fraction ($^{210}\text{Pb}_{\text{ex}}$) is

typically estimated as the difference between the total ^{210}Pb activity and the activity of ^{226}Ra , one of its precursors (Appleby and Oldfield, 1978).

A module has been added to SOMPROF in order to use measurements of $^{210}\text{Pb}_{\text{ex}}$ as a tracer for SOM transport (Figure 3.1). The modelled $^{210}\text{Pb}_{\text{ex}}$ concentration profile is controlled by atmospheric input, radioactive decay, and organic matter input, decomposition and transport. The $^{210}\text{Pb}_{\text{ex}}$ module is based on the following assumptions: (i) variations in time of the atmospheric $^{210}\text{Pb}_{\text{ex}}$ input are negligible; (ii) $^{210}\text{Pb}_{\text{ex}}$ is input only into the L horizon; (iii) once in the soil, $^{210}\text{Pb}_{\text{ex}}$ binds immediately and irreversibly to any organic matter pool; (iv) $^{210}\text{Pb}_{\text{ex}}$ “follows” the organic matter to which it is bound through the decomposition and transport processes; and (v) aside from transport, $^{210}\text{Pb}_{\text{ex}}$ is lost only due to radioactive decay, at a fixed rate of 0.0311 yr^{-1} .

Since $^{210}\text{Pb}_{\text{ex}}$ is only input into the L horizon, which contains no root litter, no $^{210}\text{Pb}_{\text{ex}}$ is associated with this pool. Furthermore, external input of organic matter as litter has a diluting effect on $^{210}\text{Pb}_{\text{ex}}$, while loss of organic matter as CO_2 leads to an increase of mass fraction. For the organic horizons, the $^{210}\text{Pb}_{\text{ex}}$ fluxes due to organic matter flow (either by transport or transformation to another pool) are calculated by multiplying the flux from a pool by its $^{210}\text{Pb}_{\text{ex}}$ mass fraction. For the mineral soil the transport equations are solved separately for $^{210}\text{Pb}_{\text{ex}}$ associated with the FL, NLS and LS pools.

Since the atmospheric deposition rate of $^{210}\text{Pb}_{\text{ex}}$ is not generally known, the $^{210}\text{Pb}_{\text{ex}}$ fractions were normalized relative to the fractions at the mineral soil surface for comparison with observations (see section 3.2.3). Thus, the exact input rate is trivial, and was set to 1. Mineral soil $^{210}\text{Pb}_{\text{ex}}$ mass fractions, used for comparing with measurements, were calculated as the total $^{210}\text{Pb}_{\text{ex}}$ amount, summed over all organic matter pools, divided by the total mass (mineral plus organic).

3.2.2 Site descriptions

Loobos

Loobos is a Scots pine (*Pinus sylvestris*) forest on a well drained, sandy soil in the Netherlands ($52^\circ 10' 0'' \text{ N}$; $5^\circ 44' 38'' \text{ E}$). The climate is temperate/oceanic with an average annual precipitation of 966 mm and an average temperature of 10°C (WUR, Alterra, 2011). The area, which was originally covered by shifting sands, was planted with pine trees in the early twentieth century. Currently, the forest floor is covered with a dense understorey of wavy hair grass (*Deschampsia flexuosa*) that roots primarily in the organic layer. Due to its young age, the soil is classified as Cambic or Haplic Arenosol (IUSS Working Group WRB, 2007; Smit, 1999), but shows clear signs of the onset of podzolization. Because of the high content of quartzitic sand ($> 94\%$) the soil is very poor, which is reflected by a low pH (3–4) and nutrient concentrations, and a virtual absence of soil fauna (Emmer, 1995; Smit, 1999). Organic matter is comprised mostly of mor humus in a thick organic layer of circa 11 cm, and

organic carbon fractions in the mineral soil are very low.

Half-hourly measurements of soil moisture and temperature were performed continuously at five depths (5, 13, 30, 60, 110 cm). Data for the period 1 May 2005 to 31 December 2008 was used to derive an average annual cycle of soil temperature and moisture which was used for the simulations. Additionally, aboveground litter fall measurements on a two to four weeks basis for the period 2000 to 2008 were used to derive an average annual cycle for aboveground litter input. Since the carbon content of the litter was not determined, we used a fixed C fraction of 50%. Bulk density was calculated by the model according to a function from Federer et al. (1993), based on hypothetical bulk densities of pure mineral and pure organic soil (set to 1400 and 150 kg m⁻³, respectively).

Annual root litter input for the understorey was taken from Smit and Kooijman (2001) (Table 3.1), who estimated root turnover in the same forest using root ingrowth cores. To account for seasonal fluctuations of the grass layer, the annual input of both above and belowground grass litter was distributed over the year using a function based on data taken from Veresoglou and Fitter (1984), which peaks around early June. The vertical distribution of understorey root litter input was set such that approximately 95% occurs in the organic layer (Figure 3.C.1), which corresponds to in situ observations of root biomass (A. Smit, personal communication, 2009). For the root litter input from the pine trees (Table 3.1) we used data from a forest in Belgium (Brasschaat) with a similar vegetation composition, soil type, and age (Janssens et al., 2002). The root litter input for Loobos was derived by scaling the estimate from the Janssens et al. (2002) study according to net primary productivity estimates of both sites, which were taken from Luyssaert et al. (2007). The root litter input from the canopy vegetation was held constant throughout the simulation. Its vertical distribution was also derived from information from Janssens et al. (2002), as well as personal communication from J. Elbers and I. Janssens (2009). At both the Brasschaat and Loobos sites it is observed that the root biomass starts at the top of the H horizon and peaks at the mineral soil surface. Therefore, we chose a distribution function that increases linearly with depth from the top to the bottom of the H horizon. From there it decreases with depth according to a two-term exponential function: $f(z) = \exp(-20.00z) + 0.0384 \exp(-0.886z)$ (Figure 3.C.1). By this function we accounted for deep soil input from pine roots which may be important for the vertical SOM profile. Since the thickness of the H horizon is variable, the total distribution function was normalized at every time step.

The simulation length was set to 95 yr, which is the approximate time between the forest plantation and the sampling date. To account for the time needed for vegetation to develop, litter input was reduced in the initial stage, by multiplying with a function linearly increasing from 0, at the start of the simulation, to 1, after 60 yr (Emmer, 1995).

Hainich

This site is located in the Hainich national park in Central Germany, (51°4'45.36" N; 10°27'7.20" E). The forest, which has been unmanaged for the last 60–70 yr, is domi-

nated by beech (*Fagus Sylvatica*, 65 %) and ash (*Fraxinus excelsior*, 25 %) (Kutsch et al., 2010). The forest floor is covered by herbaceous vegetation (*Allium ursinum*, *Mercurialis perennis*, *Anemone nemorosa*) which peaks before canopy budbreak. The climate is temperate suboceanic/subcontinental with an average annual precipitation of 800 mm and an average temperature of 7–8 °C.

The soil is classified as Luvisol or Cambisol (IUSS Working Group WRB, 2007; Kutsch et al., 2010). It has formed in limestone overlain by a layer of loess, and is characterized by a high clay content (60 %) and a pH-H₂O of 5.9 to 7.8 (T. Persson, personal communication, 2011). The favorable soil properties support a high biological activity (Cesarz et al., 2007), corroborated by a thin organic layer and a well developed A horizon. About 90 % of the root biomass occurs above 40 cm depth. A similar distribution was used for the root litter input (Figure 3.C.1).

The oldest trees at Hainich are approximately 250 years old, but presumably the site has been covered by similar vegetation for much longer. Thus, we assumed that the soil is close to steady state, hence a 1000 yr simulation was used. For further information on the setup of the Hainich simulation we refer to the description of the reference simulation in section 2.3. The model inputs that were not included in the calibration are listed in Table 3.1.

3.2.3 Observations used for the calibration

Organic carbon measurements

For Loobos, measured carbon stocks in the L, F and H horizons and the mineral soil, and carbon mass fractions at 3 depths in the mineral profile were used in the calibration. Several profiles were affected by wind erosion; when this was the case, the affected measurements were omitted. In 2005 the soil was sampled in a regular quadratic grid at 25 points spaced 40 m apart. Organic layers were removed with a square metal frame with a side length of 25 cm. The mineral soil was sampled horizon-wise with a Pürckhauer auger, 2–3 cm wide and 1 m long. Soil samples were sieved to < 2 mm and ground. Carbon stocks in the organic layers were analyzed with a CN analyser Vario EL (Elementar Analysensysteme GmbH, Hanau, Germany); carbon fractions in the mineral soil were measured with a CN Analyser VarioMax (Elementar Analysensysteme GmbH, Hanau, Germany).

For Hainich measured stocks in the L and F/H horizon (the individual F and H horizons could not be identified), and in the mineral soil were used, as well as mass fraction measurements at 8 depths in the mineral profile. In addition, we used measured effective decomposition rate coefficients at 15 °C and soil moisture at 60 % of water holding capacity in the L and F/H horizon, and at 7 depths in the mineral profile. The sampling procedure and organic carbon measurements are described in Schrumpf et al. (2011). The decomposition rate coefficients were calculated from measurements of respiration rates measured during lab incubation of soil samples, which is described in Kutsch et al. (2010). By dividing the average respiration rate of each sample by its organic carbon content, we obtained effective decomposition rate coefficients. All measurements are listed in Table 3.C.1.

Table 3.1: Model driving data and not-estimated parameters.

Variable/Parameter	Loobos	Hainich	Units
Annual aboveground litter input	0.310	0.314 ^b	kg C m ⁻² yr ⁻¹
Canopy	0.255	0.277 ^b	
Understory	0.055 ^c	0.037 ^b	
Total annual root litter input	0.543	0.178 ^b	kg C m ⁻² yr ⁻¹
Canopy	0.118	0.148 ^b	
Understory	0.425 ^c	0.03 ^b	
Root litter distribution parameter	see text	7	m ⁻¹
Soil temperature response parameter	308.56 ^d	308.56 ^d	K
Soil moisture response parameter <i>a</i> ^e	1	1	–
Soil moisture response parameter <i>b</i> ^e	20	20	–
Soil temperature	^a	^a	K
Relative soil moisture content	^a	^a	–
Bulk density L layer	50	50	kg m ⁻³
Bulk density F layer	100	100	kg m ⁻³
Bulk density H layer	150	150	kg m ⁻³
Bulk density mineral soil	1400	^a	kg m ⁻³
Simulation period	95	1000	yr
Depth of bottom boundary	2	0.7	m

^a Variable in depth and/or time.

^b Kutsch et al. (2010); W. Kutsch (personal communication, 2009).

^c Smit and Kooijman (2001).

^d Lloyd and Taylor (1994).

^e Soil moisture response function: $g(W) = \exp(-\exp(a - bW))$.

Simulated organic carbon fractions and effective decomposition rate coefficients were interpolated to the measurement depths for comparing with measurements using piecewise Hermitian interpolation (Burden, 2004). Because organic carbon stocks and mass fractions cannot be less than zero and typically have large spatial variance, the measurements from replicate samplings can be assumed to have right-skewed distributions. We assumed that this is also the case for the effective decomposition rate measurements. Therefore, all measurements (and their corresponding model results) were log transformed for the calibration to bring the distributions closer to normal. This also reduced heteroscedasticity for the mineral soil organic carbon fractions.

²¹⁰Pb_{ex} measurements

Since local ²¹⁰Pb_{ex} measurements were not available for Loobos, we used two activity profiles from Kaste et al. (2007), for a site in the Hubbard Brook Experimental Forest, New Hampshire, USA. This site has conditions similar to those at Loobos in terms of vegetation, soil texture, soil pH, and soil biological activity (Bormann and Likens,

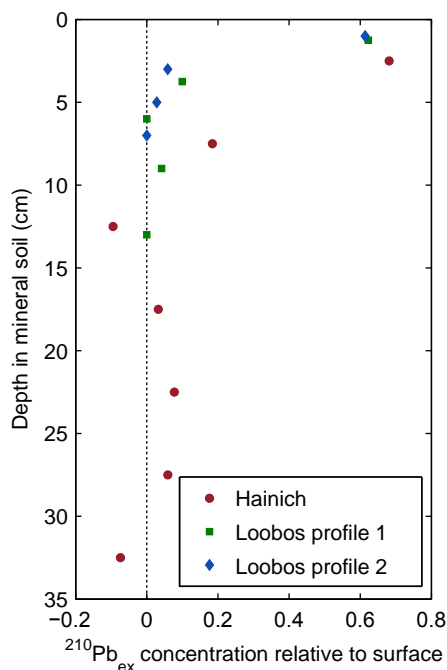


Figure 3.2: Measured $^{210}\text{Pb}_{\text{ex}}$ concentrations used for the calibration. Concentrations are relative to the values at the surface. Note that the $^{210}\text{Pb}_{\text{ex}}$ measurements for Loobos are taken from an equivalent site (Kaste et al., 2007).

1994). Furthermore, pedological processes related to podzol formation are occurring at both sites. The two sites differ with respect to age, since the Loobos soil is very young. However, in view of the relatively fast decay rate of ^{210}Pb , and the shallow distribution of the $^{210}\text{Pb}_{\text{ex}}$ profile (Figure 3.2), we assume that it is close to steady state at both sites.

Local $^{210}\text{Pb}_{\text{ex}}$ measurements at Hainich were performed for a study by Fujiyoshi and Sawamura (2004, R. Fujiyoshi, personal communication, 2008). Although these measurements were corrected for in situ formed ^{210}Pb by subtracting the ^{226}Ra activity (R. Fujiyoshi, personal communication, 2008), the activity profile did not approach zero with depth, hence this method did presumably not account for all supported ^{210}Pb . Therefore, we assumed that the $^{210}\text{Pb}_{\text{ex}}$ concentration is zero from approximately 12.5 cm downwards. The supported ^{210}Pb activity was estimated as the average below this depth, and all data was corrected by subtracting this average. (Note that in several cases this produced negative concentrations.)

Only mineral soil $^{210}\text{Pb}_{\text{ex}}$ measurements were used in the calibration (Figure 3.2 and Table 3.C.1). The profiles of both sites, as well as those predicted by the model, were normalized by dividing them by the $^{210}\text{Pb}_{\text{ex}}$ activity at the surface of the mineral soil, which was estimated using piecewise Hermitian extrapolation. Simulated

Table 3.2: The model parameters estimated in the calibration. Note that the prior distributions were only used for calibration setup 3. The lower bound for all parameters is zero; the upper bound is given in the table.

Parameter	Symbol	Units	Prior distribution in calibr. setup 3	Upper bound
Decomposition rate coefficients at 10°C and optimal soil moisture				
Aboveground litter	k_{AGL}	yr^{-1}	$\text{Log}-\mathcal{N}(-0.23, 0.74)$	3
Root litter	k_{RL}	yr^{-1}	$\text{Log}-\mathcal{N}(-0.23, 0.74)$	3
Fragmented litter	k_{FL}	yr^{-1}	$\text{Log}-\mathcal{N}(-0.23, 0.74)$	3
Non-leachable slow organic matter	k_{NLS}	yr^{-1}	$\text{Log}-\mathcal{N}(-2.23, 1.00)$	3
Leachable slow organic matter	k_{LS}	yr^{-1}	$\text{Log}-\mathcal{N}(-2.23, 1.00)$	3
Transformation fractions				
Aboveground litter–fragmented litter	$\alpha_{AGL \rightarrow FL}$	–	$\text{Logit}-\mathcal{N}(0.43, 0.95)$	1
Fragmented litter–non-leachable slow	$\alpha_{FL \rightarrow NLS}$	–	$\text{Logit}-\mathcal{N}(-0.93, 0.98)$	$1, (1 - \alpha_{FL \rightarrow LS})$
Fragmented litter–leachable slow	$\alpha_{FL \rightarrow LS}$	–	$\text{Logit}-\mathcal{N}(-0.93, 0.98)$	$1, (1 - \alpha_{FL \rightarrow NLS})$
Root litter–non-leachable slow	$\alpha_{RL \rightarrow NLS}$	–	$\text{Logit}-\mathcal{N}(-0.93, 0.98)$	$1, (1 - \alpha_{RL \rightarrow LS})$
Root litter–leachable slow	$\alpha_{RL \rightarrow LS}$	–	$\text{Logit}-\mathcal{N}(-0.93, 0.98)$	$1, (1 - \alpha_{RL \rightarrow NLS})$
Transport parameters				
Bioturbation rate	B	$\text{kg m}^{-2} \text{yr}^{-1}$	uniform	3
Mixing length	l_m	m	uniform	3
Liquid phase transport (advection) rate	v	m yr^{-1}	uniform	0.1

$^{210}\text{Pb}_{\text{ex}}$ fractions and effective decomposition rate coefficients were interpolated to the measurement depths also using Hermitian interpolation, for comparing with measurements. Because of the negative observed values for Hainich, no log-transformations was used for the $^{210}\text{Pb}_{\text{ex}}$ data.

3.2.4 Bayesian calibration

We performed Bayesian estimation of 13 model parameters: five decomposition rate coefficients, five transformation fractions, and three transport parameters (Table 3.2). Bayesian calibration is aimed at deriving the posterior probability distribution $p(\boldsymbol{\theta}|\mathbf{O})$ of the model parameters $\boldsymbol{\theta}$ based on the misfit between the model results and the observations \mathbf{O} , and the a priori probability distribution of the parameters (Mosegaard and Sambridge, 2002). According to Bayes' theorem, the posterior distribution is defined as:

$$p(\boldsymbol{\theta}|\mathbf{O}) = c p(\boldsymbol{\theta}) p(\mathbf{O}|\boldsymbol{\theta}), \quad (3.6)$$

where $p(\boldsymbol{\theta})$ is the prior probability distribution, expressing our knowledge of the parameters prior to the calibration, and c is a normalization constant, ensuring that the integral over the distribution equals 1. $p(\mathbf{O}|\boldsymbol{\theta})$ is a likelihood function which expresses the probability of the observations \mathbf{O} , given the parameters $\boldsymbol{\theta}$ (Gelman et al., 2004, Chap. 1).

The calibrations were performed in three setups, in which $^{210}\text{Pb}_{\text{ex}}$ data and prior knowledge were stepwise added, in order to investigate the information content of each source of information. For both sites, we ran calibrations in the following setups:

1. excluding $^{210}\text{Pb}_{\text{ex}}$ data and with weak priors;
2. including $^{210}\text{Pb}_{\text{ex}}$ data and with weak priors;
3. including $^{210}\text{Pb}_{\text{ex}}$ data and with strong priors.

Calibration setup 3 represents our best estimate of the model parameters.

Likelihood function

As discussed in section 3.2.3, different types of observed variables were used in the calibration, referred to as “data streams”. For any data stream i the observations O_i may be seen as the sum of the model prediction $M_i(\boldsymbol{\theta})$ plus a stochastic residual term ϵ_i :

$$O_i = M_i(\boldsymbol{\theta}) + \epsilon_i, \quad i = 1, 2 \dots I \quad (3.7)$$

Note that for all data streams except $^{210}\text{Pb}_{\text{ex}}$ the model prediction and measurements were log-transformed. We assumed that the residuals are normally distributed with variance σ_i , which may be different for each data stream. The conditional likelihood function for a given σ_i is defined by the joint distribution of the residuals of all data streams:

$$p(\mathbf{O}|\boldsymbol{\theta}, \boldsymbol{\sigma}^2) \propto \prod_{i=1}^I \sigma_i^{-N_i} \exp\left(-\frac{1}{2\sigma_i^2} SS_i(\boldsymbol{\theta})\right). \quad (3.8)$$

Note that we did not consider correlations between the different variables. $SS_i(\boldsymbol{\theta})$ is the sum of squared residuals for data stream i over all N_i data points:

$$SS_i(\boldsymbol{\theta}) = \sum_{n=1}^{N_i} (O_{i,n} - M_{i,n}(\boldsymbol{\theta}))^2. \quad (3.9)$$

Multiple replicate measurements, if available, were all individually included in $S_i(\boldsymbol{\theta})$, meaning a single model prediction was compared to multiple observations. For the mineral soil profile measurements from all depth levels were considered to be part of the same data stream, i.e. the residuals were assumed to have the same distribution.

The variance of the residuals σ_i^2 is usually determined by both model related errors (deficiencies in the model structure, errors in forcing data) as well as observational uncertainty (spatial heterogeneity, measurement errors). In some cases it may

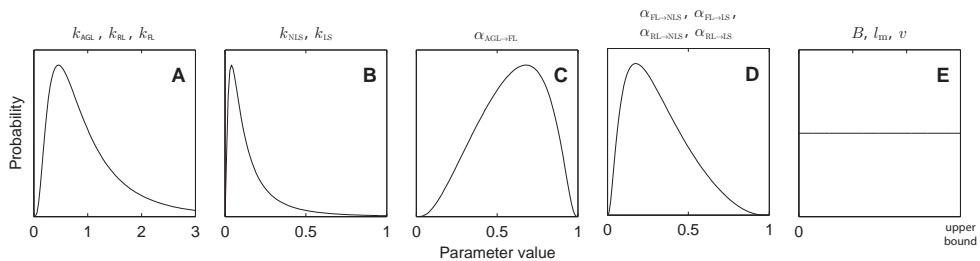


Figure 3.3: Prior probability distributions of the model parameters used for calibration setup 3. See Table 3.2 for the parameters of the distribution functions. All distributions are bounded at zero and an upper bound which are given in Table 3.2.

be estimated a priori based on knowledge of the model and the measurement uncertainty (Knorr et al., 2005; Rayner et al., 2005; van Oijen et al., 2005), but in general it must be considered unknown. For certain prior distributions σ_i can be analytically integrated out of the joint likelihood function $p(\mathbf{O}, \boldsymbol{\sigma}^2 | \boldsymbol{\theta})$, yielding the marginal distribution $p(\mathbf{O} | \boldsymbol{\theta})$ (Kavetski et al., 2006; Box and Tiao, 1992). We use the uninformative prior $p(\sigma_i) \propto 1/\sigma_i$, which yields the following formulation of the likelihood function:

$$p(\mathbf{O} | \boldsymbol{\theta}) \propto \prod_{i=1}^I SS_i(\boldsymbol{\theta})^{-N_i/2}. \quad (3.10)$$

Prior parameter distributions

We performed calibration with both strong and with weak prior distributions. For the runs with weak priors, the prior probability $P(\boldsymbol{\theta})$ was simply omitted from the posterior probability definition (Equation 4.2), which resulted in a multivariate uniform distribution, within the sampling region.

For the runs with strong priors, the distributions were based on knowledge from previously published studies (section 2.2.7). The same distributions were used for both sites. Since decomposition rate coefficients cannot be negative or zero, we chose a log-normal distribution. For the litter pools (k_{AGL} , k_{RL} and k_{FL}) we used the same distributions (mode at 0.46 yr^{-1} ; Figure 3.3a). It is likely that the decomposition rate coefficient of leachable slow organic matter (k_{LS}) is lower than that of non-leachable slow organic matter (k_{NLS}), since the former is comprised mostly of material adsorbed to the mineral phase. Nevertheless, since we aimed to test this hypothesis with the measurements, we used the same prior distributions for the decomposition rate coefficient of both pools (mode at 0.04 yr^{-1} ; Figure 3.3b).

We used logit-normal prior distributions for the transformation fractions. This distribution is similar to the beta distribution and is bounded between 0 and 1 (Mead, 1965). For $\alpha_{AGL \rightarrow FL}$ a distribution with the mode at 0.68 was used (Figure 3.3c), while for the other conversion fractions ($\alpha_{RL \rightarrow NLS}$, $\alpha_{RL \rightarrow LS}$, $\alpha_{FL \rightarrow NLS}$, and $\alpha_{FL \rightarrow LS}$) the same prior was used with the mode at 0.18 (Figure 3.3d). Since relatively little a priori

information about the SOM transport parameters (B , l_m , and v) is available, we used uniform priors for all calibrations (Figure 3.3e).

For all calibration setups, the sampling was constrained to a bounded region in parameter space. This constraint was included since preliminary runs showed that some parameters may be unconstrained at the upper bound by the data, due to over-parameterization. The lower bounds for all parameters were set to zero; the upper bounds are listed in Table 3.2. Additionally, since decomposition must not lead to a net formation of material, the sum of transformation fraction for root litter ($\alpha_{RL \rightarrow NLS} + \alpha_{RL \rightarrow LS}$) and fragmented litter ($\alpha_{FL \rightarrow NLS} + \alpha_{FL \rightarrow LS}$) pools was bounded to 1.

Monte Carlo simulations

The complexity of SOMPROF precludes analytical model inversion or expression of the normalizing constant in Equation (3.6). Therefore, we approximated the posterior distribution using a Markov Chain Monte Carlo algorithm. Such algorithms obtain a sample of the posterior distribution by performing a random walk through parameter space. They are increasingly used for calibrating ecosystem models against eddy-covariance measurements and satellite data (Knorr et al., 2005; Fox et al., 2009) and have been applied to calibrate soil carbon models as well (Yeluripati et al., 2009; Scharnagl et al., 2010; de Bruijn and Butterbach-Bahl, 2010). We used the Metropolis algorithm DREAM(ZS) (Laloy and Vrugt, 2012), a successor to DREAM (Vrugt et al., 2009), which has been shown to perform well for complex, multimodal distributions. Further information concerning the calibration setup can be found in Appendix 3.A.1.

Additionally, we performed forward Monte Carlo simulations based on the posterior distributions. 5000 simulations were made with parameter sets selected at regular intervals from the posterior sample. For these simulations the non-leachable slow (NLS) and leachable slow (LS) organic matter pools were split into fractions originating from fragmented litter (FL) and root litter (RL), in order to trace the source of organic matter. Otherwise, the setup of the simulations was the same as those made for the calibration runs.

To study the importance of root litter input, bioturbation, and liquid phase transport for the formation of the SOM profile, the contribution of these processes was quantified. We estimated the amount of organic carbon that would be derived from these three processes for the steady state, giving an indication of their importance for long time scales. Note that the organic carbon derived from root litter input also includes material that is transformed from root litter to the slow pools, NLS and LS. Furthermore, bioturbation and liquid phase transport can lead to a net loss of organic matter at a given depth, as opposed to root litter input which only leads to gain. Thus, the amount of organic carbon derived from the transport processes may be negative for certain depths. However, the sum of three organic carbon fractions must be positive. Further description of these calculations is given in Appendix 3.B.

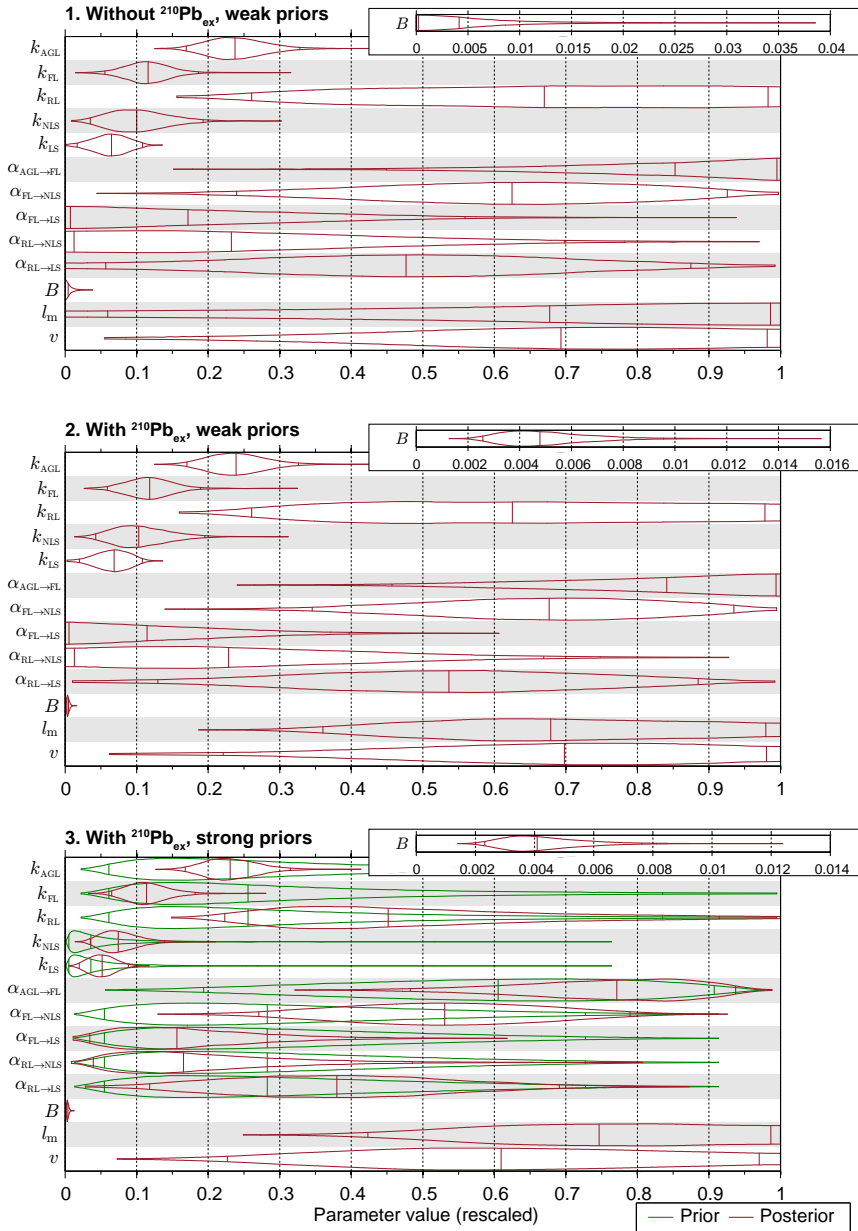


Figure 3.4: Posterior distributions for the three setups for Loobos. The “violins” depict the marginal distribution for each parameter. The three vertical lines inside the violins indicate the median and the 95 % confidence bounds. The parameters are normalized to the sampling ranges (see Table 3.2).

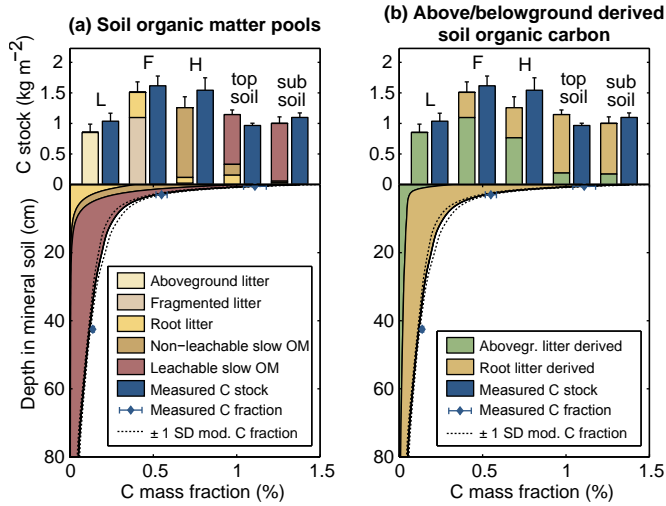


Figure 3.5: Organic carbon measurements and corresponding model results of forward Monte Carlo simulations for Loobos, based on posterior distribution of calibration setup 3. **a.** stocks and fractions of the model pools; **b.** above vs belowground derived organic matter. L, F, and H refer to the organic horizons (see section 3.2.1); topsoil: 0–30 cm; subsoil: > 30 cm; OM: organic matter. All model results are averages over the Monte Carlo ensemble; errorbars denote one standard error of the mean for the measurements and one standard deviation (SD) for the model results.

3.3 Results

3.3.1 Loobos

Figure 3.4 depicts the marginal posterior distributions for the three calibrations for Loobos (see also Table 3.C.2). For calibration setups 1 and 2 several parameters have wide distributions compared to the sampling range, which shows they are poorly constrained by the observations. Furthermore, for some of the parameters (k_{RL} , $\alpha_{FL \rightarrow LS}$, $\alpha_{RL \rightarrow NLS}$, l_m , and v) the highest density point appears to lie at or near the upper or lower bound. Adding $^{210}\text{Pb}_{\text{ex}}$ improved the constraint of the bioturbation related parameters (B and l_m) but had otherwise no major effect on the marginal distributions. Inclusion of prior knowledge reduced uncertainty, particularly for the parameters that are poorly constrained by the data.

The results of the forward simulations (Figure 3.5a, additional results shown in Figure 3.C.5) indicate that leachable slow organic matter (LS) is the most abundant pool, followed by non-leachable slow organic matter (NLS). LS particularly dominates the mineral soil, being virtually the only pool below 20 cm. Figure 3.5b shows that most organic matter in the mineral soil is derived from root litter, but above-ground derived SOM is present up to great depths, due to fast downward migration by liquid phase transport. Figure 3.6a shows the organic matter transport fluxes in

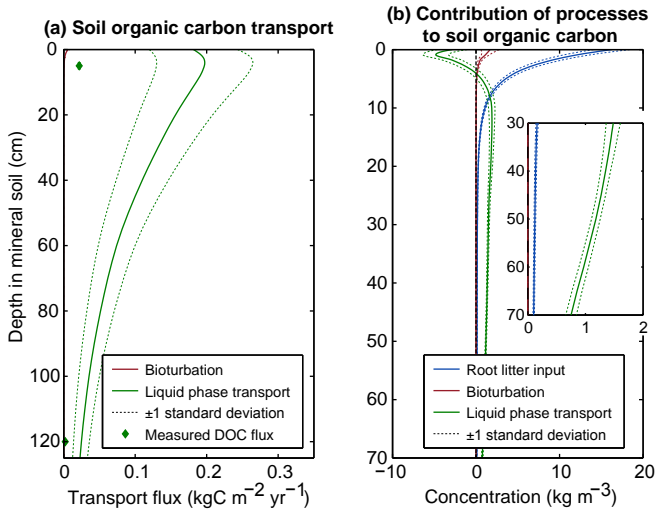


Figure 3.6: Simulated organic carbon fluxes from forward Monte Carlo simulations for Loo-bos, based on posterior distribution of calibration setup 3 (note the different scales on the y axes). All quantities are averages over the last simulation year and the Monte Carlo ensemble. **a.** organic carbon transport fluxes and measured dissolved organic carbon (DOC) fluxes (Kindler et al., 2011; not used in the calibration). Note the indistinct bioturbation flux in the upper left corner. **b.** Contributions of the different processes to soil organic matter profile in mineral soil (see section 3.2.4).

the mineral soil. Clearly, transport due to bioturbation plays almost no role; virtually all transport occurs by movement with the liquid phase. Figure 3.6b, which depicts the amount of organic carbon in the steady state derived from the three processes, corroborates the importance of liquid phase transport. The negative concentrations for this process indicate it causes organic matter from near the surface – mainly root litter derived – to be moved downward to greater depths, where it is the dominant mechanism of input.

3.3.2 Hainich

For Hainich the posterior distribution is multimodal for all calibration setups, comprising three distinct optima. For analysis the modes were sampled individually in separate calibration runs. An additional calibration run was performed in which all modes were sampled simultaneously to assure that the multimodality is not an artifact of the sampling (see Figure 3.C.4). The marginal distributions for all calibration setups and all modes are depicted in Figure 3.7 (see also Table 3.C.2). While the distributions of most parameters differ between the modes, the most prominent differences can be seen for the decomposition rate coefficients of root litter (k_{RL}), non-leachable slow (k_{NLS}), and leachable slow (k_{LS}) organic matter. For each of the modes, one of these three parameters is tightly constrained at the lower end of the

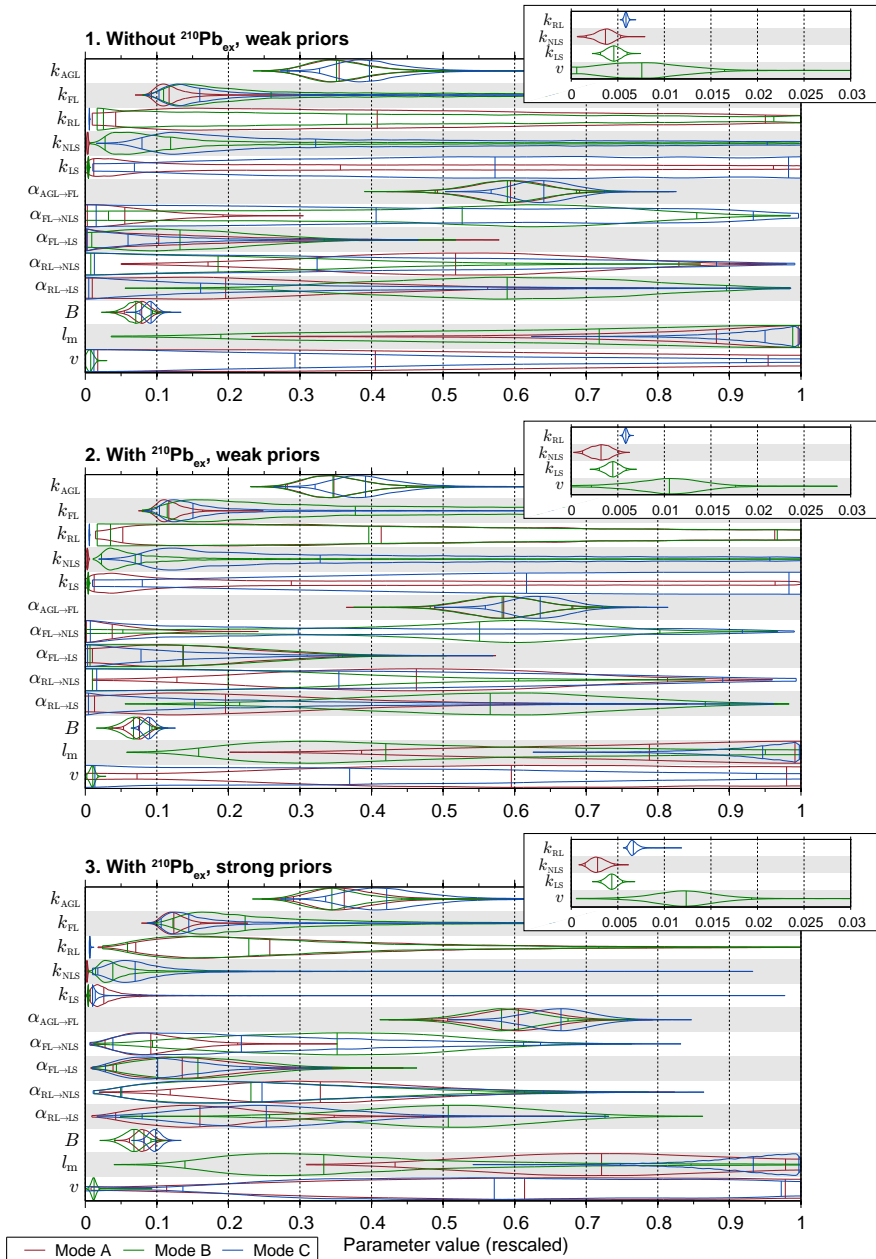


Figure 3.7: Posterior distributions for the three calibration setups for Hainich. The “violins” depict the marginal distribution for each parameter. The three posterior modes are plotted separately in the same graph. The three vertical lines inside the violins indicate the median and the 95% confidence bounds. The parameters are normalized to the sampling ranges (see Table 3.2).

Table 3.3: Minimum misfit value (see Equation 3.11) in the posterior sample for each of the modes for Hainich for the three calibration setups. Note that the misfit values of calibration setup 2 are lower than those of calibration setup 1. This is caused by the fact that the misfit values for the $^{210}\text{Pb}_{\text{ex}}$ are negative due to the small number of data points (cf Equation 3.10).

Calibration setup	Mode A	Mode B	Mode C
1: Excl. $^{210}\text{Pb}_{\text{ex}}$; weak priors	140.14	140.31	141.87
2: Incl. $^{210}\text{Pb}_{\text{ex}}$; weak priors	131.27	129.43	135.04
3: Incl. $^{210}\text{Pb}_{\text{ex}}$; strong priors	146.56	142.9	157.57

range, while the other two have wide distributions at higher values.

Addition of $^{210}\text{Pb}_{\text{ex}}$ to the observations caused shifts and reduction of uncertainty for some parameters (e.g. v for mode A, l_m for mode B), but had in general no major effects on the posterior. Changing from weak to strong priors reduced uncertainty for parameters that are poorly constrained by the observations.

The comparative probability of the modes cannot be inferred from Figure 3.7, since the distributions are scaled to the same height. To compare the modes we introduce the “misfit” $S(\theta)$ as the negative logarithm of the unnormalized posterior density (Mosegaard and Sambridge, 2002):

$$S(\theta) = -\ln(p(\theta) p(\mathbf{O}|\theta)) = -\ln(p(\theta)) - \sum_{i=1}^I \ln \left(SS_i(\theta)^{-N_i/2} \right), \quad (3.11)$$

where $SS_i(\theta)$ is defined according to Equation (9). A lower misfit indicates a higher posterior density and a better fit to the observations and priors. Note that the contribution of a single data stream to $S(\theta)$ may be negative for a high fit and/or small N_i . The modes are compared according to the lowest misfit in the calibration samples (Table 3.3). This shows that the three calibrations setups differ notably in terms of the comparative probability of the modes. In calibration 1 the three modes have similar misfit. Introduction of $^{210}\text{Pb}_{\text{ex}}$ and prior information to the calibration caused the misfit of mode C to increase markedly compared to A and B, which is explained by a somewhat poorer fit to the $^{210}\text{Pb}_{\text{ex}}$ measurements (results not shown), as well as the very low root litter decomposition rate coefficient, which conflicts with prior knowledge.

Figure 3.8a depicts the simulated organic matter stocks and fractions of the three modes for calibration setup 3 (additional results are shown in Figures 3.C.5 and 3.C.6). The different parameter values for the three modes give rise to quite different model results, despite the fact that the quantities of total organic matter are very similar and match the observations well. In each of the three modes, a different pool dominates the total stocks: non-leachable slow OM for mode A; leachable slow OM for mode B, and root litter for mode C. These contrasts are mainly explained by the differing decomposition rate coefficients of these three pools. Figure 3.8b shows that modes A and B have very similar contributions of above and belowground litter, whereas for mode C the root litter derived organic carbon is considerably larger.

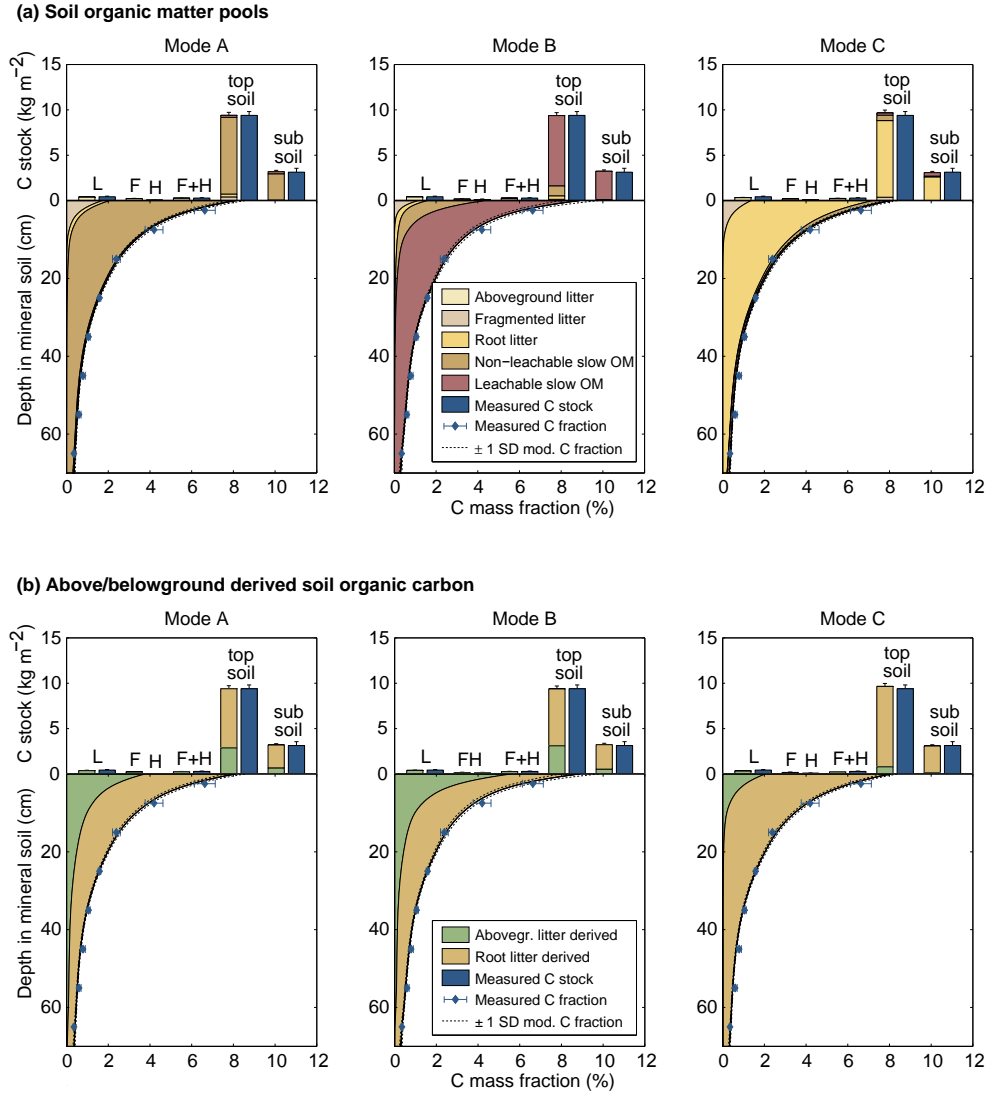


Figure 3.8: Organic carbon measurements and corresponding model results of forward Monte Carlo simulations for Hainich, based on the three posterior modes of calibration setup 3. **a.** stocks and fractions of the model pools; **b.** above vs belowground derived organic matter. L, F, and H refer to the organic horizons (see section 3.2.1); topsoil: 0–30 cm; subsoil: > 30 cm; OM: organic matter. All model results are averages over the Monte Carlo ensemble; errorbars denote one standard error of the mean for the measurements and one standard deviation (SD) for the model results.

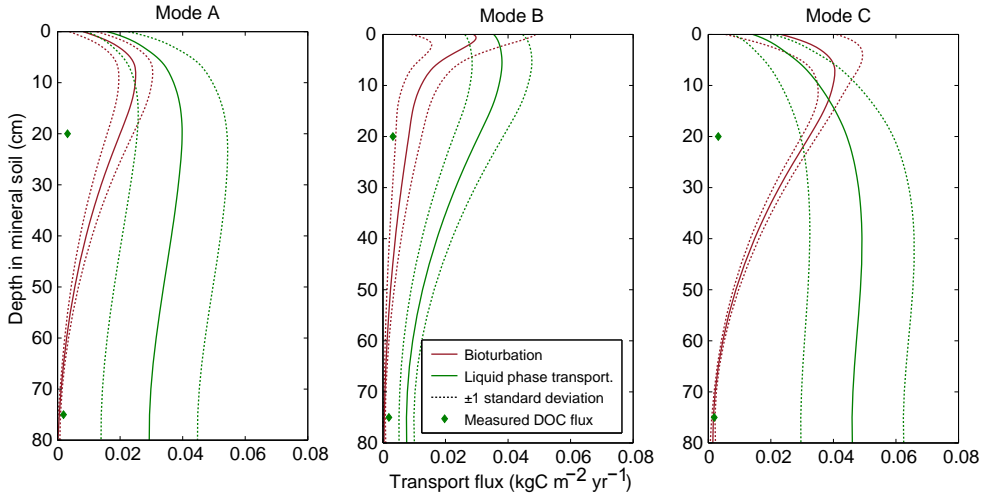
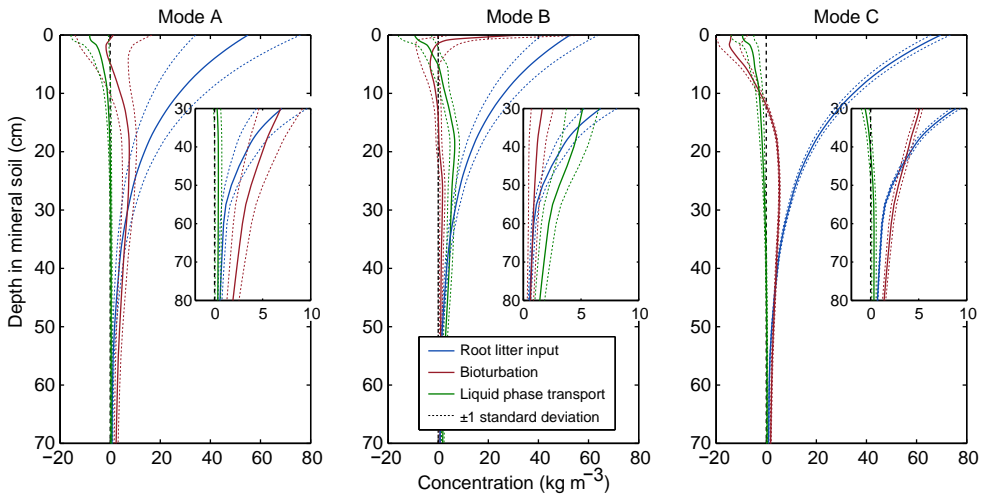
(a) Soil organic carbon transport**(b) Contribution of processes to soil organic carbon**

Figure 3.9: Simulated organic carbon fluxes from forward Monte Carlo simulations for Hainich, based on the three modes of the posterior distribution of calibration setup 3 (note the different scales on the y axes). All quantities are averages over the last simulation year and the Monte Carlo ensemble. **a.** organic carbon transport fluxes and measured dissolved organic carbon (DOC) fluxes (Kindler et al., 2011; not used in the calibration); **b.** contribution of the different processes to soil organic matter profile in mineral soil (see section 3.2.4).

The differences between the modes are further demonstrated by the different organic matter transport fluxes (Figure 3.9a). Interestingly, modes A and C, which have the lowest amounts of the leachable slow organic matter pool, show the highest liquid phase transport fluxes, which is explained by the high advection rates. Figure 3.9b shows that for all modes root litter input is an important process for long term organic matter storage. For modes A and B most organic carbon is present as the slow pools NLS and LS derived from root litter, while for mode C RL itself is stable. The effects of the transport processes are generally smaller than those of root litter input. However, they represent an important mechanism for moving organic matter from shallow levels to deeper layers, as indicated by the negative values near the surface.

3.4 Discussion

3.4.1 Loobos

The calibration results for Loobos suggest that leachable slow (LS) OM is the most abundant organic matter fraction. Its transport with the liquid phase, representing dissolved organic matter leaching, is largely responsible for downward SOM movement and formation of the vertical SOM profile in general. Although the decomposition rate coefficient of this pool (k_{LS}) is the lowest, its distribution tends to quite high values (optimum approximately 0.189 yr^{-1} in calibration setup 3; Figure 3.4-3; Table 3.C.2). Particularly considering that LS is the only pool in the deep soil, where decomposition is slow, we would expect a lower value for k_{LS} . The prior distribution of this parameter used in calibration setup 3, which tends to lower values, caused only a slight downward shift in the posterior. Due to its large variance, the posterior distribution of k_{LS} does allow for somewhat lower, more realistic values. Furthermore, there are quite strong correlations between parameters related to the LS pool (Figure 3.C.7), which indicate that a decrease of the formation of LS (determined by $\alpha_{FL \rightarrow LS}$ and $\alpha_{RL \rightarrow LS}$) can be compensated by a decrease of the liquid phase transport rate v or the decomposition rate coefficient k_{LS} , both controlling the loss of this pool.

Although SOMPROF was not developed to simulate dissolved organic matter transport, the modelled liquid phase transport fluxes should represent the average movement of dissolved organic carbon (DOC) over long timescales¹. Figure 3.6a shows that simulated liquid phase transport fluxes are an order of magnitude higher than DOC fluxes measured by Kindler et al. (2011), which points to a too high value of the advection rate v . However, the high uncertainty of both the rate and fluxes of liquid phase transport shows that the observations used in the calibration can also be explained with somewhat lower values. A lower value for v would be accompanied by a lower decomposition rate coefficient of LS, since the two parameters are strongly correlated (Figure 3.C.7). Thus, it is likely that additional observations constraining the deep soil decomposition rate coefficient, such as radiocarbon measurements, would lead to a more realistic estimate of liquid phase transport rate.

¹While the LS pool represents mostly material adsorbed to the mineral phase, the transport of this pool occurs only by the small fraction that is mobile and thus corresponds to DOC fluxes.

Notwithstanding the over-estimated liquid phase transport fluxes, the relative importance of organic matter leaching over bioturbation is in good agreement with the soil conditions and humus form at Loobos. Soil fauna is virtually absent, and the high concentration of sand supports fast water infiltration and has a low adsorptive capacity, thus allowing high dissolved organic matter fluxes.

3.4.2 Hainich

The presence of multiple modes in the posterior distributions for Hainich is illustrative of the equifinality problem discussed in the introduction. Since the modes represent separate isolated regions in parameter space, they may be seen as distinct explanations for the observations, in terms of the processes represented in the model. In calibration setup 1 the three modes have similar misfit (Table 3.3). The addition of $^{210}\text{Pb}_{\text{ex}}$ to the calibration led to a shift in the comparative misfit, causing mode B to become dominant. Switching to strong priors further increased these differences. Based on these results we can discard mode C with some certainty. The difference between modes A and B, however, is relatively small, hence in view of unconsidered uncertainties (see section 3.4.6) we cannot fully ignore mode A as possible explanation for the observations.

Figure 3.9a shows that for all modes the modelled advective flux is substantially larger than the DOC fluxes measured by Kindler et al. (2011). However, for mode B the overestimation is less pronounced, particularly in the subsoil. For modes A and C modelled advective flux as well as its uncertainty are very high. Contrastingly, the contribution of advection to input in the profile is very small and well constrained for both modes (Figure 3.9b). The reason is that the advective fluxes have relatively small vertical gradients. This also explains the high uncertainty of the advective flow (and the advection rate v) for these modes: as long as its gradient does not change, the actual flux can vary relatively freely.

The abundance of LS and the low rate of liquid phase transport for mode B agrees well with expectations based on the soil texture at Hainich. The high clay content impedes water infiltration, while favoring adsorption of organic matter, slowing down both dissolved organic matter leaching and decomposition of organic matter. This is corroborated by organic matter density fractionation measurements at the site (M. Schrumpp, unpublished data, 2011). These indicate that 81–93 % of the organic matter is present in the heavy fraction, which is known to comprise mostly material in organo-mineral complexes (Golchin et al., 1994). Although the model pools can presumably not be compared directly to the measured density fractions, this is clearly in support of mode B, since leachable slow OM represents mostly material adsorbed to the mineral phase (sections 3.2.1 and 2.2.4). Based on these arguments we conclude that mode B represents the most likely explanation for the observations at Hainich.

The results of the forward simulations for mode B (Figures 3.8 and 3.9) suggest that root input is the most important process at Hainich. Although root litter itself represents only a small fraction, its decomposition products (mainly LS) constitute the bulk of the total SOM. The effects of the transport processes are generally small

compared to material derived from root litter input. However, particularly advection causes loss of material near the surface, and input into deeper layers. The relative importance of root derived SOM agrees well with recent findings by Tefs and Gleixner (2012), who found, based on ^{14}C profile measurements, that soil organic carbon dynamics at Hainich are mainly determined by root input.

3.4.3 Comparison between sites

It is difficult to explain why the posterior distributions for Loobos do not display multimodality, like the distributions for Hainich. One possible explanation is the fact that the observed mineral soil C profile for Loobos clearly consists of two zones: one with a fast decrease with depth between 0 and 10 cm, and one below this, with a much slower decrease. It is conceivable that such a profile can only be explained by a situation where diffusion (bioturbation) operates only near the surface, while advection (liquid phase transport) acts in the complete profile. For Hainich, on the other hand, the C profile is smoother, thus allowing it to be explained by different mechanisms.

In the following discussion we will only consider mode B for Hainich. When comparing the marginal parameter distributions for both sites (see Figure 3.C.3) it is apparent that the decomposition rates of the AGL and FL pools are higher for Hainich than for Loobos, while the reverse is true for RL, NLS, and LS. This agrees well with expectations: the low pH of the coniferous litter at Loobos may slow decomposition in the organic layer, hence we can expect the pools that are important there to have low decomposition rates. On the other hand, the high clay content at Hainich likely stabilizes organic matter in the mineral soil, leading to lower decomposition rates of the pools that dominate there. Comparison further shows that the decomposition rate coefficient of the main pool LS is markedly lower for Hainich, and much less uncertain. This is presumably explained by the observations of the effective decomposition rate coefficients. For the deep soil this data directly constrains the decomposition rate coefficient of LS since this is virtually the only pool there (see also Figure 3.C.6). In view of the considerable effort involved with such measurements, a study into the value of such data for inferring SOMPROF parameters would be valuable. However, in general care must be taken when using lab measurements to infer parameters for field conditions. Furthermore, for the decomposition rate coefficients of the slow pools, very long incubation times may be required (Scharnagl et al., 2010).

The two sites differ strongly with respect to the organic matter transport parameters, with Hainich having a higher bioturbation rate, and Loobos having a higher liquid phase transport rate. This is in good agreement with the differences between the two sites in terms of biological activity and soil texture.

3.4.4 Implications for soil organic matter cycling

The fact that leachable slow organic matter pool constitutes the bulk of SOM for both sites emphasizes the importance of organo-mineral interactions for soil carbon cy-

cling. However, this interpretation relies on the assumption that mineral-associated organic matter is correctly represented by the LS pool. Mathematically, the only difference between the NLS and LS pools lies in the transport behavior: diffusion-only versus diffusion and advection. The question is whether this distinction correctly represents the differences between stable particulate and adsorbed organic matter in reality. The good agreement of our results with density fractionation measurements at Hainich, as well as the environmental conditions at both sites suggests that an explanation where LS dominates might indeed be appropriate. Furthermore, many studies have demonstrated the importance of mineral associations for long-term carbon preservation (Eusterhues et al., 2003; Mikutta et al., 2006; Kögel-Knabner et al., 2008; Kalbitz and Kaiser, 2008). In contrast, others have indicated the presence of root-derived particulate material in podzol B horizons, and questioned the relevance of mineral associated material for mineral soil organic matter fractions (Nierop, 1998; Nierop and Buurman, 1999; Buurman and Jongmans, 2005).

The predominance of root derived material predicted for both sites (Figures 3.5b and 3.8b, mode B) underlines the importance of roots for organic matter input in the mineral soil, which is in agreement with previous studies (Kong and Six, 2010; Rasse et al., 2005). For Hainich the root input also strongly determines the vertical distribution of SOM (Figure 3.9), whereas for Loobos also redistribution of organic material by liquid phase transport is a major factor (Figure 3.6). Based on analysis of a large database of SOM profiles, Jobbagy and Jackson (2000) found that root/shoot allocation, together with the root biomass distribution, explains the vertical SOM profile in the upper part of the soil while clay content was found to be more important at greater depths. The effects of texture are not considered in this study, but Figures 3.6b and 3.9b show that the relative importance of liquid phase transport becomes greater with depth. This supports the findings of Jobbagy and Jackson (2000) since this mechanism is likely strongly controlled by soil texture.

3.4.5 The use of $^{210}\text{Pb}_{\text{ex}}$ measurements

The addition of $^{210}\text{Pb}_{\text{ex}}$ to the calibration had no major effects on the posterior distributions. For Loobos, the $^{210}\text{Pb}_{\text{ex}}$ measurements improved the constraint of the parameters related to bioturbation, while for Hainich they improved constraint of the mixing length for mode B, and caused an increase of the misfit of mode B and C relative to mode A. The fact that the $^{210}\text{Pb}_{\text{ex}}$ data influenced only parameters related to bioturbation may be explained by the fact that the profiles used here are quite shallow, due to the relatively fast decay rate of the isotope (cf Figure 3.2). These measurements are therefore presumably most informative for the topsoil, where bioturbation is more important.

For both sites, the measured $^{210}\text{Pb}_{\text{ex}}$ profile was already well matched by the model in calibration setup 1, in which these measurements were not included. This indicates that these observations can be explained well in conjunction with the organic carbon measurements, which supports the model structure. It also suggests

that the $^{210}\text{Pb}_{\text{ex}}$ data from Kaste et al. (2007) is consistent with the conditions at Loobos.

The use of $^{210}\text{Pb}_{\text{ex}}$ as a tracer for SOM transport relies on the assumption that Pb adsorbs strongly to organic matter, both particulate and in solution. Based on $^{210}\text{Pb}_{\text{ex}}$ and ^{14}C profiles, Dörr and Münnich (1989) found that transport rates of $^{210}\text{Pb}_{\text{ex}}$ were very close to those of organic matter, suggesting that the two are indeed strongly linked. Although Pb is known to occur also in association with the mineral phase and inorganic complexes (Schroth et al., 2008), the affinity of Pb to particulate organic matter is well established, in view of its strong retention in organic layers and topsoils over short timescales (Kaste et al., 2003; Kylander et al., 2008; Schroth et al., 2008), as well as by adsorption studies (Logan et al., 1997; Sauve et al., 2000). The effect of DOM movement on Pb migration is less clear, because it is difficult to predict the behavior of Pb adsorbed to the organic matter that is transformed to the dissolved fraction. Several researchers have indicated the importance of DOM and colloidal organic matter for Pb movement in soil (Miller and Friedland, 1994; Wang and Benoit, 1997; Urban et al., 1990; Friedland et al., 1992). Furthermore, adsorption studies have found that Pb adsorbs readily to humic and fulvic acids (Logan et al., 1997; Turner et al., 1986), while movement of dissolved Pb^{2+} was found to be unimportant (Wang and Benoit, 1997).

In summary, further study on this topic is needed, but we believe that use of $^{210}\text{Pb}_{\text{ex}}$ as a tracer for SOM transport is well defensible. Despite the limited constraint gained in this study, this isotope can be useful as a tracer for SOM transport, provided that more replicate measurements are available to reduce uncertainty. Particularly in combination with other tracers, such as ^{14}C or ^{137}Cs , $^{210}\text{Pb}_{\text{ex}}$ may be quite informative.

3.4.6 Methodological constraints and model validity

For both sites, many strong correlations exist between different combinations of model parameters (Figure 3.C.7) which indicates that the model is over-parameterized with respect to the available data. Furthermore, for all calibration setups there is at least one decomposition rate coefficient for which high values are not constrained by the observations (Figures 3.4 and 3.7). Since the predicted stock of a pool is inversely proportional to its decomposition rate coefficient, these pools are present in very small amounts, which shows that SOMPROF has at least one redundant organic matter pool, given the available data. This is further demonstrated by a strong negative correlation between decomposition rate coefficient of FL and RL for Loobos (Figure 3.C.7), indicating that these pools are essentially “competing” as explanation for the observed carbon stocks and fractions. In order to obtain better constraint, additional observations are needed. Obvious candidates for such data are carbon isotopes (^{13}C or ^{14}C) measurements, of both organic matter and heterotrophic respiration.

There are numerous uncertainties that were not considered in the calibration. In view of practical limitations on the number of parameters that can be estimated si-

multaneously, we focused on the inherently unmeasurable parameters, on which little prior information was available. Many other model inputs, with varying degrees of uncertainty, were held fixed, including the temperature and moisture data, the litter input rates, and the temperature and moisture response parameters. Another source of uncertainty is associated with site history. The sites included in this study were selected for having a relatively well-known and constant history, but particularly for Hainich there have undoubtedly been past fluctuations in the forcing that were not considered. Finally, considerable uncertainty is related to the model structure, specifically to the simple representations of organic matter decomposition and transport in SOMPROF, as well as the behavior of $^{210}\text{Pb}_{\text{ex}}$. These unconsidered variabilities call for care when interpreting the results. Further, it may be advisable to inflate the variance of the posterior distributions when using them as priors for a follow-up study, or for predictive simulations. Nevertheless, we believe that the parameters that were estimated constitute the most important uncertainties.

The good fit to the observations indicates that SOMPROF is able to reproduce widely different SOM profiles, based on realistic parameter values. Furthermore, the consistency of the results with site conditions and the good fit to the $^{210}\text{Pb}_{\text{ex}}$ measurements (even when they are not included in the calibration) are encouraging and support the validity of SOMPROF for temperate forests. The validity for other ecosystems such as grasslands and tropical and boreal forests is yet to be established. Also, comparison to other types of measurements is needed, both to improve constraint of the processes, and to further evaluate the model. Examples of such data include carbon isotopes, heterotrophic respiration rates, and chronosequence measurements. The strong overestimation of the advective flux compared measured DOC flux rates suggests the need for modifications to the transport scheme. Addition of the DOC measurements to the calibration should reveal if the model can reproduce this data with acceptable loss of fit for the other observations. If not, it may be necessary to introduce depth dependence of the advection rate, for example by linking to average water fluxes and soil texture. Finally, further study should explore whether simplification of the model by removal of organic matter pools is warranted. If so, a possible modification would involve merging the root litter and fragmented litter pools, which are functionally very similar.

3.5 Concluding remarks

In order to study the processes involved in SOM profile formation we performed Bayesian estimation of SOMPROF model parameters for Loobos and Hainich, based on organic carbon and $^{210}\text{Pb}_{\text{ex}}$ measurements as well as prior knowledge. The final calibration yielded a multimodal posterior distribution for Hainich, with two dominant modes corresponding to two distinct explanations for the observations. One mode was found to be most realistic in the light of ancillary measurements, and *in situ* soil conditions. For Loobos the posterior distribution is unimodal.

For both Loobos and the most probable mode for Hainich, most of the organic matter is comprised of the leachable slow organic matter pool, which represents ma-

terial that is mostly adsorbed, but potentially leachable. The results further indicate that for both sites most organic matter in the mineral soil is derived from root inputs. For Hainich root input also determines the vertical distribution of SOM, whereas for Loobos downward advective movement of SOM, representing liquid phase transport, represents a major control. These results agree well with other measurements and *in situ* conditions.

The $^{210}\text{Pb}_{\text{ex}}$ measurements improved constraint of the parameters related to bioturbation and reduced the probability of one of the modes for Hainich, but had otherwise no major influence on the posterior distributions. Nevertheless, since the $^{210}\text{Pb}_{\text{ex}}$ observations could be reproduced well together with the organic carbon measurements, we believe this isotope holds value as a SOM tracer.

Our study illustrates the difficulties with explaining the vertical SOM profile caused by the convolution of several mechanisms. Soil carbon profile measurements are necessary but in general not sufficient for resolving the processes. Ancillary measurements such as respiration rates or tracers are needed and even then the model may remain over-parameterized. Bayesian calibration using Markov Chain Monte Carlo, is an invaluable tool for such problems since it helps to identify (non-linear) parameter correlations and the existence of multiple modes, which with traditional calibration tools could easily have gone unnoticed. Furthermore, inclusion of prior knowledge mitigates the adverse effects of over-parameterization.

For future large scale application of SOMPROF sets of characteristic parameter values for different soils and ecosystems are required. With results of the current study and future calibrations progressively stronger prior distributions can be derived, which can be used for sites where fewer observations are available.

Appendix 3.A Markov chain Monte Carlo scheme

3.A.1 The Metropolis algorithm

The Metropolis algorithm (Metropolis et al., 1953) samples the posterior distribution by means of a Markov chain which performs a random walk in parameter space. At each iteration i proposals of the parameters θ^* are generated by taking a (semi-)random step from the current position θ^i . The model is run with the proposed parameter set and the unnormalized posterior probability density ($p(\theta)p(\mathbf{O}|\theta)$) of the proposal is evaluated. The proposal is subsequently accepted or rejected according to the Metropolis rule, which defines the chance for acceptance as:

$$s = \min \left\{ \frac{p(\mathbf{O}|\theta^*)p(\theta^*)\lambda(\theta^*)}{p(\mathbf{O}|\theta^i)p(\theta^i)\lambda(\theta^i)}, 1 \right\}, \quad (3.A.1)$$

where $\lambda(\theta)$ is a factor which may be included to remove the effects of sampling in transformed parameter space (see section 3.A.2). The decision for acceptance or rejection is made using a random number from a uniform distribution on the unit interval. In case of acceptance, the chain moves to the position of the proposal; in case of rejection the chain stays at the current position, which is thus sampled again.

We used the DREAM(ZS) algorithm (Laloy and Vrugt, 2012), an adaptation of the DREAM (DiffeRential Evolution Adaptive Metropolis) algorithm which uses multiple chains in parallel and automatically adapts the scale and orientation of the proposal distribution.

3.A.2 Parameter transformations

Since calibration algorithms generally perform better for distributions that are close to Gaussian, the random walk performed was in transformed parameter space for all calibration setups. For the decomposition rate coefficients (k_i) and transport rates (B, l_m, v) a log transformation was applied:

$$\theta' = \ln(\theta), \quad (3.A.2)$$

and for the transformation fractions $\alpha_{i \rightarrow j}$ a logit transformation was used:

$$\theta' = \text{logit}(\theta) = \ln \left(\frac{\theta}{1 - \theta} \right), \quad (3.A.3)$$

where θ' is the transformed parameter value and θ is the untransformed parameter value, used as input for SOMPROF.

From the rules for change of variables for probability density functions it follows that performing the random walk in transformed space affects the sampled distribution. Suppose we apply Monte Carlo sampling according to some density function $f(\theta)$ and our samples θ' are generated in transformed space according to $\theta' = g(\theta)$. Then our sampled target distribution will be:

$$\tau(\theta) \propto \left| \frac{d}{d\theta} g(\theta) \right| f(\theta). \quad (3.A.4)$$

The factor in vertical bars is the Jacobian of the transformation; or inverse transformation, depending on what is the scale of interest (see e.g. Box and Cox, 1964). This effect was removed by multiplying the posterior density by the reciprocal of the Jacobian, which is the factor $\lambda(\theta)$ in Equation 3.A.1. For a log transformation:

$$\lambda(\theta) = \theta, \quad (3.A.5)$$

and for a logit transformation:

$$\lambda(\theta) = \theta - \theta^2. \quad (3.A.6)$$

3.A.3 Calibration setup

For each calibration first an exploratory run was performed, intended to search for different posterior modes. For this run, at least 20 chains were run in parallel, with starting points widely dispersed in the sampling region using Latin hypercube sampling. Furthermore, the posterior cost was reduced using a cost-reduction factor of 0.1, multiplied with the log posterior density. This effectively “flattens” the posterior,

allowing the chains to escape from local modes and to take bigger steps, thus covering more area. After all modes of interest were identified in the exploratory run, secondary runs without cost reduction were performed with eight chains, started near each mode.

The convergence of the chains was evaluated using the Gelman-Rubin index (Gelman et al., 2004, Chap. 11), which is proportional to the ratio of the between-chain variance and the within-chain variance, and declines to 1 when different chains converge on the same distribution. All chains were run until the convergence index was ≤ 1.01 for all parameters, with at least 100 000 iterations per chain.

After the secondary runs, a variable number of iterations was removed from the start of each chain (the burn-in). Next, the remaining chains for each mode were merged and thinned to 10 000 iterations for analysis by selecting iterations in regular intervals. The continuous posterior distributions depicted in the Figures 3.4 and 3.7 were derived using kernel density estimation.

Appendix 3.B Calculation of process contributions to the SOM profile

In SOMPROF there are five processes that cause input or redistribution of the organic matter pools in the mineral soil: root litter input (RLI), formation due to fragmented litter decomposition (FLdec), formation due to root litter decomposition (RLdec), bioturbation (BT), and liquid phase transport (LPT). Obviously, not every organic matter pool is influenced by each process. The average fluxes (in $\text{kg C m}^{-3} \text{ yr}^{-1}$) over the last simulation year of these processes are calculated by SOMPROF in the forward Monte Carlo runs, yielding the following flux rates: $F_{\text{FL}}^{\text{BT}}$, $F_{\text{RL}}^{\text{RLI}}$, $F_{\text{RL}}^{\text{BT}}$, $F_{\text{NLS}}^{\text{FLdec}}$, $F_{\text{NLS}}^{\text{RLdec}}$, $F_{\text{NLS}}^{\text{BT}}$, $F_{\text{LS}}^{\text{FLdec}}$, $F_{\text{LS}}^{\text{RLdec}}$, $F_{\text{LS}}^{\text{BT}}$, and $F_{\text{LS}}^{\text{LPT}}$. Note that the net input/output of organic matter due to bioturbation/diffusion and liquid phase transport/advection are not equal to the flux rates of these processes (as depicted in Figure 3.6-1 and 3.9-1), but are defined as the vertical derivative of the transport fluxes. For a system with discrete layers, this means the difference between the flux at the top and at the bottom of a layer. The relative importance of each of these fluxes for long term SOM storage, may be estimated by dividing them by the decomposition rate coefficient of the respective pools, yielding an organic carbon concentration for the steady state (kg C m^{-3}):

$$C_i^j = \frac{F_i^j}{k_i}, \quad (3.B.1)$$

for any pool i and process j . Since root litter at any depth may come from either root litter input or bioturbation, also the decomposition products of root litter (NLS and

LS) may be split into fractions that come from these two sources:

$$C_{\text{NLS}}^{\text{RLdec,RLI}} = \frac{C_{\text{RL}}^{\text{RLI}}}{C_{\text{RL}}^{\text{RLI}} + C_{\text{RL}}^{\text{BT}}} C_{\text{NLS}}^{\text{RLdec}}, \quad (3.B.2a)$$

$$C_{\text{NLS}}^{\text{RLdec,BT}} = \frac{C_{\text{RL}}^{\text{BT}}}{C_{\text{RL}}^{\text{RLI}} + C_{\text{RL}}^{\text{BT}}} C_{\text{NLS}}^{\text{RLdec}}, \quad (3.B.2b)$$

$$C_{\text{LS}}^{\text{RLdec,RLI}} = \frac{C_{\text{RL}}^{\text{RLI}}}{C_{\text{RL}}^{\text{RLI}} + C_{\text{RL}}^{\text{BT}}} C_{\text{LS}}^{\text{RLdec}}, \quad (3.B.2c)$$

$$C_{\text{LS}}^{\text{RLdec,BT}} = \frac{C_{\text{RL}}^{\text{BT}}}{C_{\text{RL}}^{\text{RLI}} + C_{\text{RL}}^{\text{BT}}} C_{\text{LS}}^{\text{RLdec}}. \quad (3.B.2d)$$

The calculations above yields 12 carbon concentrations: $C_{\text{FL}}^{\text{BT}}$, $C_{\text{RL}}^{\text{RLI}}$, $C_{\text{RL}}^{\text{BT}}$, $C_{\text{NLS}}^{\text{FLdec}}$, $C_{\text{NLS}}^{\text{RLdec,RLI}}$, $C_{\text{NLS}}^{\text{RLdec,BT}}$, $C_{\text{NLS}}^{\text{BT}}$, $C_{\text{LS}}^{\text{FLdec}}$, $C_{\text{LS}}^{\text{RLdec,RLI}}$, $C_{\text{LS}}^{\text{RLdec,BT}}$, $C_{\text{LS}}^{\text{BT}}$, and $C_{\text{LS}}^{\text{LPT}}$. Note that the sum of these concentrations is not necessarily equal to the simulated total concentration because (i) the simulated SOM profile may not be in steady state, and (ii) the effects of soil temperature and moisture are not accounted for when estimating the steady state concentration. However, since all the pools respond equally to soil temperature and moisture, the relative distribution of the organic matter over the pools is correct for the steady state.

To quantify the importance of the three processes root litter input, bioturbation and liquid phase transport, the organic carbon concentrations are summed as follows:

$$C_{\text{RLI}}^{\text{RLI}} = C_{\text{RL}}^{\text{RLI}} + C_{\text{NLS}}^{\text{RLdec,RLI}} + C_{\text{LS}}^{\text{RLdec,RLI}}, \quad (3.B.3a)$$

$$C_{\text{BT}}^{\text{BT}} = C_{\text{FL}}^{\text{BT}} + C_{\text{RL}}^{\text{BT}} + C_{\text{NLS}}^{\text{BT}} + C_{\text{NLS}}^{\text{FLdec}} + C_{\text{NLS}}^{\text{RLdec,BT}} + C_{\text{LS}}^{\text{RLdec,BT}} + C_{\text{LS}}^{\text{FLdec}} + C_{\text{LS}}^{\text{BT}}, \quad (3.B.3b)$$

$$C_{\text{LPT}}^{\text{LPT}} = C_{\text{LS}}^{\text{LPT}}. \quad (3.B.3c)$$

Since the transport processes may also cause loss of organic matter at a given depth, their contributions to the total organic carbon may also be negative. However, the sum over all contributions must be positive, and equal to the total steady state organic carbon concentration for a simulation with temperature and moisture constant at 15 °C and 1, respectively.

Appendix 3.C Supplementary material

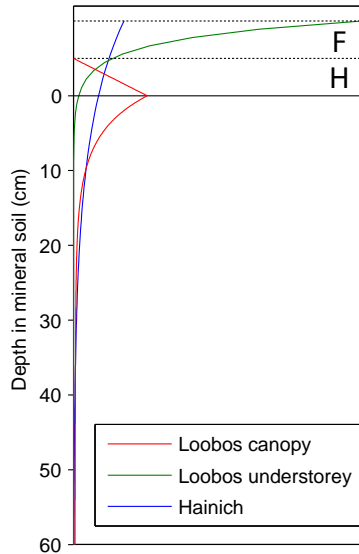


Figure 3.C.1: Vertical distribution of the root litter input for Loobos and Hainich used in the simulations. For Loobos different distribution functions were used for the canopy and understorey. The canopy distribution function consists of two parts: a linearly increasing function from zero to 1.0384 from the top to the bottom of H horizon for the organic layer; and a two-term exponential function for the mineral soil: $f(z) = \exp(-20.00 z) + 0.0384 \exp(-0.886 z)$ (with z the depth in the mineral soil in m). For the understorey at Loobos, and all root input at Hainich, a single-term exponential function starting at the top of the F horizon was used ($f(z) = \exp(-40 z)$ for Loobos; $f(z) = \exp(-7 z)$ for Hainich). All curves are normalized so that the integral equals 1.

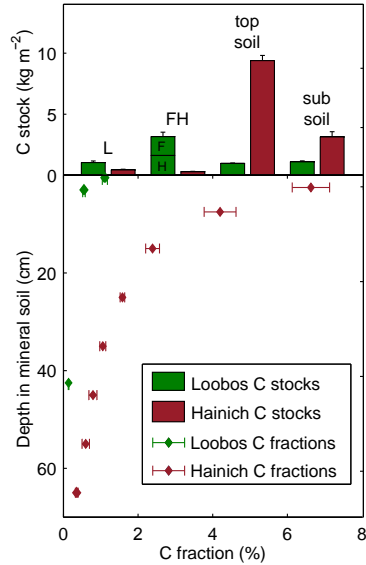


Figure 3.C.2: Measured organic carbon stocks and mass fractions at Loobos and Hainich. All quantities are means. Errorbars indicate one standard error of the mean.

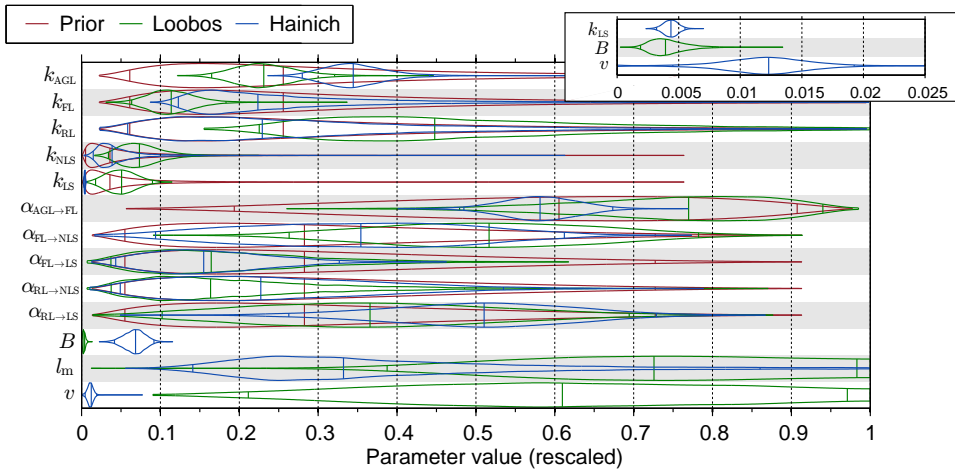


Figure 3.C.3: Marginal posterior distributions for Loobos and Hainich (mode B), calibration setup 3. The “violins” depict the marginal distribution for each parameter. The three vertical lines inside the violins indicate the median and the 95% confidence bounds.

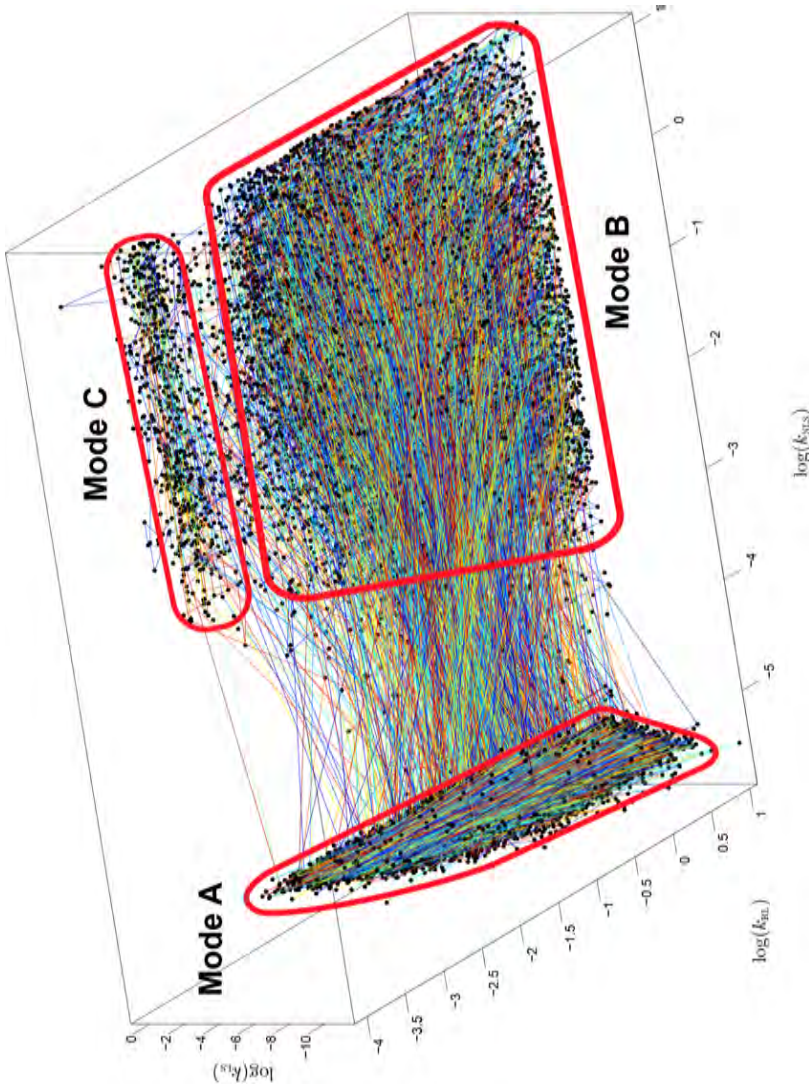


Figure 3.C.4: Trace plot of 20 chains sampling the three modes for Hainich for calibration setup 3. The sample was obtained in a supplementary run with the DREAM(ZS) algorithm, estimating only the parameters that differ significantly between the modes: k_{RL} , k_{NLS} , k_{MS} and v (not shown). All other parameters were fixed at the average over the three modes. The variance of the distribution was artificially inflated by a factor 5. The chains were started widely dispersed in the parameter space using Latin hypercube sampling, and were run for 200,000 iterations. The algorithm converged for all parameters (Gelman-Rubin index ≤ 1.01). The many lines between the modes indicate the chains jumping back and forth between them.

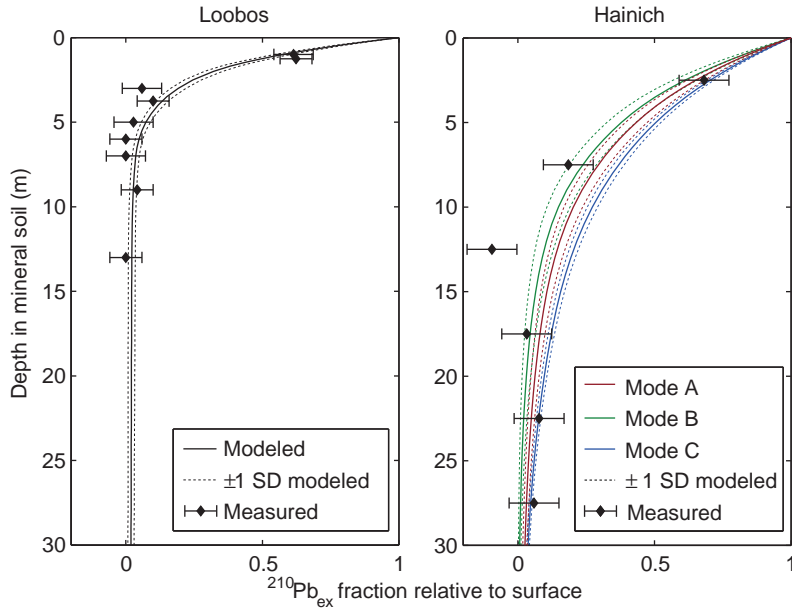


Figure 3.C.5: Measured $^{210}\text{Pb}_{\text{ex}}$ fractions relative to surface and corresponding model results for both sites, calibration setup 3. Model results are averages and standard deviations over the Monte Carlo ensemble. Note that the observed $^{210}\text{Pb}_{\text{ex}}$ profile was not measured at Loobos but at an equivalent site.

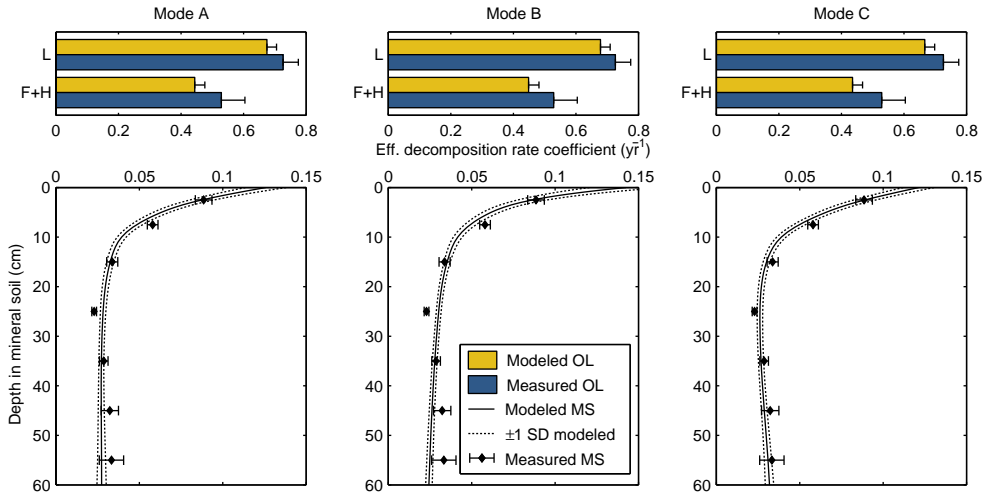


Figure 3.C.6: Measured effective decomposition rate coefficients and corresponding model results for Hainich, calibration setup 3. Depicted model results are averages and standard deviations over the Monte Carlo ensemble. Errorbars for the measurements indicate one standard error of the mean.

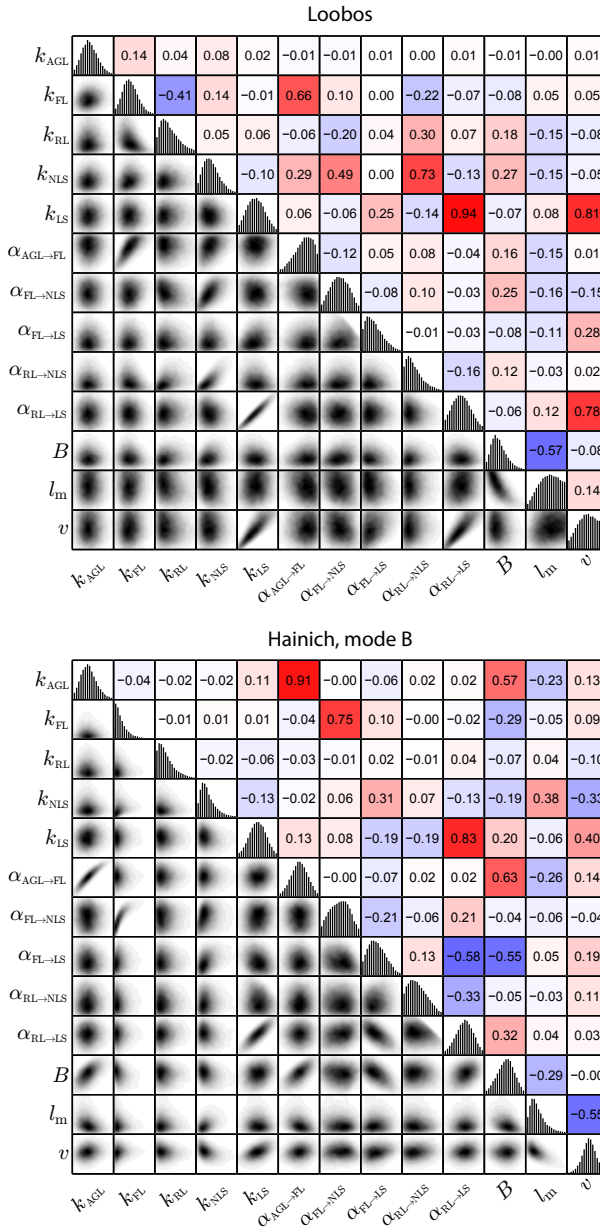


Figure 3.C.7: Correlation matrix of the posterior sample for calibration 3 (including $^{210}\text{Pb}_{\text{ex}}$ and strong priors) for Loobos and mode B for Hainich. The figures shows the correlations for each possible combination of two parameters. In the lower triangle bivariate probability density plots are depicted. In the upper triangle the correlation coefficients are shown, with blue indicating negative correlations and red positive correlations. On the diagonal histograms of the univariate marginal distribution for each parameter are shown.

Table 3.C.1: Observations used in the calibrations. Numbers are means and standard deviations of replicate samplings. Depth is relative to mineral soil surface. $^{210}\text{Pb}_{\text{ex}}$ fractions have been preprocessed and are relative to surface fraction (see section 3.2.3).

Description	Depth (cm)	Mean	s.d.	N
Loobos				
L horizon C stock (kg C m^{-2})	n.a.	1.08	0.619	24
F horizon C stock (kg C m^{-2})	n.a.	1.65	0.729	24
H horizon C stock (kg C m^{-2})	n.a.	1.56	0.979	24
Mineral soil C stock (kg C m^{-2})	n.a.	2.07	0.417	21
	0.5	1.11	0.312	21
Mineral soil C fraction (%)	3	0.550	0.153	21
	42.5	0.138	0.0413	21
Mineral soil $^{210}\text{Pb}_{\text{ex}}$ fraction (-), profile 1	1.25	0.623	-	1
	3.75	0.100	-	1
	6	0	-	1
	9	0.042	-	1
	13	0	-	1
Mineral soil $^{210}\text{Pb}_{\text{ex}}$ fraction (-), profile 2	1	0.614	-	1
	3	0.059	-	1
	5	0.028	-	1
	7	0	-	1
Hainich				
L horizon C stock (kg C m^{-2})	n.a.	0.432	0.188	10
F/H horizon C stock (kg C m^{-2})	n.a.	0.283	0.115	10
Mineral soil C stock (kg C m^{-2})	n.a.	12.5	1.65	10
	2.5	6.63	1.50	9
	7.5	4.20	1.35	10
	15	2.400	0.0584	10
Mineral soil C fraction (%)	25	1.58	0.0196	10
	35	1.06	0.0253	10
	45	0.791	0.0337	10
	55	0.0597	0.0298	9
	65	0.0355	0.007	4
L horizon eff. decomp. rate coeff. (yr^{-1})	n.a.	0.685	0.0929	10
F/H horizon eff. decomp. rate coeff. (yr^{-1})	n.a.	0.459	0.0942	10
	2.5	0.0886	0.0150	10
	7.5	0.0580	0.00960	10
	15	0.0338	0.00992	10
Mineral soil effective decomposition rate coeff. (yr^{-1})	25	0.0229	0.00424	10
	35	0.0287	0.00774	10
	45	0.0323	0.0156	10
	55	0.0333	0.0206	9
	2.5	0.681	-	1
	7.5	0.185	-	1
	12.5	-0.0949	-	1
Mineral soil $^{210}\text{Pb}_{\text{ex}}$ fraction (-)	17.5	0.0324	-	1
	22.5	0.0776	-	1
	27.5	0.0590	-	1
	32.5	-0.0740	-	1

Table 3.C.2: Properties of the marginal posterior distributions for both sites for calibration setup 3 (with $^{210}\text{Pb}_{\text{ex}}$ and strong priors). For each site/mode the 2.5 % quantile (upper), the sample with highest posterior density (middle), and the 97.5 % quantile (lower) are shown.

	k_{AGL} yr^{-1}	k_{FL} yr^{-1}	k_{RL} yr^{-1}	k_{NLS} yr^{-1}	k_{LS} yr^{-1}	$\alpha_{\text{AGL} \rightarrow \text{FL}}$ —	$\alpha_{\text{FL} \rightarrow \text{FL}}$ —	$\alpha_{\text{FL} \rightarrow \text{NLS}}$ —	$\alpha_{\text{FL} \rightarrow \text{LS}}$ —	$\alpha_{\text{RL} \rightarrow \text{NLS}}$ —	$\alpha_{\text{RL} \rightarrow \text{LS}}$ —	B $\text{kg m}^{-2} \text{yr}^{-1}$	l_m m	v m yr^{-1}
Loobos														
	0.495	0.19	0.676	0.102	0.0531	0.479	0.263	0.0372	0.0372	0.0376	0.102	0.00571	1.16	0.0211
	0.735	0.297	1.68	0.184	0.189	0.658	0.5	0.171	0.171	0.148	0.487	0.00943	2.53	0.0651
	0.962	0.55	2.72	0.42	0.27	0.94	0.782	0.429	0.429	0.486	0.694	0.0232	2.95	0.0971
Hainich														
	0.873	0.3	0.212	0.00447	0.021	0.506	0.0276	0.0388	0.0388	0.119	0.0424	0.185	1.3	0.0114
Mode A	1.08	0.381	0.598	0.00776	0.104	0.607	0.0845	0.149	0.149	0.309	0.162	0.256	1.86	0.0834
	1.45	0.484	2.35	0.0139	0.378	0.705	0.213	0.293	0.293	0.614	0.348	0.31	2.94	0.0978
	0.839	0.368	0.176	0.0444	0.00962	0.485	0.0939	0.0434	0.0434	0.0491	0.263	0.125	0.423	0.000453
Mode B	1.1	0.746	0.788	0.0779	0.013	0.61	0.404	0.142	0.142	0.222	0.488	0.233	0.583	0.00137
	1.32	2.13	2.16	0.44	0.0165	0.674	0.612	0.327	0.327	0.535	0.729	0.276	2.58	0.00192
	1.01	0.318	0.018	0.0526	0.0306	0.582	0.0386	0.0283	0.0283	0.0511	0.0795	0.247	2.24	0.0136
Mode C	1.21	0.439	0.0202	0.201	0.0389	0.647	0.247	0.0975	0.0975	0.304	0.284	0.285	2.94	0.052
	1.76	1.1	0.0241	0.701	0.134	0.757	0.636	0.23	0.23	0.641	0.473	0.348	2.99	0.0972

Chapter 4

The use of radiocarbon to constrain current and future soil organic matter turnover and transport in a temperate forest

We investigated the merits of radiocarbon measurements for estimating soil organic matter (SOM) turnover and vertical transport for a temperate deciduous forest. Eleven parameters defining decomposition and transport in the soil carbon model SOMPROF were estimated using a Bayesian approach, based on organic carbon stocks and mass fractions, and radiocarbon concentration of SOM and heterotrophic respiration. The addition of radiocarbon data had strong effects on the parameter distribution, most importantly causing a reduction of the decomposition and production rate of the slowest SOM pool by an order of magnitude, and a similar reduction in SOM transport with the liquid phase. The modified parameters led to changes in the partitioning of SOM over the different model pools and a strong reduction of advective fluxes. The calibration results were subsequently used to perform transient soil carbon projections for the period 1901–2100. These projections show an increase of soil carbon in the topsoil and a decrease in the subsoil, adding to a net gain overall. Near the end of the 21st century total carbon stocks stabilize and—for the radiocarbon-constrained model—start to decrease. However, the changes over time were small compared to the total stocks. The predictions based on the calibrations with and without radiocarbon were in general quite similar, but the former showed a significantly higher heterotrophic respiration flux, which is explained by lower losses of carbon with the liquid phase. The uncertainty of the predicted total soil carbon stock was only slightly decreased and was increased for individual depth compartments.

Based on: M. C. Braakhekke, C. Beer, M. Schrumpf, A. Ekici, B. Ahrens, M.R. Hoosbeek, B. Kruijt, P. Kabat, and M. Reichstein
Accepted on condition of minor revision for Journal of Geophysical Research:
Biogeosciences

4.1 Introduction

Recent studies have called attention to the soil as an important source of uncertainty in the prediction of terrestrial carbon cycling (Jones and Falloon, 2009; Sitch et al., 2008; Arora and Matthews, 2009). For example, based on a reanalysis of results from Friedlingstein et al. (2006), Jones and Falloon (2009) concluded that the spread of future predicted land carbon storage by earth system models is explained for a large part by varying responses of global soil carbon stocks. A similar result was found by Sitch et al. (2008) in an intercomparison study of dynamic global vegetation models. Because of the large amount of carbon stored globally in soils, uncertainty in representation of soil carbon cycling in earth system models can propagate to considerable variation in predicted atmospheric CO_2 and climate change.

In the context of climate change, the main purpose of a soil carbon model is to predict carbon storage in, and fluxes from, the soil in response to environmental factors. Therefore, soil carbon models applied at large scale have typically been calibrated to reproduce observed, or at least reasonable, carbon stocks and heterotrophic respiration fluxes. Since soil organic matter (SOM) comprises a mixture of materials with different turnover times, it is usually modelled as several pools or compartments with different decomposition rates. The number of pools varies widely but most models include at least three SOM fractions in order to adequately represent the spectrum of turnover rates observed in reality (Manzoni and Porporato, 2009). Since each pool requires one or more parameters to characterize its behavior, the degrees of freedom of a soil carbon model increase rapidly with each additional pool. Consequently, measured carbon stocks and fluxes alone are in general not sufficient to estimate all parameters of a multi-pool soil carbon model. Depending on the number of pools, one or more additional sources of information characterizing the organic matter turnover are required. In absence of such data, a clear best parameter set may not exist. Instead, there may be one or more large regions in parameter space that yield optimal, or almost optimal, fit to observations (chapter 3). Selecting a single parameter set in such a region may result in a model that is right for the wrong reason and gives biased predictions when extrapolated to different conditions (Beven, 2006).

The cosmogenic carbon isotope ^{14}C , generally referred to as radiocarbon, has proven to be an ideal tool for quantifying SOM turnover (Gaudinski et al., 2000; Trumbore, 2009). Because of its relatively constant natural formation rate, the availability of accurate past records of atmospheric concentrations, and its long half-life of 5,730 years, it can represent the decomposition rates of the most stable organic matter fractions. Furthermore, the large increase of the atmospheric radiocarbon fraction due to nuclear weapons testing in the 1960s allows it to be used for quantifying decadal turnover rates as well. Hence, it has been used extensively for calibrating and evaluating soil carbon models (Jenkinson and Coleman, 1994; Michalzik et al., 2003; Petersen et al., 2005; Jenkinson and Coleman, 2008).

Studies in which radiocarbon was measured at multiple levels in the soil profile have shown that SOM generally becomes older with depth (Trumbore et al., 1995; Rumpel et al., 2002; Schrumpf et al., 2013). It has been suggested that certain mech-

anisms that cause stabilization of organic matter are comparatively more important in the subsoil (Rumpel et al., 2012). Examples of such mechanisms include: sorption to minerals; oxygen, energy, or nutrient limitation of microbes; and spatial inaccessibility of SOM. Conversely, the vertical radiocarbon gradient can also be explained by transport of SOM. Since effective transport rates are generally quite low, the time needed for material to reach deeper levels will cause a vertical age gradient (Kaiser and Kalbitz, 2012). Furthermore, downward migration leads to vertical segregation of organic matter, causing slower fractions to become more prominent with depth (Elzein and Balesdent, 1995). Indeed, when combined with vertical transport, a multi-pool soil carbon model will inevitably show decrease of average turnover rates with depth. This suggests that profile measurements of SOM and radiocarbon may provide additional constraint on turnover rates, if combined with a vertical transport model. On the other hand, since SOM transport rates are poorly known, they need to be estimated in addition, which partially negates the improved constraint on the decomposition parameters.

We aimed to study the merits of radiocarbon measurements for characterizing SOM turnover and vertical transport in a temperate deciduous forest in Germany. To this end, radiocarbon activity of soil organic matter and heterotrophic respiration were used together with organic carbon measurements to estimate parameters of the soil carbon model SOMPROF with a Bayesian calibration approach. SOMPROF (chapter 2) is a vertically explicit SOM model that simulates the distribution of organic matter over the mineral soil profile and surface organic layers. It is based on simple but explicit representations of bioturbation (mixing by the soil fauna), liquid phase transport, (root) litter input, and decomposition. A previous calibration study for the same site without radiocarbon indicated that the vertical SOM profile can be explained in several ways (chapter 3). Here, we used a reduced version of the model and studied how the addition of radiocarbon data affects the parameters by performing calibrations with and without these observations. The calibrations were performed in a Bayesian framework with Monte Carlo inversion, allowing full characterization of parameter distributions and inclusion of prior knowledge. Furthermore, it was studied how the updated parameters and their uncertainty affect predictions of future soil carbon cycling under conditions of climate change. Based on the results of the calibrations an ensemble of forward simulations until 2100 were run, using litter fluxes and soil climate predicted by the land surface model JSBACH (Raddatz et al., 2007).

4.2 Methods

4.2.1 Model description and simulation setup

The SOMPROF model and simulation setup have previously been described elsewhere (chapters 2 and 3). Hence, we only provide a general description of the model here, and focus on the changes with respect to these texts.

SOMPROF simulates organic carbon stocks and mass fractions in the mineral

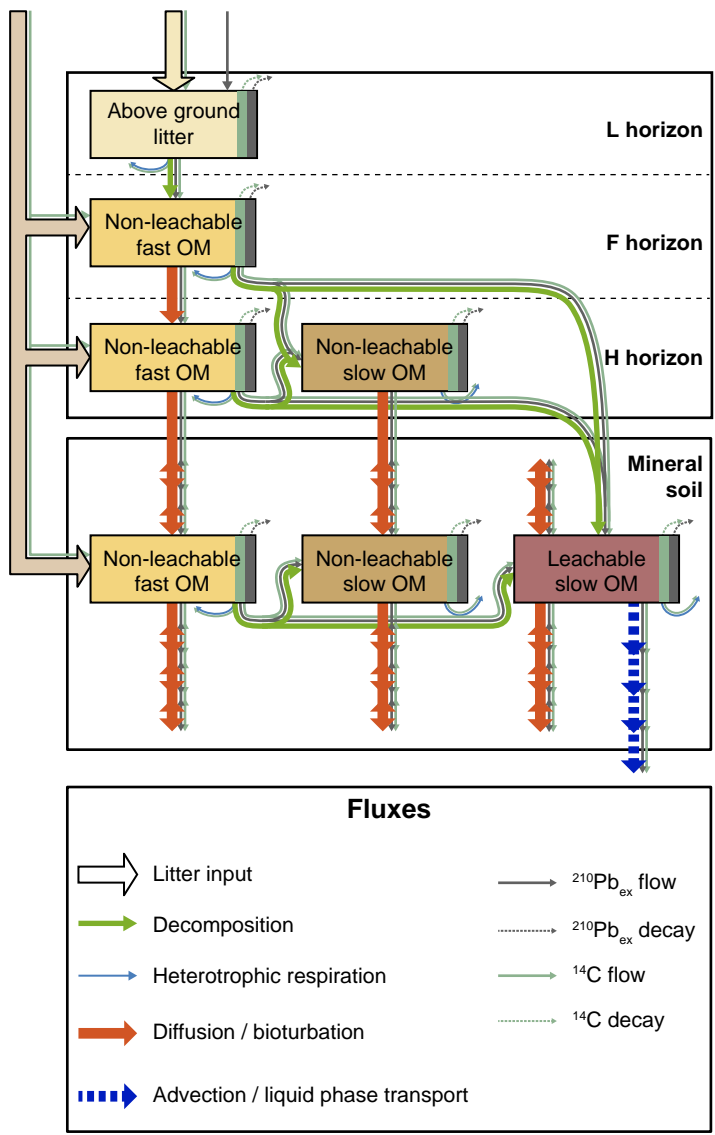


Figure 4.1: Structure of the SOMPROF model.

soil and three surface organic horizons: L, F and H (Figure 4.1). The model accounts for organic matter (OM) input by roots and aboveground litter fall, decomposition, and two mechanisms for vertical OM transport: bioturbation (mixing of the soil by the soil fauna) and movement with the liquid phase. The model further includes a module simulating the profile of excess lead-210 ($^{210}\text{Pb}_{\text{ex}}$), a radiogenic isotope which can be used as a tracer for SOM transport.

The version of SOMPROF used in this study contains four OM pools: aboveground litter (AGL), non-leachable fast organic matter (NLF), non-leachable slow organic matter (NLS), and leachable slow organic matter (LS). Decomposition of the OM pools is simulated as first order kinetics, controlled by the decomposition rate k (yr^{-1}). The decomposition rate is corrected for soil temperature and moisture profiles, but otherwise independent of depth. The decomposition flux is partitioned by transformation fractions α (-) into a part that flows to more decomposed pools and a part that is lost as CO_2 (heterotrophic respiration). Previously, the NLF pool was split into two pools: fragmented litter, which represented fresh litter transformed in a first decomposition step, and root litter, representing organic matter input by roots. In a calibration study (chapter 3) it was found that the observations could constrain the decomposition rate coefficient for only one of these two pools, which suggests that one of them is redundant. Since the two pools are very similar in terms of quality and transport behavior, we chose to merge them into the NLF pool since this removes three parameters.

Organic matter input occurs as aboveground litter in the L horizon, and over the whole profile due to input from roots as non-leachable fast OM. Root input is vertically distributed according to a function of depth, starting at the top of the F horizon and exponentially declining, determined by a shape parameter β (m^{-1}).

Vertical transport due to bioturbation in the organic layer is represented by a fixed downward flux to the underlying horizon, or into the mineral soil. This flux is defined by the bioturbation rate B ($\text{kg m}^{-2} \text{yr}^{-1}$), and is distributed over the organic matter pools. Aboveground litter is the only pool not moved by bioturbation, and as such is only present in the L horizon. In the mineral soil bioturbation is simulated as a diffusion process, with the diffusivity D_{BT} determined by the bioturbation rate and the mixing length l_m (m) according to:

$$D_{\text{BT}} = \frac{1}{2} \frac{B}{\rho} l_m, \quad (4.1)$$

where ρ is the bulk density, which may vary with depth. In the simulations for the calibrations ρ was based on local measurements, while for the projection simulations (section 4.2.5) it was determined from the local organic matter fraction using a pedotransfer function from Federer et al. (1993). Transport of organic matter with the liquid phase is only considered for the mineral soil and may lead to loss of organic matter over the lower boundary. It is simulated as an advection process, controlled by the advection rate v (m yr^{-1}). Only the leachable slow organic matter pool is subject to advection. The parameters controlling vertical transport, B , l_m , and v , are all assumed to be constant with depth, although diffusivity may be variable due to bulk density differences.

The simulations for the calibrations covered the period 1810–2009, with monthly time steps. The model was forced by repeated average annual cycles of litter fluxes and soil temperature and moisture, which were derived from *in situ* measurements (section 2.3.2). Lead-210 input was held constant at 1; the absolute values were not required since both the modelled and measured $^{210}\text{Pb}_{\text{ex}}$ profile were normalized with respect to the value at the soil surface (section 3.2.3). Additional model input is presented in Table 4.B.1. The forcing for the radiocarbon model is discussed below.

In view of the high age of the Hainich forest and the absence of any known major land-use changes in the past (see section 4.2.2), it was assumed that the soil is in steady state at the start of the simulation, for average constant forcing. A Newton-Raphson root-finding algorithm (Press et al., 1996, Ch. 9) was used to directly estimate the steady state for given parameter values.

Radiocarbon simulation

Radiocarbon (^{14}C) is a cosmogenic radioisotope formed in the upper atmosphere by interactions between cosmic radiation and atmospheric nitrogen. Additionally, above-ground nuclear weapons testing, mostly during the 1960s, produced a large amount of radiocarbon, roughly doubling the atmospheric activity in less than 10 years (the “bomb-peak”). The $^{14}\text{C}/^{12}\text{C}$ ratio of carbon incorporated in organic tissue is determined by the atmospheric ratio at the time of fixation, as well as fractionation effects due to the mass difference between the isotopes. Since the exchange with the atmosphere ceases after uptake, the radiocarbon activity of fixed carbon is influenced only by radioactive decay and mixing with other organic carbon sources. This allows radiocarbon to be used as a tracer to quantify carbon flows and average turnover rates. Particularly valuable in the context of soil carbon cycling is the combined use of radiocarbon of SOM and of heterotrophic respiration. These two variables contain information on turnover rates of slow and fast fractions, respectively (Sierra et al., 2012).

Radiocarbon measurements are generally reported in one of two units: percent modern and $\Delta^{14}\text{C}$ (Trumbore, 2009). Both quantities compare the radiocarbon activity of the sample to that of a generally accepted standard. Furthermore, both units are corrected for isotope fractionation due to biochemical processes by normalization based on the ^{13}C activity.

SOMPROM was extended with a module simulating radiocarbon cycling in soil organic matter (Figure 4.1). The radiocarbon calculations were based on units of percent modern, corrected for the decay of the standard since 1950. This quantity is directly proportional to the true radiocarbon activity. Input of radiocarbon into the soil profile was determined as the product of the litter flux and the atmospheric radiocarbon fraction at the simulation time minus a fixed lag period. This lag time accounts for the time spent by the carbon in the vegetation. The lag time for root litter was estimated at 8 years, based on literature (Gaudinski et al., 2000) and local radiocarbon measurements of roots (data not shown). For aboveground litter a lag time of 1 year was used. Several records of atmospheric $\Delta^{14}\text{C}$ were combined to construct a time series for the radiocarbon fraction of the litter input (Stuiver et al.,

1998; Reimer et al., 2004; Levin and Kromer, 2004; Hua and Barbetti, 2004, I. Levin, personal communication, 2011). The initial conditions at the start of the simulation were calculated based on a fixed input equal to the average of the last 5,000 years before the simulation ($\Delta^{14}\text{C} = 10.02\text{‰}$). For the simulation period (1810–2009) a time series of variable atmospheric radiocarbon content was used (Figure 4.B.1).

Once present in the soil, radiocarbon follows all flows of organic carbon represented in the model: decomposition, heterotrophic respiration, bioturbation, and liquid phase transport. Additionally, radiocarbon is lost by radioactive decay at a rate of $1.21 \times 10^{-4} \text{ yr}^{-1}$. For the organic layer all radiocarbon flows were determined simply by multiplying the organic carbon fluxes from a given pool by its radiocarbon fraction. For the mineral soil separate partial differential equations were composed for each pool which account for all relevant processes. These equations were solved numerically using the same techniques as used for organic carbon.

4.2.2 Site description

The study site is located in a deciduous old-growth forest in the Hainich national park in Germany ($51^{\circ}4'45.36'' \text{ N}$; $10^{\circ}27'7.20'' \text{ E}$). The climate is temperate subcontinental with an average annual precipitation of 800 mm and average temperature of 7–8 °C. The main tree species are beech (*Fagus sylvatica*) and ash (*Fraxinus excelsior*), and the soil is covered by herbaceous vegetation (*Allium ursinum*, *Mercurialis perennis*, *Anemone nemorosa*) from April to October (Knohl et al., 2003). The main soil type is Cambisol (IUSS Working Group WRB, 2007), formed in loess on limestone bedrock with a depth of 50–70 cm. The soils are fertile, with a high clay content and pH. A thin mull-type organic layer of 3–5 cm, and a well developed A horizon of 5–10 cm, indicate a high biological activity and fast decomposition. Prior to the establishment of the national park in 1997, the forest was used by the military for approximately 60 years. Hence, the site has been unmanaged for at least 70 years. In the preceding centuries the forest was used extensively as coppice. Currently, the ages of the trees cover a wide range of up to 250 years. Large amounts of standing dead wood and woody debris on the forest floor attest to the forest's unmanaged character.

4.2.3 Observations used in the calibration

Measurements of seven variables were used in the calibration (Table 4.1). For several variables multiple values were included, representing different replicates, depths, or points in time. Model-data fit was calculated for model predictions at the sampling time of the corresponding measurements. Most observations can be expected to have right-skewed distributions since they have a theoretical lower bound at zero and large spatial variance. Therefore, all measurement variables, except lead-210, were log-transformed for the calibration, in order to bring their distributions closer to normal. Since the lead-210 data used here is the fraction in excess to the amount that was formed *in situ*, this quantity may also be negative (see section 3.2.3); hence it was not log transformed.

Table 4.1: Measured variables used in the calibration. Depth increments refer both to layers in the mineral soil as well as organic horizons. Total no. of data points represents the sum over all years, depth increments, and replicates. Note that the radiocarbon measurements were only included for calibration wC14.

Name	No. of depth increments	Measurement year(s)	No. of data points
C stock	3 ^a	2004, 2009	60
C fraction ^b	7	2004, 2007	136
Effective decomposition rate coefficient ^c	9	2004	89
Lead-210 activity ^b	7	2001	7
Total heterotrophic respiration	1	2000–2007	8
Radiocarbon of SOM ^a	up to 9	2001, 2004, 2009	112
Radiocarbon of heterotrophic respiration ^{b,c}	4	2001	4

^a L, F/H, and total mineral soil.

^b Only for the mineral soil.

^c Based on lab incubations.

C stocks and mass fractions were measured in 2004 and 2009 for up to 7 depth levels and 10 replicates (Schrumpf et al., 2011). Effective decomposition rate coefficients were determined from respired CO_2 during lab incubations of samples taken in 2004 (Kutsch et al., 2010). Measurements of lead-210 activity were taken from Fujiyoshi and Sawamura (2004), and were normalized and corrected for *in situ* formed lead-210, as described in section 3.2.3. Total average heterotrophic respiration for the years 2000–2007 was taken from Kutsch et al. (2010) who estimated it using field measurements of soil respiration and a model for autotrophic respiration. Radiocarbon measurements of both SOM and heterotrophic respiration in 2001 were taken from Hahn and Buchmann (2004). Additionally, measurements of radiocarbon of SOM for 2004 and 2009 were included (Schrumpf et al., in prep.).

4.2.4 Bayesian calibration

We performed calibration runs in two setups: without radiocarbon observations (woC14) and with radiocarbon observations (wC14). The parameter estimation was performed with a Bayesian approach. Bayesian calibration is aimed at deriving the posterior distribution, which is the distribution of the parameters conditional on prior knowledge, the model structure, and the observations. It is defined (up to a constant) as the product of prior distribution $p(\theta)$, which expresses knowledge about the model parameters θ prior to the calibration, and the likelihood function $p(\mathbf{O}|\theta)$, which defines the probability of the measurements \mathbf{O} , given model parameters θ (Gelman et al., 2004):

Table 4.2: The model parameters estimated in the calibration. The lower bound for all parameters is zero; the upper bound is given in the table.

Parameter	Symbol	Units	Prior distribution	Upper bound
Decomposition rate coefficients at 10 °C and optimal soil moisture				
Aboveground litter	k_{AGL}	yr^{-1}	$\text{Log}-\mathcal{N}(-0.23, 0.74)$	3
Non-leachable fast OM	k_{NLF}	yr^{-1}	$\text{Log}-\mathcal{N}(-0.23, 0.74)$	3
Non-leachable slow OM	k_{NLS}	yr^{-1}	$\text{Log}-\mathcal{N}(-2.23, 1.00)$	3
Leachable slow OM	k_{LS}	yr^{-1}	$\text{Log}-\mathcal{N}(-2.23, 1.00)$	3
Transformation fractions				
Aboveground litter–Non-leachable fast OM	$\alpha_{\text{AGL} \rightarrow \text{NLF}}$	–	$\text{Logit}-\mathcal{N}(0.43, 0.95)$	1
Non-leachable fast OM–non-leachable slow OM	$\alpha_{\text{NLF} \rightarrow \text{NLS}}$	–	$\text{Logit}-\mathcal{N}(-0.93, 0.98)$	1, (1 – $\alpha_{\text{NLF} \rightarrow \text{LS}}$)
Non-leachable fast OM–leachable slow	$\alpha_{\text{NLF} \rightarrow \text{LS}}$	–	$\text{Logit}-\mathcal{N}(-0.93, 0.98)$	1, (1 – $\alpha_{\text{NLF} \rightarrow \text{NLS}}$)
Transport parameters				
Bioturbation rate	B	$\text{kg m}^{-2} \text{yr}^{-1}$	uniform	3
Mixing length	l_m	m	uniform	3
Liquid phase transport (advection) rate	v	m yr^{-1}	uniform	0.1
Shape parameter for root litter input profile	β	m^{-1}	$\mathcal{N}(7, 1.2)$	14

$$p(\boldsymbol{\theta}|\mathbf{O}) \propto p(\boldsymbol{\theta}) p(\mathbf{O}|\boldsymbol{\theta}). \quad (4.2)$$

In the current study the observations comprised several “data streams”, i.e. variables for which the distribution of the model-data residuals is expected to be different. Measurements at different horizons and depth levels were considered part of the same data stream, while measurements at different time points were treated as separate data streams. The overall likelihood was defined as the product of the likelihoods for all individual data streams:

$$p(\boldsymbol{\theta}|\mathbf{O}) = \prod_{i=1}^I p_i(\mathbf{O}_i|\boldsymbol{\theta}), \quad (4.3)$$

where I is the total number of data streams. As implied by equation (4.3), correlations between data streams were not considered. For all data streams a Gaussian likelihood function was used. For a data stream i with N_i data points, the conditional likelihood function for given $\boldsymbol{\theta}$ and standard deviation σ_i is defined as:

$$p(\mathbf{O}_i|\boldsymbol{\theta}, \sigma_i) \propto \sigma_i^{-N_i} \exp\left(-\frac{1}{2\sigma_i^2} SS_i(\boldsymbol{\theta}, \mathbf{O}_i)\right). \quad (4.4)$$

$SS_i(\boldsymbol{\theta}, \mathbf{O}_i)$ is the sum of squared residuals for data stream i :

$$SS_i(\boldsymbol{\theta}, \mathbf{O}_i) = \sum_{n=1}^{N_i} (O_{i,n} - M_i(\boldsymbol{\theta}))^2, \quad (4.5)$$

where $O_{i,n}$ is the measured value for replicate n and $M_i(\boldsymbol{\theta})$ is the model prediction for parameters $\boldsymbol{\theta}$. Replicate measurements, when available, were all included individually in $SS_i(\boldsymbol{\theta})$, which means that single model predictions were compared to several observed quantities. The standard deviation of the model–data residuals σ_i depends on both measurement– and modelling–related errors and is usually not known a priori. It may be estimated as an additional parameter during the calibration (Gelman et al., 2004), but since we are not particularly interested in σ_i , an expedient approach is to remove it from the likelihood function by integration (Kavetski et al., 2006). The resulting likelihood function represents the distribution of the residuals marginalized over all values of σ_i . For all data streams we chose the uninformative Jeffreys prior for σ_i ($p(\sigma_i) \propto 1/\sigma_i$). This yields the following formulation for the marginal likelihood function:

$$p(\mathbf{O}_i|\boldsymbol{\theta}) = SS_i(\boldsymbol{\theta}, \mathbf{O}_i)^{-N_i/2}. \quad (4.6)$$

Eleven model parameters were estimated: seven parameters related to decomposition, three parameters related to transport, and one parameter quantifying the vertical distribution of root litter input (Table 4.2). Prior distributions for all parameters were the same as used in chapter 3, except for the shape parameter for root litter input. Log-normal prior distributions were used for the decomposition rates and transport parameters. For the transformation fractions logit-normal priors were

used, which is similar to the beta distribution and bounded between zero and one. Finally, for the shape parameter for root litter input a normal distribution was used with the mean at 7 m^{-1} , which is the approximate value for the profile of the root biomass at Hainich. The priors are depicted together with the posterior distributions in Figure 4.2.

The posterior distributions were approximated with a Markov Chain Monte Carlo approach using the DREAM(ZS) algorithm (Laloy and Vrugt, 2012). Additional information about the calibration can be found in the appendix.

4.2.5 Projection simulations

In order to study soil carbon cycling under conditions of climate change, we performed model projections for the period 1901–2100 based on the calibration results. The parameter sets of the posterior distributions for both calibrations obtained with Monte Carlo sampling were used to run an ensemble of 500 model simulations. The setup of these simulations was identical to those made for the calibrations, with the exception that the mineral soil bulk density was calculated based on the modelled organic matter fraction, instead of measurements.

The forcing variables for the simulation projections (above/belowground litter flux, soil moisture, and soil temperature) were obtained from a simulation run with the ecosystem model JSBACH. Part of the MPI earth system model, JSBACH simulates land-atmosphere exchange of energy, water and carbon dioxide (Raddatz et al., 2007; Brovkin et al., 2009). Its representation of canopy processes such as photosynthesis, respiration, and transpiration is based on the BETHY model (Knorr, 2000), with several extensions to represent phenology and carbon cycling (Raddatz et al., 2007), and soil freeze-thaw processes (Ekici et al., 2013).

Vegetation carbon pools were brought to equilibrium by a 1000-year spin-up procedure using 1901–1930 climate and atmospheric carbon dioxide concentration for 1901 (296 ppm). Next, the model was run with transient climate and CO_2 for the period 1901–2100. The global atmospheric carbon dioxide concentration followed the CMIP5 protocol (Meinshausen et al., 2011). The 1901–2100 climate data set consisted of WATCH forcing data (Weedon et al., 2010) for the period 1901–1978, bias-corrected ERA-Interim data (Dee et al., 2011) for the period 1979–2010, and a bias-corrected outputs from the regional climate model KNMI-RACMO for the period 2011–2100. KNMI-RACMO results came from the ENSEMBLES multi-model scenario experiment (Christensen et al., 2008, <http://www.ensembles-eu.org/>). For this experiment the model was driven by lateral boundary conditions derived by the ECHAM5 model, based on the SRES A1B greenhouse gas and aerosol scenario. Bias correction was applied to the ERA-Interim and RACMO results based on the overlapping time period (1979–2010), according to Piani et al. (2010), in order to ensure a consistent time series (Beer et al., *subm.*).

4.3 Results

4.3.1 Calibration

Posterior distribution

Both the calibration setup without radiocarbon (woC14) and with radiocarbon (wC14) yielded a multimodal posterior distribution with two relevant optima. One of the two modes scored clearly better in terms of the maximum posterior density. We focus on this mode for discussing the results. The posterior distribution and model predictions for the sub-dominant mode are presented in Figures 4.B.7–4.B.12. Figure 4.2 shows the marginal distributions for the prior and the posterior of both calibration setups. Compared to the prior the uncertainty of all parameters was reduced, already without including radiocarbon data. Adding radiocarbon led to further constraint for most of the parameters, with the exception of k_{AGL} , $\alpha_{\text{AGL}\rightarrow\text{NLF}}$, $\alpha_{\text{NLF}\rightarrow\text{LS}}$, and B . Particularly strong changes are observed for parameters related to the non-leachable slow (NLS) organic matter pool. The mean decomposition rate coefficient (k_{NLS}) is reduced from $5.7 \times 10^{-3} \text{ yr}^{-1}$ to $4.4 \times 10^{-4} \text{ yr}^{-1}$ (Table 4.B.2), corresponding an increase of turnover time from roughly 150 yr to 2000 yr. Additionally, the flow from non-leachable fast (NLF) organic matter to NLS, as determined by $\alpha_{\text{NLF}\rightarrow\text{NLS}}$, is strongly reduced. Hence, NLS is formed at a lower rate, but it is also more stable. Also the variance of k_{NLS} and $\alpha_{\text{NLF}\rightarrow\text{NLS}}$ is an order of magnitude lower when radiocarbon is included. However, the width of these distributions should be considered relative to the mean, since the two are likely correlated over different calibrations. Hence, it is more appropriate to compare the coefficient of variation (standard deviation relative to the mean) which shows a reduction by a factor of around 2 for the two parameters.

A further prominent difference between the two calibrations is apparent for the advection rate v . When radiocarbon is omitted v has a wide distribution with the marginal mode at the upper bound, whereas with radiocarbon data v is strongly constrained at the lower end of the range.

Model results

Figure 4.3 shows modelled and measured soil carbon stocks and profiles in March 2009. In both calibration setups the total simulated C stocks and mass fractions are well constrained, having less spread than the observations. Addition of radiocarbon led to a decreased fit to observed carbon stocks and mass fractions. The vertical organic carbon distribution became shallower, with overestimated stocks in the organic layer and topsoil and underestimated stocks in the subsoil. Further, the distribution over the different model pools in the topsoil changed, with leachable slow (LS) organic matter becoming more prominent.

Strong differences between the two calibrations are also apparent for the modelled organic matter transport fluxes by bioturbation (diffusion) and liquid phase transport (advection) (Figure 4.4). Addition of radiocarbon led to a reduction of the

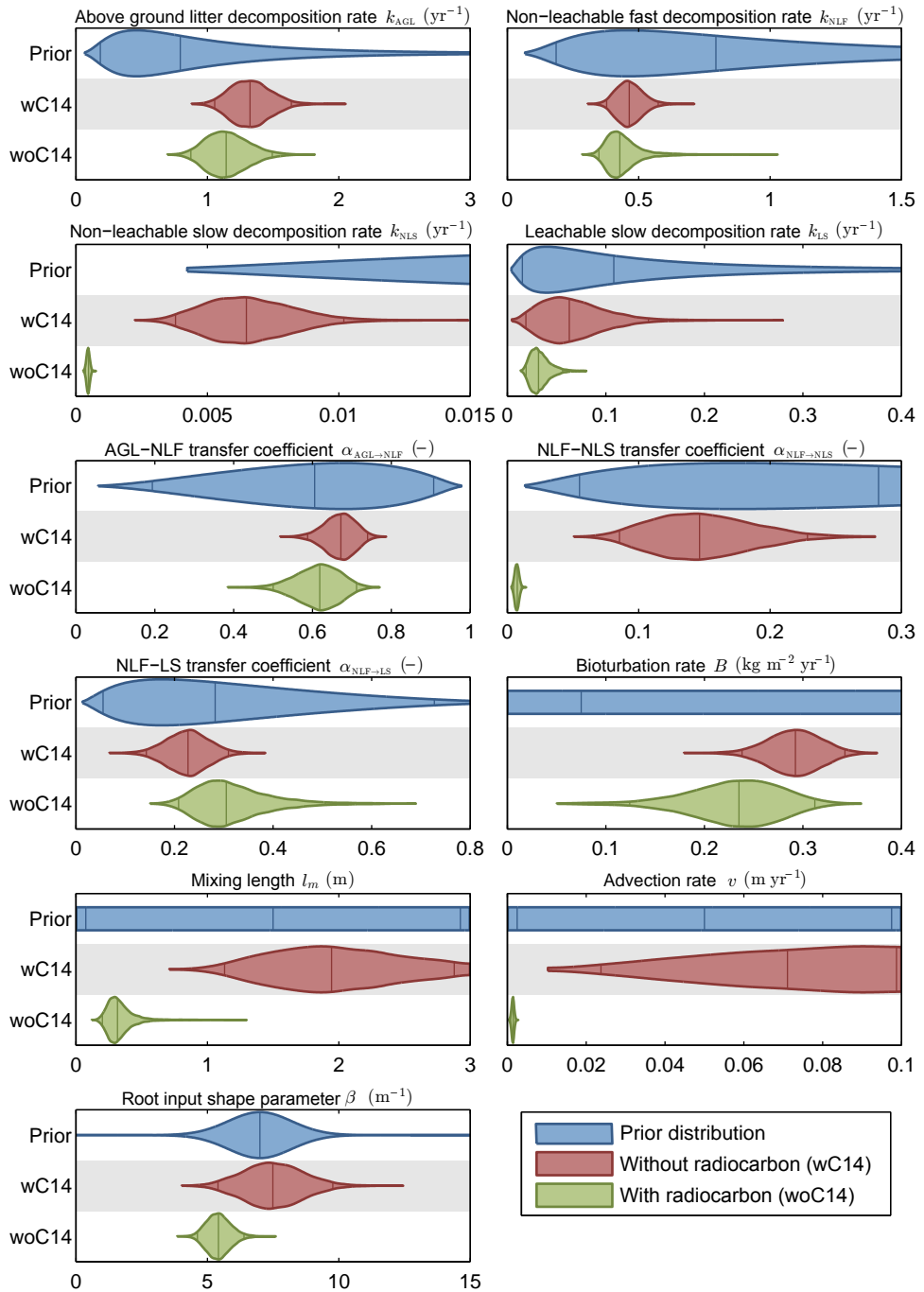


Figure 4.2: Violin plots of the marginal prior and posterior distributions. The three vertical lines inside the violins indicate the median and the 95% confidence bounds.

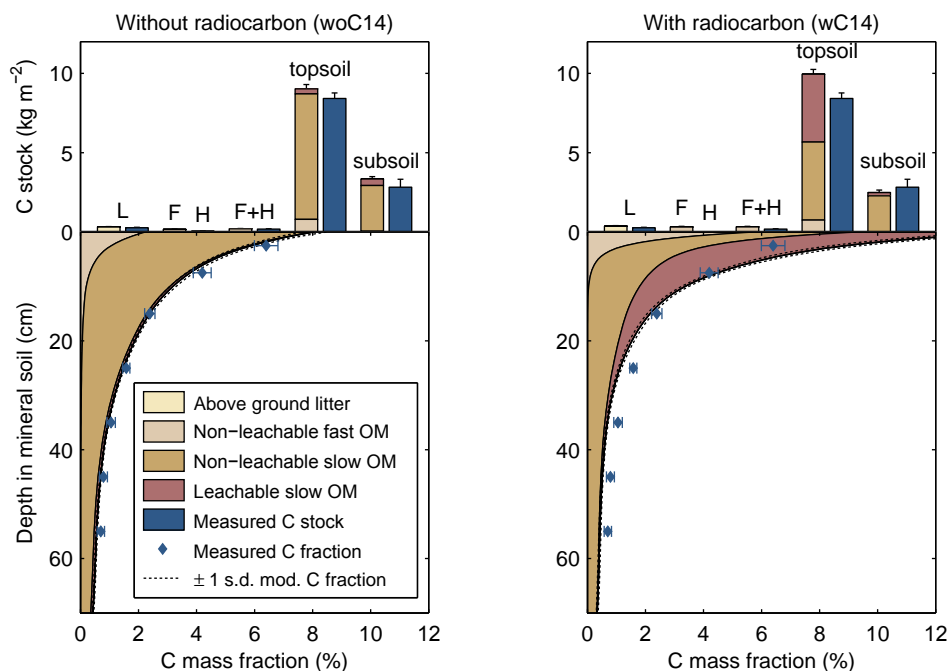


Figure 4.3: Organic carbon measurements and corresponding model results. L, F, and H refer to the organic horizons (see section 4.2.1); topsoil: 0–30 cm; subsoil: > 30 cm; OM: organic matter. All model results are ensemble means; errorbars denote one standard error of the mean for the measurements and one standard deviation (s.d.) for the model results.

flux rates of both mechanisms, which can be attributed to the reduced values of B , l_m , and v . We additionally plotted *in situ* measured dissolved organic carbon (DOC) fluxes from Kindler et al. (2011). These measurements were not included in the calibration, since the representation of liquid phase transport flow in SOMPROF was not intended for simulation of DOC. However, the simulated advective flux should roughly correspond to DOC transport. Although the advective flux is still overestimated compared to the observations, the strong reduction in flow due to radiocarbon addition is a clear improvement.

Figure 4.5 shows the measured and modelled radiocarbon activities for both organic matter and heterotrophic respiration. Measured $\Delta^{14}\text{C}$ of SOM in the mineral soil shows a clear negative gradient, indicating that SOM age increases with depth. The model results show a similar profile, but underestimate the radiocarbon activity in the deep soil. Measured $\Delta^{14}\text{C}$ of heterotrophic respiration is always higher than that of SOM, which shows that respired carbon is younger than the average total organic matter. Similar to SOM, $\Delta^{14}\text{C}$ of respired CO_2 decreases with depth. Modelled $\Delta^{14}\text{C}$ of heterotrophic respiration generally agrees with the observations, although the peak at 10 cm in the modelled vertical profile is not present for the

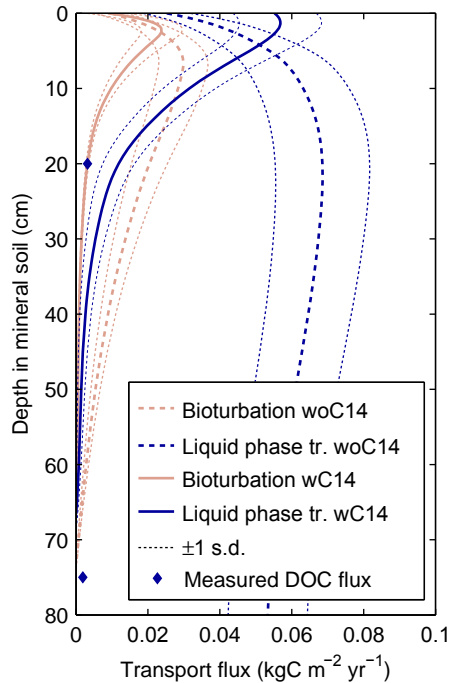


Figure 4.4: Simulated and measured organic carbon transport fluxes. Model results are ensemble means averaged over the last simulation year. Measured DOC fluxes (not used in the calibration) were taken from Kindler et al. (2011).

measurements.

Figure 4.5 further shows strong differences between the $\Delta^{14}\text{C}$ profiles of the organic matter pools. These differences are mostly explained by the decomposition rates of the pools, as well as their transport behavior. NLS has markedly lower $\Delta^{14}\text{C}$ values than the other two pools in the mineral soil, indicating it contains on average much older carbon. The profile of LS shows a clear maximum around 8 cm depth, which is caused by the bomb peak travelling downwards through the profile. Contrary to the other pools, non-leachable fast (NLF) organic matter shows almost no vertical gradient in the mineral soil, since it originates mostly from root input, which has the same radiocarbon signal everywhere. Since NLS and LS are the most abundant pools in the mineral soil, they determine the $\Delta^{14}\text{C}$ signature there, with the importance of NLS increasing with depth. In contrast, the $\Delta^{14}\text{C}$ of heterotrophic respiration is determined mostly by the LS pool and, near the surface, by NLF.

4.3.2 Projection simulations

The JSBACH ecosystem model predicts both increasing litter fluxes and soil temperatures (Figure 4.6). However, while temperatures keep rising throughout the simula-

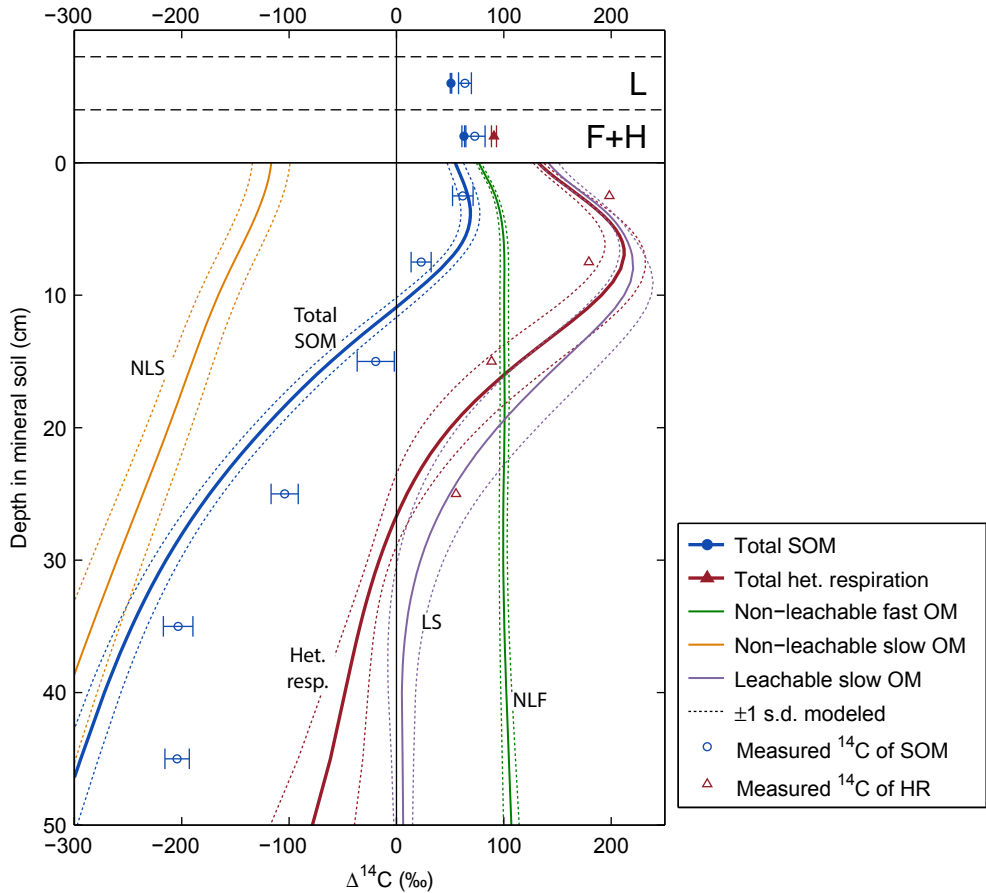


Figure 4.5: Modelled and measured $\Delta^{14}\text{C}$ for organic matter (March 2009) and heterotrophic respiration (April 2001). Model results are means and standard deviation over the simulation ensemble based on parameters from calibration wC14. Measured $\Delta^{14}\text{C}$ of heterotrophic respiration were taken from Hahn and Buchmann (2004). Additionally the $\Delta^{14}\text{C}$ values of the individual model pools (March 2009) are depicted. Note that the comparability between the OM $\Delta^{14}\text{C}$ and respiration $\Delta^{14}\text{C}$ is limited because they are shown for different years.

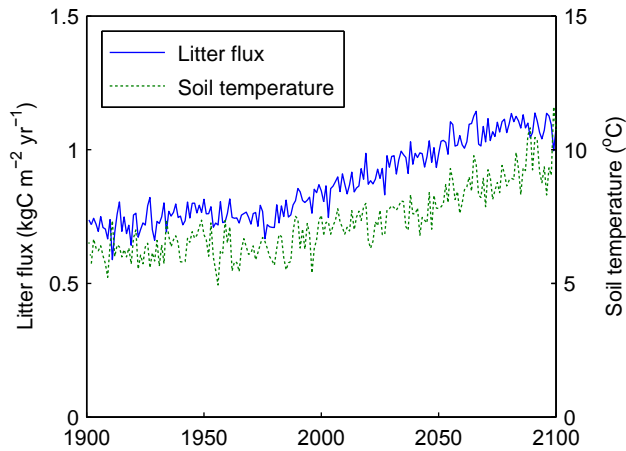


Figure 4.6: Annual total litter fluxes (above- + belowground) and average soil temperature at 8 cm depth at Hainich between 1901 and 2100, simulated by the JSBACH land surface model.

tion, litter fluxes stabilize near the end of the century. Average soil moisture did not change notably during the simulation period. Already at the start of the simulation in 1901, the litter fluxes calculated by JSBACH are markedly higher than the *in situ* measurements used in the calibration (cf Table 4.B.1). As a result, also the predicted soil carbon stocks based on the JSBACH forcing are higher than observations (Figure 4.B.6). However, for reasons discussed in section 4.4.2, we did not correct the JSBACH litter fluxes. Rather than the absolute quantities, we focus on the relative change of simulated carbon stocks over time.

Since the strongest changes in temperature and litter fluxes occur between 1980 and 2100, we limit the discussion of the results to this period. For both calibrations, the simulated organic carbon stocks for the complete profile grow initially but level off during the second half of the 21st century, and for calibration wC14, start to decrease (Figure 4.7A–B). However, the overall soil carbon gain is mainly caused by the topsoil; in the subsoil stocks are in fact decreasing. The simulated total C stock for the two calibration setups diverge over time, with calibration woC14 showing a stronger increase. Again, these differences are mainly explained by changes in the topsoil. The relative predictive uncertainty of the C stocks is depicted in Figure 4.7C as the coefficient of variation over the ensemble. Surprisingly, adding radiocarbon data to the calibration caused an *increase* of the relative uncertainty for the top- and subsoil and organic layer, individually. In contrast, the uncertainty for the total soil C stock is slightly reduced.

Figure 4.8 shows the simulated heterotrophic respiration flux. The average respiration became notably higher (approximately 10%) due to the addition of radiocarbon data. Furthermore, the uncertainty of simulated flux is reduced by roughly 90%.

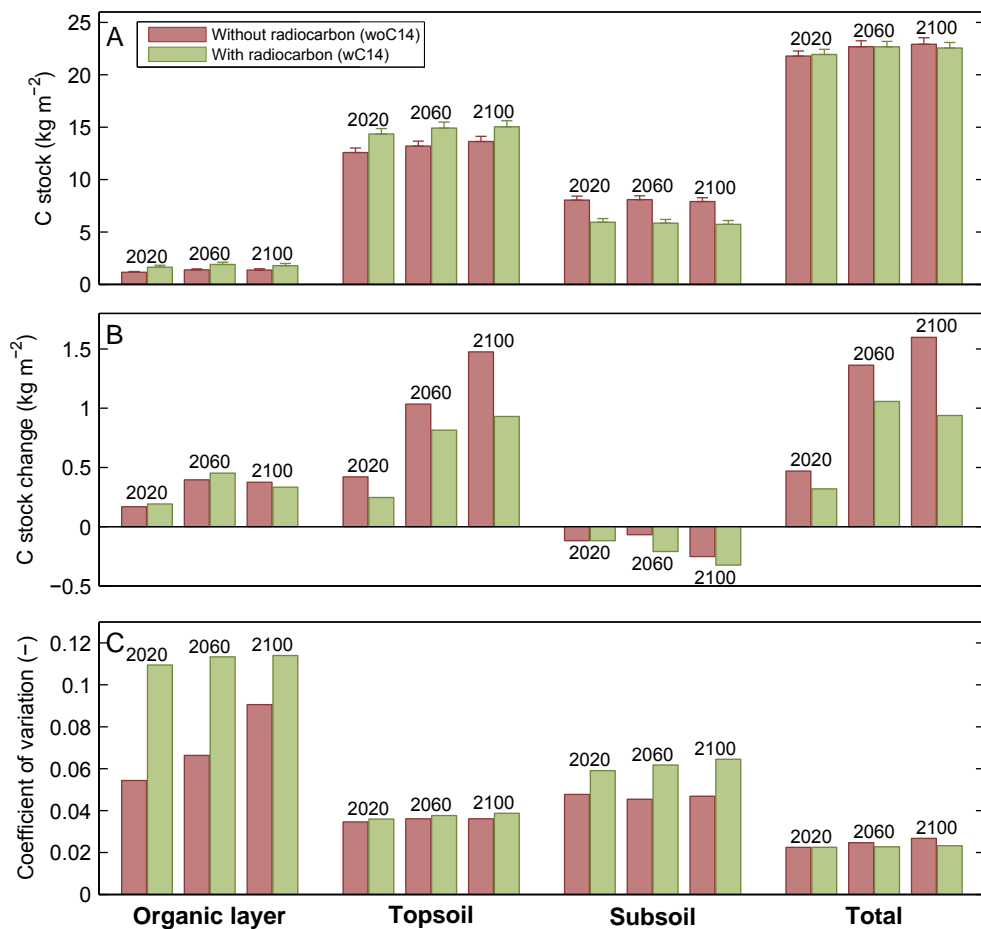


Figure 4.7: Soil carbon projections based on JSBACH predictions. A. total soil C stocks including 95% confidence bounds. B. change in C stocks relative to values in 1980. C. coefficient of variation (standard deviation relative to mean) over the ensemble for the C stocks.

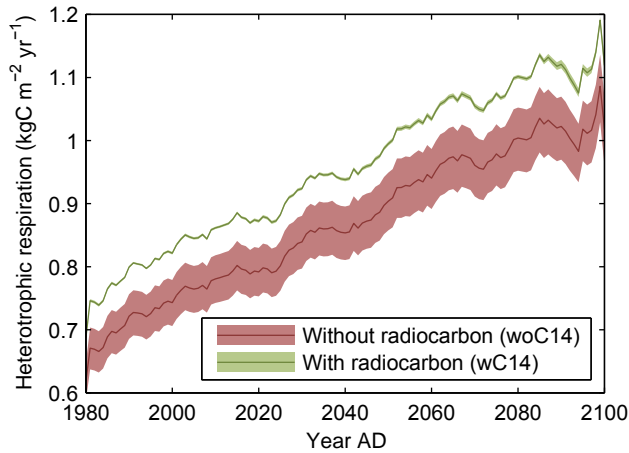


Figure 4.8: Heterotrophic respiration fluxes for the projections based on JSBACH predictions. The shaded areas indicated the 95% confidence range. The data was smoothed using a 10 year moving average window.

4.4 Discussion

4.4.1 Calibration

As mentioned earlier, the posterior distribution for both calibrations has two major optima. A similar result was obtained previously in chapter 3, where three relevant modes were found¹. The modes differ markedly in the distribution of SOM over the different pools and transport flux rates (Figures 4.B.8–4.B.10). Conversely, the predicted stocks in the projection simulations are quite similar (Figure 4.B.12). The mode for which we presented the results in the main text scored consistently better in both calibrations (log posterior density difference of ~ 7 and 10 for calibration woC14 and wC14, respectively), as well in several other setups that were tried. However, it is likely that the performance difference is overestimated since a number of uncertainty sources were not considered, most notably the forcing history and possible deviations from the steady state. Future efforts should focus on integrating additional variables that may help to identify the correct mode, such as physical and chemical SOM fractions.

The remainder of the discussion focusses on the dominant mode. The addition of radiocarbon data to the calibration caused major changes in the posterior distribution (Figure 4.2). For several parameters (k_{NLS} , $\alpha_{\text{NLF} \rightarrow \text{NLS}}$, l_m and v), there is virtually no overlap between the marginal distributions of both calibration setups, which indicates that the radiocarbon data is to some extent inconsistent with the other sources of information. Analysis of the different terms of the likelihood function shows a reduced fit to the mineral organic carbon mass fractions and the total heterotrophic

¹The two modes found here correspond approximately to modes A and B in chapter 3

respiration for the calibration with radiocarbon data (wC14). This is also apparent from graphical inspection of these variables (Figures 4.3 and 4.B.8). More important, however, is the increased disagreement with the prior distributions for k_{NLS} and $\alpha_{\text{NLF} \rightarrow \text{NLS}}$. Our prior estimates for these parameters were too high. Interestingly, for some parameters the marginal distributions became wider. This seems counter intuitive: additional information leads to more uncertainty. The explanation lies in the fact that correlations between parameters are stronger for calibration wC14 (Figure 4.B.4). This demonstrates the importance of considering the correlation structure when assessing the information gain, and when selecting a parameter set for forward simulations.

The addition of radiocarbon data to the calibration led to the introduction of a highly stable organic matter pool, turning over on millennial time scales. Also in previous studies it was found that a passive pool is required in order to reproduce measured radiocarbon activity (Perruchoud et al., 1999; Petersen et al., 2005; Gaudinski et al., 2000; Koarashi et al., 2012). For example, the inert organic matter (IOM) pool in the soil carbon model RothC is included primarily in order to reproduce observed radiocarbon ages (Falloon et al., 2000). Compared to similar studies with vertically explicit models (Elzein and Balesdent, 1995; van Dam et al., 1997; Baisden et al., 2002), our estimate of the slowest turnover rate is somewhat higher but in the same order of magnitude.

The measured radiocarbon data shows a negative depth gradient in the mineral soil (Figure 4.5). This gradient need not necessarily be caused by a change in average turnover rates with depth. Due to the time needed for vertical transport, also a homogenous SOM pool will show an age—and thus a radiocarbon—gradient with depth (cf the $\Delta^{14}\text{C}$ profile of NLS, Figure 4.5). However, apparently this mechanism alone cannot explain the observed profile. Since decomposition rates are not explicitly reduced with depth, additionally a change in the mixing ratio of the SOM pools with depth is required. This presumably explains the increased abundance of the leachable slow (LS) organic matter pool in the topsoil (Figure 4.3) and improved constraint of the advection rate v , for calibration wC14.

Both the measured and the modelled radiocarbon profile display a maximum below the surface, which is caused by the spike in the atmospheric radiocarbon activity due to nuclear weapons testing in 1964 (the bomb peak). This peak causes a similar maximum in the vertical profile which is reduced and travelling downward over time due to organic matter transport. In the modelled profile the peak is located at approximately 4cm depth in the mineral soil, while for the measurements the peak appears to be still in the F/H horizon. This suggests that the vertical organic matter transport is overestimated by the model. The modelled $\Delta^{14}\text{C}$ profile of heterotrophic respiration also displays a peak, located somewhat deeper ($\sim 6\text{cm}$), indicating that labile organic matter is transported faster than the slow pools. However, the measured $\Delta^{14}\text{C}$ for heterotrophic respiration do not display a peak. This may indicate that decomposition of root derived material is more important than shown by the model. On the other hand, no replicates were available for these measurements and the lab incubations may not be fully representative for *in situ* conditions (see section 4.4.3).

4.4.2 Projection simulations

Simulated soil carbon dynamics

As discussed in section 4.3.2, the litter fluxes predicted by JSBACH are markedly higher than estimates based on *in situ* measurements (Kutsch et al., 2010), causing a likewise overestimation of stocks in the soil carbon projections. An additional experiment for which the litter fluxes were corrected, showed more realistic carbon stocks. However, we chose to show only the original results without correction, for several reasons. First, more than in absolute quantities we are interested the *relative* SOM dynamics, which change only marginally when litter fluxes are adjusted downwards. Second, the current study was performed with future large scale gridded simulations in mind in which the two models are coupled. In such applications correction of fluxes based on local measurements would be infeasible and undesirable, since it would lead to disappearance of carbon from the system, rendering the net ecosystem fluxes meaningless.

The JSBACH model predicts both increasing soil temperatures and litter fluxes for the period 1901–2100 (Figure 4.6), the latter caused by increased vegetation productivity due to CO₂ fertilization. These two trends affect soil carbon stocks in opposite directions. However, while the litter input fluxes level off near the end of the simulation, the temperatures keep rising. This is reflected by the dynamics of the total soil carbon projections (Figure 4.7): the net balance decreases in the second of half of the 21st century and, for calibration wC14, turns negative. Similar future trajectories with initial carbon uptake, followed by levelling off or carbon loss, have been predicted in global simulation studies (Cramer et al., 2001; Sitch et al., 2008; Friedlingstein et al., 2006; Jones and Falloon, 2009).

The results further suggest that the soil at Hainich is currently gaining carbon, which agrees with previous studies based on repeated inventories (Kutsch et al., 2010; Tefs and Gleixner, 2012; Schrumpp et al., *subm.*). Notwithstanding, there are several unconsidered sources of uncertainty that potentially affect the simulated soil carbon stocks. First, the version of JSBACH used in this study does not consider nitrogen cycling. It has been suggested that vegetation models that ignore nitrogen limitation on productivity may overestimate carbon sequestration due to CO₂ fertilization (Hungate et al., 2003). Second, due to insufficient data availability, the temperature sensitivity of decomposition was not included in the calibration, but held fixed at the value reported by Lloyd and Taylor (1994). There is still little consensus regarding exact temperature sensitivity (Davidson and Janssens, 2006), which causes considerable uncertainty of predicted future soil carbon stocks (Jones and Falloon, 2009).

Interestingly, the topsoil and the subsoil show opposite responses to changes in forcing: topsoil C stocks increase while subsoil C stocks decrease. Clearly, the increased carbon input remains mostly near the surface, while at deeper levels net losses occur due to accelerated decomposition. Whether this would also occur in reality for the given conditions, is difficult to ascertain. Several mechanisms that may influence the SOM dynamics as a function of depth are currently not represented in the model since they are poorly understood. First, all SOM pools in the model have

the same response function for temperature. In reality the temperature sensitivity of decomposition may differ among different organic matter fractions, although this is still uncertain (Conant et al., 2011). Second, it has been shown that increased input of fresh litter in the subsoil may destabilize old SOM due to priming of microbial activity (Fontaine et al., 2007). Third, increased belowground productivity may lead to deeper root distributions (Iversen, 2010), causing also deeper input of SOM. Nevertheless, this result demonstrates that different parts of the SOM profile can respond differently to environmental changes. Thus, topsoil carbon dynamics should not be simply extrapolated downwards in order to derive changes in the subsoil.

Differences between calibrations

An important difference between the two calibrations lies in the predicted loss of carbon over the lower boundary by advection (Figure 4.4), which is unrealistically high for calibration woC14, up to 20% of the litter input. The smaller advective flux rates for wC14 also constitute a strong improvement compared to measured DOC fluxes. A further consequence is the markedly higher heterotrophic respiration flux (Figure 4.8) due to the steady state assumption in the calibration. Interestingly, compared to the observations, heterotrophic respiration is overestimated in calibration wC14 (Figure 4.B.3). This suggests that the steady state assumption is incorrect, and that the soil is in fact gaining carbon. The relative contributions of advection and respiration to the total loss is highly relevant for soil carbon dynamics under climate change, because the latter is sensitive to temperature while the former is not. This presumably also explains why calibration wC14 shows stronger carbon losses near the end of the simulation. Parameter sets applied for predictive simulations should produce realistic advective losses in order to avoid biased results.

An unexpected result is the larger spread for the carbon stocks in the organic layer, topsoil, and subsoil individually, in calibration wC14 (Figure 4.7C). Remarkably, adding information to the calibration led to an increase of predictive uncertainty for these variables. Conversely, for the total profile the uncertainty was slightly reduced. This indicates that the vertical distribution of SOM became more uncertain. A further explanation may lie in the fact that the predicted amount of a model pool is ultimately determined by the ratio of the input rate and the decomposition rate coefficient. Figure 4.9 shows the distribution of the ratio of $\alpha_{\text{NLF} \rightarrow \text{NLS}}$ and k_{NLS} , which determines the total amount of the NLS pool. The spread for this ratio has become wider, despite the reduced spread of these parameters individually (Figure 4.2; cf also Figure 4.B.4). This is presumably caused by disagreement between the organic C and radiocarbon observations (see Figure 4.3 and section 4.4.1). This conflict means that for parameter changes in certain directions a reduced fit to the organic C data is compensated by an improved fit to the radiocarbon data. As a result, parameter sets that were previously assigned low likelihood due to poor fit to the organic carbon data may become more probable when the radiocarbon data is included, causing the predictive uncertainty for organic carbon to increase.

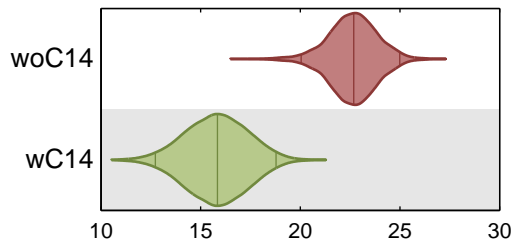


Figure 4.9: Posterior distribution for the ratio of $\alpha_{\text{NLF} \rightarrow \text{NLS}}$ and k_{NLS} for the two calibrations.

4.4.3 Methodological constraints

The effective decomposition rate observations, as well as the radiocarbon activity of the heterotrophic respiration were derived from measured fluxes from soil samples incubated in the lab, which may not be fully representative of conditions in the field. Simulated respiration rates were corrected for temperature and moisture in the lab incubation, but disturbance of the soil samples may have stimulated respiration, leading to overestimated decomposition rates, which was not accounted for. The effective decomposition rates are underestimated for calibration wC14 (Figure 4.B.5), which suggests this problem is relevant here. Furthermore, disturbance may also affect the radiocarbon signal of the respired CO_2 due to increased decomposition of old SOM (Fontaine et al., 2007).

For the calibration it was assumed that the average organic carbon stocks are in steady state, and that radiocarbon is in steady state at the start of the simulation, in 1800. Furthermore, the uncertainty of the past forcing was not considered. The Hainich forest has a relatively constant and well known history without major land use changes (Waeldchen et al., 2013, section 4.2.2). Nevertheless, as discussed in section 4.4.2, model results and previous studies point to a positive soil carbon balance in the present. Furthermore, due to the long turnover times of NLS for calibration wC14, forcing fluctuations may affect the soil carbon for hundreds of years. Methods have been proposed to relax the steady state assumption (Wutzler and Reichstein, 2007; Yeluripati et al., 2009; Carvalhais et al., 2010), but the available data here is insufficient to accurately constrain the net soil carbon balance. In view of these unconsidered uncertainties, it is advisable to inflate the variance of our posterior distribution for future calibrations.

4.4.4 The use of radiocarbon data for constraining SOM turnover and transport

When radiocarbon data was omitted from the calibration, the observed C stocks and profile were well reproduced, but with a strongly overestimated turnover rate for the slowest SOM pool. This exemplifies the problem of an incorrect model producing correct results, as discussed in the introduction. The obvious question is: to what extent does this lead to incorrect predictions and does avoiding these errors warrant

the considerable cost and labor that comes with radiocarbon measurements? The future predictions for the two calibration setups diverge for the transient simulations. However, in relative terms the differences are quite small (Figure 4.7A).

Nevertheless, we believe that SOM dynamics should be simulated based on accurate turnover rates, for several reasons. First, there is in general no guarantee that biases in the parameter estimates will be small enough that predictive errors are negligible. For other studies the overestimation of the turnover rate may be more severe (cf the Loobos site in chapter 3). Several studies have shown that the partitioning of total SOM over different turnover fractions is highly relevant for transient predictions (Telles et al., 2003; Jones et al., 2005). Furthermore, on longer time scales or in situations with more rapid environmental changes (e.g. land-use change or disturbances) overestimation of the transient response is more likely to occur. Second, as previously discussed, the response of decomposition to temperature may differ between SOM fractions (Conant et al., 2011). If this is the case, the distribution of total SOM over the different fractions is obviously highly relevant under conditions of climate change. Finally, consensus is emerging that the notion of SOM pools with fixed, intrinsic decomposition rates is incorrect. Rather, stabilization of SOM is the result of biological, physical, and chemical processes that may be reversible under the right conditions (Schmidt et al., 2011). Parameterization of these mechanisms and their effects on SOM decomposition requires accurate estimation of turnover rates.

Since C stock observations do not contain information about the dynamic behavior of soil carbon, it is generally advisable to include one or more additional observations that directly relate to turnover when calibrating soil carbon models. Several candidate measurements are available, such as heterotrophic respiration rates (either in situ or in lab incubations), ^{13}C , and observations from chronosequences. However, in general radiocarbon is one of the best choices, particularly when dynamics of the slowest organic matter fractions are of interest (Trumbore, 2009). Models that represent the complete vertical profile, such as SOMPROF, will generally require information on long time scale dynamics because of the very low turnover rates typical in the subsoil.

The fact that radiocarbon data led to an increase of predictive uncertainty in this study does not invalidate its use for constraining SOM transport and turnover. As discussed above, this is presumably related to the model's inability to fully fit both the radiocarbon and C profile data. Hence, the radiocarbon data showed that predictive uncertainty for the C stocks was previously underestimated. It does not mean that the addition of this data led to a loss of information. Since Bayesian calibration constitutes conditioning of the model on (new) data, the uncertainty of the combined distribution of the predictions for all data streams cannot become higher.

4.5 Conclusions

The addition of radiocarbon data to the calibration had large effects on the posterior parameter distribution. Strongest changes occurred for the parameters controlling

the formation and decomposition of the slowest organic matter pool, which were both strongly reduced. Additionally, the advection rate was reduced, resulting in more realistic predictions of SOM transport with the liquid phase. These results demonstrate that, without constraint on long time scale turnover rates, the model may produce correct results based on incorrect parameterization.

Future projections show increasing carbon stocks initially, with levelling off, and—for the radiocarbon constrained model—carbon losses, near the end of the 21st century. The modified parameters had only small relative effects on carbon stock projections, but led to markedly lower advective carbon losses, and higher heterotrophic respiration. Radiocarbon data further led to a slight reduction of predictive uncertainty for the total carbon stock and a strong reduction for heterotrophic respiration.

Our results illustrate the risk of obtaining biased parameters, when available observations hold limited or no information on the dynamic behavior of SOM. Despite the absence of strong changes of the model predictions we believe that radiocarbon is a valuable tool for constraining soil carbon models, particularly vertically explicit models such as SOMPROF.

Appendix 4.A Approximation of the posterior using Markov Chain Monte Carlo

Since the complexity of the model precludes analytical derivation of the posterior probability density function, the distribution was approximated with a Metropolis algorithm. This algorithm samples the posterior distribution by means of a Markov chain which performs a random walk in parameter space. At each iteration i proposals of the parameters θ^* are generated by taking a (semi-)random step from the current position θ^i . The model is run with the proposed parameter set and the unnormalized posterior probability density ($p(\theta)p(\mathbf{O}|\theta)$) of the proposal is evaluated. The proposal is subsequently accepted or rejected according to the Metropolis rule, which defines the chance for acceptance as:

$$s = \min \left\{ \frac{p(\mathbf{O}|\theta^*)p(\theta^*)}{p(\mathbf{O}|\theta^i)p(\theta^i)}, 1 \right\}. \quad (4.A.1)$$

The decision for acceptance or rejection is made using a random number from a uniform distribution on the unit interval. In case of acceptance, the chain moves to the position of the proposal; in case of rejection the chain stays at the current position, which is thus sampled again.

The specific algorithm used here was DREAM(ZS) (Laloy and Vrugt, 2012), an adaptation of the DREAM (DiffeRential Evolution Adaptive Metropolis) algorithm which uses multiple chains in parallel and automatically adapts the scale and orientation of the proposal distribution. Eight chains were run for each calibration. The convergence of the chains was evaluated using the Gelman-Rubin index (Gelman et al., 2004, Chap. 11), which is proportional to the ratio of the between-chain variance and the within-chain variance, and declines to 1 when the chains converge on

the same distribution. All chains were run until the convergence index was ≤ 1.01 for all parameters, with at least 100000 iterations per chain. After the runs, a variable number of iterations was removed from the start of each chain (the “burn-in”). Next, the remaining samples of all chains were merged and thinned to 10000 iterations for analysis by selecting iterations in regular intervals. Marginal probability distributions depicted in Figure 4.2 were derived using kernel density estimation (Bowman and Azzalini, 1997). For the model results depicted in Figures 4.3–4.5 5000 simulations were made based on parameters sets from the Monte Carlo samples.

Appendix 4.B Supplementary material

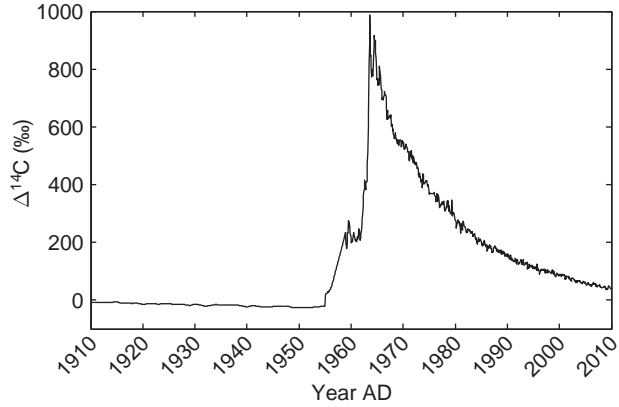


Figure 4.B.1: Atmospheric radiocarbon content used in the simulations.

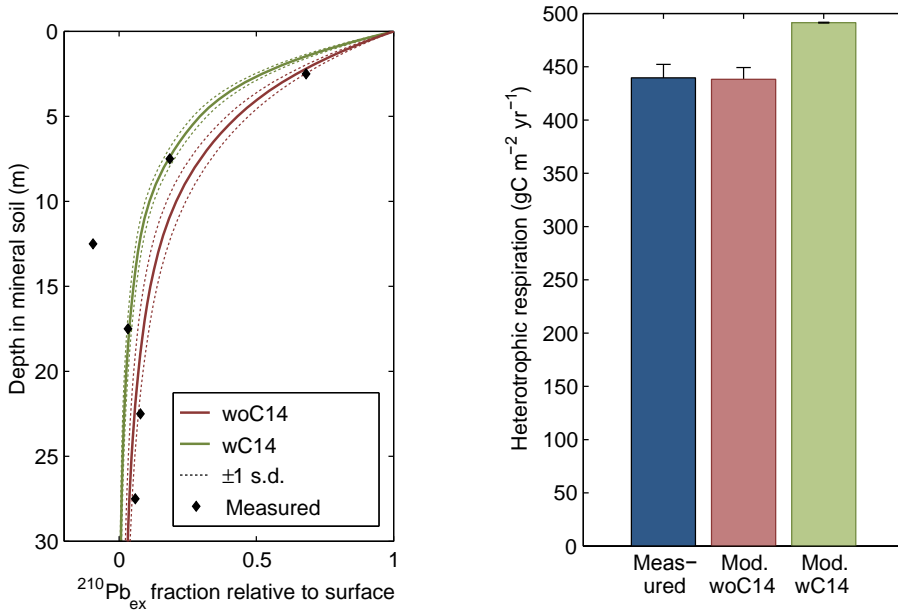


Figure 4.B.2: Measured lead-210 fractions relative to surface and corresponding model results. Model results are averages and standard deviations over the Monte Carlo ensembles.

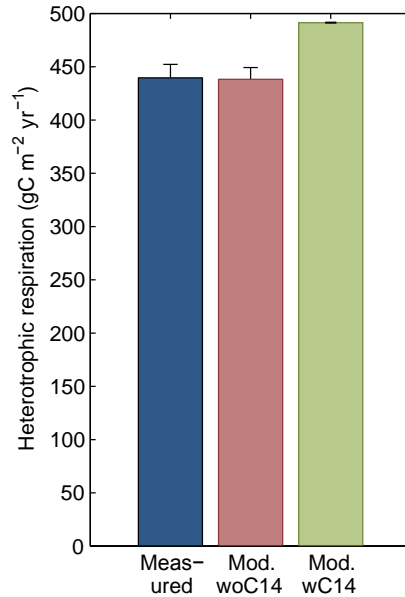


Figure 4.B.3: Measured and modelled total annual heterotrophic respiration. Model results are averages and standard deviations over the Monte Carlo ensembles. Errorbars for the measurements indicate one standard error of the mean.

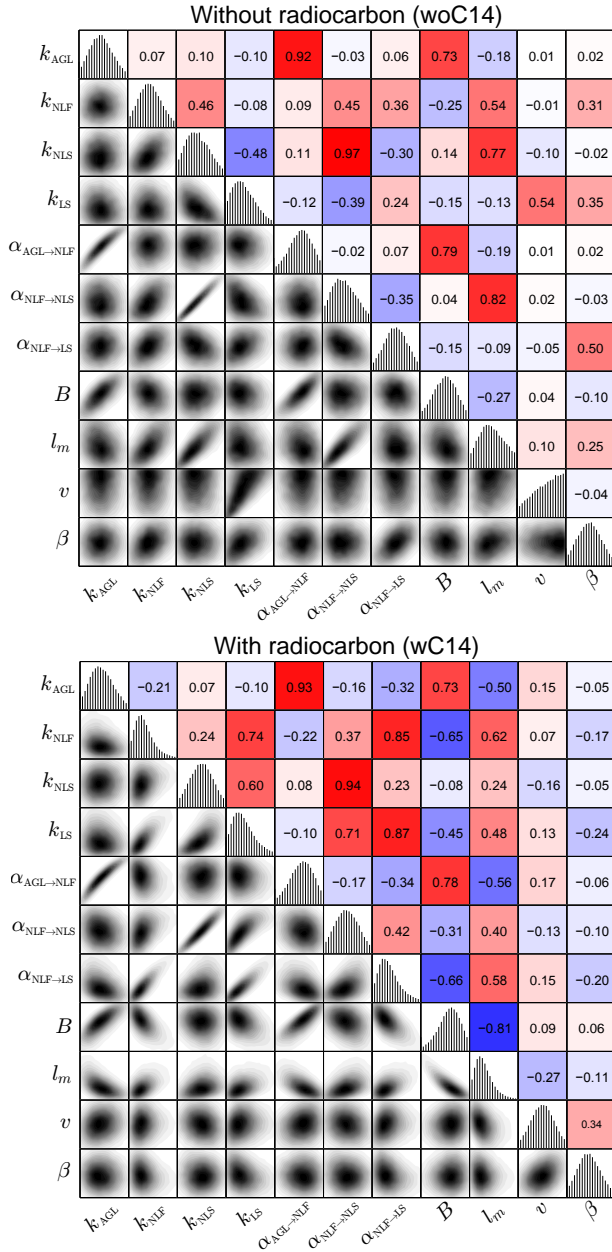


Figure 4.B.4: Correlation matrix of the posterior parameter distribution for the two calibrations. The figures show the correlations for each possible combination of two parameters. In the lower triangle bivariate probability density plots are depicted. In the upper triangle the correlation coefficients are shown, with blue indicating negative correlations and red positive correlations. On the diagonal histograms of the univariate marginal distribution for each parameter are shown.

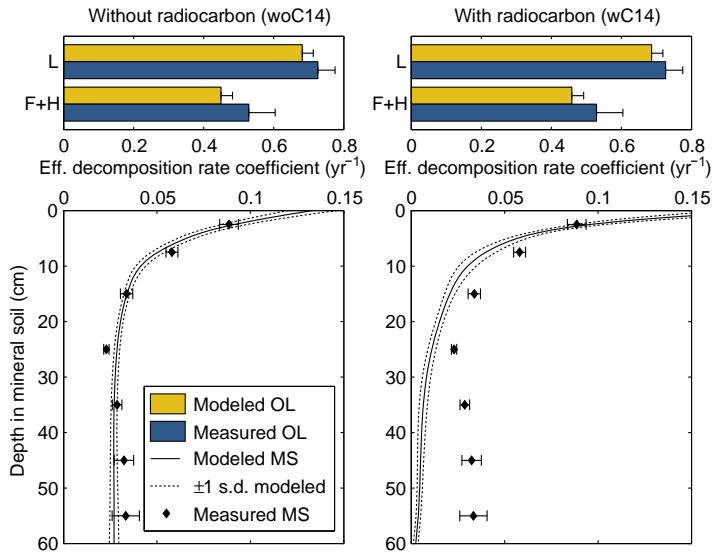


Figure 4.B.5: Measured effective decomposition rate coefficients and corresponding model results. Depicted model results are averages and standard deviations over the Monte Carlo ensemble. Errorbars for the measurements indicate one standard error of the mean.

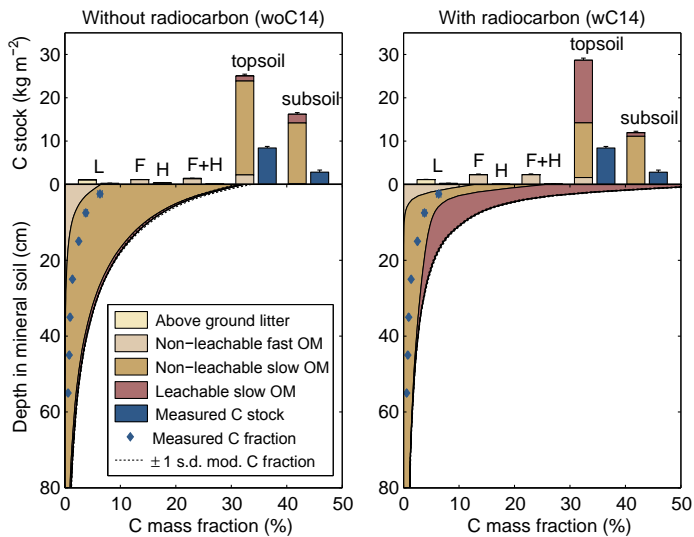


Figure 4.B.6: Organic carbon measurements for 2009 and corresponding model results based on JSBACH forcing. L, F, and H refer to the organic horizons; topsoil: 0–30 cm; subsoil: > 30 cm; OM: organic matter. All model results are ensemble means; errorbars denote one standard error of the mean for the measurements and one standard deviation (s.d.) for the model results.

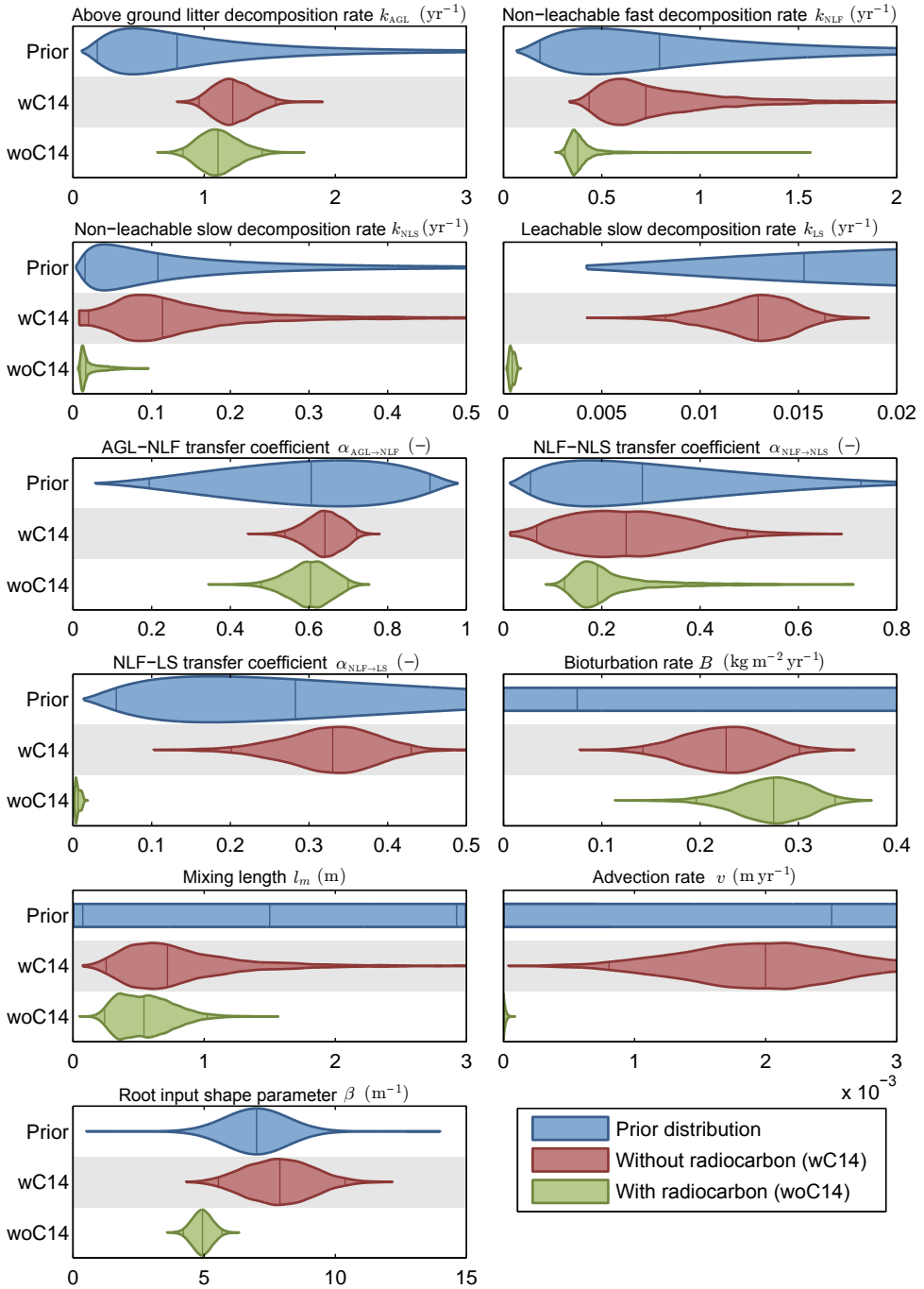


Figure 4.B.7: Violin plots marginal prior and posterior distributions for the sub-dominant mode. The three vertical lines inside the violins indicate the median and the 95% confidence bounds.

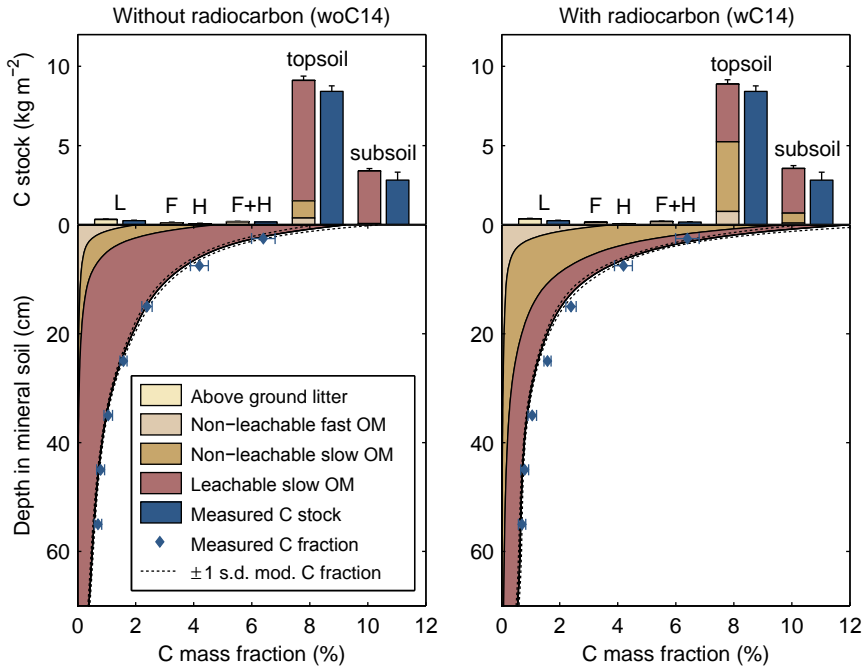


Figure 4.B.8: Organic carbon measurements and corresponding model results based on samples from the sub-dominant mode. L, F, and H refer to the organic horizons; topsoil: 0–30 cm; subsoil: > 30 cm; OM: organic matter. All model results are ensemble means; errorbars denote one standard error of the mean for the measurements and one standard deviation (s.d.) for the model results.

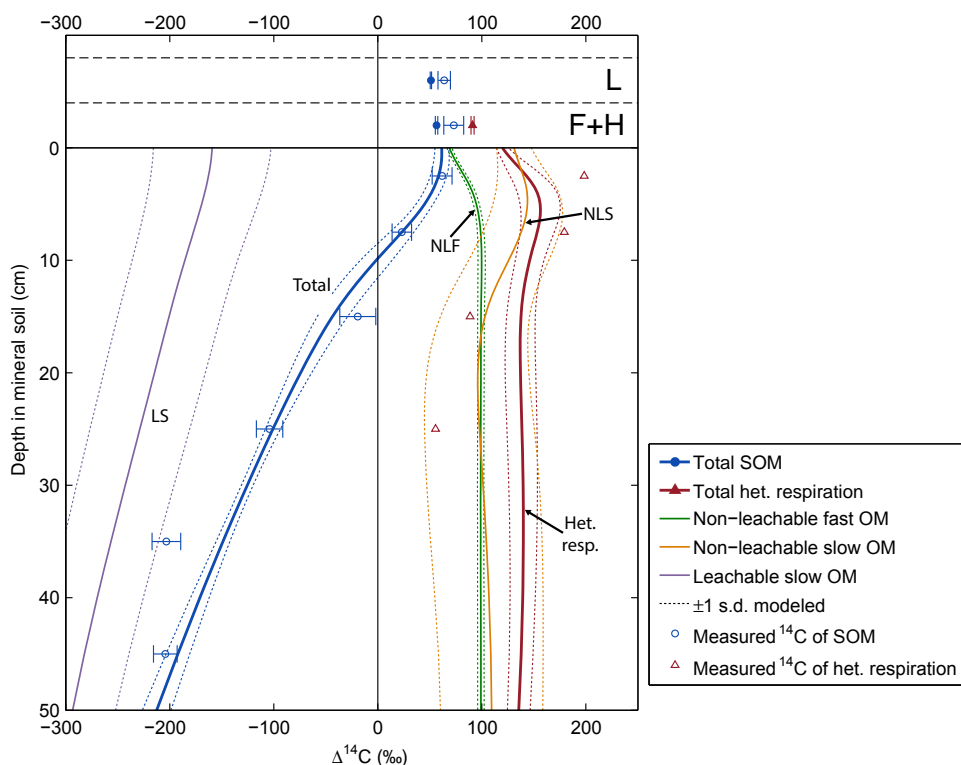


Figure 4.B.9: Measured $\Delta^{14}\text{C}$ for organic matter (March 2009) and heterotrophic respiration (April 2001) and corresponding model results based on samples from the sub-dominant mode for calibration wC14. Model results are means and standard deviation over the simulation ensemble. Additionally the $\Delta^{14}\text{C}$ values of the individual model pools (March 2009) are depicted. Note that the comparability between the OM $\Delta^{14}\text{C}$ and respiration $\Delta^{14}\text{C}$ is limited because they are shown for different years.

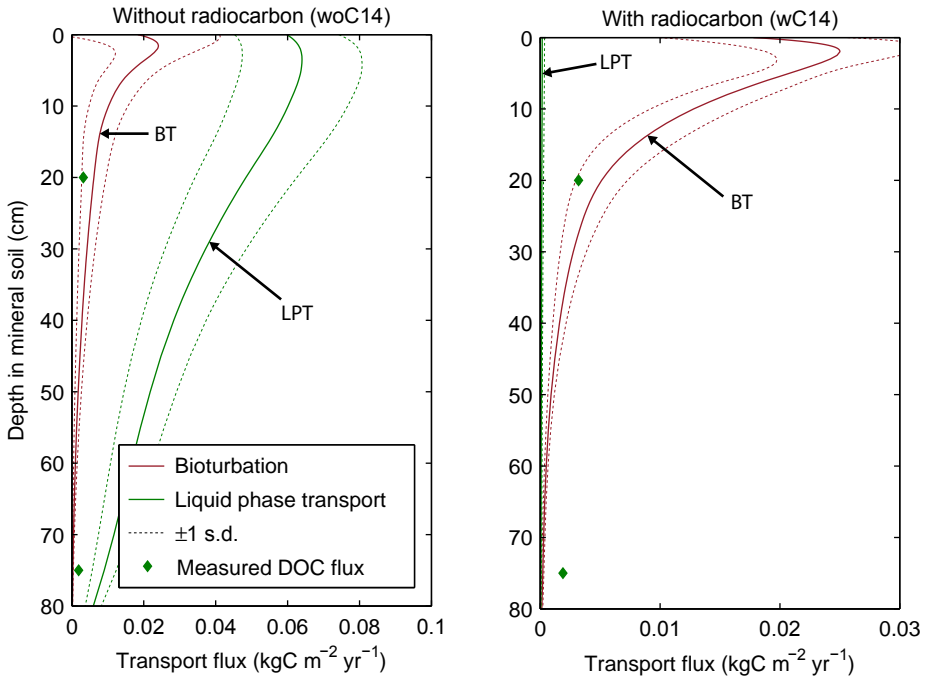


Figure 4.B.10: Modelled organic carbon transport fluxes based on samples from the sub-dominant mode and measured dissolved organic carbon fluxes. Model results are ensemble means and standard deviations averaged over the last simulation year. Measured DOC fluxes were taken from Kindler et al. (2011).

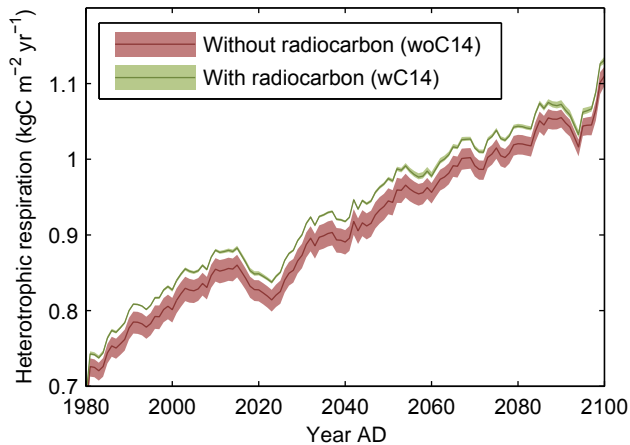


Figure 4.B.11: Modelled heterotrophic respiration for projection simulations until 2100 based on samples from the sub-dominant mode and JSBACH forcing data. Lines indicate ensemble means and shaded areas indicate 95% confidence bounds.

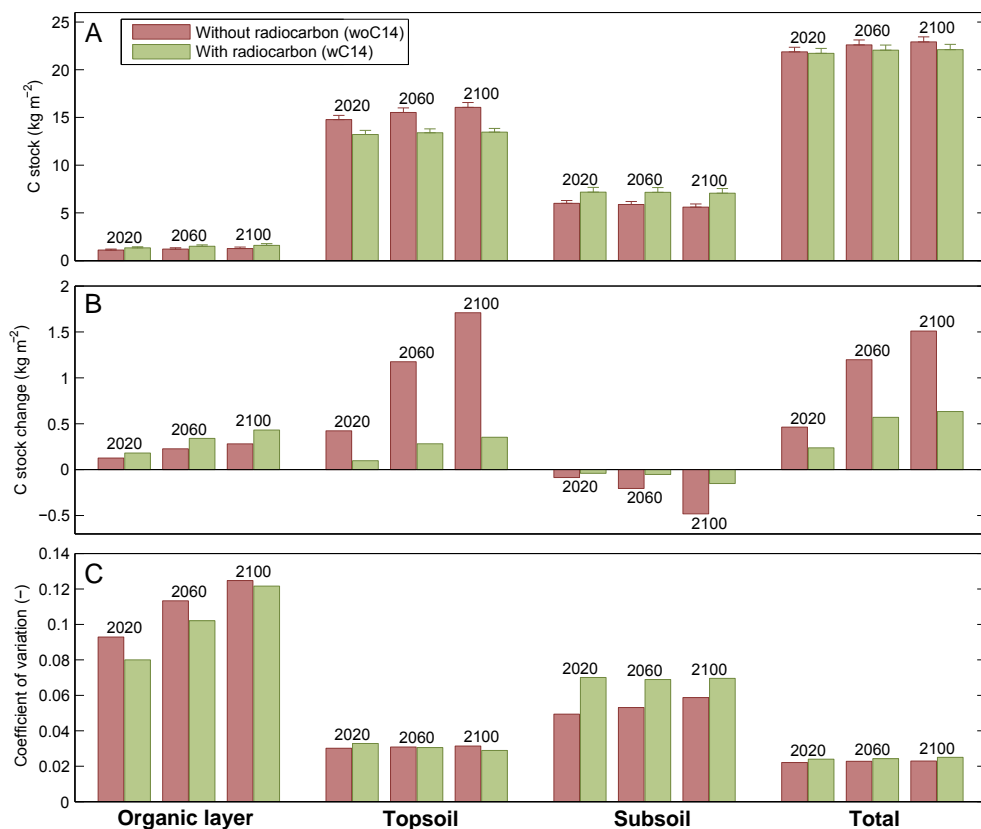


Figure 4.B.12: Modelled C stock results of projection until 2100 based on samples from the sub-dominant mode and JSBACH forcing data. A. total soil C stocks including standard deviation over the Monte Carlo ensemble. B. change in C stocks relative to values in 1980. C. coefficient of variation (standard deviation relative to mean) over the ensemble for the C stocks.

Table 4.B.1: Model driving data and not-estimated parameters.

Variable/Parameter	Value
Annual aboveground litter input ^{a,b}	0.314 kg C m ⁻² yr ⁻¹
Canopy	0.277 kg C m ⁻² yr ⁻¹
Understory	0.037 kg C m ⁻² yr ⁻¹
Total annual root litter input ^{a,b}	0.178 kg C m ⁻² yr ⁻¹
Canopy	0.148 kg C m ⁻² yr ⁻¹
Understory	0.03 kg C m ⁻² yr ⁻¹
Average soil moisture ^{a,c,d}	0.361
Average soil temperature ^{a,c}	7.653 °C
Soil temperature response parameter	308.56 ^e K
Soil moisture response parameter <i>a</i> ^f	1
Soil moisture response parameter <i>b</i> ^f	20
Bulk density L horizon	50 kg m ⁻³
Bulk density F horizon	100 kg m ⁻³
Bulk density H horizon ^g	150 kg m ⁻³
Bulk density mineral soil ^a	785.63–1350.3 kg m ⁻³
Bulk density pure mineral soil ^h	1300 kg m ⁻³
Initial depth of bottom boundary	0.7 m

^a Only used in calibration simulations.

^b Kutsch et al. (2010); W. Kutsch (personal communication, 2009).

^c Average over year and profile.

^d Fraction of maximum available water.

^e Lloyd and Taylor (1994)

^f Soil moisture response function: $g(W) = \exp(-\exp(a - bW))$; (Subke et al., 2003).

^g Also used in projection simulations as bulk density of pure organic soil.

^h Used in projection simulations to determine bulk density using pedotransfer function (Federer et al., 1993).

Table 4.B.2: Properties of the marginal posterior distributions for both calibrations (with and without radiocarbon) and both modes. For each parameter the 2.5 % quantile, the sample with highest posterior density (Opt.), and the 97.5 % quantile are shown.

Setup	k_{AGL} yr^{-1}	k_{NLF} yr^{-1}	k_{NLS} yr^{-1}	k_{LS} yr^{-1}	$\alpha_{\text{AGL} \rightarrow \text{NLF}}$ —	$\alpha_{\text{NLF} \rightarrow \text{NLS}}$ —	$\alpha_{\text{NLF} \rightarrow \text{LS}}$ —	B $\text{kg m}^{-2} \text{yr}^{-1}$	l_m m	v m yr^{-1}	β m^{-1}
Dominant mode											
2.5%	1.053	0.3779	0.003785	0.01896	0.5882	0.08471	0.1434	0.237	1.126	0.02322	5.394
woC14 Opt.	1.366	0.4365	0.005664	0.06945	0.687	0.127	0.2254	0.3095	1.586	0.06497	7.231
95%	1.645	0.5743	0.01019	0.1432	0.7397	0.2282	0.3107	0.3426	2.878	0.09868	9.791
2.5%	0.8752	0.3487	0.0003618	0.01912	0.4991	0.004723	0.209	0.1229	0.202	0.0008569	4.603
wC14 Opt.	1.187	0.3869	0.0004355	0.0239	0.6387	0.006184	0.2493	0.2758	0.2491	0.001373	5.269
95%	1.492	0.6163	0.0005933	0.05653	0.7106	0.01071	0.5079	0.3116	0.6193	0.002104	6.404
Sub-dominant mode											
2.5%	0.9565	0.4358	0.01979	0.008266	0.5378	0.06756	0.2009	0.1417	0.2563	0.0008034	5.54
woC14 Opt.	1.282	0.5443	0.05198	0.01239	0.6548	0.1756	0.3003	0.2666	0.5779	0.002127	7.848
97.5%	1.55	1.926	0.4966	0.01632	0.722	0.493	0.4304	0.3019	2.037	0.003415	10.35
2.5%	0.8425	0.3129	0.009128	0.0002474	0.479	0.1248	0.002604	0.1968	0.2469	3.223e-07	4.206
wC14 Opt.	1.074	0.3601	0.01264	0.000351	0.588	0.1741	0.004136	0.272	0.6864	4.939e-06	4.902
95%	1.439	0.6858	0.06145	0.0007039	0.699	0.4644	0.01397	0.337	1.027	4.312e-05	5.679

Chapter 5

General discussion and conclusions

5.1 Introduction

The past two decades have seen a huge increase in the number studies on processes that govern soil carbon cycling. The understanding gained from these studies needs to be transferred to models so that predictions of future climate change can be improved. However, it is becoming increasingly clear that the zero-dimensional approach currently applied in most large scale models is too simplistic to accommodate new process descriptions. For the next generation of models a representation of the vertical heterogeneity of soil organic matter (SOM) will need to be developed in order improve simulation of cycling of carbon and other elements, as well as soil physical processes.

This chapter reflects on the structure of the SOMPROF model and the calibration results, and summarizes the main findings regarding the formation of the vertical SOM profile. Furthermore, several recommendations for potential improvements to the model structure and calibration approach, as well as future large scale applications, are made.

5.2 Key results of this study

The SOMPROF model described in chapter 2 is a new, vertically explicit scheme that simulates soil organic matter dynamics. It represents the vertical distribution of SOM in the mineral soil profile and surface organic horizons by accounting for vertical SOM movement by bioturbation and liquid phase transport, and the vertical distribution of input by roots. Simulations have demonstrated that the model is able to predict realistic SOM profiles and organic layer masses, based on reasonable parameter values. Results from sensitivity analyses show that temporal variability of heterotrophic respiration is influenced by the vertical SOM distribution.

The model was calibrated using a Bayesian approach based on measurements for two deciduous forest sites with contrasting soil conditions (chapter 3). The results give insights into the determinants of the SOM profile, highlighting differences be-

tween the two sites in terms of the relative importance of root input, bioturbation, and liquid phase transport. Furthermore, for one site the calibration yielded a posterior parameter distribution with several modes, which demonstrated the difficulties arising from convolution of the different processes. Inclusion of measurements of $^{210}\text{Pb}_{\text{ex}}$ as a tracer for SOM transport helped to identify the most probable mode, but did not have major effects on the parameter distributions.

In a subsequent calibration study (chapter 4) the use of radiocarbon (^{14}C) data was investigated. Including this data in the calibration data strongly reduced the estimated decomposition rate of the slowest SOM pool, indicating that this parameter was previously overestimated. A prognostic simulation for the period 1910–2100 under conditions of increasing litter input and temperature showed diverging responses for different parts of the SOM profile. The addition of radiocarbon data caused minimal reduction of prediction uncertainty but did reveal inconsistency between the model and different observed variables.

5.3 The SOMPROF model

The development of the SOMPROF model structure was constrained by two considerations: parsimony and fidelity. The parsimony constraint limits the maximum complexity, so that parameters can be estimated with an acceptable degree of certainty. Since the number of studies on the vertical SOM distribution and SOM transport processes is relatively small, little prior information is available to determine parameter values for unvisited sites. Hence parameter estimation based on observations is required. Since calibration rapidly becomes more difficult with increasing degrees of freedom (Tarantola, 2005), limiting the number of parameters by choosing simple mathematical formulations is expedient. On the other hand, the need for fidelity to the natural system limits the degree of simplification. This fidelity is desirable for several reasons. First, in order to be applied for climate change simulations, the model should capture the dynamic response to changes in litter input and environmental conditions. A purely empirical description is less likely to correctly simulate temporal dynamics. Second, parameters that represent real physical quantities are preferred because prior knowledge is less likely to be available for purely empirical parameters. Furthermore, such physical quantities can be better related to environmental covariates.

Examples of parsimony motivated choices in SOMPROF are the representation of liquid phase transport as a simple advection process, and the constancy of parameters with depth (section 2.2). Conversely, the choice to represent bioturbation and liquid phase transport by separate formulations (contrary to most models; c.f. section 1.2.6), is motivated by the need for fidelity.

As discussed in chapter 1, this work is not the first study aimed on modelling the vertical SOM profile (see references in section 1.2.6). Most notable are the recent works by Jenkinson and Coleman (2008) and Koven et al. (2013), which represent significant steps forward in the addition of the vertical dimension to prognostic soil carbon models. The work by Koven et al. (2013), dealing with an extension of the

Community Land Model (CLM4), likely represents the first global application of a dynamic SOM profile model. The structure of this model is quite similar to that of SOMPROF. Both include a multi-pool decomposition model with first order kinetics, combined with diffusion and advection. An advantage of SOMPROF is the explicit representation of the surface organic layer, which will be beneficial for simulation of soil moisture and heat transport.

The current study also took a more rigorous approach to parameter estimation compared to earlier works. With one exception (Guenet et al., 2013), none of the previous studies applied a Bayesian approach, and few discussed parameter identifiability and equifinality. Furthermore, previous studies did not attempt to relate mathematical descriptions of SOM transport to specific processes in the field. Although challenging, individual parameterization of transport mechanisms will likely make the model robust when applied for different sites and under changing conditions.

Parallel efforts at developing different model representations for the SOM profile should not be seen as redundant. Scientific development ultimately benefits from existence of multiple formulations, both to identify superior descriptions, as well as to assess uncertainty of predictions originating from the model structure.

5.4 Determinants of the soil organic matter profile

Combined with the posterior parameter distributions, SOMPROF can offer valuable insights into the development of SOM profiles. An approach was developed to estimate the amount of organic matter deriving from root input, bioturbation, and liquid phase transport for the steady state (section 3.2.4 and 3.B). This provides an estimate of the relative importance of these processes as a function of depth. The analysis shows that the two sites studied in this study differ considerably in this respect (Figures 3.6b and 3.9b). At Loobos, a poor sandy Arenosol, liquid phase transport appears to be a major determinant of the SOM profile, removing organic matter from near the surface and depositing it in the rest of the profile. For Hainich, a rich Cambisol with a high clay content, root input and bioturbation are important. The differences between the two sites agree well with expectations based on site conditions, which is encouraging and supports the validity of the approach. The results also show that the effects of SOM transport processes can in general not be ignored. Using the root biomass distribution as an approximation of the SOM profile would likely lead to a too shallow distribution.

Because of the convolution of the processes, as well as difficulties measuring them *in situ*, inversion of a mechanistic model may be the only way to quantify them simultaneously, particularly on long time scales. At the same time, the entanglement of processes also constitutes the most important obstacle in this study. It was anticipated that the different processes could be separated in the model inversion by representing them with different mathematical formulations: diffusion and advection. Similarly, the choice for a separate SOM pool that is transported by advection was aimed at separating particulate and potentially mobile SOM fractions (section 2.2.4). For Hainich this proved challenging, as demonstrated by the existence of multiple

modes in the parameter distributions, characterized by different relative importance of the SOM pools and transport mechanisms (sections 3.3.2 and 4.3.1). Furthermore, changes to the model structure and addition of new calibration data in chapter 4 led to a change of the dominant mode. Clearly the calibration data and prior distributions did not contain sufficient information to fully disentangle the mechanisms. For Loobos the separation of processes was more successful (section 3.3.1), which is remarkable, considering that less data was used for this site. It is possible that the bounds of the prior distribution excluded other potential modes from the posterior. However, as demonstrated by the Hainich results, a model may be right for the wrong reason, which is not revealed in the calibration. Hence it would be advisable to verify the Loobos results with additional observations. In particular observations pertaining to SOM turnover are needed, in view of the overestimated decomposition rate coefficients of the slowest SOM fraction. Various sources of uncertainty and convolution of processes are further discussed in section 5.6.2.

5.5 Vertical soil organic matter transport

5.5.1 Bioturbation

In SOMPROF bioturbation in the mineral soil is modelled as a diffusive process (section 2.2.4). The validity of diffusion as a mechanistic description of bioturbation has been questioned by researchers in the field of benthic geochemistry (Boudreau, 1986b; Meysman et al., 2003) because its criteria are generally violated, particularly at small spatial scales and short time scales. Other, possibly more valid, approaches have been suggested (Boudreau, 1986a, 1989; Meysman et al., 2008). Nevertheless, as an empirical approach, the diffusion model has proven to be useful to modelling bioturbation (Meysman et al., 2003). Since SOMPROF is intended to be applied at temporal and spatial scales much greater than those of biological mixing, the diffusion model is assumed to be appropriate.

The diffusion equation for soil mixing can be derived from mixing length theory (Boudreau, 1986b, Appendix 2.B), originally developed for turbulent mixing in gasses. In this approach the diffusivity ($\text{m}^2 \text{yr}^{-1}$) is assumed to be composed of the fluctuating component of the vertical advection rate ($\text{m}^3 \text{m}^{-2} \text{yr}^{-1} = \text{m yr}^{-1}$), and the mixing length l_m (m). The former can be related to the “population level reworking rate” (Wheatcroft et al., 1990, here referred to as the bioturbation rate B $\text{kg m}^{-2} \text{yr}^{-1}$), and the latter should represent the typical distance over which burrowing animals displace soil particles (Boudreau, 1986b). The question arises to what extent B and l_m correspond to these quantities in reality. Paton et al. (1995) compiled a comprehensive list of soil reworking rate estimates for various soil animal groups. For earthworms, the most important and well-studied bioturbating organism, the listed rates range between 0.0063 and 26.8 $\text{kg m}^{-2} \text{yr}^{-1}$, with most values between 0.1 and 5 $\text{kg m}^{-2} \text{yr}^{-1}$. For Hainich, where earthworms are presumably responsible for most of the mixing, the estimates of this study are approximately 0.23 $\text{kg m}^{-2} \text{yr}^{-1}$ and 0.27 $\text{kg m}^{-2} \text{yr}^{-1}$, for the dominant and sub-dominant modes, respectively (chap-

ter 4, calibration wC14). Hence, the estimate obtained in this study is in the lower end of the range, but compares well.

The mixing length l_m is more difficult to link to a measurable quantity. Wheatcroft et al. (1990) suggested using body length of the burrowing organism for bioturbation in sediments. However, Meysman et al. (2003) pointed out that typical displacement distance is likely larger, because animals move while feeding, and additional transport occurs due to collapse of burrows. Again, assuming earthworms as the main agent of mixing, typical body length is in the range of 5–15 cm for the dominant species at Hainich (*Aporrectodea caliginosa*; Cesarz et al., 2007). The estimates obtained in this study for Hainich are approximately 34 cm, and 56 cm for the dominant and sub-dominant modes (chapter 4, calibration wC14)—notably higher but in the right order of magnitude.

Since field estimates of the soil displacement rates are influenced by large uncertainty from various sources (section 1.2.4), they are only useful as a rough approximation to B . For the mixing length l_m direct measurement may be impossible. Estimates of B and l_m in the SOMPROF inversion are likely also influenced by the fact that the former is used as the potential flux of material between the organic horizons and into the mineral soil (section 2.2.4). Furthermore, soil mixing due to bioturbation is a much more complex process than the picture of turbulent exchange in mixing length theory (Francois et al., 1997). Hence, the diffusivity should be seen as an effective parameter, which cannot be directly measured. Soil reworking rate measurements are useful as an environmental covariate that can be empirically linked to the diffusivity. Mixing length theory suggests that a simple linear relationship is appropriate.

The bioturbation rate B (and thus the diffusivity) is assumed constant with depth in SOMPROF. This choice was made for reasons of parsimony and the fact that very little is known about the depth distribution of mixing intensity. Nevertheless, this is obviously a simplification since soil fauna biomass and reworking activity are highest in the topsoil (Paton et al., 1995). It should be studied if a decreasing bioturbation rate with depth yields better results. Boudreau (1998) suggested relating the bio-diffusivity in sediments to the local concentration of labile organic matter since mixing is related to feeding. This approach has the advantage that it does not introduce additional parameters.

5.5.2 Liquid phase transport

In SOMPROF liquid phase transport is simulated with a one-parameter advection model for a potentially mobile SOM pool (leachable slow (LS) organic matter), representing both dissolved organic matter (DOM) in solution and adsorbed to the solid phase (section 2.2.4). Several other published SOM profile models also use a simple advection approach (e.g. Elzein and Balesdent, 1995). The representation in SOMPROF is somewhat more detailed compared to these models because of the assumption that only one pool is moved by advection. This means that the concentration of material that is susceptible to advection can vary with depth independently from the overall SOM concentration. Furthermore, it means that decomposability and

susceptibility to advective transport are inherently linked.

The scheme for liquid phase transport in SOMPROF relies on several assumptions: (i) The fractions of DOM in solution and adsorbed to the solid phase are assumed to be in equilibrium. Since the typical time scale of water flow is much shorter than that of ad- and desorption, this assumption generally does not hold (Gjettermann et al., 2007). This may lead to both over- and underestimation of simulated fluxes, hence the errors may average out over long time scales. However, the precise errors are highly dependent on the specific conditions, and depth in the profile. For soils with fast water fluxes it may lead to underestimation of loss of carbon over the lower boundary. (ii) The adsorption isotherm is assumed to be linear, with no saturation effects. This is in general not true since the capacity of minerals for adsorption decreases with increasing adsorbed organic matter (Hassink, 1997). This may lead to underestimated advective fluxes particularly for the topsoil. (iii) The advection rate is assumed constant with depth. Based on measured dissolved organic carbon fluxes, Sanderman et al. (2008) found decreasing advection rates with depth. This is to be expected since average downward water fluxes are lower in the deep soil, due to root water uptake, decreasing hydraulic conductivity with depth, and the fact that precipitation first leads to increased water storage, when soil is dry. (iv) Lateral DOM transport is assumed negligible. The rate of lateral water flow is dependent on the slope but in many soils presumably some lateral DOM flow occurs (McDowell and Likens, 1988). This represents an additional loss term of soil carbon that is not considered.

Several more realistic approaches have been published that explicitly simulate DOM concentrations and fluxes (e.g. Michalzik et al., 2003; Neff and Asner, 2001; Gjettermann et al., 2008). However, applying these schemes in SOMPROF is difficult because they require detailed information to parameterize adsorption and simulation of water fluxes at short time scales (≤ 1 d). Furthermore, since DOM in the soil solution represents only a small fraction compared to the total organic matter it not of interest for the SOM profile as such.

A potential improvement of the representation of liquid phase transport would involve replacing the advection rate by a linear function of long term average (simulated) water fluxes as a function of depth. The slope of this function then represents the retardation factor, accounting for the reduction of dissolved organic matter transport due to interactions with the solid phase, and should thus only be dependent on sorptive properties of the soil. A further advantage is that this would automatically reduce advective transport rates with depth.

5.5.3 Comparison of transport parameters with previous estimates

Diffusivities and advection rates of organic matter have been measured in a number of other studies (section 1.2.6; Table 5.1). In most studies the approach to determine transport parameters was similar to the method applied here: inversion of a SOM profile model based on measurements. Many researchers used soil organic carbon concentration and radiocarbon. In several cases transport rates were based on profiles of tracers other than ^{14}C (Kaste et al., 2007; Jarvis et al., 2010; Yoo et al., 2011;

Dörr and Münnich, 1991). In one study advection rates were estimated based on measured dissolved organic carbon fluxes (Sanderman et al., 2008).

Table 5.1 lists previously determined diffusivities and advection rates and the best estimates derived in this study. The parameters derived here generally compare well with those of other studies. The studies which included both transport mechanisms generally have somewhat higher diffusivities and lower advection rates. The latter may be explained by the fact that only part of the organic matter is moved by advection SOMPROF while in other studies based on SOM measurements, all SOM was assumed to be transported by this mechanism.

In addition to local environmental factors, parameter estimates are influenced by the methodology used to infer them. Relevant aspects include: (i) the type of observations included; (ii) the structure of the transport model, particularly the included transport mechanisms: diffusion, advection, or both; (iii) when SOM data is included, the structure of the decomposition model; (iv) which parameters are estimated in the calibration. Particularly the choice to include either diffusion, advection, or both is highly relevant. Since the overall vertical transport is partitioned between the included formulations, omission of one can be expected to lead to increase of the rate of the other. Moreover, Bruun et al. (2007) found that the advection rate differed by two orders of magnitude depending on whether or not SOM is split into fractions that are affected by each mechanism. The included formulations vary among studies and often clear justification for the choice is lacking. Presumably, most authors were not interested in separating transport mechanisms and linking them to specific processes. Most studies include only advection, even though this formulation is likely incorrect for mixing processes (Boudreau, 1986b). The importance of the model structure for parameter estimates was demonstrated by Guenet et al. (2013), who estimated SOM transport and decomposition parameters using data from a long term bare fallow experiment. They tested various models and found that the structure of the decomposition model affects the transport parameters.

Hence, parameters are specific to the model structure and should not be transferred carelessly. In light of this problem it is advisable to develop model structures that involve physically meaningful parameters which can be estimated using other approaches, such as the bioturbation rate B in SOMPROF. Furthermore, addition of observations that pertain to specific processes may improve comparability between approaches (see section 5.6.3). Finally, in addition to parameter estimates, observations that were used to derive them should be published.

5.6 Calibration

5.6.1 Convolution of processes

A major challenge in this study is disentangling the processes relevant to SOM profile dynamics: bioturbation, liquid phase transport, rhizodeposition, and decomposition. Since these processes are difficult to observe directly, their rates can often

Table 5.1: SOM transport rates previously published and derived in this study. Studies for which transport processes other than bioturbation and liquid phase transport are relevant are not included, as well as studies where calibration was performed manually. When USDA soil classes were reported they were converted to the FAO system based on Spaargaren and Batjes (1995). NA: not applicable; NR: not reported; (D)OC: (dissolved) organic carbon; ON: organic nitrogen.

Source	Diffusivity ($\text{cm}^2 \text{yr}^{-1}$)	Advection rate (cm yr^{-1})	Location	Ecosystem type	Soil	Observations
Elzein and Balesdent (1995)	5.15	0.013	Kattinkar, India	Tropical forest	Ferralsol	OC, ^{14}C
Elzein and Balesdent (1995)	16.6	0.034	Para, Brazil	Tropical forest	Ferralsol	OC, ^{14}C
Elzein and Balesdent (1995)	5.29	0.048	Bahia, Brazil	Tropical forest	Ferralsol	OC, ^{14}C
Elzein and Balesdent (1995)	0.94	0.06	France	Forest	Podzol	OC, ^{14}C
Elzein and Balesdent (1995)	1.48	0.042	France	Deciduous forest	Luvisol	OC, ^{14}C , $\leq 50 \mu\text{m}$ frac.
Bruun et al. (2007)	0.99 ^a	0.23 ^a	NA	NA	NA ^b	^{14}C
Jarvis et al. (2010) ^c	0.3	NA	Sweden	Grassland	Dystric Cambisol	^{137}Cs
Baisden et al. (2002)	NA	0.05, 0.026, 0.010 ^d	California	Grassland	Gravelly loam	OC, ON, ^{14}C
Baisden and Parfitt (2007)	NA	0.6, 0.09, 0.019 ^d	New Zealand	Grassland	Ferralic Cambisol	OC, ^{14}C
Baisden and Parfitt (2007)	NA	0.06, 0.13, 0.025 ^d	California, USA	Grassland	Sandy loam	OC, ^{14}C
Baisden and Parfitt (2007)	NA	0.05, 0.05, 0.05 ^d	California, USA	Grassland	Loamy sand	OC, ^{14}C
Yoo et al. (2011)	NA	0.6 \pm 0.1, 2.7 \pm 0.5, 2.5 \pm 0.6 ^e	Delaware, USA	Forest	Sandy loam	OC, $^{210}\text{Pb}_{\text{ex}}$
Kaste et al. (2007)	1.1 \pm 0.3	0.07	Southeastern Australia	Forest	NR	$^{210}\text{Pb}_{\text{ex}}$, ^{241}Am , ^{137}Cs
Kaste et al. (2007)	2.1 \pm 0.4	0.11	California, USA	Grassland	NR	$^{210}\text{Pb}_{\text{ex}}$, ^{241}Am , ^{137}Cs
Kaste et al. (2007)	1.0 \pm 0.3	0.1–0.2	New Hampshire, USA	Grassland	Podzol	^7Be , $^{210}\text{Pb}_{\text{ex}}$
Sanderman et al. (2008)	NA	0.105 \pm 0.020	California, USA	Coniferous forest	Haplic Acrisol	DOC fluxes
Sanderman et al. (2008)	NA	0.045 \pm 0.007	California, USA	Grassland	Haplic Phaeozem	DOC fluxes

^a 76 % moved by diffusion; 24 % moved by advection

^b Mesocosm amended with ^{14}C labelled straw 41 years previous; no root input

^c Model included diffusion, non-local mixing, and dispersion in water phase

^d Separate transport rates determined for different SOM pools

^e Separate transport rates determined for three soil layers up to 46 cm depth

Table 5.1: SOM transport rates previously published and derived in this study. (continued)

Source	Diffusivity ($\text{cm}^2 \text{yr}^{-1}$)	Advection rate ($\text{cm} \text{yr}^{-1}$)	Location	Ecosystem type	Soil type	Observations
Dörr and Münnich (1989)	NA	0.16 ± 0.04	Germany	Mixed forest	Sandy	OC, ^{14}C
Dörr and Münnich (1989)	NA	0.12 ± 0.03	Germany	Deciduous forest	Loamy	OC, ^{14}C
Dörr and Münnich (1989)	NA	0.06 ± 0.02	Germany	Mixed forest	Sandy	OC, ^{14}C
Dörr and Münnich (1989)	NA	0.08 ± 0.02	Germany	Coniferous forest	Clayey/loamy	OC, ^{14}C
O'Brien and Stout (1978)	13.2	NA	New Zealand	Pasture	Ferralitic Cambisol	OC, ^{14}C
van Dam et al. (1997)	0.42	NA	Costa Rica	Tropical forest/pasture	Humic Cambisol	OC, ^{14}C , ^{13}C
van Dam et al. (1997)	3.97	NA	Costa Rica	Tropical forest/pasture	Umbric Andosol	OC, ^{14}C , ^{13}C
Dörr and Münnich (1991)	NA	0.083 ± 0.039	Europe ^a	Forest	Various ^a	$^{210}\text{Pb}_{\text{ex}}$
This study, Ch. 3	0.092 ± 0.026^b	0.61 ± 0.21	The Netherlands, Loobos	Coniferous forest	Arenosol	see Ch. 3
This study, Ch. 3 ^c	0.97 ± 0.47^b	0.120 ± 0.040	Germany, Hainich	Deciduous forest	Cambisol	see Ch. 4
This study, Ch. 4 ^d	0.320 ± 0.048^b	0.150 ± 0.032	Germany, Hainich	Deciduous forest	Cambisol	see Ch. 4

^a Mean rate for 49 forest soils in Europe

^b Determined from B and l_m according to equation (2.2) using the average bulk density over the profile.

^c Calibration setup 3, dominant mode

^d Calibration wC14, dominant mode

only be inferred using model inversion. For each of these mechanisms a mathematical description requires at least one parameter. The same organic matter profile can be obtained with several parameter sets, corresponding to different contributions of the processes. This situation is referred to as “equifinality” (Beven, 2006). The inversion of a model based on data that holds insufficient information will constitute an ill-posed problem, i.e. it does not have a unique optimal solution. In Bayesian inference equifinality may lead to an undesirably large region of significant probability in the posterior distribution. The relevance of this problem for this study is demonstrated by poorly constrained parameters and the existence of multiple modes (see chapters 3 and 4).

The multimodality of the posterior distribution for Hainich is a remarkable and important result of this study (section 3.3.2). Reports in literature of multimodal parameter distributions for ecological models are scarce (e.g. Rahn et al., 2012). However, this does not necessarily mean that this is a rare occurrence. Likelihood surfaces for parameters of non-linear models often have local optima (Tarantola, 2005). The aim of model inversion is often to derive a single optimal parameter set, hence existence of multiple acceptable explanations for observations is presumably considered undesirable (Beven, 2006). It is therefore plausible that sub-dominant modes are simply discarded in favor of the optimal mode, and not reported.

There are several reasons to be careful with discarding sub-dominant modes. First, in view of unconsidered sources of uncertainty (see section 5.6.2), the difference between the maximum posterior probability of the modes is likely to be overestimated. Second, as shown in chapters 3 and 4, the addition of new information to the calibration leads to large shifts in the maximum probability. These shifts can cause a previously sub-dominant mode to become dominant. This occurred in chapter 4 of this study when the model was modified and additional calibration data was added.

It must be noted that the possibility that the multimodality is an artifact of the modelling approach cannot be completely excluded. It has been demonstrated that errors introduced by the numerical solution of the model can cause irregularities in the likelihood surface, resulting in apparent multimodality (Schoups et al., 2010). If this problem were relevant here it would likely not change the fact that different regions in parameter space give similar fit to the data, but rather that connections between these regions go unnoticed. Additional study using more accurate numerical schemes is advisable.

5.6.2 Sources of uncertainty

The posterior parameter distribution in Bayesian calibration derives from the prior probability density function and the likelihood function. The latter is determined by the (dis)agreement between model predictions and calibration data. Misfit between model output and measurements originates from different sources, which are related to both the model and the measurements (Raupach et al., 2005).

Uncertainty of the calibration measurements. The observations used for the parameter estimation are affected by several sources of uncertainty including: spatial hetero-

geneity, heterogeneity of the analyzed soil samples, and errors arising from the treatment and analysis in the lab. Spatial heterogeneity forms likely the largest contribution to these errors. This type of uncertainty can be reduced and quantified by repeated sampling and measurements.

Errors in the model structure. Biased predictions can result from incorrect or missing representation of processes and interactions (Gupta et al., 2012). Such misrepresentations may be either deliberate, motivated by limited availability of computational resources and model input, or unintentional due to a lack of understanding of the modelled system. For example, in view of the intended large scale application of SOMPROF, the representation of liquid phase transport of organic matter was deliberately kept simple (see section 5.5). Conversely, the correct representation of decomposition is mainly limited by lack of understanding.

Errors in the uncalibrated model input. Ideally, the uncalibrated model input should be well known but this is often not the case (Kavetski et al., 2006). For example, the rate of rhizodeposition is very difficult to measure, and may be more uncertain than the soil carbon profile itself. Furthermore, soil temperature, moisture and litter input are needed for the complete duration of the simulation, spanning up to thousands of years. Since these quantities vary considerably over time, current measurements may be a quite poor representation of these variables in the past. The model input was estimated from local measurements and assumed exactly known, hence this source of errors has not been considered here.

Scale mismatch between model input, calibration data, and model structure. Inconsistency between the characteristic spatial and temporal scales of the model and observations used for input and parameter estimation may cause model-data disagreement (Raupach et al., 2005). For example, the soil temperature and moisture data used for model forcing, were measured in one or two profiles while the soil carbon measurements were based on many repeated samplings spread out over a large area, thus representing a larger scale. Ideally, all measurements should be representative for the spatial and temporal scale for which the model is valid (Reichstein and Beer, 2008) but in practice this is often not feasible.

Ideally, the posterior parameter distribution should reflect all the above mentioned error sources, to allow correct assessment of the uncertainty of model projections. However, in practice this is very difficult. In the calibrations of this study several uncertainties were ignored, which likely means that the spread of the posterior is underestimated. First, a large ignored source of uncertainty is represented by the uncalibrated model input. Several recently developed methods may be used to include these errors in Bayesian calibration (Kavetski et al., 2006; Vrugt et al., 2008). Second, uncertainty may go unnoticed if the model is right for the wrong reason, i.e. it reproduces the observations based on an incorrect parameterization. This is demonstrated by the changes to the posterior distribution caused by the addition of radiocarbon to the observations, discussed in chapter 4. This problem may be addressed by also considering model output variables for which no observations are available. For example, even without local radiocarbon observations for Hainich, it would be clear that the radiocarbon profile predicted by model woC14 is unre-

alistic. Such prior knowledge for model results could be applied in the parameter estimation. Similar to the prior distributions for the model parameters, prior density functions for model output could be used to improve parameter estimates. Finally, overoptimistic uncertainty estimates may result from oversimplified representation of the system motivated by the parsimony principle. If the inclination to avoid overparameterization leads one to neglect relevant mechanisms, uncertainty of parameters may be underestimated (Reichert and Omlin, 1997). When the model is extrapolated outside the calibration domain in prognostic simulations, this in turn can cause to underestimated uncertainty of predictions.

5.6.3 Observations for calibration

The model inversions in this study have shown that SOM profile measurements alone do not provide adequate constraint on the model parameters, since these observations are the integrated result of all processes represented in the model. A multiple constraint approach with several additional information sources is necessary to capture the individual processes. The complementary data streams used in this study (see Table 4.1) provided mostly information on SOM turnover at both long (radiocarbon of SOM) and short (radiocarbon of heterotrophic respiration, effective decomposition rates) time scales. As discussed in chapter 4, particularly the radiocarbon data of SOM proved to be very helpful to improve estimates of SOM turnover rates.

The use of excess lead-210 ($^{210}\text{Pb}_{\text{ex}}$) as a tracer for SOM transport was studied in chapter 3. The potential value of this isotope as a tracer lies in the fact that it binds to the solid phase but is not part of organic molecules, hence its profile is less dependent on decomposition. Furthermore, its loss due to radioactive decay is exactly known. Nevertheless, this observation added limited additional information to the model inversion. Compared to the effects of radiocarbon the changes to the posterior distribution by adding $^{210}\text{Pb}_{\text{ex}}$ were relatively small. A likely cause is that this tracer is mainly useful for disentangling overall SOM transport from root input, but this appears to be a less important problem than separating the different transport mechanisms. A drawback of $^{210}\text{Pb}_{\text{ex}}$ is that it needs to be separated from the fraction that is formed from *in situ* ^{222}Rn decay. Furthermore, it is not fully clear to what extent this tracer can represent liquid phase transport (see section 3.4.5). Despite these problems this isotope has potential as a complementary data stream. A study with high resolution profile measurements of lead-210 and more replicate samplings, together with other observations and inverse modelling, would be helpful to further assess the value of this isotope.

There are several other possible radioisotopes similar to lead-210 that can be useful for constraining SOM transport, originating from both natural and anthropogenic sources. Natural isotopes that are formed due to cosmic radiation or decay of natural parent isotopes are useful because of their relatively constant formation, which means the profile is usually in equilibrium. Hence, the input rate can be eliminated from the equations by normalizing the concentrations relative to the surface value, as was done for $^{210}\text{Pb}_{\text{ex}}$ (see section 3.2.3). ^7Be is a natural isotope that may be useful

as a SOM tracer (Kaste et al., 2007). Anthropogenic isotopes are formed by nuclear weapons testing and nuclear accidents. These isotopes are usually not in steady state and require time series of their input rates. However, when accurate records are available they may be very informative. ^{241}Am and ^{137}Cs are potentially useful (Kaste et al., 2007), although there is some indication that the latter may move independently of organic matter in soils (Dörr and Münnich, 1989, 1991).

Since convolution of bioturbation and liquid phase transport proved to be an important challenge, observations that pertain specifically to either mechanism would be advantageous. An obvious candidate is data of dissolved organic matter (DOM) flux rates (Sanderman et al., 2008; Kindler et al., 2011). Since DOM transport is an additional pathway of loss from the soil, these fluxes may be also quite useful to constrain the total soil carbon balance. However, these measurements may be relatively costly and labor intensive. Furthermore, fluxes should be measured for a year or longer, in view of short term variability.

A promising technique for studying bioturbation is optically stimulated luminescence (OSL). This method measures the time since mineral (quartz and feldspar) grains were last exposed to sunlight, and has been suggested as a useful approach to quantify soil mixing as well as erosion and deposition (Wilkinson and Humphreys, 2005). However, OSL would presumably not be useful for soils with a thick organic layer.

5.7 Recommendations for further development

A range of future developments and applications of SOMPROF can be envisaged. These are related to: (i) Extensions that may potentially improve predictions of SOM profile dynamics and extend the validity of the model. Some of these have already been discussed in section 5.5. (ii) Potential synergies with other process descriptions, such as heat and moisture transport and microbial dynamics. (iii) Large scale application of SOMPROF in a global ecosystem or earth system model.

5.7.1 Extensions of the model structure

Temperature sensitivity of decomposition. The effect of temperature on decomposition is considered in the model but was not included in the calibration. Considering the relevance for feedbacks to climate change the temperature sensitivity should be included in the calibration if sufficient data is available. Furthermore, it has been suggested that temperature sensitivity varies between SOM fractions (Conant et al., 2011). Although this is still uncertain, the effects of various assumptions in relation to the vertical profile can be studied.

Depth dependence of decomposition rates. In several previously published models decomposition rates are explicitly reduced with depth to account for less favorable conditions in the subsoil or depth dependent stabilization mechanisms (Jenkinson and Coleman, 2008; Koven et al., 2013). In inverse parameter estimation this assumption may help to reduce the disagreement between SOM concentration and radiocarbon

activity that was found in chapter 4. However, depth dependence of decomposition can also be achieved by explicitly accounting for certain mechanisms or microbial dynamics (see next point).

Microbial dynamics and substrate interactions. It has been suggested that energy limitation of decomposers may contribute significantly to soil carbon stabilization (Fontaine et al., 2007). Several recent publications have presented model structures that simulate these mechanisms (Fontaine and Barot, 2005; Wutzler and Reichstein, 2007, 2013). Coupling of such a scheme with a vertically explicit representation of SOM has potentially major effects on predictions of soil carbon cycling (Guenet et al., 2013).

Root distribution. The vertical distribution of roots (and thus rhizodeposition) differs among vegetation types and depends on other factors, such as moisture and nutrient availability. Furthermore, increase of vegetation productivity due to rising atmospheric CO₂ concentration may be associated with deepening of root distributions (Iversen, 2010). In combination with substrate interactions (see point above) this may also lead to shifts in decomposition dynamics.

Nitrogen dynamics. Decomposition is partially controlled by soil nitrogen availability. Nitrogen deposition may cause shifts in microbial activity that lead to stabilization of SOM (Janssens et al., 2010). Furthermore, plant growth and thus litter input is strongly influenced by nitrogen availability.

Extension to other soil types and ecosystems. The current structure of SOMPROF with three organic surface horizons is mainly designed for forests and may not be appropriate for other ecosystems. For example, in grasslands organic matter tends to accumulate within the mineral soil, rather than on top, when conditions are unfavorable for decomposition (van Delft et al., 2006). Furthermore, in certain ecosystems other mechanisms for organic matter transport are relevant, such as ploughing in croplands and cryoturbation in permafrost soils.

5.7.2 Coupling to physical soil processes

The effect of soil organic matter concentration on soil hydrological parameters may be represented by pedotransfer functions (PTFs). PTFs are empirical models that predict soil properties that are difficult to measure based on more readily available data, such as texture and organic matter content. Several useful PTFs have been published (Rawls et al., 2003; Saxton and Rawls, 2006).

In soil hydrological models the surface organic layer is sometimes treated similar to the mineral soil, by representing it as a separate layer with different properties (Ashby, 1999). However, in view of the strong differences between these two parts of the profile, this approach may not be appropriate. Several models have been developed in which the organic layer is represented by a separate submodel (Schaap et al., 1997; Ogee and Brunet, 2002; Neto et al., 2012).

Soil thermal properties (thermal conductivity and heat capacity) can be determined from the fractions of solid and liquid constituents (Farouki, 1981). Soil organic matter generally acts as an insulator, particularly in the form of a surface organic layer, which was found to be important in permafrost soils (Harden et al., 2006).

Several model structures have been published that simulate these effects (Lawrence and Slater, 2008; Mölders and Romanovsky, 2006).

5.7.3 Large scale parameterization

The need for parameter estimates represents the most important challenge for SOMPROF application at large spatial scales. To perform simulations for unvisited sites relationships between parameters and known or predictable environmental variables need to be derived. In large scale applications, ecosystem models are typically run for spatial grids with resolutions ranging from 0.5 degrees latitude and longitude, for simulations of terrestrial ecosystems only (uncoupled), to 3–5 degrees, in earth system simulations (coupled) (Stouffer et al., 2011). The vegetation parameters that describe processes such as photosynthesis are determined from the dominant plant functional type in each grid cell, which may be prescribed or predicted by a biogeographical submodel. Parameters for soil hydrology and heat flux are typically based on local soil properties.

The free SOMPROF parameters include decomposition rate coefficients k_i , transformation fractions $\alpha_{i \rightarrow j}$, and the transport parameters: the bioturbation rate B , mixing length l_m , and advection rate v (section 2.2.7). Most of these can best be linked to soil properties, rather than vegetation type. However, the choice of covariates is limited by available data at global scale (FAO et al., 2012). The appropriate covariates depend on the specific model parameter. The bioturbation rate B is determined by the biomass and activity of the soil fauna groups relevant to mixing, mainly earthworms, ants, and termites. The activity of earthworms can likely best be linked to base saturation or Ca concentration (Reich et al., 2005), while biogeography of ants and termites is related to climate and vegetation type (Gotelli and Ellison, 2002). Ideally, the mixing length l_m should be related to the main soil fauna species, but in practice it may be difficult to determine a clear relationship. It may be reasonable to use a single global value.

The advection rate v , defining liquid phase transport rates is determined by vertical water fluxes and soil properties influencing adsorption. Average water fluxes may be estimated by a soil hydrological model. As discussed in section 5.5.2, if advection rates are linked to water flow, it may be replaced with the retardation factor, which should mainly depend on adsorption. In dissolved organic matter transport models adsorption capacity is often linked to Al and Fe content (Moore and Desouza, 1992), but this information is presumably not available at global scale. Clay content may be a good alternative.

Parameters determining the decomposition of litter are related to the C : N or lignin : N ratio of the litter (see section 1.2.1) which can be linked to vegetation type (Berg and McClaugherty, 2008). Parameters of decomposition in the mineral soil are sometimes linked to clay content (Hassink, 1997), although many models use fixed global parameters.

Derivation of global parameter sets requires additional model inversions for new sites. In particular, calibrations are needed for new ecosystems including grasslands, and tropical and boreal forests. As is evident in chapters 3 and 4, these calibrations

require a relatively large amount of data, both for model input and to constrain parameters. It is unlikely that the number of sites for which this data is available is sufficient to derive a global parameterization. Some variables may be estimated using other methods, e.g. from model predictions or based on measurements for comparable ecosystems, but this will add additional uncertainty.

In view of these difficulties the Bayesian approach is highly recommendable since posterior distributions can be used as priors in subsequent calibrations in order to reduce uncertainty. Model inversions can be performed first for sites with high data availability, such as those used in this study, to construct increasingly narrow parameter distributions. Those distributions can subsequently be used for sites for which less data is available. In this case, full approximation of the posterior distribution using Markov Chain Monte Carlo sampling may be too time consuming and computationally demanding. If the posterior distribution is assumed to be normal, a gradient search algorithm (e.g. quasi-Newton) with a Bayesian cost function can be applied. A useful approach in this context may be hierarchical modelling. With this method parameter sets for multiple sites can be estimated simultaneously with their relationships with environmental covariates. Hierarchical Bayes is the Bayesian equivalent of this method. It allows the incorporation of prior knowledge on the relationship between the model parameters and covariates, by defining “hyperpriors”: prior distributions for the parameters that define the priors of parameters at a lower model level (Clark, 2005).

5.8 Conclusions

In this thesis research I developed a numerical model, SOMPROF, for dynamic simulation of the vertical soil organic matter (SOM) profile, and estimated parameters based on measurements. Specific attention was given to explicit description of relevant processes, expected large scale application as a part of ecosystem models, and assessment of parameter and prediction uncertainty. Based on this work the following overarching conclusions can be drawn:

1. In most natural and undisturbed soils the vertical SOM distribution is determined by the combined effects of bioturbation, liquid phase transport, above- and belowground litter input, and decomposition. The SOMPROF model structure, developed in this study, contains simple but realistic parameterizations of these processes, including diffusion and advection, representing bioturbation and liquid phase transport, respectively. SOMPROF is able to simulate SOM profiles that compare well to profiles observed in the field.
2. Estimation of the parameters describing these processes based on measurements in two contrasting forest sites shows that (i) SOM transport can have a considerable influence on the vertical SOM distribution, and (ii) the relative importance of root input and the two transport processes differ substantially between sites.

3. Convolution of the relevant processes, in particular the two transport mechanisms, poses a considerable challenge for quantifying them by model inversion. This problem can lead to poorly constrained model parameters and existence of multiple adequate parameter sets for the same observations. Bayesian inference is arguably the best tool for such problems, since it allows uncertainty to be both assessed, by approximation of parameter distributions, and reduced, by incorporation of prior knowledge obtained in previous studies.
4. Because of the entanglement of processes, inclusion of sufficient and appropriate observations is critical to the parameter estimation. Data on SOM stocks and fractions alone are in general insufficient. Additional data streams are required in order to constrain individual mechanisms. Excess lead-210 is a potential candidate for such data, although it did not add significant constraint in this study. Additionally, observations pertaining to SOM turnover, such as radiocarbon activity and respiration rates, are important to correctly assess decomposition rates.
5. Prognostic simulations suggest that the response to changes in litter input and temperature can vary over the vertical SOM profile. Therefore estimation of responses of the organic carbon stocks for the total soil based on topsoil dynamics alone may lead to biased results.

Mechanistic modelling of the vertical soil organic matter profile is still in its infancy. While a large body of literature exists on models of organic matter decomposition, models of processes such as bioturbation and liquid phase transport are relatively scarce. Fortunately, research into these topics is growing, but there is some need for haste, since the understanding of the processes is lagging behind the need for a parameterization for prognostic simulations.

The SOMPROF model developed in this study can be used to assess the relative importance of different mechanisms that determine the SOM profile and for prognostic simulations as a part of an ecosystem model. But perhaps the most important part of the value of this study lies in the identification of challenges related to SOM profile modelling, and the development of methods to deal with them. I hope that this thesis will stimulate collection of new data by field and lab researchers, and help modelers to use this data, in order to test and improve SOMPROF and other related models.

References

- Alban, D. H. and Berry, E. C. (1994). Effects of earthworm invasion on morphology, carbon, and nitrogen of a forest soil. *Applied Soil Ecology*, 1(3):243–249.
- Allison, S. D., Wallenstein, M. D., and Bradford, M. A. (2010). Soil-carbon response to warming dependent on microbial physiology. *Nature Geoscience*, 3(5):336–340.
- Anderson, L., Comas, L., Lakso, A., and Eissenstat, D. (2003). Multiple risk factors in root survivorship: a 4-year study in Concord grape. *New Phytologist*, 158(3):489–501.
- Appleby, P. G. and Oldfield, F. (1978). The calculation of lead-210 dates assuming a constant rate of supply of unsupported ^{210}Pb to the sediment. *Catena*, 5(1):1–8.
- Arai, H. and Tokuchi, N. (2010). Factors contributing to greater soil organic carbon accumulation after afforestation in a Japanese coniferous plantation as determined by stable and radioactive isotopes. *Geoderma*, 157(34):243–251.
- Arblaster, J., Dufresne, J.-L., Fichefet, T., Friedlingstein, P., Gao, X., Gutowski Jr, W., Johns, T., Krinner, G., Shongwe, M., Tebaldi, C., Weaver, A., and Wehner, M. (2013). Long-term climate change: Projections, commitments and irreversibility. In Cubasch, U., Wuebbles, D., Chen, D., Facchini, M., Frame, D., Mahowald, N., and Winther, J.-G., editors, *Climate Change 2013: The Physical Science Basis. Contribution of Working Group I to the Fifth Assessment Report of the Intergovernmental Panel on Climate Change*.
- Arora, V. K. and Matthews, H. D. (2009). Characterizing uncertainty in modeling primary terrestrial ecosystem processes. *Global Biogeochemical Cycles*, 23:GB2016.
- Arrouays, D. and Pelissier, P. (1994). Modeling carbon storage profiles in temperate forest humic loamy soils of France. *Soil Science*, 157(3):185–192.
- Ashby, M. (1999). Modelling the water and energy balances of Amazonian rainforest and pasture using Anglo-Brazilian Amazonian climate observation study data. *Agricultural and Forest Meteorology*, 94(2):79–101.
- Baisden, W. T., Amundson, R., Brenner, D. L., Cook, A. C., Kendall, C., and Harden, J. W. (2002). A multiisotope C and N modeling analysis of soil organic matter turnover and transport as a function of soil depth in a California annual grassland soil chronosequence. *Global Biogeochemical Cycles*, 16(4):82.
- Baisden, W. T. and Parfitt, R. L. (2007). Bomb C-14 enrichment indicates decadal C pool in deep soil? *Biogeochemistry*, 85(1):59–68.
- Bard, Y. (1974). *Nonlinear parameter estimation*. Academic Press.
- Batjes, N. H. (1996). Total carbon and nitrogen in the soils of the world. *European Journal of Soil Science*, 47(2):151–163.
- Beer, C., Weber, U., Tomelleri, E., Carvalhais, N., Mahecha, M. D., and Reichstein, M. Harmonized long-term climate data for assessing the effect of changing variability on land-atmosphere CO₂ fluxes. Submitted to *Journal of Climate*.
- Berg, B. and McClaugherty, C. (2008). *Plant litter: decomposition, humus formation, carbon seques-*

- tration. Springer, Berlin [u.a.], second edition.
- Beven, K. (2006). A manifesto for the equifinality thesis. *Journal of Hydrology*, 320:18–36.
- Beven, K. and Freer, J. (2001). Equifinality, data assimilation, and uncertainty estimation in mechanistic modelling of complex environmental systems using the GLUE methodology. *Journal of Hydrology*, 249(1-4):11–29.
- Blagodatsky, S. and Richter, O. (1998). Microbial growth in soil and nitrogen turnover: A theoretical model considering the activity state of microorganisms. *Soil Biology & Biochemistry*, 30(13):1743–1755.
- Blume, H. and Leinweber, P. (2004). Plaggen soils: landscape history, properties, and classification. *Journal of Plant Nutrition and Soil Science*, 167(3):319–327.
- Bockheim, J. G. (2007). Importance of cryoturbation in redistributing organic carbon in permafrost-affected soils. *Soil Science Society of America Journal*, 71(4):1335–1342.
- Bohlen, P., Pelletier, D., Groffman, P., Fahey, T., and Fisk, M. (2004). Influence of earthworm invasion on redistribution and retention of soil carbon and nitrogen in northern temperate forests. *Ecosystems*, 7(1):13–27.
- Bormann, F. and Likens, G. (1994). *Pattern and process in a forested ecosystem: disturbance, development, and the steady state based on the Hubbard Brook ecosystem study*. Springer-Verlag.
- Bosatta, E. and Ågren, G. (1985). Theoretical-analysis of decomposition of heterogeneous substrates. *Soil Biology & Biochemistry*, 17(5):601–610.
- Bosatta, E. and Ågren, G. I. (1996). Theoretical analyses of carbon and nutrient dynamics in soil profiles. *Soil Biology & Biochemistry*, 28(10-11):1523–1531.
- Bottcher, J. and Springob, G. (2001). A carbon balance model for organic layers of acid forest soils. *Journal of Plant Nutrition and Soil Science*, 164(4):399–405.
- Boudreau, B. (1986a). Mathematics of tracer mixing in sediments II. nonlocal mixing and biological conveyor-belt phenomena. *American Journal of Science*, 286(3):199–238.
- Boudreau, B. (1989). The diffusion and telegraph equations in diagenetic modeling. *Geochimica et Cosmochimica Acta*, 53(8):1857–1866.
- Boudreau, B. P. (1986b). Mathematics of tracer mixing in sediments I, spatially-dependent, diffusive mixing. *American Journal of Science*, 286(3):161–198.
- Boudreau, B. P. (1998). Mean mixed depth of sediments: The wherefore and the why. *Limnology and Oceanography*, 43(3):524–526.
- Bowman, A. and Azzalini, A. (1997). *Applied Smoothing Techniques for Data Analysis: The Kernel Approach with S-Plus Illustrations*. OUP Oxford.
- Box, G. E. P. and Cox, D. R. (1964). An analysis of transformations. *Journal of the Royal Statistical Society Series B-Statistical Methodology*, 26(2):211–252.
- Box, G. E. P. and Tiao, G. C. (1992). *Bayesian Inference in Statistical Analysis*. Wiley.
- Brovelli, A., Battle-Aguilar, J., and Barry, D. A. (2012). Analysis of carbon and nitrogen dynamics in riparian soils: Model development. *Science of the Total Environment*, 429:231–245.
- Brovkin, V., Raddatz, T., Reick, C. H., Claussen, M., and Gayler, V. (2009). Global biogeophysical interactions between forest and climate. *Geophysical Research Letters*, 36:L07405.
- Brussaard, L., Behan-Pelletier, V., Bignell, D., Brown, V., Didden, W., Folgarait, P., Fragoso, C., Freckman, D., Gupta, V., Hattori, T., Hawksworth, D., Klopatek, C., Lavelle, P., Malloch, D., Rusek, J., Soderstrom, B., Tiedje, J., and Virginia, R. (1997). Biodiversity and ecosystem functioning in soil. *Ambio*, 26(8):563–570.
- Bruun, S., Christensen, B. T., Thomsen, I. K., Jensen, E. S., and Jensen, L. S. (2007). Modeling vertical movement of organic matter in a soil incubated for 41 years with ¹⁴C labeled straw. *Soil Biology & Biochemistry*, 39(1):368–371.
- Bunzl, K. (2002). Transport of fallout radiocesium in the soil by bioturbation: a random walk model and application to a forest soil with a high abundance of earthworms. *Science of the*

- Total Environment*, 293(1-3):191–200.
- Burden, R. L. (2004). *Numerical analysis*. Belmont, California, Brooks/Cole, 8th edition edition.
- Buurman, P. and Jongmans, A. G. (2005). Podzolisation and soil organic matter dynamics. *Geoderma*, 125(1-2):71–83.
- Carvalho, N., Reichstein, M., Ciais, P., Collatz, G. J., Mahecha, M. D., Montagnani, L., Papale, D., Rambal, S., and Seixas, J. (2010). Identification of vegetation and soil carbon pools out of equilibrium in a process model via eddy covariance and biometric constraints. *Global Change Biology*, 16(10):2813–2829.
- Cesarz, S., Fahrenholz, N., Migge-Kleian, S., Platner, C., and Schaefer, M. (2007). Earthworm communities in relation to tree diversity in a deciduous forest. *European Journal of Soil Biology*, 43:S61–S67.
- Chabbi, A., Koegel-Knabner, I., and Rumpel, C. (2009). Stabilised carbon in subsoil horizons is located in spatially distinct parts of the soil profile. *Soil Biology & Biochemistry*, 41(2):256–261.
- Chapin, F., Chapin, F., Matson, P., and Vitousek, P. (2002). *Principles of Terrestrial Ecosystem Ecology*. Springer.
- Chertov, O. and Komarov, A. (1997). SOMM: A model of soil organic matter dynamics. *Ecological Modelling*, 94(2-3):177–189.
- Chertov, O., Komarov, A., Nadporozhskaya, M., Bykhovets, S., and Zudin, S. (2001). ROMUL - a model of forest soil organic matter dynamics as a substantial tool for forest ecosystem modeling. *Ecological Modelling*, 138(1-3):289–308.
- Choi, J., Francois-Carcaillet, F., and Boudreau, B. (2002). Lattice-automaton bioturbation simulator (LABS): implementation for small deposit feeders. *Computers & Geosciences*, 28(2):213–222.
- Christensen, B. T. (1996). Matching measurable soil organic matter fractions with conceptual pools in simulation models of carbon turnover: Revision of model structure. In Powlson, D. S., Smith, P., and Smith, J. U., editors, *Evaluation of soil organic matter models using existing, long-term datasets*, volume 38 of *NATO ASI Series I*, page 143159. Springer, Berlin.
- Christensen, J. H., Boberg, F., Christensen, O. B., and Lucas-Picher, P. (2008). On the need for bias correction of regional climate change projections of temperature and precipitation. *Geophysical Research Letters*, 35(20):L20709.
- Clark, D., Brown, S., Kicklighter, D., Chambers, J., Thomlinson, J., and Ni, J. (2001). Measuring net primary production in forests: Concepts and field methods. *Ecological Applications*, 11(2):356–370.
- Clark, J. (2005). Why environmental scientists are becoming Bayesians. *Ecology Letters*, 8(1):2–14.
- Conant, R. T., Ryan, M. G., Agren, G. I., Birge, H. E., Davidson, E. A., Eliasson, P. E., Evans, S. E., Frey, S. D., Giardina, C. P., Hopkins, F. M., Hyvonen, R., Kirschbaum, M. U. F., Lavalley, J. M., Leifeld, J., Parton, W. J., Steinweg, J. M., Wallenstein, M. D., Wetterstedt, J. A. M., and Bradford, M. A. (2011). Temperature and soil organic matter decomposition rates - synthesis of current knowledge and a way forward. *Global Change Biology*, 17(11):3392–3404.
- Conant, R. T., Steinweg, J. M., Haddix, M. L., Paul, E. A., Plante, A. F., and Six, J. (2008). Experimental warming shows that decomposition temperature sensitivity increases with soil organic matter recalcitrance. *Ecology*, 89(9):2384–2391.
- Cramer, W., Bondeau, A., Woodward, F., Prentice, I., Betts, R., Brovkin, V., Cox, P., Fisher, V., Foley, J., Friend, A., Kucharik, C., Lomas, M., Ramankutty, N., Sitch, S., Smith, B., White, A., and Young-Molling, C. (2001). Global response of terrestrial ecosystem structure and function to CO₂ and climate change: results from six dynamic global vegetation models.

- Global Change Biology*, 7(4):357–373.
- Davidson, E. A. and Janssens, I. A. (2006). Temperature sensitivity of soil carbon decomposition and feedbacks to climate change. *Nature*, 440(7081):165–173.
- Davidson, E. A., Savage, K. E., Trumbore, S. E., and Borken, W. (2006). Vertical partitioning of CO₂ production within a temperate forest soil. *Global Change Biology*, 12(6):944–956.
- de Bruijn, A. M. G. and Butterbach-Bahl, K. (2010). Linking carbon and nitrogen mineralization with microbial responses to substrate availability - the DECONIT model. *Plant and Soil*, 328(1-2):271–290.
- Dee, D., Uppala, S., Simmons, A., Berrisford, P., Poli, P., Kobayashi, S., Andrae, U., Balmaseda, M., Balsamo, G., Bauer, P., et al. (2011). The ERA-Interim reanalysis: Configuration and performance of the data assimilation system. *Quarterly Journal of the Royal Meteorological Society*, 137(656):553–597.
- Diochon, A. C. and Kellman, L. (2009). Physical fractionation of soil organic matter: Destabilization of deep soil carbon following harvesting of a temperate coniferous forest. *Journal of Geophysical Research-Biogeosciences*, 114:G01016.
- Dörr, H. and Münnich, K. O. (1989). Downward movement of soil organic matter and its influence on trace-element transport (²¹⁰Pb, ¹³⁷Cs) in the soil. *Radiocarbon*, 31(3):655–663.
- Dörr, H. and Münnich, K. O. (1991). Lead and cesium transport in European forest soils. *Water Air and Soil Pollution*, 57-58:809–818.
- Driessen, P. and Dudal, R. (1991). *The Major Soils of the World: Lecture Notes on Their Geography, Formation, Properties and Use*. Agricultural University Wageningen, Department of Soil Science & Geology.
- Drigo, B., Kowalchuk, G. A., and van Veen, J. A. (2008). Climate change goes underground: effects of elevated atmospheric CO₂ on microbial community structure and activities in the rhizosphere. *Biology and Fertility of Soils*, 44(5):667–679.
- Ehleringer, J., Buchmann, N., and Flanagan, L. (2000). Carbon isotope ratios in belowground carbon cycle processes. *Ecological Applications*, 10(2):412–422.
- Ekici, A., Beer, C., Hagemann, S., and Hauck, C. (2013). Improved soil physics for simulating high latitude permafrost regions by the JSBACH terrestrial ecosystem model. *Geoscientific Model Development Discussions*, 6(2):2655–2698.
- Elzein, A. and Balesdent, J. (1995). Mechanistic simulation of vertical distribution of carbon concentrations and residence times in soils. *Soil Science Society of America Journal*, 59(5):1328–1335.
- Emmer, I. M. (1995). *Humus form and soil development during a primary succession of monoculture Pinus sylvestris on poor sandy soils*. PhD thesis, University of Amsterdam, Amsterdam.
- Eswaran, H., Vandenberg, E., and Reich, P. (1993). Organic-carbon in soils of the world. *Soil Science Society of America Journal*, 57(1):192–194.
- Eusterhues, K., Rumpel, C., Kleber, M., and Kögel-Knabner, I. (2003). Stabilisation of soil organic matter by interactions with minerals as revealed by mineral dissolution and oxidative degradation. *Organic Geochemistry*, 34(12):1591–1600.
- Falloon, P., Smith, P., Coleman, K., and Marshall, S. (2000). How important is inert organic matter for predictive soil carbon modelling using the Rothamsted carbon model? *Soil Biology & Biochemistry*, 32(3):433–436.
- Fang, C. M., Smith, P., Moncrieff, J. B., and Smith, J. U. (2005). Similar response of labile and resistant soil organic matter pools to changes in temperature. *Nature*, 433(7021):57–59.
- FAO, IIASA, ISRIC, ISSCAS, and JRC (2012). Harmonized world soil database (version 1.2).
- Farouki, O. T. (1981). The thermal properties of soils. Technical report, USACRREL.
- Federer, C. A., Turcotte, D. E., and Smith, C. T. (1993). The organic fraction–bulk density relationship and the expression of nutrient content in forest soils. *Canadian Journal of Forest*

- Research*, 23(6):1026–1032.
- Feng, X., Peterson, J., Quideau, S., Virginia, R., Graham, R., Sonder, L., and Chadwick, O. (1999). Distribution, accumulation, and fluxes of soil carbon in four monoculture lysimeters at San Dimas experimental forest, California. *Geochimica et Cosmochimica Acta*, 63(9):1319–1333.
- Fierer, N., Chadwick, O. A., and Trumbore, S. E. (2005). Production of CO₂ in soil profiles of a California annual grassland. *Ecosystems*, 8(4):412–429.
- Fontaine, S. and Barot, S. (2005). Size and functional diversity of microbe populations control plant persistence and long-term soil carbon accumulation. *Ecology Letters*, 8(10):1075–1087.
- Fontaine, S., Barot, S., Barre, P., Bdioui, N., Mary, B., and Rumpel, C. (2007). Stability of organic carbon in deep soil layers controlled by fresh carbon supply. *Nature*, 450(7167):277–U10.
- Fox, A., Williams, M., Richardson, A. D., Cameron, D., Gove, J. H., Quaipe, T., Ricciuto, D., Reichstein, M., Tomelleri, E., Trudinger, C. M., and Van Wijk, M. T. (2009). The REFLEX project: Comparing different algorithms and implementations for the inversion of a terrestrial ecosystem model against eddy covariance data. *Agricultural and Forest Meteorology*, 149(10):1597–1615.
- Francois, F., Poggiale, J., Durbec, J., and Stora, G. (1997). A new approach for the modelling of sediment reworking induced by a macrobenthic community. *Acta Biotheoretica*, 45(3-4):295–319.
- Freier, K. P., Glaser, B., and Zech, W. (2010). Mathematical modeling of soil carbon turnover in natural Podocarpus forest and Eucalyptus plantation in Ethiopia using compound specific $\delta^{13}\text{C}$ analysis. *Global Change Biology*, 16(5):1487–1502.
- Friedland, A. J., Craig, B. W., Miller, E. K., Herrick, G. T., Siccama, T. G., and Johnson, A. H. (1992). Decreasing lead levels in the forest floor of the northeastern USA. *Ambio*, 21(6):400–403.
- Friedlingstein, P., Cox, P., Betts, R., Bopp, L., Von Bloh, W., Brovkin, V., Cadule, P., Doney, S., Eby, M., Fung, I., Bala, G., John, J., Jones, C., Joos, F., Kato, T., Kawamiya, M., Knorr, W., Lindsay, K., Matthews, H. D., Raddatz, T., Rayner, P., Reick, C., Roeckner, E., Schnitzler, K. G., Schnur, R., Strassmann, K., Weaver, A. J., Yoshikawa, C., and Zeng, N. (2006). Climate-carbon cycle feedback analysis: Results from the C⁴MIP model intercomparison. *Journal of Climate*, 19(14):3337–3353.
- Fujiyoshi, R. and Sawamura, S. (2004). Mesoscale variability of vertical profiles of environmental radionuclides (K-40, Ra-226, Pb-210 and Cs-137) in temperate forest soils in Germany. *Science of the Total Environment*, 320(2-3):177–188.
- Gaudinski, J., Trumbore, S., Davidson, E., and Zheng, S. (2000). Soil carbon cycling in a temperate forest: radiocarbon-based estimates of residence times, sequestration rates and partitioning of fluxes. *Biogeochemistry*, 51(1):33–69.
- Gaudinski, J. B., Torn, M. S., Riley, W. J., Dawson, T. E., Joslin, J. D., and Majdi, H. (2010). Measuring and modeling the spectrum of fine-root turnover times in three forests using isotopes, minirhizotrons, and the Radix model. *Global Biogeochemical Cycles*, 24:GB3029.
- Gelman, A., Carlin, J. B., Stern, S., and Rubin, D. B. (2004). *Bayesian data analysis*. Chapman & Hall.
- Gjettermann, B., Styczen, M., Hansen, H. C. B., Vinther, F. P., and Hansen, S. (2008). Challenges in modelling dissolved organic matter dynamics in agricultural soil using DAISY. *Soil Biology & Biochemistry*, 40(6):1506–1518.
- Gjettermann, B., Styczen, M., Hansen, S., Borggaard, O. K., and Hansen, H. C. B. (2007). Sorption and fractionation of dissolved organic matter and associated phosphorus in agricultural soil. *Journal Of Environmental Quality*, 36(3):753–763.
- Golchin, A., Oades, J. M., Skjemstad, J. O., and Clarke, P. (1994). Soil-structure and carbon

- cycling. *Australian Journal of Soil Research*, 32(5):1043–1068.
- Gotelli, N. and Ellison, A. (2002). Biogeography at a regional scale: Determinants of ant species density in New England bogs and forests. *Ecology*, 83(6):1604–1609.
- Grant, R., Juma, N., and McGill, W. (1993). Simulation of carbon and nitrogen transformations in soil - mineralization. *Soil Biology & Biochemistry*, 25(10):1317–1329.
- Gregorich, E. G., Ellert, B. H., Drury, C. F., and Liang, B. C. (1996). Fertilization effects on soil organic matter turnover and corn residue C storage. *Soil Science Society of America Journal*, 60(2):472–476.
- Guenet, B., Eglin, T., Vasilyeva, N., Peylin, P., Ciais, P., and Chenu, C. (2013). The relative importance of decomposition and transport mechanisms in accounting for soil organic carbon profiles. *Biogeosciences*, 10(4):2379–2392.
- Gupta, H. V., Clark, M. P., Vrugt, J. A., Abramowitz, G., and Ye, M. (2012). Towards a comprehensive assessment of model structural adequacy. *Water Resources Research*, 48:W08301.
- Hahn, V. and Buchmann, N. (2004). A new model for soil organic carbon turnover using bomb carbon. *Global Biogeochemical Cycles*, 18(1):GB1019.
- Hansen, S., Jensen, H., Nielsen, N., and Svendsen, H. (1991). Simulation of nitrogen dynamics and biomass production in winter-wheat using the Danish simulation-model DAISY. *Fertilizer Research*, 27(2-3):245–259.
- Harden, J. W., Manies, K. L., Turetsky, M. R., and Neff, J. C. (2006). Effects of wildfire and permafrost on soil organic matter and soil climate in interior Alaska. *Global Change Biology*, 12(12):2391–2403.
- Hashimoto, S., Tanaka, N., Kume, T., Yoshifuji, N., Hotta, N., Tanaka, K., and Suzuki, M. (2007). Seasonality of vertically partitioned soil CO₂ production in temperate and tropical forest. *Journal of Forest Research*, 12(3):209–221.
- Hassink, J. (1997). The capacity of soils to preserve organic C and N by their association with clay and silt particles. *Plant and Soil*, 191(1):77–87.
- He, Q. and Walling, D. E. (1997). The distribution of fallout Cs-137 and Pb-210 in undisturbed and cultivated soils. *Applied Radiation and Isotopes*, 48(5):677–690.
- Heimann, M. and Reichstein, M. (2008). Terrestrial ecosystem carbon dynamics and climate feedbacks. *Nature*, 451(7176):289–292.
- Heinemeyer, A., Croft, S., Garnett, M. H., Gloor, E., Holden, J., Lomas, M. R., and Ineson, P. (2010). The MILLENNIA peat cohort model: predicting past, present and future soil carbon budgets and fluxes under changing climates in peatlands. *Climate Research*, 45(1, 24):207–226.
- Hilinski, T. (2001). Implementation of exponential depth distribution of organic carbon in the CENTURY model. <http://nrel.colostate.edu/projects/century5/reference/html/Century/exp-c-distrib.htm>. Date retrieved: 8 September 2013.
- Hinze, J. (1975). *Turbulence*. McGraw-Hill series in mechanical engineering. McGraw-Hill, New York, second edition.
- Högberg, P. (1997). Tansley review No 95 - N-15 natural abundance in soil-plant systems. *New Phytologist*, 137(2):179–203.
- Hole, F. (1961). A classification of pedoturbations and some other processes and factors of soil formation in relation to isotropism and anisotropism. *Soil Science*, 91:375–377.
- Hoosbeek, M. R. and Scarascia-Mugnozza, G. E. (2009). Increased litter build up and soil organic matter stabilization in a poplar plantation after 6 years of atmospheric CO₂ enrichment (FACE): Final results of POP-EuroFACE compared to other forest FACE experiments. *Ecosystems*, 12(2):220–239.
- Hua, Q. and Barbetti, M. (2004). Review of tropospheric bomb C-14 data for carbon cycle modeling and age calibration purposes. *Radiocarbon*, 46(3):1273–1298.

- Huang, K., Toride, N., and Genuchten, M. T. (1995). Experimental investigation of solute transport in large, homogeneous and heterogeneous, saturated soil columns. *Transport in Porous Media*, 18(3):283–302.
- Hungate, B., Dukes, J., Shaw, M., Luo, Y., and Field, C. (2003). Nitrogen and climate change. *Science*, 302(5650):1512–1513.
- IUSS Working Group WRB (2007). World reference base for soil resources 2006, first update 2007. Technical report, FAO.
- Iversen, C. M. (2010). Digging deeper: fine-root responses to rising atmospheric CO₂ concentration in forested ecosystems. *New Phytologist*, 186(2):346–357.
- Jackson, R., Canadell, J., Ehleringer, J., Mooney, H., Sala, O., and Schulze, E. (1996). A global analysis of root distributions for terrestrial biomes. *Oecologia*, 108(3):389–411.
- Jackson, R., Schenk, H., Jobbagy, E., Canadell, J., Colello, G., Dickinson, R., Field, C., Friedlingstein, P., Heimann, M., Hibbard, K., Kicklighter, D., Kleidon, A., Neilson, R., Parton, W., Sala, O., and Sykes, M. (2000). Belowground consequences of vegetation change and their treatment in models. *Ecological Applications*, 10(2):470–483.
- Janssens, I. A., Dieleman, W., Luysaert, S., Subke, J. A., Reichstein, M., Ceulemans, R., Ciais, P., Dolman, A. J., Grace, J., Matteucci, G., Papale, D., Piao, S. L., Schulze, E. D., Tang, J., and Law, B. E. (2010). Reduction of forest soil respiration in response to nitrogen deposition. *Nature Geoscience*, 3(5):315–322.
- Janssens, I. A., Sampson, D. A., Curiel-Yuste, J., Carrara, A., and Ceulemans, R. (2002). The carbon cost of fine root turnover in a Scots pine forest. *Forest Ecology and Management*, 168(13):231–240.
- Jarvis, N. J., Taylor, A., Larsbo, M., Etana, A., and Rosen, K. (2010). Modelling the effects of bioturbation on the re-distribution of ¹³⁷Cs in an undisturbed grassland soil. *European Journal of Soil Science*, 61(1):24–34.
- Jenkinson, D. and Coleman, K. (1994). Calculating the annual input of organic-matter to soil from measurements of total organic-carbon and radiocarbon. *European Journal of Soil Science*, 45(2):167–174.
- Jenkinson, D. S. (1990). The turnover of organic carbon and nitrogen in soil. *Philosophical Transactions of the Royal Society of London Series B-Biological Sciences*, 329(1255):361–368.
- Jenkinson, D. S. and Coleman, K. (2008). The turnover of organic carbon in subsoils. part 2. Modelling carbon turnover. *European Journal of Soil Science*, 59(2):400–413.
- Jenkinson, D. S. and Rayner, J. H. (1977). Turnover of soil organic matter in some of the Rothamsted classical experiments. *Soil Science*, 123(5):298–305.
- Jenny, H. (1980). *The soil resource: origin and behavior*. Ecological studies. Springer-Verlag.
- Jobbagy, E. G. and Jackson, R. B. (2000). The vertical distribution of soil organic carbon and its relation to climate and vegetation. *Ecological Applications*, 10(2):423–436.
- Johnson, D., Domier, J., and Johnson, D. (2005). Animating the biodynamics of soil thickness using process vector analysis: a dynamic denudation approach to soil formation. *Geomorphology*, 67(1-2):23–46.
- Johnson, D., Watson-Stegner, D., Johnson, D., and Schaetzl, R. (1987). Proisotropic and proanisotropic processes of pedoturbation. *Soil Science*, 143(4):278–292.
- Johnson, D. W., Murphy, J. D., Rau, B. M., and Miller, W. W. (2011). Subsurface carbon contents: Some case studies in forest soils. *Forest Science*, 57(1, SI):3–10.
- Jones, C. and Falloon, P. (2009). Sources of uncertainty in global modelling of future soil organic carbon storage. In Baveye, P., Laba, M., and Mysiak, J., editors, *Uncertainties in environmental modelling and consequences for policy making*, NATO Science for Peace and Security Series C-Environmental Security, pages 283–315. NATO.
- Jones, C., McConnell, C., Coleman, K., Cox, P., Falloon, P., Jenkinson, D., and Powlson, D.

- (2005). Global climate change and soil carbon stocks; predictions from two contrasting models for the turnover of organic carbon in soil. *Global Change Biology*, 11(1):154–166.
- Jones, C. D., Cox, P., and Huntingford, C. (2003). Uncertainty in climate-carbon-cycle projections associated with the sensitivity of soil respiration to temperature. *Tellus Series B-Chemical and Physical Meteorology*, 55(2):642–648.
- Jones, C. D., Cox, P. M., and Huntingford, C. (2006). Climate-carbon cycle feedbacks under stabilization: uncertainty and observational constraints. *Tellus Series B-Chemical and Physical Meteorology*, 58(5):603–613.
- Kaiser, K. and Guggenberger, G. (2000). The role of DOM sorption to mineral surfaces in the preservation of organic matter in soils. *Organic Geochemistry*, 31(7-8):711–725.
- Kaiser, K. and Kalbitz, K. (2012). Cycling downwards - dissolved organic matter in soils. *Soil Biology & Biochemistry*, 52:29–32.
- Kalbitz, K. and Kaiser, K. (2008). Contribution of dissolved organic matter to carbon storage in forest mineral soils. *Journal of Plant Nutrition and Soil Science*, 171(1):52–60.
- Kalbitz, K., Solinger, S., Park, J. H., Michalzik, B., and Matzner, E. (2000). Controls on the dynamics of dissolved organic matter in soils: A review. *Soil Science*, 165(4):277–304.
- Kaste, J. M., Friedland, A. J., and Sturup, S. (2003). Using stable and radioactive isotopes to trace atmospherically deposited Pb in montane forest soils. *Environmental Science & Technology*, 37(16):3560–3567.
- Kaste, J. M., Heimsath, A. M., and Bostick, B. C. (2007). Short-term soil mixing quantified with fallout radionuclides. *Geology*, 35(3):243–246.
- Kavetski, D., Kuczera, G., and Franks, S. W. (2006). Bayesian analysis of input uncertainty in hydrological modeling: 1. theory. *Water Resources Research*, 42(3):W03407.
- Kempen, B., Brus, D. J., and Stoorvogel, J. J. (2011). Three-dimensional mapping of soil organic matter content using soil type-specific depth functions. *Geoderma*, 162(1-2):107–123.
- Kindler, R., Siemens, J., Kaiser, K., Walmsley, D. C., Bernhofer, C., Buchmann, N., Cellier, P., Eugster, W., Gleixner, G., Grunwald, T., Heim, A., Ibrom, A., Jones, S. K., Jones, M., Klumpp, K., Kutsch, W., Larsen, K. S., Lehuger, S., Loubet, B., McKenzie, R., Moors, E., Osborne, B., Pilegaard, K., Rebmann, C., Saunders, M., Schmidt, M. W. I., Schrumpf, M., Seyfferth, J., Skiba, U., Soussana, J. F., Sutton, M. A., Tefs, C., Vowinkel, B., Zeeman, M. J., and Kaupenjohann, M. (2011). Dissolved carbon leaching from soil is a crucial component of the net ecosystem carbon balance. *Global Change Biology*, 17(2):1167–1185.
- Kirkby, M. (1977). Soil development models as a component of slope models. *Earth Surface Processes and Landforms*, 2(2-3):203–230.
- Kleber, M. (2010). What is recalcitrant soil organic matter? *Environmental Chemistry*, 7(4):320–332.
- Knohl, A., Schulze, E., Kolle, O., and Buchmann, N. (2003). Large carbon uptake by an unmanaged 250-year-old deciduous forest in Central Germany. *Agricultural and Forest Meteorology*, 118(3-4):151–167.
- Knorr, W. (2000). Annual and interannual CO₂ exchanges of the terrestrial biosphere: Process-based simulations and uncertainties. *Global Ecology and Biogeography*, 9(3):225–252.
- Knorr, W., Prentice, I. C., House, J. I., and Holland, E. A. (2005). Long-term sensitivity of soil carbon turnover to warming. *Nature*, 433(7023):298–301.
- Koarashi, J., Hockaday, W. C., Masiello, C. A., and Trumbore, S. E. (2012). Dynamics of decadal cycling carbon in subsurface soils. *Journal of Geophysical Research-Biogeosciences*, 117:G03033.
- Kögel-Knabner, I., Guggenberger, G., Kleber, M., Kandeler, E., Kalbitz, K., Scheu, S., Eusterhues, K., and Leinweber, P. (2008). Organo-mineral associations in temperate soils: Integrating biology, mineralogy, and organic matter chemistry. *Journal of Plant Nutrition and*

- Soil Science*, 171(1):61–82.
- Kong, A. Y. Y. and Six, J. (2010). Tracing root vs. residue carbon into soils from conventional and alternative cropping systems. *Soil Science Society of America Journal*, 74(4):1201–1210.
- Koven, C., Friedlingstein, P., Ciais, P., Khvorostyanov, D., Krinner, G., and Tarnocai, C. (2009). On the formation of high-latitude soil carbon stocks: Effects of cryoturbation and insulation by organic matter in a land surface model. *Geophysical Research Letters*, 36:L21501.
- Koven, C. D., Riley, W. J., Subin, Z. M., Tang, J. Y., Torn, M. S., Collins, W. D., Bonan, G. B., Lawrence, D. M., and Swenson, S. C. (2013). The effect of vertically resolved soil biogeochemistry and alternate soil C and N models on C dynamics of CLM4. *Biogeosciences*, 10(11):7109–7131.
- Kutsch, W., Persson, T., Schrumppf, M., Moyano, F., Mund, M., Andersson, S., and Schulze, E.-D. (2010). Heterotrophic soil respiration and soil carbon dynamics in the deciduous Hainich forest obtained by three approaches. *Biogeochemistry*, 100:167–183.
- Kylander, M. E., Cortizas, A. M., Rauch, S., and Weiss, D. J. (2008). Lead penetration and leaching in a complex temperate soil profile. *Environmental Science & Technology*, 42(9):3177–3184.
- Laloy, E. and Vrugt, J. A. (2012). High-dimensional posterior exploration of hydrologic models using multiple-try DREAM(ZS) and high-performance computing. *Water Resources Research*, 48:W01526.
- Lawrence, D. M. and Slater, A. G. (2008). Incorporating organic soil into a global climate model. *Climate Dynamics*, 30(2-3):145–160.
- Lebret, M., Nys, C., and Forgeard, F. (2001). Litter production in an Atlantic beech (*Fagus sylvatica* L.) time sequence. *Annals of Forest Science*, 58(7):755–768.
- Levin, I. and Kromer, B. (2004). The tropospheric CO₂-C-14 level in mid-latitudes of the Northern Hemisphere (1959-2003). *Radiocarbon*, 46(3):1261–1272.
- Li, C., Frolking, S., and Frolking, T. (1992). A model of nitrous-oxide evolution from soil driven by rainfall events .1. model structure and sensitivity. *Journal of Geophysical Research-Atmospheres*, 97(D9):9759–9776.
- Lloyd, J. and Taylor, J. A. (1994). On the temperature dependence of soil respiration. *Functional Ecology*, 8(3):315–323.
- Logan, E. M., Pulford, I. D., Cook, G. T., and MacKenzie, A. B. (1997). Complexation of Cu²⁺ and Pb²⁺ by peat and humic acid. *European Journal of Soil Science*, 48(4):685–696.
- Lorenz, K. and Lal, R. (2005). The depth distribution of soil organic carbon in relation to land use and management and the potential of carbon sequestration in subsoil horizons. In *Advances in Agronomy, Vol 88*, pages 35–66. Elsevier Academic Press Inc, San Diego.
- Luyssaert, S., Inghima, I., Jung, M., Richardson, A. D., Reichstein, M., Papale, D., Piao, S. L., Schulze, E. D., Wingate, L., Matteucci, G., Aragao, L., Aubinet, M., Beer, C., Bernhofer, C., Black, K. G., Bonal, D., Bonnefond, J. M., Chambers, J., Ciais, P., Cook, B., Davis, K. J., Dolman, A. J., Gielen, B., Goulden, M., Grace, J., Granier, A., Grelle, A., Griffis, T., GrNwald, T., Guidolotti, G., Hanson, P. J., Harding, R., Hollinger, D. Y., Hutyrá, L. R., Kolari, P., Kruijt, B., Kutsch, W., Lagergren, F., Laurila, T., Law, B. E., Le Maire, G., Lindroth, A., Loustau, D., Malhi, Y., Mateus, J., Migliavacca, M., Misson, L., Montagnani, L., Moncrieff, J., Moors, E., Munger, J. W., Nikinmaa, E., Ollinger, S. V., Pita, G., Rebmann, C., Rouspard, O., Saigusa, N., Sanz, M. J., Seufert, G., Sierra, C., Smith, M. L., Tang, J., Valentini, R., Vesala, T., and Janssens, I. A. (2007). CO₂ balance of boreal, temperate, and tropical forests derived from a global database. *Global Change Biology*, 13(12):2509–2537.
- Mabit, L., Klik, A., Benmansour, M., Toloza, A., Geisler, A., and Gerstmann, U. C. (2009). Assessment of erosion and deposition rates within an Austrian agricultural watershed by combining Cs-137, Pb-210(ex) and conventional measurements. *Geoderma*, 150(3-4):231–239.

- Manzoni, S. and Porporato, A. (2009). Soil carbon and nitrogen mineralization: Theory and models across scales. *Soil Biology & Biochemistry*, 41(7):1355–1379.
- McDowell, W. and Likens, G. (1988). Origin, composition, and flux of dissolved organic-carbon in the Hubbard Brook valley. *Ecological Monographs*, 58(3):177–195.
- Mead, R. (1965). A generalised logit-normal distribution. *Biometrics*, 21(3):721–732.
- Meinshausen, M., Smith, S. J., Calvin, K., Daniel, J. S., Kainuma, M., Lamarque, J., Matsumoto, K., Montzka, S., Raper, S., Riahi, K., et al. (2011). The RCP greenhouse gas concentrations and their extensions from 1765 to 2300. *Climatic Change*, 109(1-2):213–241.
- Metropolis, N., Rosenbluth, A. W., Rosenbluth, M. N., Teller, A. H., and Teller, E. (1953). Equation of state calculations by fast computing machines. *Journal of Chemical Physics*, 21(6):1087–1092.
- Meysman, F., Boudreau, B., and Middelburg, J. (2005). Modeling reactive transport in sediments subject to bioturbation and compaction. *Geochimica et Cosmochimica Acta*, 69(14):3601–3617.
- Meysman, F. J. R., Boudreau, B. P., and Middelburg, J. J. (2003). Relations between local, non-local, discrete and continuous models of bioturbation. *Journal of Marine Research*, 61(3):391–410.
- Meysman, F. J. R., Boudreau, B. P., and Middelburg, J. J. (2010). When and why does bioturbation lead to diffusive mixing? *Journal of Marine Research*, 68(6):881–920.
- Meysman, F. J. R., Malyuga, V. S., Boudreau, B. P., and Middelburg, J. J. (2008). A generalized stochastic approach to particle dispersal in soils and sediments. *Geochimica et Cosmochimica Acta*, 72(14):3460–3478.
- Meysman, F. J. R., Middelburg, J. J., and Heip, C. H. R. (2006). Bioturbation: a fresh look at Darwin's last idea. *Trends in Ecology and Evolution*, 21(12):688–695.
- Michalzik, B., Kalbitz, K., Park, J. H., Solinger, S., and Matzner, E. (2001). Fluxes and concentrations of dissolved organic carbon and nitrogen - a synthesis for temperate forests. *Biogeochemistry*, 52(2):173–205.
- Michalzik, B., Tipping, E., Mulder, J., Lancho, J. F. G., Matzner, E., Bryant, C. L., Clarke, N., Lofts, S., and Esteban, M. A. V. (2003). Modelling the production and transport of dissolved organic carbon in forest soils. *Biogeochemistry*, 66(3):241–264.
- Mikutta, R., Kleber, M., Torn, M. S., and Jahn, R. (2006). Stabilization of soil organic matter: Association with minerals or chemical recalcitrance? *Biogeochemistry*, 77(1):25–56.
- Miller, E. K. and Friedland, A. J. (1994). Lead migration in forest soils - response to changing atmospheric inputs. *Environmental Science & Technology*, 28(4):662–669.
- Minasny, B., McBratney, A., Mendonca-Santos, M., Odeh, I., and Guyon, B. (2006). Prediction and digital mapping of soil carbon storage in the lower namoi valley. *Australian Journal of Soil Research*, 44(3):233–244.
- Mölders, N. and Romanovsky, V. (2006). Long-term evaluation of the hydro-thermodynamic soil-vegetation scheme's frozen ground/permafrost component using observations at Barrow, Alaska. *Journal of Geophysical Research-Atmospheres*, 111(D4):D04105.
- Moni, C., Rumpel, C., Virto, I., Chabbi, A., and Chenu, C. (2010). Relative importance of sorption versus aggregation for organic matter storage in subsoil horizons of two contrasting soils. *European Journal of Soil Science*, 61(6):958–969.
- Moore, T. and Desouza, WaAnd Koprivnjak, J. (1992). Controls on the sorption of dissolved organic-carbon by soils. *Soil Science*, 154(2):120–129.
- Mosegaard, K. and Sambridge, M. (2002). Monte Carlo analysis of inverse problems. *Inverse Problems*, 18(3):R29–R54.
- Müller-Lemans, H. and van Dorp, F. (1996). Bioturbation as a mechanism for radionuclide transport in soil: Relevance of earthworms. *Journal of Environmental Radioactivity*, 31(1):7–

- 20.
- Nadelhoffer, K. and Fry, B. (1988). Controls on natural N-15 and C-13 abundances in forest soil organic-matter. *Soil Science Society of America Journal*, 52(6):1633–1640.
- Nakane, K. and Shinozaki, K. (1978). A mathematical model of the behavior and vertical distribution of organic carbon in forest soils. *Japanese Journal of Ecology*, 28(2):111–122.
- National Oceanic and Atmospheric Administration (2013). CO₂ at NOAAs Mauna Loa Observatory reaches new milestone: Tops 400 ppm. <http://www.esrl.noaa.gov/gmd/news/7074.html>. Date Retrieved: 10 July 2013.
- Neff, J. C. and Asner, G. P. (2001). Dissolved organic carbon in terrestrial ecosystems: Synthesis and a model. *Ecosystems*, 4(1):29–48.
- Neto, A. J. S., Ribeiro, A., Lopes, D. D., Neto, O. B. D., Souza, W. G., and Santana, M. O. (2012). Simulation of rainfall interception of canopy and litter in Eucalyptus plantation in tropical climate. *Forest Science*, 58(1):54–60.
- Nguyen, C. (2003). Rhizodeposition of organic C by plants: mechanisms and controls. *Agronomie*, 23(5-6):375–396.
- Nierop, K. G. J. (1998). Origin of aliphatic compounds in a forest soil. *Organic Geochemistry*, 29(4):1009–1016.
- Nierop, K. G. J. and Buurman, P. (1999). Water-soluble organic matter in incipient podzols: accumulation in B horizons or in fibres? *European Journal of Soil Science*, 50(4):701–711.
- Nodvin, S. C., Driscoll, C. T., and Likens, G. E. (1986). Simple partitioning of anions and dissolved organic carbon in a forest soil. *Soil Science*, 142(1):27–35.
- Norby, R. J., DeLucia, E. H., Gielen, B., Calfapietra, C., Giardina, C. P., King, J. S., Ledford, J., McCarthy, H. R., Moore, D. J. P., Ceulemans, R., De Angelis, P., Finzi, A. C., Karnosky, D. F., Kubiske, M. E., Lukac, M., Pregitzer, K. S., Scarascia-Mugnozza, G. E., Schlesinger, W. H., and Oren, R. (2005). Forest response to elevated CO₂ is conserved across a broad range of productivity. *Proceedings of the National Academy of Sciences of the United States of America*, 102(50):18052–18056.
- O'Brien, B. J. and Stout, J. D. (1978). Movement and turnover of soil organic matter as indicated by carbon isotope measurements. *Soil Biology and Biochemistry*, 10(4):309–317.
- Ogee, J. and Brunet, Y. (2002). A forest floor model for heat and moisture including a litter layer. *Journal of Hydrology*, 255(1-4):212–233.
- Olson, J. (1963). Energy-storage and balance of producers and decomposers in ecological-systems. *Ecology*, 44(2):322–331.
- Omlin, M. and Reichert, P. (1999). A comparison of techniques for the estimation of model prediction uncertainty. *Ecological Modelling*, 115(1):45–59.
- Parton, W. J., Schimel, D. S., Cole, C. V., and Ojima, D. S. (1987). Analysis of factors controlling soil organic matter levels in Great Plains grasslands. *Soil Science Society of America Journal*, 51(5):1173–1179.
- Paton, T., Humphreys, G. S., and Mitchell, P. (1995). *Soils: a new global view*, chapter 3. Bioturbation, pages 33–67. Yale Univ. Press, New Haven [u.a.].
- Paustian, K., Ågren, G., and Bosatta, E. (1997). Modeling litter quality effects on decomposition and soil organic matter dynamics. In Cadisch, G. and Giller, K., editors, *Driven by nature: plant litter quality and decomposition*, pages 313–335. CABI Publishing, Wallingford.
- Perruchoud, D., Joos, F., Fischlin, A., Hajdas, I., and Bonani, G. (1999). Evaluating timescales of carbon turnover in temperate forest soils with radiocarbon data. *Global Biogeochemical Cycles*, 13(2):555–573.
- Persson, T., Karlsson, P., Seyferth, U., Sjöberg, R., and Rudebeck, A. (2000). Carbon mineralisation in European forest soils. In Schulze, E. D., editor, *Carbon and nitrogen cycling in European forest ecosystems*, Ecological Studies. Springer-Verlag GmbH, New York.

- Petersen, B., Berntsen, J., Hansen, S., and Jensen, L. (2005). CN-SIM - a model for the turnover of soil organic matter. I. long-term carbon and radiocarbon development. *Soil Biology & Biochemistry*, 37(2):359–374.
- Philips, D. A., Fox, T. C., and Six, J. (2006). Root exudation (net efflux of amino acids) may increase rhizodeposition under elevated CO₂. *Global Change Biology*, 12(3):561–567.
- Piani, C., Weedon, G., Best, M., Gomes, S., Viterbo, P., Hagemann, S., and Haerter, J. (2010). Statistical bias correction of global simulated daily precipitation and temperature for the application of hydrological models. *Journal of Hydrology*, 395(3):199–215.
- Prentice, I. C., Farquhar, G. D., Fasham, M. J. R., Goulden, M. L., Heimann, M., Jaramillo, V. J., Khashgi, H. H. S., Le Qur, C., Scholes, R. R. J., and Wallace, D. W. R. (2001). The carbon cycle and atmospheric carbon dioxide. In Houghton, J. T., Ding, Y., Griggs, D. J., Noguer, M., van der Linden, P. P. J., Dai, X., Maskell, K., and Johnson, C. A., editors, *Climate Change 2001: The Scientific Basis. Contribution of Working Group I to the Third Assessment Report of the Intergovernmental Panel on Climate Change*, pages 183–237. Cambridge University Press.
- Press, W. H., Teukolsky, S. A., Vetterling, W. T., and Flannery, B. P. (1996). *Numerical Recipes in Fortran 90 (2nd Ed.): The Art of Parallel Scientific Computing*. Cambridge University Press, New York, NY, USA.
- Raddatz, T. J., Reick, C. H., Knorr, W., Kattge, J., Roeckner, E., Schnur, R., Schnitzler, K.-G., Wetzel, P., and Jungclaus, J. (2007). Will the tropical land biosphere dominate the climate-carbon cycle feedback during the twenty-first century? *Climate dynamics*, 29(6):565–574.
- Rahn, K.-H., Werner, C., Kiese, R., Haas, E., and Butterbach-Bahl, K. (2012). Parameter-induced uncertainty quantification of soil N₂O, NO and CO₂ emission from Höglwald spruce forest (Germany) using the LandscapeDNDC model. *Biogeosciences*, 9(10):3983–3998.
- Raich, J. and Nadelhoffer, K. (1989). Belowground carbon allocation in forest ecosystems - global trends. *Ecology*, 70(5):1346–1354.
- Rasmussen, J. (2011). Why we need to restrict the use of “rhizodeposition” and the Janzen and Bruinsma equation. *Soil Biology & Biochemistry*, 43(10):2213–2214.
- Rasse, D. P., Rumpel, C., and Dignac, M.-F. (2005). Is soil carbon mostly root carbon? Mechanisms for a specific stabilisation. *Plant and Soil*, 269:341–356.
- Raupach, M., Rayner, P., Barrett, D., DeFries, R., Heimann, M., Ojima, D., Quegan, S., and Schimmler, C. (2005). Model-data synthesis in terrestrial carbon observation: methods, data requirements and data uncertainty specifications. *Global Change Biology*, 11(3):378–397.
- Rawls, W. (1983). Estimating soil bulk-density from particle-size analysis and organic-matter content. *Soil Science*, 135(2):123–125.
- Rawls, W., Pachepsky, Y., Ritchie, J., Sobecki, T., and Bloodworth, H. (2003). Effect of soil organic carbon on soil water retention. *Geoderma*, 116(1-2):61–76.
- Rayner, P. J., Scholze, M., Knorr, W., Kaminski, T., Giering, R., and Widmann, H. (2005). Two decades of terrestrial carbon fluxes from a carbon cycle data assimilation system (CCDAS). *Global Biogeochemical Cycles*, 19(2):GB2026. Rayner, P. J., Scholze, M., Knorr, W., Kaminski, T., Giering, R., Widmann, H.
- Reich, P. B., Oleksyn, J., Modrzyński, J., Mrozinski, P., Hobbie, S. E., Eissenstat, D. M., Chorover, J., Chadwick, O. A., Hale, C. M., and Tjoelker, M. G. (2005). Linking litter calcium, earthworms and soil properties: a common garden test with 14 tree species. *Ecology Letters*, 8(8):811–818.
- Reichert, P. and Omlin, M. (1997). On the usefulness of overparameterized ecological models. *Ecological Modelling*, 95(2-3):289–299.
- Reichstein, M. and Beer, C. (2008). Soil respiration across scales: The importance of a model-data integration framework for data interpretation. *Journal of Plant Nutrition and Soil Science*, 171(3):344–354.

- Reichstein, M., Katterer, T., Andren, O., Ciais, P., Schulze, E. D., Cramer, W., Papale, D., and Valentini, R. (2005). Temperature sensitivity of decomposition in relation to soil organic matter pools: critique and outlook. *Biogeosciences*, 2(4):317–321.
- Reimer, P., Baillie, M., Bard, E., Bayliss, A., Beck, J., Bertrand, C., Blackwell, P., Buck, C., Burr, G., Cutler, K., Damon, P., Edwards, R., Fairbanks, R., Friedrich, M., Guilderson, T., Hogg, A., Hughen, K., Kromer, B., McCormac, G., Manning, S., Ramsey, C., Reimer, R., Remmele, S., Southon, J., Stuiver, M., Talamo, S., Taylor, F., van der Plicht, J., and Weyhenmeyer, C. (2004). IntCal04 terrestrial radiocarbon age calibration, 0–26 cal kyr BP. *Radiocarbon*, 46(3):1029–1058.
- Rinke, A., Kuhry, P., and Dethloff, K. (2008). Importance of a soil organic layer for Arctic climate: A sensitivity study with an Arctic RCM. *Geophysical Research Letters*, 35(13):L13709.
- Rosenbloom, N., Doney, S., and Schimel, D. (2001). Geomorphic evolution of soil texture and organic matter in eroding landscapes. *Global Biogeochemical Cycles*, 15(2):365–381.
- Rumpel, C., Chabbi, A., and Marschner, B. (2012). Carbon storage and sequestration in subsoil horizons: Knowledge, gaps and potentials. In Lal, R., Lorenz, K., and Hüttl, R., editors, *Re-carbonization of the Biosphere: Ecosystems and the Global Carbon Cycle*, pages 445–464. Springer Netherlands.
- Rumpel, C. and Kögel-Knabner, I. (2011). Deep soil organic matter—a key but poorly understood component of terrestrial C cycle. *Plant and Soil*, 338(1–2):143–158.
- Rumpel, C., Kögel-Knabner, I., and Bruhn, F. (2002). Vertical distribution, age, and chemical composition of organic carbon in two forest soils of different pedogenesis. *Organic Geochemistry*, 33(10):1131–1142.
- Salomé, C., Nunan, N., Pouteau, V., Lerch, T. Z., and Chenu, C. (2010). Carbon dynamics in topsoil and in subsoil may be controlled by different regulatory mechanisms. *Global Change Biology*, 16(1):416–426.
- Salvador-Blanes, S., Minasny, B., and McBratney, A. B. (2007). Modelling long-term in situ soil profile evolution: application to the genesis of soil profiles containing stone layers. *European Journal of Soil Science*, 58(6):1535–1548.
- Sanderman, J., Baldock, J. A., and Amundson, R. (2008). Dissolved organic carbon chemistry and dynamics in contrasting forest and grassland soils. *Biogeochemistry*, 89(2):181–198.
- Saugier, B., Roy, J., and Mooney, H. (2001). Estimations of global terrestrial productivity: Converging toward a single number? In Roy, J. and Saugier, B. Mooney, H., editors, *Terrestrial Global Productivity, A Volume in the Physiological Ecology Series*. Academic Press.
- Sauve, S., Martinez, C. E., McBride, M., and Hendershot, W. (2000). Adsorption of free lead Pb^{2+} by pedogenic oxides, ferrihydrite, and leaf compost. *Soil Science Society of America Journal*, 64(2):595–599.
- Saxton, K. E. and Rawls, W. J. (2006). Soil water characteristic estimates by texture and organic matter for hydrologic solutions. *Soil Science Society of America Journal*, 70(5):1569–1578.
- Schaap, M. and Bouten, W. (1997). Forest floor evaporation in a dense Douglas fir stand. *Journal of Hydrology*, 193(1–4):97–113.
- Schaap, M., Bouten, W., and Verstraten, J. (1997). Forest floor water content dynamics in a Douglas fir stand. *Journal of Hydrology*, 201(1–4):367–383.
- Scharnagl, B., Vrugt, J. A., Vereecken, H., and Herbst, M. (2010). Information content of incubation experiments for inverse estimation of pools in the Rothamsted carbon model: a Bayesian perspective. *Biogeosciences*, 7(2):763–776.
- Scharpenseel, H. W., Becker-Heidmann, P., Neue, H. U., and Tsutsuki, K. (1989). Bomb-carbon, ^{14}C -dating and ^{13}C -measurements as tracers of organic matter dynamics as well as of morphogenetic and turbation processes. *Science of the Total Environment*, 81–82:99–110.
- Schenk, H. and Jackson, R. (2002a). The global biogeography of roots. *Ecological Monographs*,

- 72(3):311–328.
- Schenk, H. and Jackson, R. (2002b). Rooting depths, lateral root spreads and below-ground/above-ground allometries of plants in water-limited ecosystems. *Journal of Ecology*, 90(3):480–494.
- Schimel, D. (1995). Terrestrial ecosystems and the carbon-cycle. *Global Change Biology*, 1(1):77–91.
- Schimel, D. S., Braswell, B. H., Holland, E. A., McKeown, R., Ojima, D. S., Painter, T. H., Parton, W. J., and Townsend, A. R. (1994). Climatic, edaphic, and biotic controls over storage and turnover of carbon in soils. *Global Biogeochemical Cycles*, 8(3):279–293.
- Schlesinger, W. H. (1997). *Biogeochemistry: An Analysis of Global Change*. Academic Press, London, 2nd edition.
- Schmidt, M. W. I., Torn, M. S., Abiven, S., Dittmar, T., Guggenberger, G., Janssens, I. A., Kleber, M., Koegel-Knabner, I., Lehmann, J., Manning, D. A. C., Nannipieri, P., Rasse, D. P., Weiner, S., and Trumbore, S. E. (2011). Persistence of soil organic matter as an ecosystem property. *Nature*, 478(7367):49–56.
- Schoups, G., Vrugt, J. A., Fenicia, F., and de Giesen, N. C. v. (2010). Corruption of accuracy and efficiency of Markov chain Monte Carlo simulation by inaccurate numerical implementation of conceptual hydrologic models. *Water Resources Research*, 46:W10530.
- Schroth, A. W., Bostick, B. C., Kaste, J. M., and Friedland, A. J. (2008). Lead sequestration and species redistribution during soil organic matter decomposition. *Environmental Science & Technology*, 42(10):3627–3633.
- Schrumpf, M., Kaiser, K., Guggenberger, G., Persson, T., Kögel-Knabner, I., and Schulze, E.-D. (2013). Storage and stability of organic carbon in soils as related to depth, occlusion within aggregates, and attachment to minerals. *Biogeosciences*, 10(9):1675–1691.
- Schrumpf, M., Kaiser, K., and Schulze, E.-D. Soil organic carbon and total nitrogen gains in an old growth deciduous forest in Germany. Submitted to PlosOne.
- Schrumpf, M., Schulze, E. D., Kaiser, K., and Schumacher, J. (2011). How accurately can soil organic carbon stocks and stock changes be quantified by soil inventories? *Biogeosciences*, 8(5):1193–1212.
- Sierra, C. A., Trumbore, S. E., Davidson, E. A., Frey, S. D., Savage, K. E., and Hopkins, F. M. (2012). Predicting decadal trends and transient responses of radiocarbon storage and fluxes in a temperate forest soil. *Biogeosciences*, 9(8):3013–3028.
- Sitch, S., Huntingford, C., Gedney, N., Levy, P. E., Lomas, M., Piao, S. L., Betts, R., Ciais, P., Cox, P., Friedlingstein, P., Jones, C. D., Prentice, I. C., and Woodward, F. I. (2008). Evaluation of the terrestrial carbon cycle, future plant geography and climate-carbon cycle feedbacks using five Dynamic Global Vegetation Models (DGVMs). *Global Change Biology*, 14(9):2015–2039.
- Smit, A. (1999). The impact of grazing on spatial variability of humus profile properties in a grass-encroached Scots pine ecosystem. *Catena*, 36(1-2):85–98.
- Smit, A. and Kooijman, A. M. (2001). Impact of grazing on the input of organic matter and nutrients to the soil in a grass-encroached Scots pine forest. *Forest Ecology and Management*, 142(1-3):99–107.
- Smith, J., Smith, P., Monaghan, R., and MacDonald, J. (2002). When is a measured soil organic matter fraction equivalent to a model pool? *European Journal of Soil Science*, 53(3):405–416.
- Søe, A. R. B. and Buchmann, N. (2005). Spatial and temporal variations in soil respiration in relation to stand structure and soil parameters in an unmanaged beech forest. *Tree Physiology*, 25(11):1427–1436.
- Soil Classification Working Group (1998). The Canadian system of soil classification. Technical Report 1646 (Revised), Agriculture and Agri-Food Canada.

- Soil Survey Division Staff (1993). Soil survey manual. Technical Report 18, Soil Conservation Service. U.S. Department of Agriculture.
- Sombroek, W., Nachtergaele, F., and Hebel, A. (1993). Amounts, dynamics and sequestering of carbon in tropical and subtropical soils. *Ambio*, 22(7):417–426.
- Spaargaren, O. and Batjes, N. H. (1995). Report on the classification into FAO-UNESCO soil units of profiles selected from the NRCS pedon data base for IGBP-DIS. Technical report, International Soil Reference and Information Centre, Wageningen, The Netherlands.
- Stouffer, R., KE, T., and GA, M. (2011). CMIP5 long-term experimental design. *CLIVAR Exchanges*, 56:5–7.
- Stuiver, M., Reimer, P., and Braziunas, T. (1998). High-precision radiocarbon age calibration for terrestrial and marine samples. *Radiocarbon*, 40(3):1127–1151.
- Subke, J.-A. and Bahn, M. (2010). On the ‘temperature sensitivity’ of soil respiration: Can we use the immeasurable to predict the unknown? *Soil Biology & Biochemistry*, 42:1653–1656.
- Subke, J. A., Reichstein, M., and Tenhunen, J. D. (2003). Explaining temporal variation in soil CO₂ efflux in a mature spruce forest in southern Germany. *Soil Biology & Biochemistry*, 35(11):1467–1483.
- Tarantola, A. (2005). Monte Carlo methods. In *Inverse Problem Theory and Methods for Model Parameter Estimation*, chapter 2. Society for Industrial and Applied Mathematics, Philadelphia.
- Tarnocai, C., Canadell, J. G., Schuur, E. A. G., Kuhry, P., Mazhitova, G., and Zimov, S. (2009). Soil organic carbon pools in the northern circumpolar permafrost region. *Global Biogeochemical Cycles*, 23:GB2023.
- Tefs, C. and Gleixner, G. (2012). Importance of root derived carbon for soil organic matter storage in a temperate old-growth beech forest: Evidence from C, N and ¹⁴C content. *Forest Ecology and Management*, 263(0):131–137.
- Telles, E. d. C. C., de Camargo, P. B., Martinelli, L. A., Trumbore, S. E., da Costa, E. S., Santos, J., Higuchi, N., and Oliveira, R. C. (2003). Influence of soil texture on carbon dynamics and storage potential in tropical forest soils of Amazonia. *Global Biogeochemical Cycles*, 17(2):9.
- Tonneijck, F. H. and Jongmans, A. G. (2008). The influence of bioturbation on the vertical distribution of soil organic matter in volcanic ash soils: a case study in northern Ecuador. *European Journal of Soil Science*, 59(6):1063–1075.
- Trumbore, S. (2009). Radiocarbon and soil carbon dynamics. *Annual Review of Earth and Planetary Sciences*, 37:47–66.
- Trumbore, S., Davidson, E., Decamargo, P., Nepstad, D., and Martinelli, L. (1995). Belowground cycling of carbon in forests and pastures of eastern Amazonia. *Global Biogeochemical Cycles*, 9(4):515–528.
- Trumbore, S. E. (2000). Age of soil organic matter and soil respiration: Radiocarbon constraints on belowground C dynamics. *Ecological Applications*, 10(2):399–411.
- Trumbore, S. E. and Czimczik, C. I. (2008). An uncertain future for soil carbon. *Science*, 321(5895):1455–1456.
- Trumbore, S. E. and Torn, M. S. (2005). Soils and the global carbon cycle. In Holland, E. D., editor, *Soils and Global Change*. NATO Advanced Study Institute.
- Tuomi, M., Thum, T., Järvinen, H., Fronzek, S., Berg, B., Harmon, M., Trofymow, J. A., Sevanto, S., and Liski, J. (2009). Leaf litter decomposition—Estimates of global variability based on Yasso07 model. *Ecological Modelling*, 220(23):3362–3371.
- Turner, D. R., Varney, M. S., Whitfield, M., Mantoura, R. F. C., and Riley, J. P. (1986). Electrochemical studies of copper and lead complexation by fulvic-acid .1. potentiometric measurements and a critical comparison of metal-binding models. *Geochimica et Cosmochimica Acta*, 50(2):289–297.

- Urban, N. R., Eisenreich, S. J., Grigal, D. F., and Schurr, K. T. (1990). Mobility and diagenesis of Pb and Pb-210 in peat. *Geochimica et Cosmochimica Acta*, 54(12):3329–3346.
- van Breemen, N. and Burman, P. (1997). *Soil Formation*. Kluwer Academic Publishers.
- van Dam, D., Veldkamp, E., and van Breemen, N. (1997). Soil organic carbon dynamics: variability with depth in forested and deforested soils under pasture in Costa Rica. *Biogeochemistry*, 39(3):343–375.
- van Delft, B., de Waal, R., Kemmers, R., Mekking, P., and Sevink, J. (2006). Field guide humus forms, description and classification of humus forms for ecological applications. Technical report, Alterra, Research Institute for the Green Environment. <http://www.wageningenur.nl/en/Research-Results/Projects-and-programmes/Humus-forms.htm>.
- van Oijen, M., Rougier, J., and Smith, R. (2005). Bayesian calibration of process-based forest models: bridging the gap between models and data. *Tree Physiology*, 25(7):915–927.
- van Veen, J. A. and Paul, E. (1981). Organic-carbon dynamics in grassland soils .1. background information and computer-simulation. *Canadian Journal of Soil Science*, 61(2):185–201.
- Vancampenhout, K., De Vos, B., Wouters, K., Swennen, R., Burman, P., and Deckers, J. (2012). Organic matter of subsoil horizons under broadleaved forest: Highly processed or labile and plant-derived? *Soil Biology & Biochemistry*, 50:40–46.
- Veresoglou, D. S. and Fitter, A. H. (1984). Spatial and temporal patterns of growth and nutrient-uptake of 5 co-existing grasses. *Journal of Ecology*, 72(1):259–272.
- Vogt, K., Grier, C., Meier, C., and Keyes, M. (1983). Organic-matter and nutrient dynamics in forest floors of young and mature *abies-amabilis* stands in western Washington, as affected by fine-root input. *Ecological Monographs*, 53(2):139–157.
- Vogt, K., Grier, C., and Vogt, D. (1986). Production, turnover, and nutrient dynamics of above-ground and belowground detritus of world forests. *Advances in Ecological Research*, 15:303–377.
- von Lützw, M., Kögel-Knabne, I., Ludwig, B., Matzner, E., Flessa, H., Ekschmitt, K., Guggenberger, G., Marschner, B., and Kalbitz, K. (2008). Stabilization mechanisms of organic matter in four temperate soils: Development and application of a conceptual model. *Journal of Plant Nutrition and Soil Science*, 171(1):111–124.
- von Lützw, M., Kögel-Knabner, I., Ekschmitt, K., Matzner, E., Guggenberger, G., Marschner, B., and Flessa, H. (2006). Stabilization of organic matter in temperate soils: mechanisms and their relevance under different soil conditions - a review. *European Journal of Soil Science*, 57(4):426–445.
- Vrugt, J. A., ter Braak, C. J. F., Clark, M. P., Hyman, J. M., and Robinson, B. A. (2008). Treatment of input uncertainty in hydrologic modeling: Doing hydrology backward with Markov chain Monte Carlo simulation. *Water Resources Research*, 44:W00B09.
- Vrugt, J. A., ter Braak, C. J. F., Diks, C. G. H., Robinson, B. A., Hyman, J. M., and Higdon, D. (2009). Accelerating Markov Chain Monte Carlo simulation by differential evolution with self-adaptive randomized subspace sampling. *International Journal of Nonlinear Sciences and Numerical Simulation*, 10(3):273–290.
- Waldchen, J., Schulze, E.-D., Schoening, I., Schrumpf, M., and Sierra, C. (2013). The influence of changes in forest management over the past 200 years on present soil organic carbon stocks. *Forest Ecology and Management*, 289:243–254.
- Wakiyama, Y., Onda, Y., Mizugaki, S., Asai, H., and Hiramatsu, S. (2010). Soil erosion rates on forested mountain hillslopes estimated using Cs-137 and Pb-210(ex). *Geoderma*, 159(1-2):39–52.
- Walling, D. E. and He, Q. (1999). Using fallout lead-210 measurements to estimate soil erosion on cultivated land. *Soil Science Society of America Journal*, 63(5):1404–1412.
- Wang, E. X. and Benoit, G. (1997). Fate and transport of contaminant lead in spodosols: A

- simple box model analysis. *Water Air and Soil Pollution*, 95(1-4):381–397.
- Weedon, G., Gomes, S., Viterbo, P., Österle, H., Adam, J., Bellouin, N., Boucher, O., and Best, M. (2010). The WATCH forcing data 1958-2001: A meteorological forcing dataset for land surface-and hydrological-models. Technical report, WATCH Tech. Rep. 22.
- Wheatcroft, R. A., Jumars, P. A., Smith, C. R., and Nowell, A. R. M. (1990). A mechanistic view of the particulate biodiffusion coefficient: Step lengths, rest periods and transport directions. *Journal of Marine Research*, 48:177–207.
- Wilkinson, M. and Humphreys, G. (2005). Exploring pedogenesis via nuclide-based soil production rates and OSL-based bioturbation rates. *Australian Journal of Soil Research*, 43(6):767–779.
- Wilkinson, M. T., Richards, P. J., and Humphreys, G. S. (2009). Breaking ground: Pedological, geological, and ecological implications of soil bioturbation. *Earth-Science Reviews*, 97(1-4):257–272.
- WUR, Alterra (2011). Loobos site. <http://www.climatexchange.nl/sites/loobos/index.htm>. Date retrieved: 8 March 2011.
- Wutzler, T. and Reichstein, M. (2007). Soils apart from equilibrium – consequences for soil carbon balance modelling. *Biogeosciences*, 4(1):125–136.
- Wutzler, T. and Reichstein, M. (2008). Colimitation of decomposition by substrate and decomposers - a comparison of model formulations. *Biogeosciences*, 5(3):749–759.
- Wutzler, T. and Reichstein, M. (2013). Priming and substrate quality interactions in soil organic matter models. *Biogeosciences*, 10(12):2089–2103.
- Xu, X., Thornton, P. E., and Post, W. M. (2013). A global analysis of soil microbial biomass carbon, nitrogen and phosphorus in terrestrial ecosystems. *Global Ecology and Biogeography*, 22(6):737–749.
- Yeluripati, J. B., van Oijen, M., Wattenbach, M., Neftel, A., Ammann, A., Parton, W. J., and Smith, P. (2009). Bayesian calibration as a tool for initialising the carbon pools of dynamic soil models. *Soil Biology & Biochemistry*, 41(12):2579–2583.
- Yoo, K., Ji, J. L., Aufdenkampe, A., and Klaminder, J. (2011). Rates of soil mixing and associated carbon fluxes in a forest versus tilled agricultural field: Implications for modeling the soil carbon cycle. *Journal of Geophysical Research-Biogeosciences*, 116:G01014.
- Zimov, S., Schuur, E., and Chapin, F. (2006). Permafrost and the global carbon budget. *Science*, 312(5780):1612–1613.

Summary

Soil organic matter (SOM) plays an important role in the global carbon cycle and has the potential to enhance or reduce anthropogenic climate change. While measurement and modelling studies of SOM dynamics have traditionally focused on the topsoil, evidence is growing that deeper soil levels may store significant amounts of organic carbon. Often different mechanisms related to carbon cycling are relevant at different depths within the soil profile, due to strong vertical gradients of soil properties. Furthermore, processes such as heat and moisture transport are influenced by SOM and its vertical distribution. Therefore, ecosystem models can benefit from an explicit representation of the vertical distribution of SOM in the profile.

Soil organic matter, defined as all dead organic material in soil, is derived mainly from plants. Decomposer organisms (soil fauna, bacteria, and fungi) process litter and SOM, both transforming it to more decomposed compounds and releasing it to the atmosphere as CO_2 . In soil, organic matter concentrations are generally highest near the surface and decrease with depth. In certain ecosystems organic matter may accumulate at the surface as an organic layer. The SOM profile and organic layer mass vary strongly between soils and ecosystems and are determined by several processes. The relative proportions of above- and belowground litter input is relevant to the SOM profile, as well as the vertical distribution of roots. Furthermore, the vertical SOM profile is influenced by several transport mechanisms. Activity of soil fauna such as earthworms, ants, and termites causes mixing of the soil (bioturbation), leading to deepening of the SOM profile. SOM migration may also occur by movement of dissolved organic matter with infiltrating water. Vertical transport, together with microbial processing and stabilization mechanisms causes SOM to become older and more decomposed with depth. SOM turnover rates decrease along the profile by several orders of magnitude.

Although many numerical SOM models have been developed, only a small number of these is vertically explicit. These generally represent vertical SOM transport as diffusion or advection. Most of these models were not intended for (large scale) prognostic simulation and do not include an explicit formulation of the organic layer. This thesis focuses on the development of dynamic representation of the vertical SOM profile and the surface organic layer. The aim is to derive a scheme that includes the main relevant mechanisms, while being parsimonious enough for parameterizations for large spatial scales. Specific attention is given to parameter estimation based on observations.

Chapter 2 of this thesis presents SOMPROF, a new model that dynamically simulates soil carbon cycling. In the model the SOM profile is split into the mineral soil and the surface organic layer, which is further subdivided into three horizons. Aboveground litter fall leads to input at the surface while root input leads to direct input within the profile. Organic matter is split into several pools that differ in terms of decomposability, transport behavior, and mechanism of input. Decomposition is simulated as a first order decay process corrected for temperature and moisture. The model considers two SOM transport mechanisms: bioturbation and liquid phase transport. Bioturbation in the mineral soil is simulated a diffusive process. The diffusivity is determined by the bioturbation rate B and the mixing length l_m , according to mixing length theory. The bioturbation rate is further used to calculate downward flow between the organic surface horizons and across the mineral soil surface. Liquid phase transport is represented as an advection process and only simulated for the mineral soil. A specific SOM pool is defined that represents potentially mobile material. This pool accounts for both dissolved and adsorbed organic matter, thus obviating the need for explicit representation of ad- and desorption.

A simulation run was performed for a deciduous old growth forest on a Cambisol, located in Hainich, Germany, as well as a sensitivity analysis of the transport parameters. SOMPROF is able to simulate realistic SOM profiles and organic layer masses, based on reasonable parameter values. Results further show that temporal variability of heterotrophic respiration is influenced by the vertical SOM distribution.

Chapter 3 deals with calibration of SOMPROF. Due to the difficulty with observing processes such as bioturbation and liquid phase transport *in situ*, model calibration is required. However, parameter estimation is hindered by equifinality: the ability of the model to produce similar results based on different parameterization. Based on organic carbon measurements, 13 parameters related to decomposition and transport of organic matter were estimated for the Hainich site, as well as for a coniferous forest on an Arenosol, located in Loobos, The Netherlands. The value of measurements of ^{210}Pb as a tracer for SOM transport was studied by performing calibrations with and without this data. The calibration was performed with a Bayesian approach which merges information contained in the observations with prior knowledge to derive posterior parameter distributions.

The results highlight the differences between the two sites. For Loobos organic matter transport with the liquid phase appears to be important for shaping the vertical SOM profile, while the effects of bioturbation are negligible. For Hainich the calibration yielded a posterior distribution with three modes (optima), corresponding to distinctly different “explanations” for the observations. The addition of ^{210}Pb data and prior knowledge, led to identification of a favorable mode. This explanation indicates that root litter input is a dominant process for shaping the SOM profile at Hainich.

Chapter 4 presents further study on SOM profile dynamics at the Hainich site. Specifically, the value of radiocarbon (^{14}C) measurements of both SOM and heterotrophic respiration, for constraining model parameters was investigated. Using the Bayesian approach developed in the previous chapter, calibrations were run both

with and without radiocarbon observations. Additionally, the dynamic behavior of the SOM profile under global warming and increasing litter fluxes was studied. The parameter distributions obtained by the calibrations were used to perform prognostic simulations for the period 1910–2100 based on litter fluxes and soil temperature and moisture values predicted by an ecosystem model.

Posterior distributions with two modes were found, corresponding approximately to two of the three modes discussed in chapter 3. However, here a different mode was dominant. The addition of radiocarbon data to the calibration had strong effects on the parameter distribution, most importantly causing a reduction of the decomposition and production rate of the slowest SOM pool by an order of magnitude. The prognostic simulations show an increase of soil carbon in the topsoil and a decrease in the subsoil, adding up to a net gain overall. Near the end of the 21st century total carbon stocks stabilize and—for the radiocarbon-constrained model—start to decrease. However, the changes over time are small compared to the total stocks. The predictions based on the calibrations with and without radiocarbon are similar, but the former shows a markedly higher heterotrophic respiration flux and lower advective loss of organic carbon. The uncertainty of the predicted total soil carbon stock was only slightly decreased by adding radiocarbon data.

Chapter 5 presents a synthesis of the preceding chapters. The SOMPROF model is discussed in the context of parsimony and fidelity, as well as its value for gaining insights in the determinants of the SOM profile. Specific attention is given to bioturbation and liquid phase transport processes, their mathematical representation, and the parameter estimates are compared to previous studies. Furthermore, the difficulties related to calibration and sources of parameter uncertainty are explored. Model equifinality and resulting lack of parameter constraint and multimodality of the posterior distribution are an important issue in calibration of SOM profile models. Several potential observations are possible that may mitigate these problems.

Obvious next steps in the development and application of SOMPROF are its incorporation into an ecosystem model and application at large spatial scales for prognostic simulations. In this context several extensions to the model are advisable in order to improve its validity. A large challenge ahead lies in the derivation of a parameterization for different soils and ecosystems. Parameters need to be related to environmental covariates available in gridded data sets in order to apply the model for unvisited sites.

Samenvatting

De voorraden aan organische stof die opgeslagen liggen in bodems spelen een belangrijke rol in de mondiale koolstofkringloop. Processen die leiden tot af- of toename van deze bodemvoorraden kunnen het broeikas effect versterken of verzwakken. In het verleden was onderzoek naar deze processen voornamelijk gericht op de bovenste laag van de bodem. Recente studies hebben echter aangetoond dat ook diepere bodemlagen grote hoeveelheden koolstof kunnen bevatten. Doordat de meeste bodemeigenschappen een sterke verticale gradiënt vertonen, zijn er grote verschillen tussen bodemlagen in de processen die verantwoordelijk zijn voor opbouw, afbraak en transport van organische stof. Omgekeerd worden processen als transport van warmte en vocht sterk beïnvloed door de organische stof in de bodem. Het is dan ook te verwachten dat modellen van de koolstofkringloop in ecosystemen gebaat zijn bij een expliciete weergave van de verticale verdeling van organische stof in de bodem en de processen die zich daarin afspelen.

“Bodemorganischestof” is gedefinieerd als al het dode organische materiaal in de bodem. Dit materiaal is voornamelijk afkomstig van planten. Plantenresten worden verkleind en verteerd door bodemfauna, bacteriën en schimmels. Daarbij komt een deel van de koolstof vrij als CO_2 en een deel wordt omgezet in stabielere verbindingen en al of niet verplaatst naar andere bodemlagen. De uiteindelijke verticale verdeling van organische stof op en in de bodem verschilt sterk tussen ecosystemen. Deze verdeling hangt in de eerste plaats af van waar de dode plantenresten worden afgezet—bovengronds of ondergronds—en van de verdeling van de wortels. Vervolgens wordt de verticale verdeling beïnvloed door transportprocessen. Graafactiviteiten van bodemfauna, zoals regenwormen, mieren en termieten, vermengen de bodem (bioturbatie) wat leidt tot verdieping van het organischestofprofiel. Verplaatsing van organische stof gebeurt ook door neerwaarts transport van opgeloste organische stoffen met wegzijgend bodemvocht (advectie). De combinatie van verticaal transport en voortgaande omzetting door micro-organismen heeft tot gevolg dat de organische stof in diepere bodemlagen gemiddeld ouder en sterker afgebroken is dan boven in de bodem. Daardoor vermindert met de diepte ook de gemiddelde afbraaksnelheid van organische stof met enkele orden van grootte.

In de laatste decennia zijn vele dynamische simulatiemodellen ontwikkeld die de dynamiek van organische stof in de bodem beschrijven. Daarvan is echter slechts een klein aantal verticaal expliciet. De meeste modellen onderscheiden geen strooisellaag. Verticaal transport van organische stof wordt meestal weergegeven als diffusie

of advectie. Deze modellen zijn doorgaans niet ontwikkeld met het oog op voorspelling van de invloed van bodemprocessen op de mondiale koolstofkringloop.

Het in dit proefschrift beschreven onderzoek beoogt het ontwikkelen van een nieuw model voor dynamisch simulatie van de verticale verdeling van organische stof in de bodem en op het bodemoppervlak. Het doel is een model dat alle relevante processen tijdens de ontwikkeling van bodems beschrijft en toch eenvoudig genoeg voor toepassing op grote ruimtelijke schaal.

Hoofdstuk 2 geeft een beschrijving van het model SOMPROF dat organische stof in de bodem en organische laag simuleert. In dit model is het organischestofprofiel gesplitst in de minerale bodem (met een geleidelijk verlopend organischestofgehalte) en een organische toplaag, die verdeeld is in drie subhorizonten. De aanvoer van organisch materiaal vindt plaats door bovengrondse strooiselval en diepteafhankelijke aanvoer door wortels. De organische stof wordt verdeeld in fracties die verschillen qua aanvoermechanisme (boven- of ondergronds), afbraaksnelheid en transportgedrag. Afbraak wordt weergegeven als een eerste-orde kinetisch proces en gecorrigeerd voor temperatuur en bodemvocht. Het model bevat twee transportmechanismen: bioturbatie en verplaatsing met bodemvocht. Bioturbatie in de minerale bodem wordt gesimuleerd als een diffusieproces. De diffusieconstante hangt af van de bioturbatiesnelheid (B) en de menglengte (l_m), volgens de menglengtetheorie van turbulente stroming. Voor de organische toplaag wordt de bioturbatiesnelheid gebruikt om het neerwaarts transport tussen de horizonten te berekenen. Transport met bodemvocht wordt beschreven als een advectieproces (alleen in de minerale bodem). Het model beschrijft een aparte fractie potentieel mobiele organische stof die zowel opgelost als geadsorbeerd organisch materiaal omvat, wat afzonderlijke simulatie van adsorptie en desorptie van organische stof overbodig maakt.

Het model SOMPROF is gebruikt om de verdeling van organische stof in de bodem te simuleren op basis van meetgegevens afkomstig uit een loofbos op een Cambisol in Hainich (Duitsland). Tevens is een gevoeligheidsanalyse uitgevoerd voor de transportparameters in SOMPROF. Simulaties op basis van redelijke parameterwaarden leverden verdelingen op die goed overeenkomen met metingen. De resultaten tonen verder aan dat de temporele variatie van de heterotrofe respiratie op seizoenstijdschaal afhangt van de diepteverdeling van organische stof in de bodem.

Hoofdstuk 3 behandelt de kalibratie van SOMPROF. Processen als bioturbatie en transport met bodemvocht kunnen moeilijk in het veld worden gemeten. Daarom moeten de parameters die deze processen beschrijven worden geschat. Dit wordt echter bemoeilijkt door equifinaliteit: het verschijnsel dat dezelfde modeluitkomst kan worden bereikt met verschillende parametercombinaties. Op basis van meetgegevens uit Hainich is een schatting gemaakt van de waarden van 13 parameters die nodig zijn voor de beschrijving van afbraak en transport van organische stof. Hetzelfde is gedaan met meetgegevens uit Loobos, een naaldbos op een Arenosol in Nederland. De kalibraties zijn uitgevoerd volgens een Bayesiaanse methode. Deze methode combineert informatie afkomstig uit metingen met bestaande voorkennis om te komen tot een *a posteriori* kansverdeling van modelparameters. Tevens is het nut van metingen van lood-210 (^{210}Pb) als een tracer voor transport van organische stof onderzocht. Kalibraties zijn uitgevoerd met en zonder metingen van het lood-

210 gehalte in de bodem.

De resultaten onderstrepen de verschillen tussen de twee onderzoekslocaties. Voor Loobos blijkt transport met het bodemvocht een belangrijke rol te spelen bij de uiteindelijke verdeling van organische stof in de bodem, terwijl de rol van bioturbatie minimaal is. Voor Hainich leverde de kalibratie een parameter verdeling met drie optima (modi) op, welke corresponderen met verschillende verklaringen voor de metingen. Door voorkennis en gegevens van lood-210 gehalten bij de kalibratie te betrekken kon de meest waarschijnlijke modus worden geïdentificeerd. De parameterwaarden van deze modus tonen aan dat de aanvoer van organische stof door wortels in belangrijke mate bepalend is voor de uiteindelijke verdeling van organische stof in de bodem van Hainich.

Hoofdstuk 4 gaat dieper in op de dynamiek van organische stof in de bodem bij Hainich. Om te onderzoeken of metingen van koolstof-14 (^{14}C) gehalten in de organische stof en de CO_2 -emissie gebruikt kunnen worden om de schatting van modelparameters te verbeteren, zijn nieuwe kalibraties uitgevoerd met en zonder koolstof-14 data. Hiervoor is een vereenvoudigde versie van het model gebruikt. Daarnaast is de ontwikkeling van het organischestofprofiel gesimuleerd voor een toekomstscenario met toenemende bodemtemperatuur en strooiselproductie, zoals berekend met een ecosysteemmodel voor de periode 1910–2100. Daarbij zijn parameterwaarden gebruikt die bij de kalibraties van SOMPROF waren gevonden.

De nieuwe kalibraties, zowel met als zonder koolstof-14 data, leverden een bimodale *a posteriori* parameterverdeling op. De twee modi komen bij benadering overeen met twee van de drie modi die in hoofdstuk 3 werden gevonden. Nu was echter een andere modus dominant door het gebruik van een vereenvoudigde versie van het model. Toevoeging van koolstof-14 data aan de kalibratie had grote gevolgen voor de parameterwaarden: de geschatte afbraak- en productiesnelheid van de langzaamste organischestoffractie werd een orde van grootte kleiner om de hoge leeftijd van organische stof in de diepe bodem, aangegeven door de koolstof-14 data, te kunnen reproduceren. De simulaties met het toekomstscenario voorspellen een toename van organische stof bovenin het profiel en een afname in diepere bodemlagen. De totale voorraad organische stof in de bodem neemt aanvankelijk toe en vlakt af tegen het einde van 21ste eeuw. Voor het model gekalibreerd met koolstof-14 data begint organische stof af te nemen aan het eind van de simulatie.

Zowel de veranderingen in de tijd als de verschillen tussen de simulaties voor beide kalibraties zijn echter klein in verhouding tot de totale koolstofvoorraden. De simulaties met medeneming van koolstof-14 data voorspellen grotere koolstofverliezen door heterotrofe respiratie en kleinere verliezen door advectie. De onzekerheid in de voorspelling van de organischestofvoorraad werd slechts weinig verminderd door toevoeging van koolstof-14 data aan het model.

Hoofdstuk 5 is een synthese van de voorgaande hoofdstukken. Het model SOMPROF wordt besproken in de context van parsimonie en natuurgetrouwheid. Bijzondere aandacht wordt besteed aan de betekenis en wiskundige formulering van bioturbatie en transport van organische stof met bodemvocht. De geschatte transportsnelheden worden vergeleken met waarden die in eerdere studies zijn gevonden. Ook de moeilijkheden bij het schatten van parameterwaarden worden besproken.

Het verschijnsel equifinaliteit is een belangrijke bron van onzekerheid bij het kalibreren van modellen die de dynamiek van organische stof in de bodem beschrijven. Verschillende aanvullende metingen worden genoemd die deze problemen zouden kunnen verminderen.

Voordat het model SOMPROF kan worden opgenomen in een ecosysteemmodel van de mondiale koolstofkringloop zijn aanpassingen en uitbreidingen nodig om de validiteit van het model te verbeteren. Een grote uitdaging ligt in het toepassen van SOMPROF voor verschillende bodems en ecosystemen. Daartoe moeten relaties tussen de parameters van het model en omgevingsvariabelen, zoals bodem- en vegetatietype en klimaat, worden afgeleid.

About the author

Curriculum Vitae

Maarten Braakhekke was born on 19 April 1979 in Ede, The Netherlands. From 1991 he followed secondary education at the Dorenweerd College in Doorwerth and Oosterbeek and he received his diploma in 1997. Before moving on to university education Maarten spent seven months in Australia on a work-and-travel program. In 1998 he started his study Soil-Water-Atmosphere at Wageningen University. Rather than specializing in one of the three disciplines soil science, hydrology, or meteorology, as was customary, he chose to compile his own course program which was interdisciplinary, with focus on terrestrial ecosystem modelling. He carried out a major thesis on modelling carbon dioxide transport in soil, and a practical internship on measuring greenhouse gas production in peat mesocosms. In 2006 he received his MSc degree. In the same year Maarten joined the Max-Planck Institute for Biogeochemistry in Jena, Germany, initially as a research scientist. From 2007 he started working on his PhD research in the recently-established junior research group of Markus Reichstein on Biogeochemical Model-Data Integration. His PhD work was carried out partially in the Earth System Science group at Wageningen University, which also co-funded his research. Maarten completed his PhD project in 2013 and currently continues his research as a PostDoc at the Department of Biogeochemical Integration in at the MPI-BGC, while being based mainly at the ESS group in Wageningen.

Publications

- **Braakhekke, M. C.**, C. Beer, M. Schrumpf, A. Ekici, B. Ahrens, M.R. Hoosbeek, B. Kruijt, P. Kabat, and M. Reichstein. *The use of radiocarbon to constrain current and future soil organic matter turnover and transport in a temperate forest*. Accepted for publication in Journal of Geophysical Research: Biogeosciences
- **Braakhekke, M. C.**, T. Wutzler, C. Beer, J. Kattge, M. Schrumpf, I. Schöning, M.R. Hoosbeek, B. Kruijt, P. Kabat, and M. Reichstein. *Modeling the vertical soil organic matter profile using Bayesian parameter estimation*. Biogeosciences 10 (2013): 399-420
- **Braakhekke, M. C.**, C. Beer, M. R. Hoosbeek, M. Reichstein, B. Kruijt, M. Schrumpf, and P. Kabat. *SOMPROF: A Vertically Explicit Soil Organic Matter Model*. Ecological Modelling 222, no. 10 (2011): 1712-1730.
- Mahecha, M. D., M. Reichstein, M. Jung, S. I. Seneviratne, S. Zaehle, C. Beer, **M. C. Braakhekke**, N. Carvalhais, H. Lange, G. Le Maire, and E. Moors. *Comparing Observations and Process-Based Simulations of Biosphere-Atmosphere Exchanges on Multiple Timescales*. Journal of Geophysical Research-Biogeosciences 115, (2010).
- Weber, U., M. Jung, M. Reichstein, C. Beer, **M. C. Braakhekke**, V. Lehsten, D. Ghent, J. Kaduk, N. Viovy, P. Ciais, N. Gobron, and C. R. Odenbeck. *The Interannual Variability of Africa's Ecosystem Productivity: A Multi-Model Analysis*. Biogeosciences 6, no. 2 (2009): 285-295.

Selected oral presentations

- **Braakhekke, M. C.**, M. Reichstein, B. Kruijt, M. R. Hoosbeek, C. Beer, C. Reick, M. Heimann, and P. Kabat. 2009. *Modelling the vertical profile of soil organic matter in terrestrial ecosystems*. International Symposium on Soil Organic Matter Dynamics, Colorado Springs, Colorado, USA, July 6-9, 2009
- **Braakhekke, M. C.**, C. Beer, M. R. Hoosbeek, M. Reichstein, J. Kattge, T. Wutzler, B. Kruijt, M. Schrumpf, and P. Kabat. 2010. *Mechanistic modeling of the vertical soil organic matter profile in terrestrial ecosystems*. EGU General Assembly, Session Soil Organic Matter: structures, functions, management strategies, and C cycle, Vienna, Austria, May 2-7, 2010
- **Braakhekke, M. C.**, T. Wutzler, M. Reichstein, J. Kattge, C. Beer, M. Schrumpf, M. R. Hoosbeek, , B. Kruijt, and P. Kabat. 2011. *Explaining the vertical SOM profile using Bayesian inversion and lead-210 measurements*. EGU General Assembly, Session Soil organic carbon (SOC) dynamics at different spatial scales, Vienna, Austria, April 3-8, 2011
- **Braakhekke, M. C.**, T. Wutzler, M. Reichstein, J. Kattge, C. Beer, M. Schrumpf, M. R. Hoosbeek, I. Schöning, B. Kruijt, and P. Kabat. 2011. *Modeling the vertical SOM profile using Bayesian inversion and ²¹⁰Pb measurements*. International Symposium on Soil Organic Matter 2011, Leuven, Belgium, July 11-14, 2011
- **Braakhekke, M. C.**, T. Wutzler, M. Reichstein, J. Kattge, C. Beer, M. Schrumpf, , I. Schöning, M. R. Hoosbeek, , B. Kruijt, and P. Kabat. 2011. *Studying the vertical SOM profile using inverse modeling and tracers: A case study for the isotope lead-210*. SIBAE Cost-action workshop on "Integrating vertical dimension in soil carbon studies/models using natural abundance of stable isotopes", Nancy, France, 17-20 October 2011



Netherlands Research School for the
Socio-Economic and Natural Sciences of the Environment

C E R T I F I C A T E

The Netherlands Research School for the
Socio-Economic and Natural Sciences of the Environment
(SENSE), declares that

***Maarten Christiaan
Braakhekke***

born on 19 April 1979 in Ede, the Netherlands

has successfully fulfilled all requirements of the
Educational Programme of SENSE.

Wageningen, 24 January 2014

the Chairman of the SENSE board

Prof. dr. Rik Leemans

the SENSE Director of Education

Dr. Ad van Dommelen

The SENSE Research School has been accredited by the Royal Netherlands Academy of Arts and Sciences (KNAW)



K O N I N K L I J K E N E D E R L A N D S E
A K A D E M I E V A N W E T E N S C H A P P E N



The SENSE Research School declares that **Mr. Maarten Christiaan Braakhekke** has successfully fulfilled all requirements of the Educational PhD Programme of SENSE with a work load of 45 ECTS, including the following activities:

SENSE PhD Courses

- o Environmental Research in Context
- o Research Context Activity: Co-organising Symposium Session and Round Table discussion at Eurosoil Congress (Bari, Italy – 2-6 July 2012)
- o Bayesian Statistics
- o Uncertainty Analysis

Other PhD Courses

- o Introduction to Earth Systems Science and Modelling
- o EaSyMS Summer School on Earth System Modelling
- o Advanced Scientific Writing

Oral Presentations

- o *Towards a more realistic, three-dimensional description of the soil system in global carbon cycle models.* Retreat of the International Max Planck Research School for Earth System Modelling, 10-12 October 2007, Hamburg, Germany
- o *Modelling the vertical profile of soil organic matter in terrestrial ecosystems.* International Symposium on Soil Organic Matter Dynamics, 6-9 July 2009, Colorado Springs, Colorado, USA
- o *Modelling the vertical profile of soil organic matter.* EGU general assembly, 2-7 May 2010, Vienna, Austria
- o *Modelling the vertical SOM profile using Bayesian inversion and ²¹⁰Pb measurements.* International Symposium on Soil Organic Matter, 11-14 July 2011, Leuven, Belgium
- o *Studying the vertical SOM profile using inverse modelling and tracers: A case study for the isotope lead-210.* SIBAE workshop: Integrating vertical dimension in soil carbon studies/models using natural abundance of stable isotopes, 17-20 October 2011, Nancy, France

SENSE Coordinator PhD Education



Dr. ing. Monique Gulickx

The research described in this thesis was financially supported by the European Research Council, the Earth System Science Group of Wageningen University, and Alterra, Wageningen UR.

Financial support from Wageningen University for printing this thesis is gratefully acknowledged.

